



Universidade de
Aveiro
2014

Departamento de Engenharia de Materiais e
Cerâmica

Saurabh Kapoor

**Vidros bioactivos isentos de alcalinos para
regeneração óssea**

**Alkali-Free Bioactive Glasses For Bone
Regeneration**



Saurabh Kapoor

Alkali-Free Bioactive Glasses For Bone Regeneration

Tese apresentada à Universidade de Aveiro para cumprimento dos requisitos necessários à obtenção do grau de Doutor em Ciência e Engenharia de Materiais, realizada sob a orientação científica do José Maria da Fonte Ferreira, Professor Associado com Agregação do Departamento de Engenharia Cerâmica e do Vidro da Universidade de Aveiro, e do Doutor Ashutosh Goel, Professor adjunto da Universidade Rutgers New Jersey, USA.

Apoio financeiro do POCTI no âmbito
do III Quadro Comunitário de Apoio,
através dos projectos:
PTDC/CTM-CER/114209/2009-
FCOMP-01-0124
PTDC/CTM/099489-FCOMP-01-0124-
FEDER-099371

Dedicated to my parents, my sister and sugandha

o júri

presidente

Prof. Doutor Luís Filipe Pinheiro de Castro
Professor Catedrático da Universidade de Aveiro

Prof. Doutor João Carlos Matias Celestino Gomes da Rocha
Professor Catedrático da Universidade de Aveiro

Prof. Doutora Maria Filomena Rabaça Roque Botelho
Professora Catedrática da Faculdade de Medicina da universidade de Coimbra

Prof. Doutor José Maria da Fonte Ferreira
Professor Associado com Agregação da Universidade de Aveiro (Orientador)

Doutor Pedro Lopes Granja
Investigador Principal do Instituto de Engenharia Biomédica da Universidade do Porto

Prof. Doutora Maria Clara Henriques Batista Gonçalves
Professora Auxiliar do Instituto Superior Técnico da Universidade de Lisboa

I would like to express my heartiest appreciation and thanks to my supervisor Professor J.M.F Ferreira, for supporting me during these past 3 years, you have been a tremendous mentor for me. He has been actively interested in my work and has always been available to advise me. I am very grateful for his patience, motivation, enthusiasm, and immense knowledge in bioactive glasses that, taken together, make him a great mentor. I would like to thank you for encouraging my research and for providing all possible facilities and funding for me to complete my PhD. He is an excellent example a person with so much humility and trying to help in whatever possible way he can.

I would like to express my immense gratitude to Dr. Ashutosh Goel for believing in me since i met you in 2010 Amritsar, for being a brother to me and guiding me in every possible way during my PhD, always trying make things work for me. His patience, flexibility, genuine caring and concern, and faith in me during the dissertation process enabled me to enjoy my Ph.D. He's been motivating, encouraging, has never judged nor pushed when he knew I needed to juggle priorities.

Acknowledgements

I would like to thank Dr. Rajan Saini for being a friend, mentor during my undergraduate and post graduate days and for encouraging me to pursue research during my masters.

My heartiest thanks to Dr. Rohit Chopra and Dr. Jaskirat Singh for being there and helping and supporting me throughout my academic years

My gratitude is also extended to Dr. Susana Olhero for her friendship and support. Without her I would not have been able to complete my work.

I would like to express my gratitude to Dr. Ajay Kaushal (also laboratory Colleague) for his friendship since the first day of my arrival in Aveiro and for teaching me important aspects of research and life.

Appreciation also goes to my laboratory colleagues and friends, whose expertise and knowledge added considerably to my experience. Their friendship was a great support in the most difficult times and doubts: Anuraag Gaddam, Allu Amarnath Reddy, Rupam Sen, Budhendra K. Singh, Paula Torres, Catarina Marques, Hugo Fernandes and B C Jamaliah.

My sincere thanks to Prof. Hae-Won Kim, Prof. Vikram Dhuna and Prof. Pedro L Granja for performing cell-culture studies the glasses samples which were helpful in showing the efficiency of our glasses.

My immense gratitude to Professor Maria J. Pascual for supporting by performing HSM measurements on my samples which were very helpful in understanding the sintering and crystallization behaviour of studied glasses in this dissertation.

To all colleagues and technicians of DEMaC and CICECO for the support to this work.

palavras-chave

Vidros, vitrocerâmicos, estrutura, bioatividade, sinterização.

resumo

Os vidros e vitrocerâmicos bioactivos fazem parte da chamada terceira geração de biomateriais, i.e., materiais que estimulam uma resposta especial quando em contacto com fluidos biológicos, capaz de conduzir ao estabelecimento de ligações fortes entre a sua superfície e os tecidos vivos. O presente estudo visou o estudo e desenvolvimento de vidros bioactivos à base de dióxido e isentos de metais alcalinos que apresentem um bom comportamento na sinterização, elevados índices de bioactividade, e taxas de dissolução / degradação compatíveis com as almejadas aplicações em regeneração óssea e em engenharia de tecidos. Procurou-se ainda entender as relações entre a estrutura e as propriedades dos vidros bioactivos estudados. De acordo com esta perspectiva, estudaram-se várias composições de vidros bioactivos pertencentes ao sistema Dióxido (CaMgSi₂O₆) – Fluorapatite (Ca₅(PO₄)₃F) – Fosfato de tricálcico (3CaO•P₂O₅). Todas as composições vítreas foram preparados por fusão, seguida de fritagem em água fria, e caracterizados através de um conjunto de técnicas complementares de caracterização. Os vitrocerâmicos foram obtidos por sinterização das fritas de vidro moídas e compactadas, seguida de tratamento térmico adequado para promover os fenómenos de nucleação e cristalização. Além disso, algumas composições vítreas seleccionadas foram dopadas com vários iões funcionais e os seus efeitos na estrutura vítrea, na sua propensão para a sinterização, e nos comportamentos *in vitro* em termos de bio-degradação e bio-mineralização foram avaliados. Os efeitos das mesmas variáveis no processo de devitrificação (nucleação e cristalização) dos vidros e formação de materiais vitrocerâmicos foram também investigados. Algumas composições de vítreas apresentaram taxas de bio-mineralização elevadas, expressas através da formação de camadas superficiais de hidroxiapatite após 1-12 h de imersão num fluido fisiológico simulado (SBF). Todas as composições vítreas apresentaram taxas de degradação mais baixas quando comparadas com a do 45S5 Bioglass[®]. Alguns vidros bioactivos revelaram comportamentos *in vitro* excelentes, sendo a taxa de bio-mineralização dos co-dopados com zinco e estrôncio dependente da dose incorporada de dopantes. Os materiais estudados demonstraram boa aptidão para aplicações em regeneração óssea e para o fabrico de estruturas de suporte em engenharia de tecidos.

keywords

Glasses, glass-ceramics, structure, bioactivity, sintering.

abstract

Bioactive glasses and glass-ceramics are a class of *third generation* biomaterials which elicit a special response on their surface when in contact with biological fluids, leading to strong bonding to living tissues. The purpose of the present study was to develop diopside based alkali-free bioactive glasses in order to achieve good sintering behaviour, high bioactivity, and a dissolution/degradation rates compatible with the target applications in bone regeneration and tissue engineering. Another aim was to understand the structure-property relationships in the investigated bioactive glasses. In this quest, various glass compositions within the Diopside ($\text{CaMgSi}_2\text{O}_6$) – Fluorapatite ($\text{Ca}_5(\text{PO}_4)_3\text{F}$) – Tricalcium phosphate ($3\text{CaO}\cdot\text{P}_2\text{O}_5$) system have been investigated. All the glasses were prepared by melt-quenching technique and characterized by a wide array of complementary characterization techniques. The glass-ceramics were produced by sintering of glass powders compacts followed by a suitable heat treatment to promote the nucleation and crystallization phenomena. Furthermore, selected parent glass compositions were doped with several functional ions and an attempt to understand their effects on the glass structure, sintering ability and on the *in vitro* bio-degradation and bio-mineralization behaviours of the glasses was made. The effects of the same variables on the devitrification (nucleation and crystallization) behaviour of glasses to form bioactive glass-ceramics were also investigated. Some of the glasses exhibited high bio-mineralization rates, expressed by the formation of a surface hydroxyapatite layer within 1–12 h of immersion in a simulated body fluid (SBF) solution. All the glasses showed relatively lower degradation rates in comparison to that of 45S5 Bioglass[®]. Some of the glasses showed very good *in vitro* behaviour and the glasses co-doped with zinc and strontium showed an *in vitro* dose dependent behaviour. The as-designed bioactive glasses and glass–ceramic materials are excellent candidates for applications in bone regeneration and for the fabrication of scaffolds for tissue engineering.

Contents

List of figures.....	xix
List of tables.....	xxv
List of abbreviations	xxvii
List of publications	xxix
1. Introduction.....	3
2. State of the art.....	7
2.1 Need for Biomaterials for bone regeneration.....	7
2.2 Biomaterials for bone repair.....	8
2.3 Bioactive glasses	10
2.4 Glass structure and bioactivity	13
2.5 Mechanism of HCA layer deposition.....	15
2.6 Role of various functional ions	16
2.6.1 Silicon	16
2.6.2 Strontium.....	17
2.6.3 Zinc	17
2.6.4 Magnesium.....	18
2.6.5 Calcium	18
2.6.6 Phosphorus	19
2.7 Introduction to the present work	20
2.7.1 Aim of the thesis	23
3. Experimental.....	27
3.1 Glass synthesis	27
3.2 Density and Molar volume.....	27
3.3 Structural characterization of glasses.....	27
3.3.1 Magic angle spinning (MAS) – Nuclear magnetic resonance (NMR) spectroscopy.....	27
3.4 Biodegradation of glasses	28

3.5 Thermal analysis	29
3.6 Preparation of glass-ceramics	30
3.7 Characterization of glass-ceramics	30
3.7.1 Mechanical Properties of sintered glass-ceramics	30
3.7.2 Microstructural characterization- SEM and EDS	30
3.8 In vitro studies.....	31
3.8.1 Alkali-free glasses for bone tissue engineering: A preliminary investigation	31
3.8.1.1 Mesenchymal stem cell proliferation	31
3.8.2 Influence of ZnO/MgO substitution on sintering, crystallization, and bio-activity of alkali-free glass-ceramics.....	32
3.8.3 Role of glass structure in defining the chemical dissolution behaviour, bioactivity and antioxidant properties of zinc- and strontium- co-doped alkali-free phosphosilicate glasses	32
3.8.3.1 In vitro cellular tests.....	32
3.8.3.1 Cell Culture studies	32
3.8.4 An experimental approach towards understanding the composition-structure- bioactivity relationships in silicate glasses	34
3.8.4.1 Cell Culture Studies	34
3.8.4.2 Cell metabolic activity	34
4 Results and Discussion	37
4.1 Alkali-free glasses for bone tissue engineering: A preliminary investigation	37
4.1.1 Introduction	37
4.1.2 Results and discussions	38
4.1.2.1 Glass forming ability.....	38
4.1.2.2 Structure of glasses (MAS – NMR spectroscopy)	39
4.1.2.3 Apatite formation and chemical degradation of glasses	40
4.1.2.4 Differential thermal analysis	45
4.1.2.5 Sintering and crystallization behaviour of glasses	46

4.1.2.6 Cellular response to sintered glass powder compacts	51
4.2.2 Conclusions	55
4.2 Structural role of zinc in biodegradation of alkali-free bioactive glasses	57
4.2.1. Introduction	57
4.2.2 Results and discussion.....	58
4.2.2.1 Glass forming ability	58
4.2.2.2 Glass structure	59
4.2.2.3 Apatite forming ability of glasses	60
4.2.2.4 Chemical degradation of glasses in Tris-HCl	63
4.2.2.5 Discussion	65
4.2.3 Conclusions	67
4.3 Influence of ZnO/MgO substitution on sintering, crystallization and bio-activity of alkali-free glass-ceramics.....	69
4.3.1 Introduction	69
4.3.2 Results and discussion.....	69
4.3.2.1 Glass-forming ability	69
4.3.2.2 Thermal analysis	69
4.3.2.3 Sintering and Crystallization behaviour.....	70
4.3.2.4 Effect of heat treatment of the structure.....	73
4.3.2.4.1 Crystalline phase evolution by XRD.....	73
4.3.2.4.2 MAS-NMR of glass-ceramics	74
4.3.2.5 Density and molar volume	75
4.3.2.6 Mechanical Behaviour	76
4.3.2.7 Apatite forming ability of glass-ceramics	77
4.3.2.8 Mesenchymal cell activity and alkaline phosphatase activity.....	79
4.3.3 Conclusions	83

4.4 Role of glass structure in defining the chemical dissolution behaviour, bioactivity and antioxidant properties of zinc- and strontium- co-doped alkali-free phosphosilicate glasses	85
4.4.1 Introduction	85
4.4.2 Results	86
4.4.2.1 Glass forming ability	86
4.4.2.2 Structure of glasses	87
4.4.2.3 SBF immersion studies	90
4.4.2.4 Chemical degradation of glasses in Tris-HCl	95
4.4.2.5 Cellular response on bioactive glasses	97
4.4.2.5.1 In vitro proliferation of MG63 cells	97
4.4.3 Discussion	98
4.4.4 Conclusions	101
4.5 Thermo-mechanical behaviour of alkali-free bioactive glass-ceramics co-doped with strontium and zinc	103
4.5.1 Introduction	103
4.5.2. Results and Discussion.....	103
4.5.2.1 Glass-forming ability	103
4.5.2.2 Thermal analysis	104
4.5.2.3 Sintering and Crystallization behaviour.....	105
4.5.2.4 Structural transformation in glasses during heat treatment:.....	108
4.5.2.4.1 XRD	108
4.5.2.5 Mechanical Behaviour:	110
4.6 Understanding the influence of composition on structure bioactive and thermal behaviour of Diopside – Tricalcium phosphate based glasses.....	113
4.6.1 Introduction	113
4.6.2 Results	113
4.6.2.1 Glass forming ability.....	113

4.6.2.2 Structure of glasses by MAS-NMR	114
4.6.2.3 SBF immersion studies	115
4.6.2.4 Chemical degradation of glasses in Tris-HCl	119
4.6.2.5 Thermal analysis	120
4.6.2.6 Sintering and crystallization behaviours	121
4.6.2.7 Structural transformations during heat treatment.....	125
4.6.2.8 Density	125
4.6.2.9 Mechanical properties	126
4.6.2.10 Cell culture studies	126
4.6.3 Discussions.....	127
4.6.4 Conclusions	131
5. General conclusions	135
6. Future works	139
References.....	143

List of figures

Figure 2.1 Compositional dependence of bioactivity in Na ₂ O-CaO-SiO ₂ -P ₂ O ₅ glass system [2].....	11
Figure 2.2 2-dimensional representation of structure of silica glass [1].	13
Figure 2.3 Number of papers published per year in the field of “bioactive glass” (compiled from a literature search SCOPUS carried out in November 2014).....	20
Figure 4.1.1 X-ray diffractograms of as-quenched glass frits.....	39
Figure 4.1.2 MAS NMR spectra of investigated glasses showing the peak positions of (a) ²⁹ Si and (b) ³¹ P.	40
Figure 4.1.3 X-ray diffractograms of glass powders after immersion in SBF solution for (a) 1 h; (c) 3 h; (c) 12 h, (d) 3 days and (e) 7 days. C refers to calcite while HA refers to hydroxyapatite.....	41
Figure 4.1.4 FTIR spectra of glass powder (TCP-20) before and after immersion in SBF solution for time durations varying between 1 h – 12 h.	43
Figure 4.1.5 Graph depicting changes in pH of solution and weight loss of glass powders after immersion in Tris-HCl for 120 h.....	45
Figure 4.1.6	46
Figure 4.1.7 Comparison of DTA and HSM curves under the same heating rate (5 K min ⁻¹) for compositions (a) TCP-20 and (b) TCP-40 at the heating rate of 5 K min ⁻¹ ; (c) influence of TCP content on different thermal parameters of glasses obtained from DTA and HSM, respectively	48
Figure 4.1.8. SEM images of glass powder compacts (a) TCP-10, (b) TCP-20, (c) TCP-30, after sintering at 800 °C for 1 h, respectively while (d) and (e) represent glass composition TCP-10 after sintering at 900 °C for 1 h.	49
Figure 4.1.9 X-ray diffractograms of glass compositions after sintering at (a) 800 °C; (b) 900 °C and 1000 °C, respectively.....	50
Figure 4.1.10 Proliferation behaviour of the MSCs cultured on the glass compacts (TCP-10 and TCP-20) and the tissue culture plastic used as a control during the periods for 3, 7 and 14 days. MSCs derived from rat bone marrow were used for the assay. Statistically significance difference was noticed between the groups; control vs. TCP-10 at day 3; control vs. TCP-10 or TCP-20 at day 7 (p < 0.05, ANOVA, n = 3)	52
Figure 4.1.11 SEM images of the MSCs grown on the sintered glass powder compacts (TCP-10 and TCP-20) during culture for 7 days. Cells spread well on both glass samples in intimate	

contacts with the underlying substrates and have active cytoskeleton processes with highly elongated filopodia. Some surface cracks associated with the sample treatment for SEM are observed.....	53
Figure 4.1.12 Alkaline phosphatase activity of the MSCs during culture for 7 and 14 days on the glass compacts (TCP-10 and TCP-20) and tissue culture plastic control. Statistically significant higher level was noticed on the glass samples with respect to control at both periods; *p < 0.05, ANOVA, n = 3.....	54
Figure 4.2.1 X-ray diffractograms of as-quenched glasses.....	58
Figure 4.2.2 MAS NMR spectra of investigated glasses showing the peak positions of (a) ²⁹ Si and (b) ³¹ P.....	59
Figure 4.2.3 X-ray diffractograms of glass powders before and after immersion in SBF solution for (a) as quenched glasses (b) 1 h (c) 6 h (d) 3 days and (e) 7 days. HA refers to hydroxyapatite.....	61
Figure 4.2.4 FTIR spectra of glass powders after immersion in SBF solution for (a) 1 h and (b) 24 h.....	62
Figure 4.2.5 Graphs depicting the change in solution pH and weight loss of glass powders after immersion in Tris–HCl.....	63
Figure 4.2.6 X-ray diffractograms of glass powder after 120 days of immersion in TRIS-HCL.....	64
Figure 4.2.7 ICP-AES plots of elemental concentrations of Ca, Mg, P, Si and Zn in Tris–HCl after 120 h of immersion of glass powder. It should be noted that Si refers to SiO ₄ ⁴⁻ and P refers to PO ₄ ³⁻ species.....	65
Figure 4.3.1 DTA thermographs of glasses at a heating rate of 20 K min ⁻¹	70
Figure 4.3.2 Comparison of DTA and HSM curves under the same heating rate (5 K min ⁻¹) for compositions: (a) Zn–2, (b) Zn–4, (c) Zn–6, (d) Zn–8 and (e) Zn–10.....	72
Figure 4.3.3 X-ray diffractograms of glass-ceramics heat treated at 850 °C for 1 h.	74
Figure 4.3.4 (a) ²⁹ Si MAS-NMR and (b) ³¹ P MAS-NMR spectra of glass-ceramics heat treated at 850 °C for 1 h.	75
Figure 4.3.5 Flexural strength of the glass-ceramics heat treated at 850 °C for 1 h.....	77
Figure 4.3.6a SEM/EDS micrographs images of unpolished and non-etched glass-ceramics samples before soaking in SBF: Zn-0, Zn-4, and Zn-8.....	78
Figure 4.3.6b SEM/EDS micrographs images of unpolished and non-etched glass-ceramics samples after soaking in SBF for 7 and 14 days: (a) Zn–0, (b) Zn–4, and (c) Zn–8.....	79

Figure 4.3.7 Influence of ZnO content in glass-ceramics on cell viability during culture for up to 7 days, as assessed by CCK method. Glass-ceramics with 4 mol% ZnO showed highest growth with respect to tissue culture plastic control as well as to that of other investigated glass-ceramics.	80
Figure 4.3.8 SEM images of the MSCs grown on the sintered glass powder compacts (Zn-0, Zn-4 and Zn-8) during culture for 3 and 7 days. After 7 days, cell proliferation on glass-ceramics was better in comparison to that observed after 3 days. Glass-ceramic Zn-4 exhibited the highest rate of cell proliferation.	81
Figure 4.3.9 Alkaline phosphatase activity of the MSCs during culture for 7 and 14 days on the glass compacts (Zn-0 to Zn-8) and on tissue culture plastic control. For all the investigated glass-ceramics, irrespective of their ZnO content, ALP levels were always higher in comparison to that of control ($p < 0.05$, ANOVA, $n=3$)	82
Figure 4.4.1 X-ray diffractograms of glass powders	87
Figure 4.4.2 MAS NMR spectra of investigated glasses showing the peak positions of (a) ^{29}Si and (b) ^{31}P	88
Thus NMR results shows that $\text{Zn}^{2+}/\text{Mg}^{2+}$ and $\text{Ca}^{2+}/\text{Sr}^{2+}$ substitutions do not affect the silicate network connectivity of these glasses.	88
Figure 4.4.3 (a) ^{29}Si MAS NMR spectra and (b) ^{31}P MAS NMR spectra after deconvolution of investigated glasses.	89
Figure 4.4.4 FTIR spectra of glass powders (a) before, after (b) 1h, (c) 24h, and (d)14 days immersion in SBF.	91
Figure 4.4.5 X-ray diffractograms of glass powders after immersing the glass powders in SBF solution for (a) 1 h (b) 3 h (c) 6 h (d) 24 h (e) 3 days and (e) 14 days.	92
Figure 4.4.6 ICP plots of elemental concentration of (a) Ca, (b) P, (c) Mg, (d) Sr, (e) Si and (f) Zn, in SBF solution versus immersion time for the investigated glass powders.	94
Figure 4.4.7 X-ray diffractograms of glass powder after 120 days of immersion in TRIS-HCL.....	95
Figure 4.4.8 (a) Graphs depicting the change in solution pH and weight loss of glass powder samples (with respect to variation in ZnO and SrO content in glasses) after immersion in Tris-HCl; (b) ICP-AES plots of elemental concentrations of Ca, Mg, P, Si, Sr and Zn in Tris-HCl after 120 h of immersion of glass powder. It should be noted that Si refers to SiO_4^{4-} and P refers to PO_4^{3-} species.....	96

Figure 4.4.9 Plots showing the cell growth kinetics of the glasses (ZS-2, ZS-4, ZS-6, and ZS-8) (a) under normal condition during culture after 4 days under normal conditions (b) under H ₂ O ₂ (250 μM) induced oxidative stress in MG63 cell after 3 days. *(C for control)..	98
Figure 4.5.1 DTA thermographs of glasses at a heating rate of 20 K min ⁻¹	104
Figure 4.5.2 Oxygen density plotted against percentage zinc and strontium substitution....	105
Figure 4.5.3 Comparison of DTA and HSM curves under the same heating rate (5 K min ⁻¹) for compositions: (a) ZS-2, (b) ZS-4, (c) ZS-6, (d) ZS-8 and (e) ZS-10.	106
Figure 4.5.4 X-ray diffractograms of glass-ceramics heat treated for 1 h at: (a) 800 °C, (b) 850 °C and (c) 900 °C.	108
Figure 4.5.5 Intensity ratio of the main XRD intensity peaks of Sr-diopside to Sr-fluorapatite plotted against percentage of zinc and strontium substitution for glass-ceramics heat treated for 1 h at 850 °C and 900 °C.	109
Figure 4.5.6 SEM images and EDS results of glass-ceramic ZS-8 sintered for 1 h at: (a) 800 °C, (b) 850 °C, (c) 900 °C, after a heating rate ramp of 5 K min ⁻¹	110
Figure 4.5.7 Flexural strength of glass-ceramics heat treated for 1 h at: (a) 800 °C, (b) 850 °C and (c) 900 °C, using a heating rate of 5 K min ⁻¹	111
Figure 4.6.1 MAS NMR spectra of investigated glasses showing the peak positions of (a) ²⁹ Si and (b) ³¹ P.	114
Figure 4.6.2 FTIR spectra of the investigated glasses	115
Figure 4.6.3 FTIR spectra of glasses powders after immersion in SBF solution for (a) 1 h, (b) 24 h, (c) 3 days, and (d) 14 h.	117
Figure 4.6.4 X-ray diffractograms of glass powders before and after immersion in SBF solution for (a) 1 h (b) 24 h (c) 3 days and (d) 14 days. HA refers to hydroxyapatite	118
Figure 4.6.5 Variations in pH and weight loss of glass powders upon immersion in Tris-HCl solution for 7 days.....	119
Figure 4.6.6 X-ray diffractograms of glass powder after 120 days of immersion in TRIS-HCL.....	120
Figure 4.6.7 DTA thermographs of glasses at a heating rate of 20 K min ⁻¹	121
Figure 4.6.8 Comparison of DTA and HSM curves under the same heating rate (5 K min ⁻¹) for compositions: (a) Di-50, (b) Di-60 (c) Di-70, (d) Di-80 (e) Di-90 and (f) Di-100.....	123
Figure 4.6.10 Flexural strength of glass-ceramics heat treated for 1 h at (a) 900 °C (b) 1000 °C, and (c) 1200 °C.	126

Figure 4.6.11 Metabolic activities of hMSCs on Di-60, Di-70 and Di-90 and TCPS after 1, 3, 7, 14 and 21 days.127

List of tables

Table 2.1 Selected bioactive glass compositions (mol%).	21
Table 3.1 Infrared bands of functional groups of bioactive glasses.	28
Table 4.1.1 Nominal composition of the as-designed glasses (mol%).	37
Table 4.2.1 Nominal composition of the as-designed glasses (mol%).	58
Table 4.3.1 Thermal parameters measured from DTA and HSM at 5 K min^{-1} * $\beta = 20 \text{ K min}^{-1}$.	73
Table 4.4.1 Nominal composition of the as-designed glasses (mol%).	86
Table 4.4.2 Q^n (Si) distribution for glasses ZS-4 and ZS-10 obtained by NMR deconvolution.	88
Table 4.4.3 Q^n (P) distribution for glasses ZS-4 and ZS-10 obtained by NMR deconvolution.	89
Table 4.5.1 Thermal parameters measured from DTA at 20 K min^{-1} .	105
Table 4.6.1 Nominal composition of the as-designed glasses (mol%).	113
Table 4.6.2 Thermal parameters measured from DTA at 20 K min^{-1} .	120
Table 4.6.3 Thermal parameters ($^{\circ}\text{C}$) and A/A_0 ratio derived from DTA and HSM at 5 K min^{-1} .	122
Table 4.6.4 Density (kg m^{-3}) of glasses and glass-ceramics.	125

List of abbreviations

A-W	Apatite-Wollastonite
ALP	Alkaline Phosphatase Activity
BO	Bridging Oxygen
BMD	Bone Mineral Density
CaSR	calcium-sensing receptor
CCK	Cell counting kit
Di	Diopside
DMEM	Dulbecco's Modified Eagle Medium
DMSO	Dimethyl Sulfoxide
DNA	Deoxyribonucleic acid
DTA	Differential Thermal Analysis
EthD-1	Ethidium Homodimer-1
EDTA	Ethylene diamine tetra acetic acid
EDS	Energy-Dispersive X-Ray Spectroscopy
ELISA	Enzyme-linked immunosorbent assay
FA	Fluorapatite
FBS	Foetal bovine serum
FTIR	Fourier Transform Infrared Spectroscopy
GPCR	G-protein coupled receptor
HA	Hydroxyapatite
hMSCs	Human Mesenchymal Stem Cells
HCA	Hydroxy Carbonate Apatite
ICP	Inductively Coupled Plasma
MAS-NMR	Magic Angle Spinning– Nuclear Magnetic Resonance
MSCs	Mesenchymal Stem Cells
NBO	Non-Bridging Oxygen
NC	Network connectivity
PBS	Phosphate Buffered Saline
PGA	Polyglycolic acid
PLA	Polylactic acid
SBF	Simulated Body Fluid
SEM	Scanning Electron Microscopy

Tris	Tris (Hydroxymethyl) Aminomethane
TE	Tissue Engineering
TCPS	Tissue Culture Polystyrene
TCP	Tricalcium Phosphate
XRD	X-Ray Diffraction
v/v	Volume/volume

List of publications

1. **Saurabh Kapoor**, Ashutosh Goel, Antonio Tilocca Raghu, Vikram Dhuna, Gaurav Bhatia, Kshitija Dhuna, Jose M. F. Ferreira, *Role of glass structure in defining the chemical dissolution behaviour, bioactivity and antioxidant properties of zinc- and strontium- co-doped alkali-free phosphosilicate glasses*. **Acta Biomaterialia**, 2014; 10: 3264–78.
2. **Saurabh Kapoor**, Ashutosh Goel, Ana Filipa Correia, Maria J. Pascual, Hye-Young Lee, Hae-Won Kim, José M.F. Ferreira. *Synthesis and Characterization of Bioactive Glass-Ceramics* **Material Science and engineering C (accepted)**.
3. **Saurabh Kapoor**, Angela Semitela, Ashutosh Goel, YeXiang, Jincheng Du, Ana H Lourenço, Daniela M Sousa, Pedro L Ganja, José M. F. Ferreira. *Understanding the composition-structure-bioactivity relationships in diopside (CaO*MgO*2SiO₂) – tricalcium phosphate (3CaO*P₂O₅) glass system*, **Acta Bioamaterlia (accepted)**
4. **Saurabh Kapoor**, Ashutosh Goel, Maria J. Pascual, José M. F. Ferreira, *Thermo-mechanical behaviour of alkali free bioactive glass-ceramics co-doped with strontium and zinc*, **Journal of Non-crystalline Solids**, 2013; 375:74-82.
5. **Saurabh Kapoor**, Ashutosh Goel, Maria J. Pascual and José M. F. Ferreira, *Alkali-free bioactive Diopside – Tricalcium phosphate glass ceramics for scaffolds fabrication: sintering and crystallization behaviour*. **Journal of Non-crystalline Solids** (Invited paper for special issue on health care).
6. Ashutosh Goel, **Saurabh Kapoor**, Antonio Tilocca Raghu, Raman Rajagopal, Jose M. F. Ferreira, *Structural role of zinc in biodegradation of alkali-free bioactive glasses*, **Journal of Material Chemistry B**, 2013;1:3073-82.
7. Ashutosh Goel, **Saurabh Kapoor**, Raghu Raman Rajagopal, Maria J. Pascual, Hae-Won Kim, Jose M. F. Ferreira, *Alkali-Free bioactive glasses for bone tissue engineering: A preliminary investigation*, **Acta Biomaterialia**, 2012; 8: 361-72.

Other publications

1. Allu Amarnath Reddy, Dilshat U. Tulyaganov, Ashutosh Goel, **Saurabh Kapoor**, Maria J. Pascual, José M.F. Ferreira, *Sintering and devitrification of glass-powder compacts in the akermanite-gehlenite system*, **Journal of Materials Science**, 2013;48:4128–36.
2. Allu Amarnath Reddy, Ashutosh Goel, Dilshat U. Tulyaganov, **Saurabh Kapoor**, K Pradeesh, Maria J. Pascual, José M.F. Ferreira, *Study of calcium-magnesium-aluminum-*

- silicate (CMAS) glass and glass-ceramic sealant for solid oxide fuel cell*, **Journal of Power Sources**, 2013;231:203–12.
3. Allu Amarnath Reddy, Dilshat U. Tulyaganov, **Saurabh Kapoor** , Ashutosh Goel , Maria J. Pascual Vladislav V. Kharton and José M. F. Ferreira, *Study of melilite based glasses and glass–ceramics nucleated by Bi₂O₃ for functional application*, **RSC Advance**, 2012;2: 10955–67.

Chapter 1

Introduction

1. Introduction

A glass can be defined as an amorphous solid completely lacking in long range, periodic atomic structure, and exhibiting a region of glass transformation behaviour. Any material, inorganic, organic, or metallic formed by any technique, which exhibits glass transformation behaviour is considered to be a glass [1].

Humans have been using glass for thousands of years, from the first uses of natural glass (e.g. obsidian, a volcanic glass) for tools and arrow heads, to the early man-made glass beads and drinking vessels of the Egyptians. Since then, glass has fascinated and attracted much interest both scientifically and technologically. The multiple forms and uses of glasses are becoming increasingly important in science, industry and in general daily life. During the last century, glasses and glass-ceramics became widely used for decorative articles, optics, architectural purposes (from windows to whole glass facades), and glassware for chemical reactions or fibres for telecommunication applications. The major advantage of glasses and glass-ceramics among its ceramic counterparts is their ability to accommodate various functional ions in their amorphous or crystalline phase, thus providing the flexibility to tailor and optimize their compositions with respect to different technological applications.

In particular bioactive glasses have been a relatively young group of materials discovered in 1970's by Larry Hench. Bioactive glasses and glass-ceramics constitute a class of bioactive materials, i.e. "Materials which elicit a special response on their surface when in contact with biological fluids, leading to strong bonding to living tissue". Since its discovery, 45S5 Bioglass[®] has been used in >650,000 human patients and is being marketed for various dental and orthopaedic applications under different commercial brand names [2-4]. Due to number of attractive properties for bone regeneration and tissue engineering (TE), increasing efforts have been made towards expanding the range of potential applications and understanding the fundamental science governing the physical, chemical and thermal properties of bioactive glasses in order to develop novel compositions with superior set of properties for biomedical applications [5-10]. Irrespective of this huge success, high alkali-containing glasses face some drawbacks which do restrict their application in some of the most advanced areas of human biomedicine. High alkali-content in glasses increase their crystallization tendency upon sintering, hindering the densification process and limiting the mechanical strength of sintered materials. Further, the relatively high chemical dissolution rates of such glasses in aqueous media decrease their *in vitro* and *in vivo* efficacy [11]. All these features constitute serious drawbacks in terms of fabrication of porous scaffolds or

porous coatings, and mitigate the potential benefits that could be drawn from their usage as biomedical devices for bone regeneration and TE.

Despite many comprehensive studies leading to the development of bioactive glasses from different systems, the majority of these studies were based on 45S5 Bioglass[®] or compositions inspired by it. Therefore, this work aims at designing new alkali-free bioactive glasses in the Diopside (Hereafter referred as Di) – Tricalcium phosphate (Hereafter referred as TCP) – Fluorapatite (Hereafter referred as FA) system having good bioactive properties and to understand the structure–property relationships in the as designed glasses.

In the light of the above mentioned perspective, this dissertation comprises of five chapters. The first chapter, i.e., the Introduction, provides an outlook of the content of each chapter; the second chapter will focus on the literature survey in the field of bioactive glasses for biomedical applications, with special emphasis on alkali-free silicate systems. The second chapter has been divided into different subsections; the first section aims at providing a historical background on the development and evolution of bioactive glasses in general, while the second section outlines the motivations and purpose behind the present work. The third chapter deals with the description of the general experimental procedures and methodologies used along the thesis. It provides details about all the experimental techniques and procedures employed in order to synthesise, characterize and test our samples. Chapter four is the most important part of this work as it presents all the experimental results obtained on alkali-free glasses and glass-ceramics during past 3 years along with the pertaining discussions. In chapter five we have tried to conclude all the results and achievements obtained during this work and chapter six provides future directions in this field of research.

Several experimental techniques were used throughout this investigation aiming at a better understanding of the glass structure, biodegradation behaviour and the sintering and crystallization behaviour of the corresponding glass powder compacts. Some properties of glasses and glass-ceramics such as density, mechanical strength, were also evaluated to achieve a better understanding concerning the structure-properties relations.

Chapter 2

State of the art

2. State of the art

2.1 Need for Biomaterials for bone regeneration

Human bone is a dynamic, highly vascularised connective tissue which provides structural support and act as a protective casing for the delicate internal organs of the body [12]. It is a tissue that is constantly remodelling to adapt to mechanical stresses imposed and repair minor injuries occurring during the lifetime. However, if the injuries suffered are extensive leading to very large bone defects, the use of bone grafts is required in order to repair the damaged part.

Worldwide, millions of people are affected by degenerative and inflammatory problems related to bone and joint. In fact, they account for half of all chronic diseases in people over 50 years of age in developed countries. Further, every year there are roughly 8.9 million cases of fractures, which occur due to osteoporosis only [13]. Also, approximately 1.6 million hip fractures occur worldwide each year, by 2050 this number could reach between 4.5 million [14] and 6.3 million [15]. Current treatments for filling bone defects and subsequent repair are based on autograft and allografts. Autologous grafts are the ones which contain essential elements for bone regeneration (osteogenic cells, osteoinductive growth factors and a matrix that supports adhesion and bone growth), are collected from the individual, minimizing the risk of rejection. Although autograft present relatively good percentages of success, however the range of applications is restricted, mainly due to the limited availability of living tissues and due to donor site morbidity [16]. Further, allograft bone introduces the possibilities of immune rejection and of pathogen transmission from donor to host. Although infrequent, infections could occur in the recipient's body after the transplantation [16]. Therefore there is a severe need to search for new bone regeneration strategies in order to meet the increasing medical and socioeconomic challenge of our aging population. Hence, materials that enhance bone regeneration have a wealth of potential clinical applications from the treatment of non-union fractures to spinal fusion. Synthetic biomaterials, developed in an effort to overcome the inherent limitations of autograft and allograft, represents an alternative strategy.

2.2 Biomaterials for bone repair

A biomaterial according to the American National Institute of Health is “*Any substance (other than a drug) or combination of substances, synthetic or natural in origin, which can be used for any period of time, as a whole or as a part of a system which treats, augments, or replaces any tissue, organ, or function of the body*”. The development of novel biomaterials is an iterative process that involves the creation of increasingly safer, more reliable, less expensive and more physiologically appropriate replacements for damaged or diseased human tissues. In the last 60 years, biomaterials for orthopaedic applications have evolved from materials available from different industrial applications into the materials with inherent capabilities to interact with the biological environment and to elicit specific biological responses. Most of the problems that orthopaedic surgery has to face have not basically changed, and are practically the same that orthopaedics had to face 50 years ago; however, the choice of possible solutions has been greatly expanded because new materials have allowed the design of innovative devices. Based on the evolution of biomaterials, these can be roughly divided into three broad categories depending upon the interaction mechanisms of the materials; namely inert materials (first generation biomaterials), Bioactive and biodegradable materials (second generation), and materials designed to stimulate specific cellular responses at the molecular level (third generation) [17]. This division represent the development in the field of biomaterials based on the requirements and properties of the materials involved. The present research is still devoted to the first or the second generation depending upon their properties and application. This means that the materials that each new generation brings in do not necessarily outweigh the existing materials.

First generation biomaterials: Developed in the early 1950s [18], the principle underlying the development of first generation biomaterials was that they should be as chemically inert as possible in order to minimize the immune response to the foreign body [17]. Initially, the first generation of biomaterials consisted of already functional materials which were being applied in industrial applications (for e.g. aerospace) where mechanical properties were the main benchmark for the selection of candidate materials for implant manufacture. These biomaterials are mainly metallic or alloys (Co–Cr–Mo alloys, Ti6Al4V, etc.), ceramics (alumina, zirconia, etc.) and polymers (silicone rubber, acrylic resins) [19]. Though bio-inert in nature, these tend to form a thin non-adherent fibrous capsule over their surface with the passage of time after implantation which inhibits further interaction with tissue [20]. The thickness of the layer developed is a function of the level of reactivity of the

implant. Formation of this thin layer is attributed to the absorption of unspecific proteins that results in unspecific signalling to the cellular environment. This thin layer leads to loosening and deterioration of the mechanical fit. Eventually, surgical removal of the device is required. Therefore the development of bioactive interfaces eliciting a specific biological response and avoiding any fibrous layer was one of the main driving forces behind the development of second generation biomaterials.

Second generation of biomaterials: Developed between the years 1970-1980. These biomaterials mainly include ceramics (bioactive glasses, glass-ceramics and calcium phosphates), biodegradable polymers (polylactic acid (PLA) and polyglycolic acid (PGA) etc.) [20]. Bioactive glasses discovered by Larry Hench in 1969-1971 [21] provided an alternative to the bio-inert materials used in orthopaedic applications. These second generation biomaterials were defined by their ability to interact with the biological environment in a controlled manner to enhance the biological response and the tissue/surface bonding. Further progress of the second generation biomaterials was the development of bioresorbable or bio-absorbable materials with the ability to undergo a progressive degradation while new tissue regenerates and heals [20, 22]. Bioactivity is defined as the ability of the material to bond to bone tissue via the formation of a bone-like hydroxyapatite (HA) layer on its surface [23]. The HA phase that forms on bioactive implants is equivalent chemically and structurally to the mineral phase in the bone, and is responsible for strong interfacial bonding, allowing for bone regeneration rather than replacement.

Second generation biomaterials have been in clinical use since 1980 in many orthopaedics and dental applications, including various compositions of bioactive glasses, ceramics, glass-ceramics, and composites. Synthetic calcium phosphate ceramics have been routinely used as bone cements and coatings over metallic prosthesis to facilitate bioactive fixation [20]. Different phases of calcium phosphate ceramics are used depending upon whether a bioresorbable or bioactive material is desired. Bioactive glasses and glass-ceramics are used as middle-ear prostheses to restore the ossicular chain and treat conductive hearing loss and as oral implants to preserve the alveolar ridge from the bone resorption that follows tooth extraction [20, 24, 25]. In comparison to the bioactive glasses and glass-ceramics, calcium phosphate based cements have been used in many orthopaedic applications such as bone substitution, repair of bone fractures (including ligament fixation), cartilage, meniscus and intervertebral disc.

Third generation of biomaterials: Developed in the 21st century, third generation of biomaterials brought together separate concepts of bioresorbable and bioactive materials of second generation. The motive behind the design and development of these materials was to enhance the self-healing capabilities of the body, by the systematic stimulation of specific cellular responses at the molecular level [20]. Primarily, third generation biomaterials were developed by interchanging and intermixing of the properties of bioresorbable and bioactive materials. Consequently, these tailored biomaterials with new levels of bio-functionality have led to new approaches for the treatment of bone defects. Two main strategies have been followed during the last two decades with respect to tissue regeneration are TE and *in situ* tissue regeneration.

TE is one of the approaches in which cells planted in the scaffolds are made to proliferate and differentiate *in vitro*. These tissue-engineered constructs are then implanted into the patients to replace diseased or damaged tissues. Clinical applications include repair of articular cartilage, skin, and the vascular system, although stability of the repaired tissues needs improvement. Another method was *in situ* tissue regeneration which involved the use of biomaterials directly implanted into the body in the form of powders, solutions, or doped micro-particles to stimulate local tissue repair. These materials release controlled amount of ionic dissolution products or growth factors such as bone morphogenic protein (BMP) by diffusion or network breakdown.

2.3 Bioactive glasses

Bioactive glasses are amorphous materials, compatible with the human body; bond to bone and can stimulate new bone growth while dissolving over time. They therefore have the potential to restore diseased or damaged bone to its original state and function (bone regeneration). Bioactive glasses belong to class A of bioactive materials which are osteogenic and osteoconductive materials. The first bioactive glass (silicate based) was discovered by Larry Hench and colleagues in 1969 using melt-quench method, at the University of Florida [26]. The glass composition of the first bioactive glass was 46.1% SiO₂, 24.4% NaO, 26.9% CaO and 2.6% P₂O₅ (mol%), termed 45S5 Bioglass[®], which is now a trademarked name (Figure 2.1).

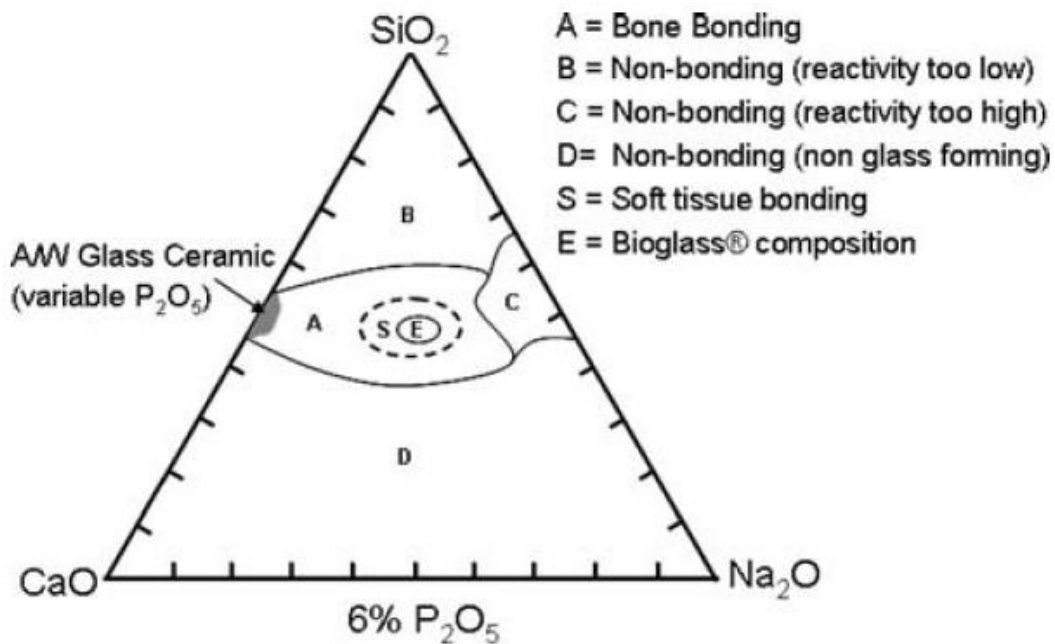


Figure 2.1 Compositional dependence of bioactivity in Na₂O-CaO-SiO₂-P₂O₅ glass system [2].

When in contact with a physiological fluid, bioactive glasses undergo a specific set of reactions, leading to the formation of an amorphous calcium phosphate (ACP) or crystalline HA phase on the surface of the glass, which is responsible for their strong bonding with the surrounding tissue [20]. Further, ionic dissolution products released from bioactive glasses (e.g. Si, Ca, P) are also reported to activate osteogenic gene expression [27, 28] and to stimulate angiogenesis [29, 30]. In addition to it, bioactive glasses offer remarkable advantages such as the ease of controlling chemical composition and, thus, the rate of degradation which make them attractive materials for orthopaedic applications. The structure and chemistry of glasses can be tailored over a wide range by changing either composition, or thermal or environmental processing history. Therefore, it is possible to design bioactive glasses with variable degradation rates to match that of bone ingrowth and remodelling.

Based on the type of glass former, there are mainly three types of bioactive glasses: the conventional silicate-based glasses; phosphate-based glasses; and borate-based glasses. Recently, there has been an increase in interest in borate based bioactive glasses [31, 32], largely due its potential ability to heal chronic wounds that would not heal under conventional treatment [33]. The soft tissue response may be due to their lower chemical durability (faster dissolution) in comparison to the silica-based counterparts [31]. Also phosphate-based glasses have shown great potential in regenerative medicine [31], as the

solubility of these glasses can be controlled by modifying their composition; therefore these glasses show additional clinical potential as resorbable materials. Thus, benefits of phosphate glasses are probably related to their very rapid solubility which is strongly composition dependent rather than bioactivity [34].

Oxide glasses are conventionally produced by melting the precursors (inorganic oxides, carbonates, fluorides and others) in precious metal or ceramic crucibles at high temperatures (for bioactive glasses typically above 1000 °C, depending on the composition). If the cooling is rapid enough (with the necessary cooling rates depending, again, on the composition) crystallization will be inhibited and an amorphous material, a glass, will result. Another common way of preparing bioactive glasses is by a polycondensation reaction from organic precursors, alkoxides such as tetraethyl orthosilicate [35]. Synthesized in the early 1990s [35], this new class of bioactive glasses displays higher compositional range of bioactivity: bioactive sol-gel glass compositions have been synthesized within the ternary $\text{SiO}_2\text{:CaO:P}_2\text{O}_5$ or even within the binary $\text{SiO}_2\text{:CaO}$ systems, and might contain between 60 and 90 mol% of silica [36, 37]. As the synthesis of glasses is highly dependent on composition and external conditions, sol-gel method gives better control over the surface and structural properties (such as surface area and porosity) of the resultant glass in comparison to melt-quenching method. The introduction of sol-gel synthesis technique has opened the research to new types of biomaterials. Many possible dopants can be introduced in a material synthesized via sol-gel. For example, it has been shown that sol-gel derived glasses containing 5 mol% ZnO resulted in increased alkaline phosphatase activity (ALP) activity and osteoblast proliferation [38].

However, in the frame of the present thesis, melt-quenching was used to prepare glasses and sol-gel derived glasses are beyond the scope of this PhD work program. Hence, the subsequent discussion will solely be based on the silicate based glasses prepared by melt-quenching.

2.4 Glass structure and bioactivity

Within the glass structure, three different components are usually described. *Network formers* are able to form amorphous materials without the need for additional components. The basic building unit of silicate glasses is the SiO_4 tetrahedron, which can be connected to neighbouring SiO_4 tetrahedra via Si—O—Si bonds, known as bridging oxygens (BO). Silicon possess a charge of 4^+ thus in the glasses when SiO_4 tetrahedral forms a network these building units can share all their four oxygen atoms to give the stoichiometry ($\text{SiO}_{4/2}$ or SiO_2 which is charge-balanced (assuming a charge of 2^- on the oxygen).

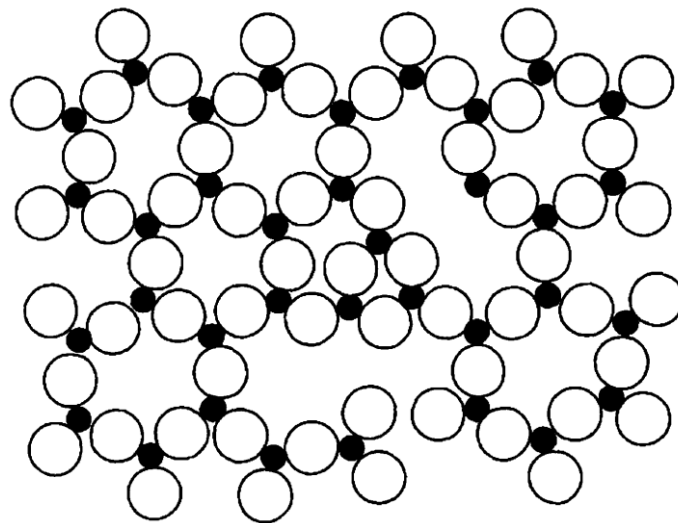


Figure 2.2 2-dimensional representation of structure of silica glass [1].

Each oxygen atom is shared between two silicon atoms, which occupy the centres of linked tetrahedra. Randomness in the structure is facilitated by the variability in the Si—O—Si angle connecting adjacent tetrahedra. Further rotation of adjacent tetrahedra around the point occupied by the oxygen atom linking the tetrahedra, and by rotation of the tetrahedra around the line connecting the linking oxygen with one of the silicon atoms results in augmentation in disorder in the structure. These tetrahedra are commonly referred to as Q^n ($n = 1, 2, 3, 4$) units, where n describes the number of BO connected to the tetrahedron. Silica glass therefore consists of Q^4 units only. A 2-dimensional representation of such a structure is shown in Figure 2.2, where the fourth oxygen, which would sit directly above the small silicon ion, is not shown.

Network modifiers, on the other hand, alter the glass structure by turning BO's (predominantly covalent in character) into non-bridging oxygens (NBO's) (Si—O- M^+

linkages, predominantly ionic in character, where M^+ is a modifier cation). Typical modifiers include the oxides of alkali or alkaline-earth metals having co-ordination number 6 or more. The more modifiers we have in the glass composition, lower is the average number of SiO_4 tetrahedra each tetrahedron is linked to. At the same time, the number of NBO's in the glass structure increases. In conventional silicate glasses, we find large concentrations of Q^4 and Q^3 units, i.e. SiO_4 tetrahedra connected to neighbouring ones in four or three directions, forming a silicate network. The relative concentrations of BO's and NBO's have an important influence on the structure and properties of the glasses. The rigidity of the glass network decreases gradually by replacing bridging atoms by non-bridging atoms.

Intermediates on the other hand can either act like typical network modifiers or enter the backbone of the glass structure, acting more like a network former. These have a co-ordination ranging from 4 to 6.

Bioactive glasses, by contrast, contain larger concentrations of network modifiers and smaller amounts of silica than conventional soda-lime silicate glasses, and they therefore consist of a more disrupted silicate network of mostly Q^2 units. According to Tilocca [5] maximum bioactivity for bioactive glasses is achieved if the structure is dominated by chains of Q^2 metasilicates, which are occasionally cross-linked through Q^3 units, whereas the Q^1 species terminate the chain. Further, the structure of glass can also be estimated based on the glass composition. Different parameters have been suggested for describing the glass structure in the literature [39-41]. Strnad [40] introduced the concept of network connectivity (NC) model to describe the average number of bridging oxygens per network forming element and to correlate the molecular structure of silicate glasses with their bioactivity (apatite forming ability). In a pure silica glass (containing no network modifiers) we have only Q^4 units, thus has a $NC = 4$. With the introduction of the network modifiers the NC decreases as the BO's are converted into NBO's. Bioactive glasses with NC value in the range of 2 and 3 are believed to show good bioactive properties (45S5 Bioglass[®] has a NC of 1.90 [39], corresponding to a structure consisting of silicate).

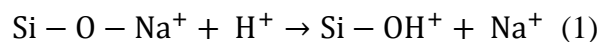
However, while NC may be a useful as a qualitative and a preliminary tool to predict the bioactivity of glasses, its predictive power rapidly decreases when: (i) a wider range of glass compositions are considered; (ii) cations of similar charge are partially substituted in the glass compositions. It has been shown that there is no straightforward correlation between the NC and the degradation behaviour bioactive glasses. For example, glass compositions with NC similar to that of 45S5 Bioglass[®] ($NC = \sim 1.95$) have been shown to exhibit slower chemical dissolution behaviour in aqueous solutions than the latter while partial substitution

of Zn^{2+} in bioactive glasses at the expense of Mg^{2+} retards the apatite forming ability of bioactive glasses despite their NC being unchanged [42].

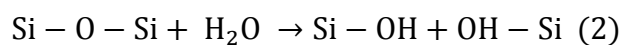
2.5 Mechanism of HCA layer deposition

Even though all the composition of silicate based bioactive glasses synthesized till date are quite different, the mechanism of HA or HCA (hydroxycarbonate apatite) formation are analogous for all of them. The apatite layer forms following solution-mediated dissolution of the glass with a mechanism very similar to conventional glass corrosion [43]. Accumulation of dissolution products causes both the chemical composition and the pH of the solution to change, providing surface sites and a pH conducive to apatite nucleation. There are five proposed stages for apatite formation in body fluid *in vivo* or in SBF *in vitro* [20].

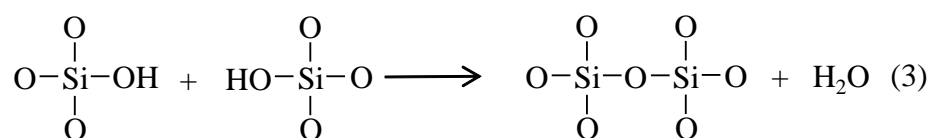
STEP 1 – Reactions for the rapid exchange of ions between the modifiers in the glass network (Na^+ and Ca^{2+}) with H^+ ions or H_3O^+ in solution, leading to hydrolysis of the groups of silica and creating silanol groups ($Si-OH$) on the glass surface. This process results in a net increase of pH of the solution due to the increasing OH ions.



STEP 2 – The increase of pH leads to attack on the glass network, breaking $Si-O-Si$ bonds. Soluble silica is lost in the form of $Si-OH$ to the solution, leaving more $Si-OH$ (silanols) at the glass-solution interface. These silanol groups play a vital role as the nucleation centres of the apatite formation.



STEP 3 – Condensation and repolymerization of SiO_2 -rich layer on the glass surface depleted in alkali and alkaline earth cations.



STEP 4 – Migration of Ca^{2+} and PO_4^{3-} groups to the surface through the silica-rich layer, forming a film rich in amorphous $CaO-P_2O_5$ on the silica-rich layer.

STEP 5 – Incorporation of hydroxyls and carbonate from solution and crystallization of the CaO–P₂O₅ film to form apatite. After the apatite layer is formed the adsorption of growth factors, attachment, proliferation and differentiation of osteoprogenitor cells are the biological mechanisms of bonding to bone. In addition to this, adsorption of adhesion proteins (e.g., fibronectin, vitronectin, etc.) is necessary condition for cellular attachment.

2.6 Role of various functional ions

The processes of bone formation and bone resorption (bone remodelling) are regulated by variety of systematic and local regulated agents including growth factors and hormones. Single inorganic ions are known to be involved in the bone formation and bone resorption (bone remodelling) and play a physiological role in angiogenesis, growth and mineralization of bone tissues. In particular, some metal ions act as enzyme co-factors and therefore influence signalling pathways and stimulate metabolic effects during tissue formation [44]. These properties make metal ions attractive for use as therapeutic agents in the fields of hard and soft TE.

Further, bioactive glasses have the ability to exhibit surface reactivity when in contact with body fluids leading to the release of ionic dissolution products (example: Si, Ca, P, Mg, F) which further stimulate the various vital mechanisms in human body like gene expression, osteoblast proliferation, angiogenesis and also provide anti-bacterial as well as anti-inflammatory effects [28, 30, 45]. In fact, it has been well established that ionic dissolution products are key to understand the behaviour of parent inorganic materials in vitro and in vivo, especially in context of TE applications [46].

2.6.1 Silicon

Silicon (Si) is a non-metallic element with an atomic weight of 28. It is the second most abundant element in the Earth's crust at 28 wt%. Si is known to be an essential element for metabolic processes related with the formation and calcification of bone tissue [44]. Silicon is present in all body tissues, but the tissues with the highest concentrations of silicon are bone and other connective tissue including skin, hair, arteries, and nails [47]. Silicon plays an important role in the formation of cross-links between collagen and proteoglycans [48-50]. *In vitro* studies have demonstrated that silicon stimulates type I collagen synthesis and osteoblast differentiation [51]. Studies in rats have demonstrated that silicon at physiological levels improves calcium incorporation in bone when compared to rats that are

deficient in silicon [52-54]. Additionally, dietary Si intake was shown to increase the bone mineral density (BMD) in men and premenopausal women. Further Si intake has shown to improve BMD by bone resorption in case of calcium deficiency in rats [55]. Moreover, it has been reported that Si has a biochemical function in bone growth processes affecting bone collagen turn over and sialic acid-containing ECM proteins like osteopontin. Moreover, orthosilicate acid ($\text{Si}(\text{OH})_4$) at physiological concentration of 10 mmol has been shown to stimulate collagen I formation in human osteoblast cells (HOC) and to stimulate osteoblastic differentiation [44].

2.6.2 Strontium

Strontium (Sr) is an abundant and widely distributed element in the geosphere, natural water and human tissues. The amount of Sr in the skeleton is only 0.335% of its Ca content [56]. The biological properties of strontium are related to its chemical similarity to calcium. Sr can accumulate in bone by exchanging with Ca in the HA crystal lattice. Thus strontium accumulates to a high degree in bone, can displace calcium in hard tissue metabolic processes and at high concentrations interferes with normal bone development. Low levels of Sr have been known to be associated with low energy fracture sites. Presence of strontium lactate enhances Ca deposition in the bone and reduces bone pain in osteoporosis patients. Sr ions have been shown to stimulate osteoblastic bone formation and to inhibit osteoclastic bone resorption both *in vitro* and *in vivo* [56, 57]. Sr drew attention as a drug for the management of osteoporosis in the 1950s. Indeed, strontium ranelate (Protelos) is a drug approved for treatment and prevention of osteoporosis. Owing to the above-mentioned beneficial aspects of Sr in bone regeneration and considering the ion releasing ability of glasses in aqueous medium, bioactive glasses incorporated with Sr have gained considerable attention in the recent past for various orthopaedic applications. Sr-containing bioactive glasses were shown to combine the known bone regenerative properties of bioactive glasses with the anabolic and anti-catabolic effects of Sr cations *in vitro* [58].

2.6.3 Zinc

Zinc (Zn) plays a vital role in bone formation, resorption and TE as it directly activates aminoacyl-tRNA synthetase (a rate-limiting enzyme at translational process of protein synthesis) in osteoblastic cells and stimulates cellular protein synthesis [42]. Zn has also been shown to stimulate gene expression of the transcription factors: runt-related transcription factor 2 (Runx2) that is related to differentiation into osteoblastic cells.

Moreover, Zn inhibits osteoclastic bone resorption by inhibiting osteoclast-like cell formation from bone marrow cells and stimulating apoptotic cell death of mature osteoclasts [42].

In case of soft tissue regeneration, Zn has been proved to be an essential element for wound healing [30, 44, 45]. It is an essential trace mineral for DNA synthesis, cell division and protein synthesis during the proliferative phase of wound healing [42]. Zn deficiency has been associated with poor wound healing and decreased breaking strength of animal wounds [44] which can result from decreased protein and collagen synthesis during healing found in Zn deficient animals. Agren et al [59] demonstrated the beneficial aspect of topically applied Zn on leg ulcer healing and wound healing in animal models. It was shown that topical zinc oxide promotes cleansing, re-epithelialisation and inhibits bacterial growth.

2.6.4 Magnesium

Magnesium (Mg) is the fourth most abundant cation in human body with approximately half of the total physiological Mg stored in bone tissue [60]. It is essential to bone metabolism and has been shown to have stimulating effects on new bone formation [61]. Mg is a co-factor for many enzymes, and stabilizes the structures of DNA and RNA. Depletion of Mg in body results in impaired bone growth, increased bone resorption and loss in trabecular bone [62, 63]. The level of Mg in the extracellular fluid ranges between 17 ppm and 25.5 ppm, where homeostasis is maintained by the kidneys and intestine [60, 64]. Although Mg levels exceeding 25.5 ppm can lead to muscular paralysis, hypotension and respiratory distress and cardiac arrest occurs for severely high serum levels of 145–170 ppm, the incidence of hyper- Mg is rare due to the efficient excretion of the element in the urine [60, 64, 65].

2.6.5 Calcium

Calcium (Ca) accounts for 1-2 % of the adult human body weight [66], and a major component of mineralized tissues, approximately 99% of body Ca is found in bone, where it serves a key role as a component of HA. Ca plays an important role in osteoblast proliferation and bone remodelling by directly activating intracellular mechanisms by affecting Ca-sensing receptors in osteoblastic cells. The influence of Ca in the body is highly concentration dependent. Maeno et al. [67] found that Ca concentrations in blood varying within the range of 4–8 mmol are suitable for osteoblast proliferation, differentiation and extracellular matrix

(ECM) mineralization, whereas higher Ca concentrations (>10 mmol) are cytotoxic. Extracellular Ca also plays an important role in the control of bone remodelling by directly regulating parathyroid cells through activation of the seven-transmembrane-spanning extracellular calcium-sensing receptor (CaSR), a member of the G-protein coupled receptor (GPCR) family [68]. Similar results were observed by Valério et al. [69], who found that extracellular Ca increases the glutamate release of osteoblastic cells. Since glutamate signalling pathways are known to play an important role for bone mechano sensitivity [70], extracellular Ca concentration must be considered as an important regulating agent in bone metabolism

2.6.6 Phosphorus

Phosphorus (P) is an essential nutrient for human and animal life. It is fundamental to growth, maintenance, and repair of all body tissues, and is necessary, along with calcium and magnesium, for proper growth and formation of bones in infants and children. P being a major component of the inorganic phase of human bone plays an important role in bone formation as it stimulates expression of matrix Gla protein (MGP), a key regulator for bone formation, in osteoblastic cells when added (10 mmol) to cell culture medium in concentration of <30 ppm [71, 72]. This release in controlled amounts has been shown to favour biomineralisation and induce expression of osteogenic messenger RNA transcripts while an increase in concentration of P beyond 30 ppm results in decrease in cell viability [72].

2.7 Introduction to the present work

Since the discovery of 45S5 Bioglass[®] in 1971 there has been a heightened interest in the science and biomedical application of bioactive glass over the last two decades, as evidenced by the growing number of publications in the field (Figure 2.3). Many artificial biomaterials based on, or inspired by Hench's glass have been developed and successfully employed in clinical applications for repairing and replacing parts of a human body

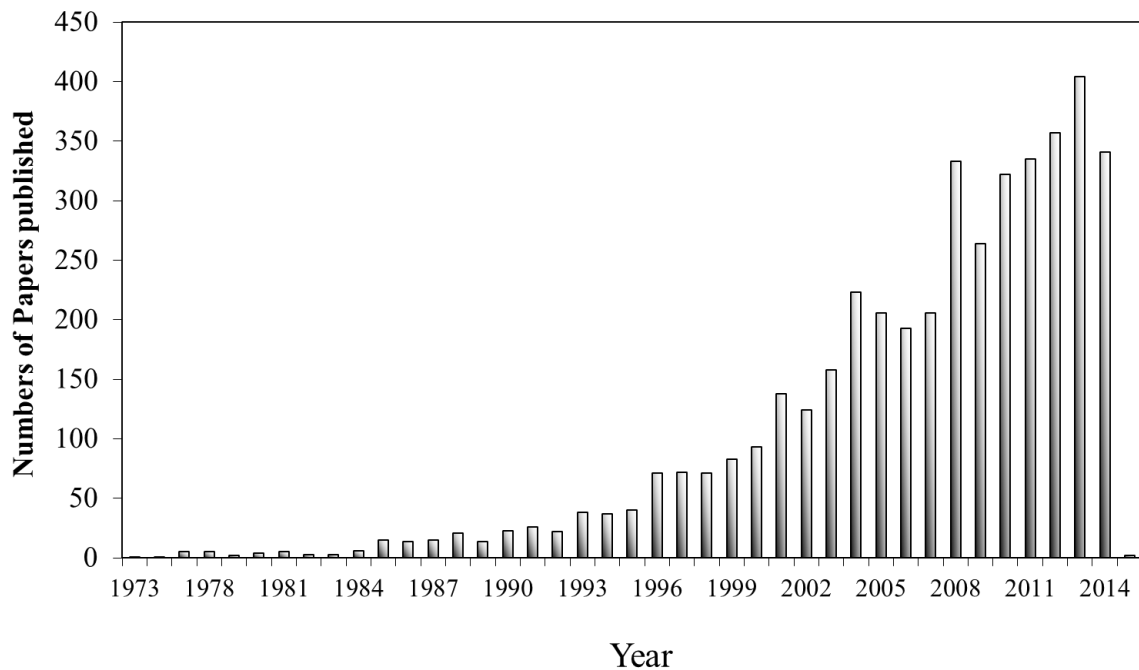


Figure 2.3 Number of papers published per year in the field of “bioactive glass” (compiled from a literature search SCOPUS carried out in November 2014).

. This field is continuously expanding: new processing routes have extended the range of applications towards new exciting directions in biomedicine [17], many of which still rely on the original Hench's base formulation, which is now considered a benchmark for the bioactive materials. Table 2.1 lists some bioactive glass compositions compiled from literature. Although the use of 45S5 Bioglass[®] in numerous clinical programs has exhibited favourable healing capability, one of the main problems associated with this glass is its high dissolution rate [73], mainly owing to its high alkali content. Our recent studies have shown that alkali-incorporation in bioactive glasses decreased their apatite forming ability during initial 72 hours of reaction with body fluids due to excessive release of sodium from the glasses [74], thus leading to apoptosis.

Table 2.1 Selected bioactive glass compositions (mol%).

	SiO ₂	P ₂ O ₅	Na ₂ O	CaO	K ₂ O	MgO	CaF ₂
45S5 [26]	46.1	2.6	24.4	26.9			
45S5F [75]	46.1	2.6	24.4	16.9			10
S53P4 [76]	53.9	1.7	22.7	21.8			
13-93 [77]	54.6	1.7	6.0	22.1	7.9	7.7	
6P61 [78]	61	2.5	10	13.5	2.4	10.7	
6P55 [78]	54.1	2.5	11.5	15.9	3.4	12.6	
A-W [79]	35.4	7.2	-	49.9	-	7.1	0.4
ICIE1[80]	49.46	1.07	26.38	23.08			
ICIE16 [80]	49.46	1.07	6.6	36.27	6.6		

With reference to the use of 45S5 Bioglass[®] *in vivo*, Vogel et al. [81] showed that this glass has good biological efficacy in cases where shorter healing periods are required (~1 month). However, this glass may not be a good option for serious injuries requiring prolonged treatment. Similarly, most of the bioactive glass compositions investigated so far and reported in papers [75-80, 82-87] and registered in a number of patents [75, 88-92] contain significant amounts of alkali oxides (Na₂O, K₂O). Although the incorporation of alkali oxides in bioactive glass is advantageous for their production, as they reduce their melting temperature, their presence in bioactive glass can reduce the usefulness of the glass *in vivo*. Often bioactive glasses for certain biomedical applications require heat treatments (coatings, sintering of porous scaffolds). When intended for coatings metal prosthesis the coefficient of thermal expansion has to match that of the metallic substrate. On the other hand, a good sintering ability is essential for achieving the required mechanical stability. These essential requirements are not fulfilled by alkali-rich bioactive glass compositions. As a matter of fact, high alkali contents degrade the working range of bioactive glasses by increasing the crystallization tendency of glass, thus rendering them unfit for use as bioactive porous scaffolds or porous coatings [93]. For example, in the case of 45S5 Bioglass[®], owing to its poor sintering ability, there have been problems with the manufacture of highly porous scaffolds possessing good mechanical. Hence, these drawbacks related to the alkali content of the bioactive glasses can be overcome by reducing the alkali contents or even by adopting alkali-free bioactive glass compositions.

The initial work for the development of alkali-free bioactive was made by Kukubo et al. in the year 1982, who designed a series of alkali-free glasses in the $3\text{CaO}\cdot\text{P}_2\text{O}_5 - \text{CaO}\cdot\text{SiO}_2 - \text{MgO}\cdot\text{CaO}\cdot 2\text{SiO}_2$ system [79]. The Apatite-Wollastonite (A-W) glass-ceramics designed by Kukubo et al. [94, 95] exhibit excellent mechanical properties as well as good *in vitro* and *in vivo* behaviour. Kasuga et al. [96] studied the effect of magnesium and aluminium on the bioactivity of the alkali-free glasses. Results indicated that Al_2O_3 tends to inhibit the apatite forming ability of the glasses and magnesium tends to slow down (but not hinder) the apatite forming ability of glasses when immersed in SBF solution. K. Ohura et al. [97] incorporated various ions into CaO-SiO_2 based glasses and studied their effect on the *in vivo* performance. The formation of a calcium phosphate layer was achieved in the all the glasses except for the ones containing Fe_2O_3 . In the mid 1990 Galliano et al. [98] investigated the influence of Mg^{2+} and Sr^{2+} on the structure and thermal behaviour of glasses in the $\text{CaO-SiO}_2\text{-P}_2\text{O}_5\text{-CaF}_2$ system. To the best of our knowledge, this is one of the foremost studies on Sr-containing bioactive glasses.

In another study, Salinas et al. [99] reported on the influence of Mg on the *in vitro* bioactivity of slightly modified A-W glasses and glass-ceramics. The results showed negligible changes in bioactivity of glasses; however, presence of Mg led to the appearance of new crystalline phases in the glass-ceramics which were able to suppress the *in vitro* bioactivity. Further, an extensive work has been done by Oliveira et al. [100-102] using ^{29}Si and ^{31}P MAS-NMR to investigate the structure *versus* bioactivity (assessed through immersing the glass samples in SBF) relationship of bioactive glasses compositions without alkali content. In 2006 Kamitakahara et al. [103] designed alkali-free Di based glass-ceramics and investigated their mechanical strength and bioactivity. They found that the flexural strength of an eutectic glass-ceramic composition 38 TCP-62 Di (wt.%) was higher than 200 MPa. However, no further studies dealing with this system have been reported since that, and our attempts to reproduce these results were unsuccessful. Recently, Kansal et al. [104-106] investigated the structure, thermal and dissolution behaviours of alkali-free glasses and glass-ceramics in Di-based glasses using MAS-NMR and ICP-AES. The as developed glasses exhibited better sintering ability than 45S5 Bioglass[®] and good *in vitro* bioactive properties.

2.7.1 Aim of the thesis

Despite of extensive amount of work done by scientists all over the world, literature survey reveals that since the earnest 1970s, most of the work in the field of bioactive glasses has been mainly focused upon understanding the compositional dependence of glass dissolution for 45S5 Bioglass[®] (46.1% SiO₂, 24.4% Na₂O, 26.9% CaO and 2.6% P₂O₅ in mole percent) or other silicate glasses with similar compositions [77, 107-109]. Further, last few years have witnessed a consistent upsurge of studies attempting correlating the atomic and molecular structure of silicate glasses with their chemical dissolution and bioactivity behaviours [5, 80, 110-112]. Simultaneously, significant efforts have been made either to unearth the influence of functional ions on the structure of bioactive glasses [113-118] or to study their influence on the chemical dissolution behaviour of glasses [119-125]. However, few attempts have been made to elucidate about the correlation between the structural role of these functional ions and the chemical degradation and bioactivity of glasses [23, 42, 87, 104, 126] especially in case of alkali-free bioactive glasses. Despite significant progress made in the pursuit of establishing relationships between chemical composition, molecular structure and bioactivity of silicate glasses, we are still not in a position to develop scientifically robust and statistically accurate models to predict the chemical dissolution and bioactivity of glasses mainly because most of the studies available in scientific literature still revolve around structure-property relationships of glasses based on or inspired by 45S5 Bioglass[®] [5, 110, 111, 127-129].

Therefore, in the present doctoral work we have tried to design and characterize glasses covering far from region of high alkali-content in an attempt to find a possible solution for the above discussed long-standing problem of alkali-containing glasses. Accordingly, the work reported in this dissertation has been directed towards fulfilment of the following aims:

1. To design alkali-free bioactive glasses having high bioactivity, lower dissolution rate and good sintering behaviour so as to prove their efficacy for bone regeneration and TE applications.
2. To understand on the structure-property relationships in alkali-free bioactive glasses
3. To understand effect of various functional ions on the structure and its implications on the biodegradation behaviour of the glasses and its impact on *in vitro* behaviour of glasses.

4. To understand the effect of these functional ions on sintering, crystallization behaviour of bioactive glasses and glass-ceramic.

We hope that the work reported in this dissertation will be a good contribution to the growing literature in the field of bioactive glasses, that will enable us to create a succinct database which can be further used to develop models for designing bioactive glasses with controlled chemical degradation rate and high bioactivity with novel applications in the field of human biomedicine.

Chapter 3

Experimental

3. Experimental

3.1 Glass synthesis

High purity powders of SiO₂ (BDH Chemicals Ltd., UK, purity >99.0%), CaCO₃ (BDH Chemicals Ltd., UK, purity >99.0%), MgCO₃ (BDH Chemicals Ltd., UK, purity >99.0%), NH₆PO₄ (Sigma Aldrich, Germany, >99.0%), ZnO (Sigma Aldrich, Germany, >99.9%), SrCO₃ (Sigma Aldrich, Germany, >99.9%) and CaF₂ (Sigma Aldrich, Germany, 325 mesh, >99.9%) were used. All the glass compositions have been prepared by melt-quenching technique. Homogeneous mixtures of batches (~100 g) obtained by ball milling, were preheated at 900 °C for 1 h for calcinations and then melted in platinum (Pt) crucibles at 1570-1590 °C for 1 h. The glasses were obtained in bulk form by casting the glass melt on a metallic mould and then annealing the glass at 500-700 °C for 1 h. The glasses were obtained in frit form by quenching of glass melts in cold water. The frits were dried and then milled in a high-speed agate mill resulting in fine glass powders with mean particle sizes of ~ 10–20 µm (determined by light scattering technique; Coulter LS 230, Beckman Coulter, Fullerton CA; Fraunhofer optical model). The amorphous/crystalline nature of frits was confirmed by X-ray diffraction (XRD) analysis (Rigaku GeigerflexD/Max, Tokyo, Japan; C Series; Cu Kα radiation; 2θ angle range 10°–60°; step 0.02° s⁻¹).

3.2 Density and Molar volume

Archimedes' method [i.e. immersion in diethyl phthalate (C₁₂H₁₄O₄) (molar mass: 222.24 g mol⁻¹; density: 1.12 g cm⁻³)] was employed to measure the apparent density of the bulk annealed glasses and glass-ceramics. Molar volume (V_m), was calculated using the density data for the bulk glasses using following relations:

$$V_m = \frac{M}{\rho}$$

Where M is the molar mass of the glass and ρ is the apparent density of the bulk glasses.

3.3 Structural characterization of glasses

3.3.1 Magic angle spinning (MAS) – Nuclear magnetic resonance (NMR) spectroscopy

The ²⁹Si MAS-NMR spectra were recorded on a Bruker ASX 400 spectrometer operating at 79.52 MHz (9.4 T) using a 7 mm probe at a spinning rate of 5 kHz and 60 seconds delay time was used. Kaolinite was used as the chemical shift reference. The ³¹P MAS-NMR spectra of glasses were recorded using 4 mm probe on a Bruker ASX 400

spectrometer operating at 161.97 MHz with 45° pulses, spinning rates of 12 kHz, a 60 s recycle delay and the chemical shift was quoted in ppm from phosphoric acid (85%).

3.3.2 Infra-red spectroscopy.

Fourier transform infrared (FTIR) spectra of the glasses (before and after immersion in SBF) were obtained using an Infrared Fourier spectrometer (FTIR, model Mattson Galaxy S-7000, USA). For this purpose glass powders were mixed with KBr in the proportion of 1/150 (by weight) and pressed into a pellet using a hand press. 64 scans for background and 64 scans per sample were made with signal gain 1. The resolution was 4 cm⁻¹. The bands were assigned as per the Table 3.1 [119, 208].

Table 3.1 Infrared bands of functional groups of bioactive glasses.

Vibration mode	Wavenumber (cm ⁻¹)
Si-O-Si	415-540
P-O bend crystal	515-530
P-O bend crystal	550-560
P-O bend amorphous	570-600
P-O bend crystal	600-610
C-O stretch	800-890
Si-O-Si tetrahedral	860-1175
Si-O stretch	1000-1100
P-O stretch	910-1040
P=O stretch	1180-1350

3.4 Biodegradation of glasses

The *in vitro* bioactivity of glasses, reflected in their capability of inducing HA-formation onto their surfaces, was investigated by immersion of glass powders in simulated body fluids (SBF) (0.10 g glass powder in 50 ml SBF solution) at 37 °C. SBF had an ionic concentration (Na⁺ 142.0, K⁺ 5.0, Ca²⁺ 2.5, Mg²⁺ 1.5, Cl⁻ 125.0, HPO₄⁻ 1.0, HCO₃²⁻ 27.0, SO₄²⁻ 0.5 mmol l⁻¹) nearly equivalent to human plasma, as discussed by Tas [130]. The powder-SBF mixtures were immediately sealed into sterilized plastic flasks and were placed in an oven at 37 °C (± 0.5 °C). The SBF solution was replaced every 48 h and sampling took place at variable times ranging from days to weeks. The experiments were performed in

duplicate in order to ensure the accuracy of results. The apatite forming ability on glass powders was followed by XRD and FTIR analysis.

The degradation tests were performed according to the standard ISO 10993–14 “Biological evaluation of medical devices – Part 14: Identification and quantification of degradation products from ceramics”. The test simulates the more frequently encountered *in vivo* pH (7.4 ± 0.1) and therefore investigates the degradation of glasses/ceramics in freshly prepared Tris–HCl buffered solution. The glass powder with particle size varying between 300 – 400 μm was added to the Tris–HCl solution (2.5 g glass powder in 50ml Tris–HCl solution). The tests were carried out without solution replacement at 37 °C and with a mixing speed of 120 rpm. The sampling was done after 120 h, when the solid and liquid phases were separated by filtering (0.22 μm , Millex GP, Millipore Corporation, USA). The solid samples were then washed in deionised water and dried in an oven to a constant weight. The structural changes (if any) in the glasses after immersion in Tris–HCl were analysed by XRD and FTIR analysis. The pH and elemental concentrations (Ca^{2+} , Sr^{2+} , Mg^{2+} , PO_5^{5-} , SiO_4^{4+}) (ICP-AES; JobinYvon, JY 70 plus, France) of the soaking solutions were measured. The relative weight loss percentage (W_L) of the glass samples after 120 h of immersion in the solutions was calculated from the following equation:

$$W_L = \left(\frac{W_0 - W_t}{W_0} \right) \times 100$$

Where W_0 refers to the weight of the glasses before immersion and W_t refers to their weight after immersion in Tris-HCl.

3.5 Thermal analysis

3.5.1 Sintering behaviour- hot stage microscope (HSM)

The sintering behaviour of the glass powders was investigated using a side-view hot stage microscope (HSM) EM 201 equipped with image analysis system and 1750/15 Leica electrical furnace. The cylindrical shaped samples with height and diameter of ~ 3 mm were prepared by cold-pressing the glass powders. The cylindrical samples were placed on a $10 \times 15 \times 1$ mm alumina (>99.5 wt% Al_2O_3) support. The temperature was measured with a Pt/Rh (6/30) thermocouple contacted under the alumina support. The microscope projects the image of the sample through a quartz window and onto the recording device. The computerized image analysis system automatically records and analyses the geometry changes of the sample during heating. The image analyser takes into account the thermal expansion of the

alumina substrate while measuring the height of the sample during firing, with the base as a reference. The HSM software calculates the percentage of decrease in height, width and area of the sample images. The measurements were conducted in air with a heating rate (β) of 5 K min⁻¹.

3.5.2 Differential thermal analysis

The values of the glass transition temperature (T_g), crystallization onset temperature (T_c) and peak temperature of crystallization (T_p) were obtained by differential thermal analysis (DTA) using a Setaram LabSys TG–DTA16 instrument (Setaram Instrumentation, France) calibrated in the temperature range 25–1000 °C. The measurements were performed using powdered glass samples (50 mg) in an alumina crucible and α -alumina powder as reference at a heating rate (β) of 5 K min⁻¹ and 20 K min⁻¹.

3.6 Preparation of glass-ceramics

Glass-ceramics can be prepared either by nucleation and crystallization through suitable heat treatments given to monolithic glasses, or by sintering and crystallization of glass powder compacts. Rectangular bars with dimensions 4 × 5 × 50 mm³ and circular disc shaped pellets with diameter 20 mm and thickness ~3 mm were prepared from fine glass powders by uniaxial pressing (80 MPa). The glass powder compacts were sintered under isothermal conditions for 1 h at the different temperatures. A slow heating rate (β) of 5 K min⁻¹ was maintained in order to prevent deformation of the samples.

3.7 Characterization of glass-ceramics

3.7.1 Mechanical Properties of sintered glass-ceramics

The mechanical properties were evaluated by measuring the three-point bending strength of rectified parallelepiped bars (3 × 4 × 50 mm³) of sintered glass-ceramics (Shimadzu Autograph AG 25 TA, Columbia, MD; 0.5 mm min⁻¹ displacement). The mean values and the standard deviation presented for shrinkage and density were obtained from (at least) ten different samples.

3.7.2 Microstructural characterization- SEM and EDS

Microstructural observations were made on polished surfaces of the sintered and heat treated glass powder compacts (chemically etched by immersion in 2 vol% HF solution for

duration of 2 min) by scanning electron microscopy (SEM; SU-70, Hitachi). In addition, energy dispersive spectroscopy (EDS; Bruker Quantax, Germany) has been utilized to study the distribution of elements.

3.8 In vitro studies

3.8.1 Alkali-free glasses for bone tissue engineering: A preliminary investigation

3.8.1.1 Mesenchymal stem cell proliferation

The biological performance of the as developed glass-ceramics was addressed by the *in vitro* cellular responses, including cell proliferation and osteoblastic differentiation. The results were compared with the tissue culture plastic used as a control. For the cellular study, mesenchymal stem cells (MSCs) derived from rat bone marrow were used. MSCs have been a potential source for the regenerative therapy of tissues including bone, because of their multipotent and self-renewal capacity without the concern of ethical issues. The experimental procedures were based on their previous work [28] and followed by the guidelines approved by the Animal Ethics Committee of Dankook University. MSCs gathered from the bone marrow of rats were maintained in a normal culture medium containing α -minimal essential medium (MEM) supplemented with 10% foetal bovine serum (FBS), 100 U ml⁻¹ penicillin and 100 mg ml⁻¹ streptomycin in a humidified atmosphere of 5% CO₂ in air at 37 °C.

MSCs maintained up to 3-4 passages were used for cellular study. The glass-ceramics were sterilized with 70% ethanol for 1 h prior to seeding cells. For the cell growth study, MSCs were seeded on each sample (15 mm × 2 mm disc type) and then cultured in the normal culture medium condition as described above. After culture for 3, 7 and 14 days, the cell growth level was analysed by the cell counting kit (CCK) assay. At each time of culturing (3 and 7 days), the CCK-8 reagent was added to each sample and incubated for 3 h at 37 °C. The absorbance was measured at a wavelength of 450 nm using a microplate reader (Molecular Devices, USA). The cell growth morphology was observed by SEM (Hitachi) after fixation the cells with 2.5% glutaraldehyde, dehydration with a graded series of ethanol (50, 70, 90 and 100%) and coating with gold.

3.8.1.2 Alkaline phosphatase activity

The osteoblastic differentiation of the MSCs on the glass-ceramics was determined by measuring the ALP activity. Cells were seeded on each sample (15 mm × 2 mm disc type), and cultured in the osteogenic medium containing 50 µg ml⁻¹ sodium ascorbate, 10 mM β -

glycerol phosphate, and 10 nM dexamethasone. After culture for 7 and 14 days, cellular samples were gathered and added to the ALP reaction media to allow an enzymatic reaction according to the manufacturer's instruction (Sigma). The quantity of samples used for the reaction was determined based on the total protein content which was determined by using a commercial DC protein assay kit (BioRad). As a result of the reaction, the product *p*-nitrophenol appears as the colour change which was then measured at an absorbance of 405 nm using a spectrophotometer.

The CCK and ALP assays were performed on three replicate samples ($n = 3$). Data were represented as means \pm standard deviations. Statistical analysis was carried out by analysis of variance (ANOVA) and significance level was considered at $p < 0.05$.

3.8.2 Influence of ZnO/MgO substitution on sintering, crystallization, and bio-activity of alkali-free glass-ceramics

Similar procedure as mention in section 3.8.1 was used.

3.8.3 Role of glass structure in defining the chemical dissolution behaviour, bioactivity and antioxidant properties of zinc- and strontium- co-doped alkali-free phosphosilicate glasses

3.8.3.1 In vitro cellular tests

For investigating the cellular responses and antioxidative effect for the developed glass compositions (ZS-2 to ZS-8), thin slices of glasses measuring ~ 1 mm of thickness were prepared by cutting and polishing the bulk annealed glasses. Tissue culture plastic was used as a control.

3.8.3.1 Cell Culture studies

Human osteosarcoma cell line MG63 was obtained from National Centre for Cell Science (NCCS), Pune, India and maintained on Dulbecco's Modified Eagle's Medium (DMEM) supplemented with streptomycin (100 U ml^{-1}), gentamycin ($100 \mu\text{g ml}^{-1}$), 10% FBS (Sigma-Aldrich) at 37°C and humid environment containing 5% CO_2 . MTT was used to assess cell integrity and potential cytotoxicity of the plant extract by monitoring the uptake of the vital mitochondrial dye, 3-[4,5-dimethylthiazol-2-yl]- 2,5-diphenyl tetrazolium bromide (MTT) by cell mitochondria.

Binding of MG63 cells to glass samples was carried out in 24 well plates. Rectangular shaped, sterilized glass slices were kept in triplicates in the 24 well plates. The wells without glass samples were considered as control. 500 μl of lymphocyte suspension at a concentration of 2×10^4 cells ml^{-1} was added to each well. The plate was then incubated at 37 °C, 5% CO_2 in air and 90% relative humidity in CO_2 incubator for 96 h. Four hours before the termination of cultures, 500 μl of MTT (2 mg ml^{-1}) prepared in serum free medium was added to each well. After 4 h, 500 μl of DMSO (Dimethyl sulfoxide) was added to each well. The blue colored formazan formed was read at 570 nm with Labsystems Multiskan EX ELISA reader against a reagent blank.

The cells on disks were fixed with freshly prepared Karnovsky's fixative (2% paraformaldehyde; 2.5% glutaraldehyde in 0.1 M phosphate buffer pH 7.4.) at 4 °C for 90 min. After fixation, the fixative was removed and cells were washed for 2 min with 0.1 M phosphate buffer. Further, cells were fixed in 1% buffered osmium tetroxide (prepared in phosphate buffer) for 90 min at 4 °C. The cells were further dehydrated with various concentrations of ethanol starting with 30% for 5 min twice and repeating the same with 50, 75, 95% and absolute ethanol. After critical point drying, cells were photographed with EVO[®] LS10 Life Science SEM.

3.8.3.2 Cytoprotective assay

Cytoprotective effect of bioactive glasses was carried out on hydrogen peroxide (H_2O_2) induced oxidative stress in human MG63 cells. The H_2O_2 dose (LD50) for cytoprotection studies was calculated by treating cells at 50% confluency with H_2O_2 (7.5 μM to 1000 μM diluted in medium) for 12 h in serum free medium. The glass slices were kept in triplicates in the 24 well plates. The wells without glass samples and H_2O_2 were considered as negative control and cells with H_2O_2 along with glass samples were kept as positive controls. 500 μl of cell suspension at a concentration of 2×10^4 cells ml^{-1} was added to each well. The plate was then incubated at 37 °C, 5% CO_2 in air and 90% relative humidity in CO_2 incubator for 72 h. The LD50 dose of H_2O_2 was given at this point to induce the oxidative stress for 12 h in the wells with and without glass samples except negative control. Four hours before the termination of cultures, 500 μl of MTT (2 mg ml^{-1}) prepared in serum free medium was added to each well. After 4 h, 500 μl of DMSO was added to each well. The blue colored formazan formed was read at 570 nm with Labsystems Multiskan EX ELISA reader against a reagent blank.

3.8.4 An experimental approach towards understanding the composition-structure-bioactivity relationships in silicate glasses

3.8.4.1 Cell Culture Studies

Human mesenchymal stem cells (hMSC, Lonza) were thawed and then cultured in 175 cm² tissue culture flasks containing DMEM (Gibco), supplemented with 10% v/v inactivated FBS (Gibco), and 1% v/v penicillin/streptomycin (P/S, Gibco). Cells were maintained at 37 °C under a 5% CO₂ humidified atmosphere. The medium was changed every third day until confluence, when cells were sub-cultured in order to prevent cell death. In order to sub-culture, the cell monolayer was washed with phosphate buffered saline (PBS) (Sigma) and incubated with a trypsin/ethylene diamine tetra acetic acid (EDTA) solution for 8 min at 37 °C to detach the cells. The effect of trypsin was then inhibited by adding culture medium at room temperature. Cells were used in the passage six.

The glass samples were autoclaved (120 °C, 20 min) and placed in untreated 48-well plates (~ 1 cm² surface area) (Cellstar[®]) to avoid cell adhesion to the bottom of the wells. The controls were wells treated with poly-D-lysine. The cells were seeded at 2×10⁴ cells per well and fresh medium was added, followed by incubation at 37 °C for 4 h to allow cell adhesion. Afterwards, fresh medium was added until it reached a final volume of 400 µl per well. To induce the hMSCs differentiation along the osteoblastic lineage, cells were also cultured with osteogenic medium: basal medium supplemented with 10 µl ml⁻¹ glycerophosphate (Sigma), 10 µl ml⁻¹ dexamethasone (Sigma), and 10 µl ml⁻¹ ascorbic acid (1.61 mg ml⁻¹) (Fluka). hMSCs were cultured on samples of the glass for periods of 1, 3, 7, 14 and 21 days. At each time point, the samples were evaluated for cell metabolic activity, viability, morphology and differentiation.

3.8.4.2 Cell metabolic activity

A resazurin method was used to assess metabolic activity at days 1, 3, 7, 14 and 21. A resazurin solution (Sigma) was added to fresh medium at a final concentration of 10% (v/v). Cells were incubated in this solution at 37 °C for 3 h, after which, 100 µl per well were transferred to a 96-well black plate and fluorescence was measured (530 nmEx/590 nmEm) in a Spectra Max Gemini XS (Molecular Devices).

Chapter 4

Results and Discussion

4 Results and Discussion

4.1 Alkali-free glasses for bone tissue engineering: A preliminary investigation

4.1.1 Introduction

The present chapter reports on a preliminary attempt to find a feasible solution for the above discussed long-standing problem of designing alkali-free bioactive glasses. In this pursuit, the alkali-free glass compositions have been designed in the system Di-FA-TCP with a general formula (Di) (90-x)-(FA)10-(TCP)x ($x = 10-40$ wt%). Table 4.1.1 presents the detailed compositions of the glasses. The present composition has been selected due to following reasons:

Table 4.1.1 Nominal composition of the as-designed glasses (mol%).

Glass	SiO ₂	P ₂ O ₅	CaO	MgO	CaF ₂
TCP-10	42.57	3.57	32	21.29	0.57
TCP-20	38.49	5.61	36.07	19.24	0.59
TCP-30	34.12	7.79	40.42	17.06	0.61
TCP-40	29.44	10.12	45.08	14.73	0.63

Di belongs to the group of inosilicates and is an important member of clinopyroxene group with composition CaMgSi₂O₆. The structure of amorphous Di is dominated by Q^2 unit which is a positive attribute for bioactivity in glasses. Also, it has been demonstrated that Di-based ceramics and glass-ceramics have no general toxicity in cell cultures and help in bone regeneration [131, 132]. Nakajima et al. [133, 134] found that Di possessed ability to form apatite in SBF and could closely bond to bone tissue when implanted in rabbits. Aza et al. [132] investigated the reactivity of the material in a natural medium of high protein content by soaking Di based ceramic pellets in human parotid saliva (HPS) over various time intervals. Also Yoganand et al. [135] synthesized bioactive glass-ceramics with the help of transferred arc plasma technique in the system CaO-MgO-SiO₂ with Di as the major crystalline phase.

In addition to the biocompatibility aspect of Di based ceramics and glass-ceramics; they are known to exhibit superior mechanical properties in comparison to many of their ceramic counterparts. Nonami et al. [131] reported significantly improved fracture toughness values for pure sintered HA with added Di. It was reported that the bending strength and fracture toughness of Di-HA composite was 2 to 3 times higher in comparison to that of

sintered HA. Therefore, owing to the presence of Di, we can expect superior mechanical properties for the glass-ceramics without compromising their biomedical characteristics.

Further, the presence of hydroxy-, oxy- or fluoro- apatite is highly favourable for biomedical applications. In particular, FA based glasses and glass-ceramics have gained attention [104, 105, 136, 137] due to their structural and chemical similarities with bone forming mineral, HA [87]. Also, fluoride is known to increase bone density and also has anti-carcinogenic properties [104]. Further, intracellular or plaque-associated enzymes have been reported to be affected by fluoride ions [104]. Alkali-free Di-FA-W bioactive glass-ceramics for replacement materials for tooth roots, dental crowns were developed by Shibuya et al. [88], while Tulyaganov et al. [138] developed glass-ceramics in ternary system tetrasilicic mica-FA-Di. Recently Kansal et al. [104, 105] reported the biodegradation behaviour of the Di-FA based glasses.

Similar to Di-FA join, glass-ceramics along Di-TCP join have been a subject of interest due to their potential biomedical applications. TCP is a typical bioresorbable material which is widely used in bone repair [139]. Also TCP ceramics bear excellent properties for bone marrow stromal cells culture towards osteogenic differentiation [140]. Therefore, the addition of TCP at the expense of Di in the glass compositions is expected to enhance their solubility as well as their bioactivity in physiological fluids. Also, the addition of TCP to Di is expected to improve its sintering ability as it has been reported that the flexural strength of eutectic glass-ceramic composition 38TCP-62Di (wt%) is higher than 200 MPa [103]. Kamitakahara et al. [103] studied the bioactivity and mechanical properties of bioactive scaffolds. Also, Ashizuka et al. [141] reported on the mechanical properties of Di-TCP based glass-ceramics. Thus it's expected that the combination of Di, FA and TCP phases is expected to result in the development of glasses with excellent bioactive properties, low chemical degradation and good sintering ability.

4.1.2 Results and discussions

4.1.2.1 Glass forming ability

For all the investigated glass compositions ($x = 10 - 40$ wt%), melting at 1570 °C for 1 h was sufficient to obtain bubble-free, transparent and amorphous glasses (Figure 4.1.1). The glass forming ability diminished with further increase in TCP content in glasses ($x > 40$ wt%) as resultant glass frits were prone to spontaneous crystallization even after super-

cooling in cold water thus, resulting in white, opaque material with FA as the only crystalline phase, as revealed by XRD analysis (not shown).

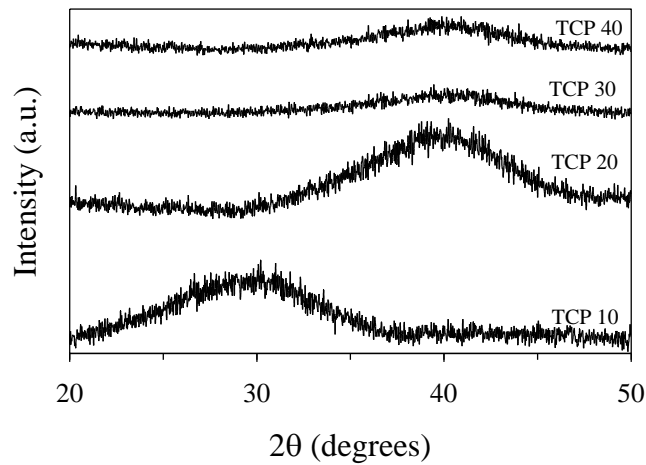


Figure 4.1.1 X-ray diffractograms of as-quenched glass frits.

4.1.2.2 Structure of glasses (MAS – NMR spectroscopy)

The molecular structure of glasses plays a crucial role in deciding their bioactivity. Therefore, understanding their structural features allows designing new glasses with improved chemical durability and tailored biodegradability for specific applications. In the present study, MAS-NMR results are presented in Figure 4.1.2, the ^{29}Si spectra (Figure 4.1.2a) for all the investigated glasses depict the dominance of Q^2 (Si) structural units in the glasses. In particular, the broad ^{29}Si spectra centred around -81 to -82 ppm indicative of Q^2 as predominant silicate species [188]. Further, with decrease in the amount of SiO_2 no change in structure was observed (TCP: 10 – 40 wt%), however a slight chemical peak shift towards more negative ppm was observed.

Further, we could not observe any significant change in peak maxima for spectra of ^{31}P nucleus with predominance of an orthophosphate-type environment (Figure 4.1.2b). In fact, the observed chemical shifts, 1–2 ppm, are close to that of the calcium orthophosphate (3.1 ppm) and that of the amorphous magnesium orthophosphate (*ca.* 0.5 ppm) [137]. However, it should be noticed that bioactivity is not solely a function of glass structure and also depends on their chemical nature [142]. According to Tilocca and Cormack [143], low contents of P_2O_5 in glasses (~ 10 mol%) enhance their bioactivity while further increase in P_2O_5 amount affects the bioactive nature of glasses in a negative manner.

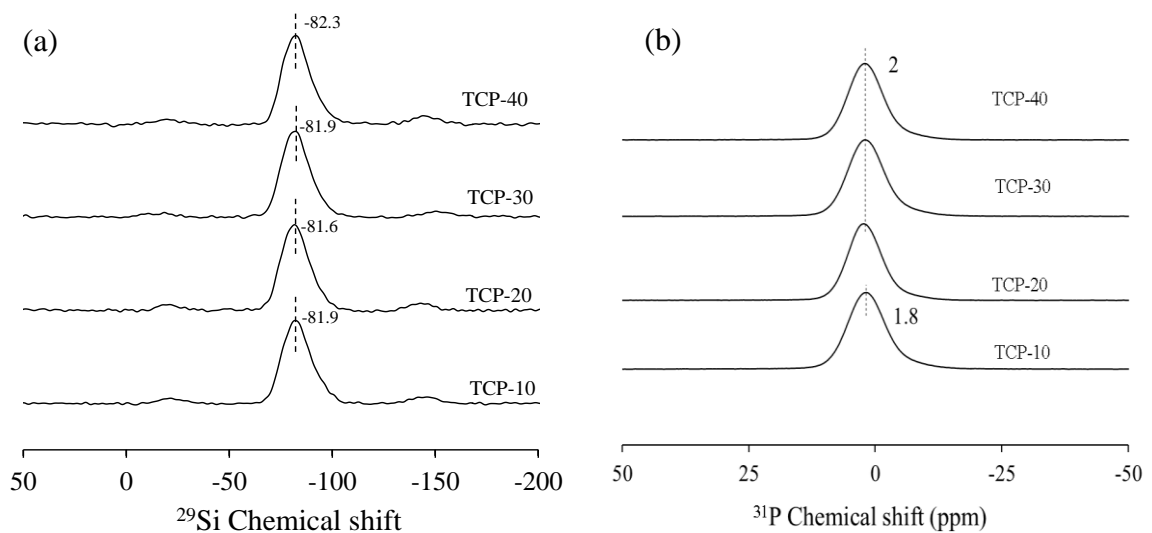


Figure 4.1.2 MAS NMR spectra of investigated glasses showing the peak positions of (a) ^{29}Si and (b) ^{31}P .

4.1.2.3 Apatite formation and chemical degradation of glasses

Immersing the materials in SBF is a relatively simple technique to evaluate the biomineralization activity and this method can be regarded as a first approach to assess bioactivity *in vitro*. However, even the preparation conditions of the SBF solution are tricky and there exist a lack of consensus regarding the usefulness of SBF tests in the literature [144]. But there are a large number of evidences about the good correlation between the biomineralization ability a given bioactive material (understood as the ability to form a carbonated apatite layer onto its surface) in SBF and its performance *in vivo* [145, 146].

The *in vitro* bioactivity analysis by immersion in SBF solution revealed the presence of apatite formation in all the glass powders. The results presented here have been mainly explained with an emphasis on glasses TCP-20 and TCP-40 due to their high potential for use in human biomedicine. The XRD patterns observed for all as-quenched glasses (Figure 4.1.1) exhibit an amorphous halo, thus depicting the absence of any crystallinity. However, the X-ray diffractograms of investigated glasses (including 45S5 Bioglass[®]) after soaking in SBF solution for time durations varying between 1 – 12 h (Figure 4.1.3) showed considerable differences in comparison to the diffractograms of their respective parent glasses. A small X-ray peak at $2\theta = 31.77^\circ$ corresponding to the formation of crystalline HA $[(\text{Ca}_5(\text{PO}_4)_3\text{OH})]$; ICDD: 00-09-0432] can be seen for glass TCP-40 after immersion in SBF for 1 h, while 45S5 Bioglass[®] suggests that calcite (CaCO_3 ; ICDD: 01-083-0577) formation under similar conditions (Figure 4.1.3a). The XRD pattern for glass TCP-20 depicted a broad amorphous halo after 1 h immersion in SBF (Fig. 4.1.3a) while the infrared spectra of this glass (Figure 4.1.4)

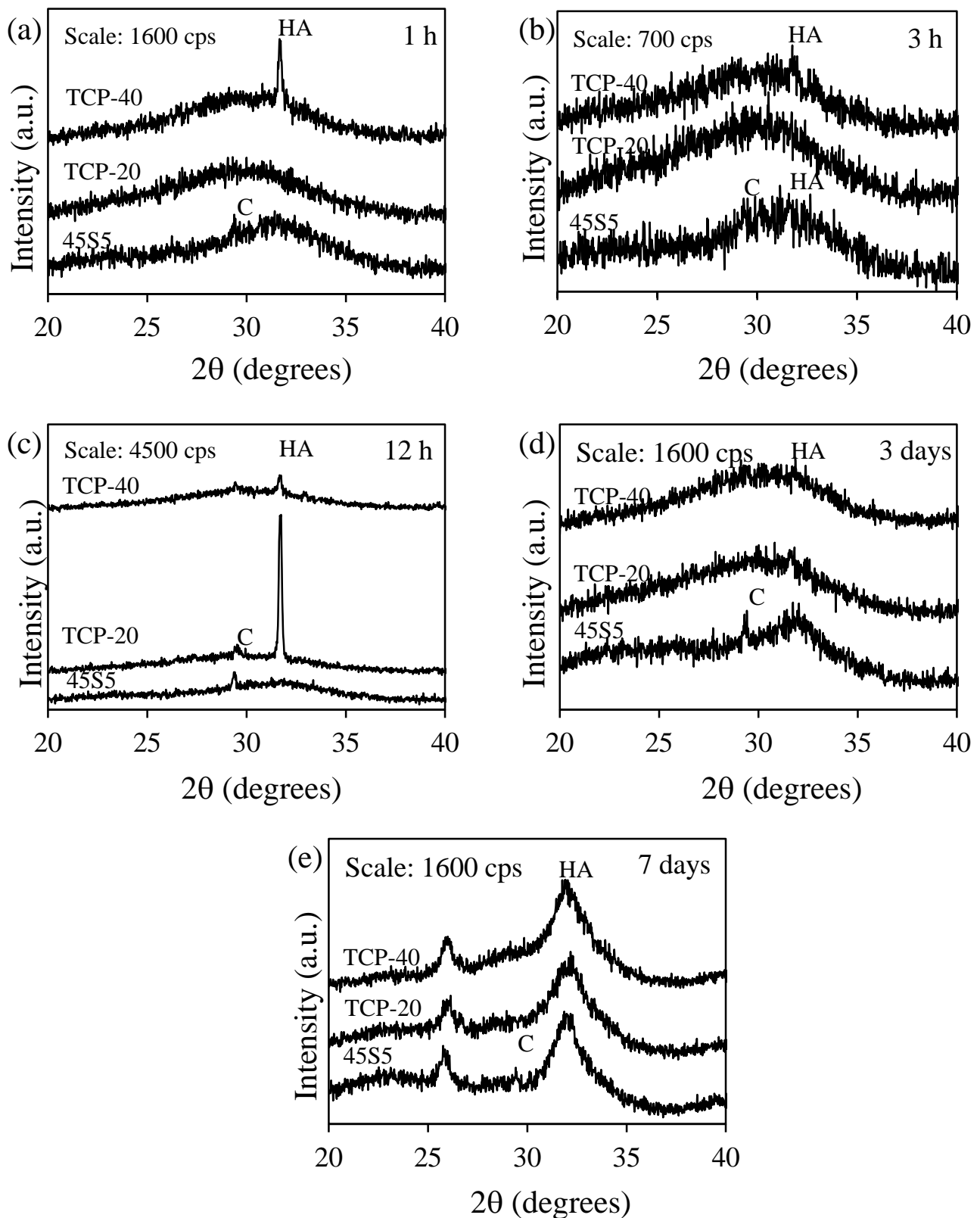


Figure 4.1.3 X-ray diffractograms of glass powders after immersion in SBF solution for (a) 1 h; (b) 3 h; (c) 12 h, (d) 3 days and (e) 7 days. C refers to calcite while HA refers to hydroxyapatite.

exhibited significant structural differences before and after immersion in SBF. As is evident from Figure 4.1.4, a strong low frequency band centred at $\sim 480 \text{ cm}^{-1}$, ascribed to a deformation mode of silica layer that develops on the dissolving glass particles could be seen in glass TCP-20 after immersion in SBF solution for 1 h [83]. The main IR band now occurs at 1080 cm^{-1} and a nearby shoulder, centred at $\sim 1235 \text{ cm}^{-1}$ attributed to Si-O-Si vibration can be observed [147], owing to the interfacial formation of high-area silica gel layer, as postulated in Hench's inorganic reaction set [20]. These features were common for all the glasses investigated in present study. Further, band at $\sim 1440 \text{ cm}^{-1}$ along with another one at $\sim 880 \text{ cm}^{-1}$ present in all glasses corresponds to incorporation of carbonate into the apatite, resulting in hydroxyl carbonated apatite, rather than stoichiometric HA [83].

Furthermore, a small broad band was observed in case of glass TCP-20 (Figure 4.1.4) at $\sim 565 \text{ cm}^{-1}$ after immersion in SBF solution for 1 h. This is the most characteristic region for apatite and other phosphates as it corresponds to P-O bending vibrations in a PO_4^{3-} tetrahedron. A single peak in this region suggests the presence of non-apatitic or ACP, which is usually taken as an indication of presence of precursors to HA. Apatitic PO_4^{3-} groups have characteristic split bands at ~ 560 and 600 cm^{-1} , with a third signal at $\sim 575 \text{ cm}^{-1}$ observed for crystallites of small size [83, 87]. However, apart from a band at $\sim 565 \text{ cm}^{-1}$ as is evident in Figure 4.1.4, no other bands in this region could be observed for glass TCP-20 even after 12 h of immersion in SBF solution while the XRD data of the same sample as presented in Figure 4.1.3c reveals the presence of sharp peak corresponding to formation of HA along with minor amounts of calcite. It is noteworthy that no HA formation could be observed instead a small X-ray peak at $2\theta = 29.41^\circ$ corresponding to the presence of calcite was observed in 45S5 Bioglass[®] even after 12 h of immersion in SBF solution (Fig. 4.1.3c)

The increasing tendency towards development of ACP rich layer leading to formation of crystalline HA with increasing TCP content in glasses may be explained on the basis of decreasing Mg concentration in glasses. It has been reported that Mg tends to associate preferentially with phosphorus at glass surface, which consequently leads to the decrease in concentration of apatite like-calcium phosphate domains on the glass surface that are supposed to act as nucleation centres for apatite formation [148]. Also, glass compositions containing phosphorus are known to be more soluble and exhibit faster release of silica in solution. Further, isolated orthophosphate groups can be directly released without breaking any chemical bond; thus high rate of formation of HA in TCP containing glasses is likely related to the high availability of this species [149].

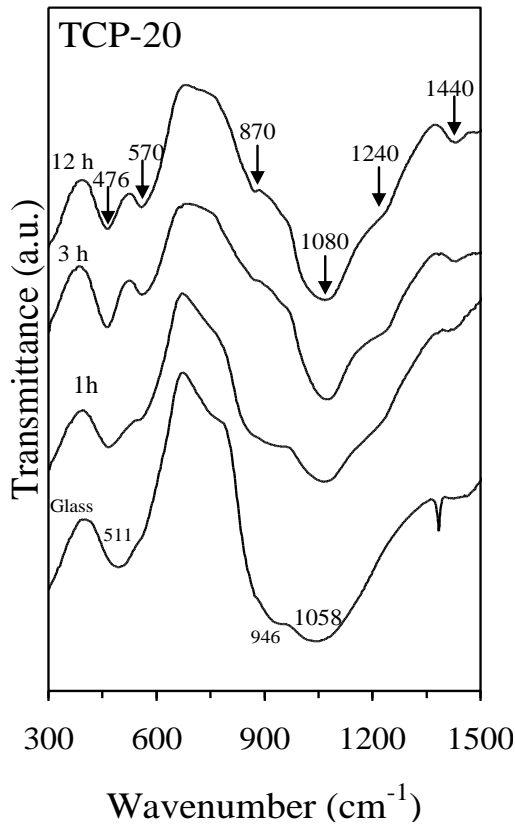


Figure 4.1.4 FTIR spectra of glass powder (TCP-20) before and after immersion in SBF solution for time durations varying between 1 h – 12 h.

The XRD data after 3 days of immersion in SBF solution (Figure 4.1.3d) depicts the highly amorphous character of glasses with a small phase reflection corresponding to HA in composition TCP-20 and TCP-40. Similar structural features could be observed in all the investigated glasses. Since intense ionic exchanges occur at the bioactive glass surface that cause major changes in the degree of super-saturation for HA formation in biological fluids, the potential for each glass to form an apatite layer can be extrapolated from the corresponding evolution of the degree of super-saturation. According to Lao et al. [122], the degree of super-saturation may be defined as: $SD = Q/K_{sp}$, where K_{sp} is the solubility product of HA in aqueous solution while Q is the ionic activity product for the formation of HA. Therefore, the solution and HA mineral phase reach equilibrium when $SD = 1$. For $SD < 1$, the dissolution of HA mineral phase is favoured, while the solution is supersaturated with respect to HA mineral and its precipitation is favoured when $SD > 1$. In the present scenario, during the initial hours of immersion of the glass in SBF, the SD increases because of dealkalinization of the glass surface, while the formation of a silica-rich layer provides

regions of low interfacial energy, thus providing favourable sites for the nucleation of HA. However, the decreasing intensity of the XRD phase reflections for the HA phase in investigated glasses after 72 h of immersion in SBF may be attributed to the changing degree of super-saturation owing to the refreshing of the SBF solution after every 48 h.

An increase in immersion time of glasses in SBF solution led to complete disappearance of calcite from the investigated glasses and depicted the formation of HA as the only crystalline phase as shown in Figure 4.1.3d. However, calcite still persisted in 45S5 glass as a minor phase along with HA even after 7 days of immersion in SBF. According to Jones et al. [150], the *in vitro* apatite forming ability of 45S5 glass decreases with increasing glass powder / SBF ratio beyond 0.002 g ml^{-1} as further increase in this value will favour the formation of calcite at the expense of HA on the glass surface. In the present study, the calcite formation in 45S5 glass may be attributed to the fact that we are exactly at this threshold value of glass powder / SBF ratio. It is noteworthy that Ca-carbonate phases present a higher solubility product ($K_{ps} \text{ calcite} = 1.7 \times 10^{-8}$) with respect to HA ($K_{ps} \text{ HA} = 1.6 \times 10^{-58}$) at pH 7.4 [83] and this should favour the precipitation of the latter. Nevertheless, Ca-carbonate phases are likely to present a higher rate of crystallization because of the presence of basic surface species (for instance: O^{2-} ions, OH^- ions or coordinatively unsaturated cation-anion pairs), which can coordinate with CO_2 , thus giving rise to many possible types of carbonate like species. According to Cerruti and Morterra [147], the carbonate formation in silica-based bioactive glasses occurs only if both CO_2 and an excess of water are present at the same time as it is believed that the gas-phase admission of both CO_2 and an excess of water mimics the long-lasting process of carbonate formation.

One of the relevant parameters in the study of glass dissolution is the kind of medium used. The pH and ionic strength of the medium play an important role in the rate at which the glasses dissolve. The variation in pH of Tris-HCl with respect to TCP content in glasses is presented in Figure 4.1.5. A slight increase in pH from 7.4 to 8.4 was observed in case of Tris-HCl with increasing TCP content in glasses while highest pH value of 9.7 was observed for the 45S5 glass, which exhibited higher dissolution rate than the investigated glasses. In the present study, an increasing pH of simulated solution with increasing TCP content in the glasses may be attributed to the increasing dissolution of Ca and Mg ions from glasses due to the dissolution of charged ion pairs $(\text{Ca-F})^+$ or $(\text{Mg-F})^+$. 45S5 glass exhibited the highest weight loss in Tris-HCl (3.7%).

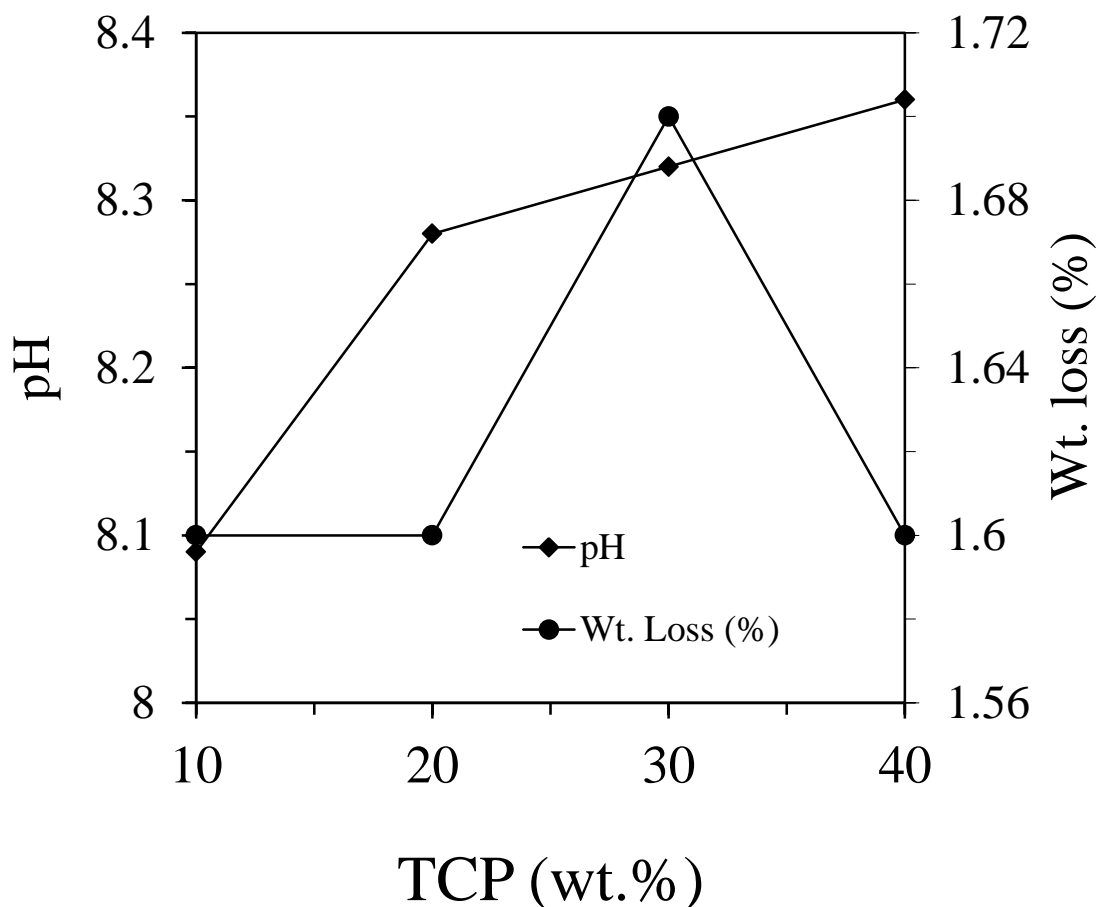


Figure 4.1.5 Graph depicting changes in pH of solution and weight loss of glass powders after immersion in Tris-HCl for 120 h.

Among all the investigated glasses, an increment in TCP content in glasses did not affect the weight loss significantly as it varied between 1.6–1.7% (Fig. 4.1.5).

4.1.2.4 Differential thermal analysis

The DTA plots of fine powders with a heating rate (β) of 20 K min^{-1} , shown in Figure 4.1.6, feature an endothermic dip in the temperature interval of $750 - 755 \text{ }^\circ\text{C}$ corresponding to T_g before T_c followed by a well-defined single exothermic crystallization curve for glasses TCP-10, TCP-20 and TCP-30. We could not observe any significant differences in the variation of T_g values with varying Di/TCP ratio in the glasses.

Further, the presence of a single crystallization exothermic peak in TCP-10 and TCP-20 samples anticipates that the resulting glass-ceramics are formed either by single crystalline phase, or derived from an almost simultaneous precipitation of different crystalline phases

(TCP-30); while the appearance of two distinct crystallization peaks (T_{p1} and T_{p2}) in glass TCP-40 points towards the formation of two different crystalline phases. The T_p values for glasses TCP-10 and TCP-20 are almost similar (i.e. 932 °C) while further decrease in Di/TCP ratio resulted in shifting of T_p to 907 °C for glass TCP-30 and 843 °C (T_{p1}) for glass TCP-40.

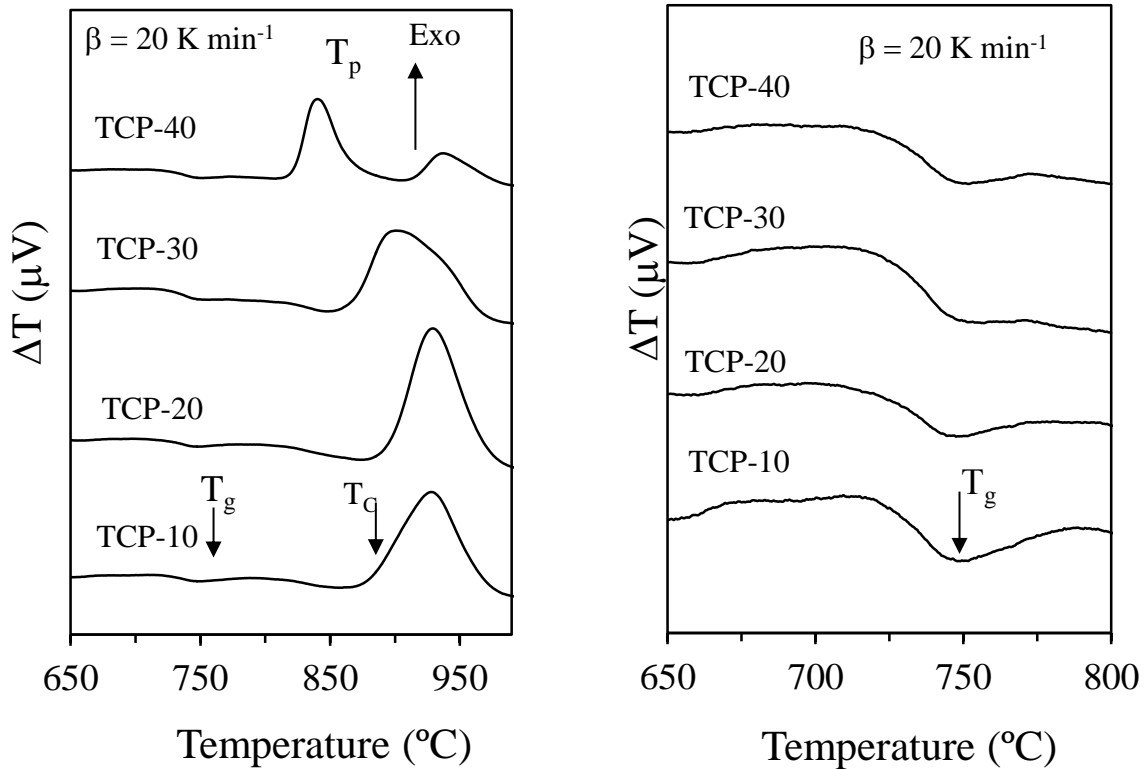


Figure 4.1.6 DTA thermographs of glasses at a heating rate of 20 K min⁻¹.

This decrease in T_p values with increasing TCP content in glasses may be attributed to their increasing crystallization tendency as will be shown further in section 4.1.6.

4.1.2.5 Sintering and crystallization behaviour of glasses

The prerequisite for optimizing the fabrication of glass-ceramics scaffolds is to understand the sintering conditions of glass powders and the interaction between sintering and crystallization of the material. By knowing the structural transformations which occur during the heat treatment of glasses, the scaffold fabrication process can be tailored, like in terms of achieving the highest possible density of the sintered scaffolds and the required crystallinity which itself controls the material's bioactivity. It is due to this reason that a comparison between DTA and HSM thermographs obtained under the same heating conditions can reveal a great deal of information in this regard. In general, two different

trends can be observed related to the sintering and crystallization behaviours of the glasses: (i) T_c occur after the final sintering stage. Therefore, under such circumstances, sintering and crystallization are independent processes. This is the required trait to obtain well sintered glass-ceramic scaffolds with good mechanical properties; (ii) T_c appears before maximum density has been reached. In this case, the crystallization process starts before complete densification, thus, preventing sintering.

In the present study both of the above mentioned trends related with sintering and crystallization behaviour of glasses have been observed depending on the glass compositions. Figure 4.1.7 presents the DTA and HSM thermographs of glasses TCP-20 (Figure 4.1.7a) and TCP-40 (Figure 4.1.7b), respectively at $\beta = 5 \text{ K min}^{-1}$ depicting a single stage sintering behaviour for the investigated glass compositions while Figure 4.1.7c presents the changes in different thermal parameters with respect to variation in TCP content in glasses. As is evident from Figure 4.1.7c, the values for temperature of first shrinkage (T_{FS} ; $\log \eta = 9.1 \pm 0.1$, where η is viscosity; dPa.s) and temperature of maximum shrinkage (T_{MS} ; $\log \eta = 7.8 \pm 0.1$) exhibited a slight decrease with increasing TCP content in glasses while values for T_c showed an initial increase and then a steep decrease with decreasing Di/TCP ratio.

With respect to T_{MS} and T_c , different trends were observed for the investigated glass compositions which can be explained with the aid of sinterability parameter (S_c), where $S_c = T_c - T_{MS}$. The parameter S_c is the measure of ability of sintering versus crystallization: the greater this difference, the more independent are the kinetics of both processes [151]. The estimated error for data points is smaller than $\pm 10\%$, approximately equal to the size of the data symbols. As can be seen from Figure 4.1.7c, the value of parameter S_c increased with increasing TCP content in the glasses until 20 wt%. However, further decrease in Di/TCP ratio led to a gradual decrease in the value of S_c with glass TCP-40 ($S_c = -24 \text{ }^\circ\text{C}$) exhibiting the lowest value for S_c . These results imply that sintering precedes crystallization in glass compositions TCP-10, TCP-20 and TCP-30 with glass composition TCP-20 exhibiting better sintering ability in comparison to the other investigated compositions.

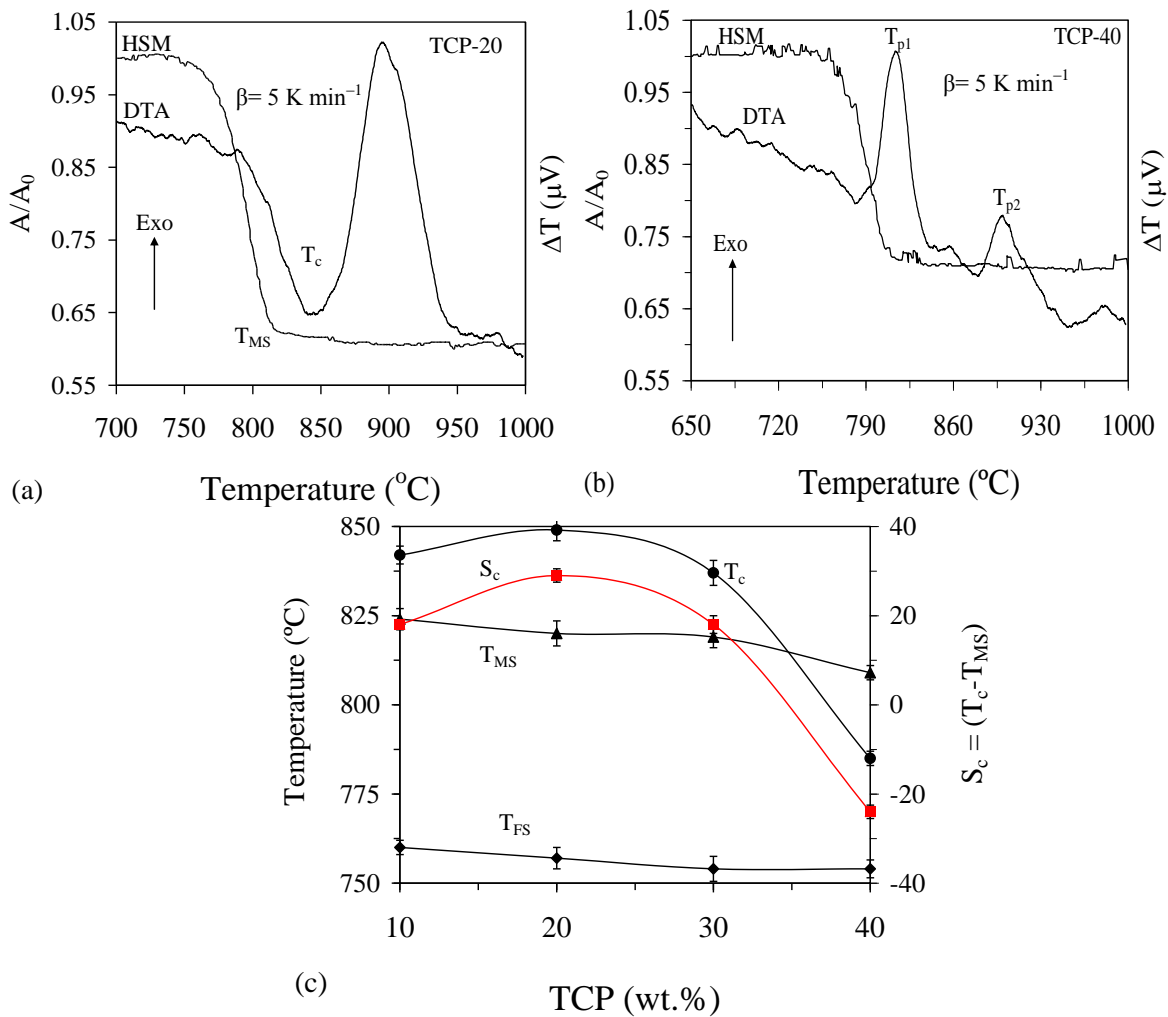


Figure 4.1.7 Comparison of DTA and HSM curves under the same heating rate (5 K min^{-1}) for compositions (a) TCP-20 and (b) TCP-40 at the heating rate of 5 K min^{-1} ; (c) influence of TCP content on different thermal parameters of glasses obtained from DTA and HSM, respectively

Therefore, we can expect well sintered, dense and mechanically stronger glass-ceramics from composition TCP-20 in comparison to its counterparts. On the other hand, crystallization precedes sintering in glass TCP-40 which should result in a poorly sintered and mechanically weak glass-ceramic material. The decreasing/poor sintering ability for glasses TCP-30 and TCP-40 is mainly due to predominance of FA in these glasses (as has been presented ahead in XRD results) which masks the influence of Di which is a crystalline phase with good mechanical strength.

Figure 4.1.8 presents the SEM images of the glass powder compacts after sintering in temperature interval of 800–900 °C for 1 h. In agreement with HSM and DTA results, the sintering of glass powder compacts at 800 °C resulted in well sintered and dense glass-

powder compacts for compositions TCP-10 (Figure 4.1.8a), TCP-20 (Figure 4.1.8b) and TCP-30 (Figure 4.1.8c), respectively, while TCP-40 resulted in a poorly sintered and mechanically weak glass powder compact.

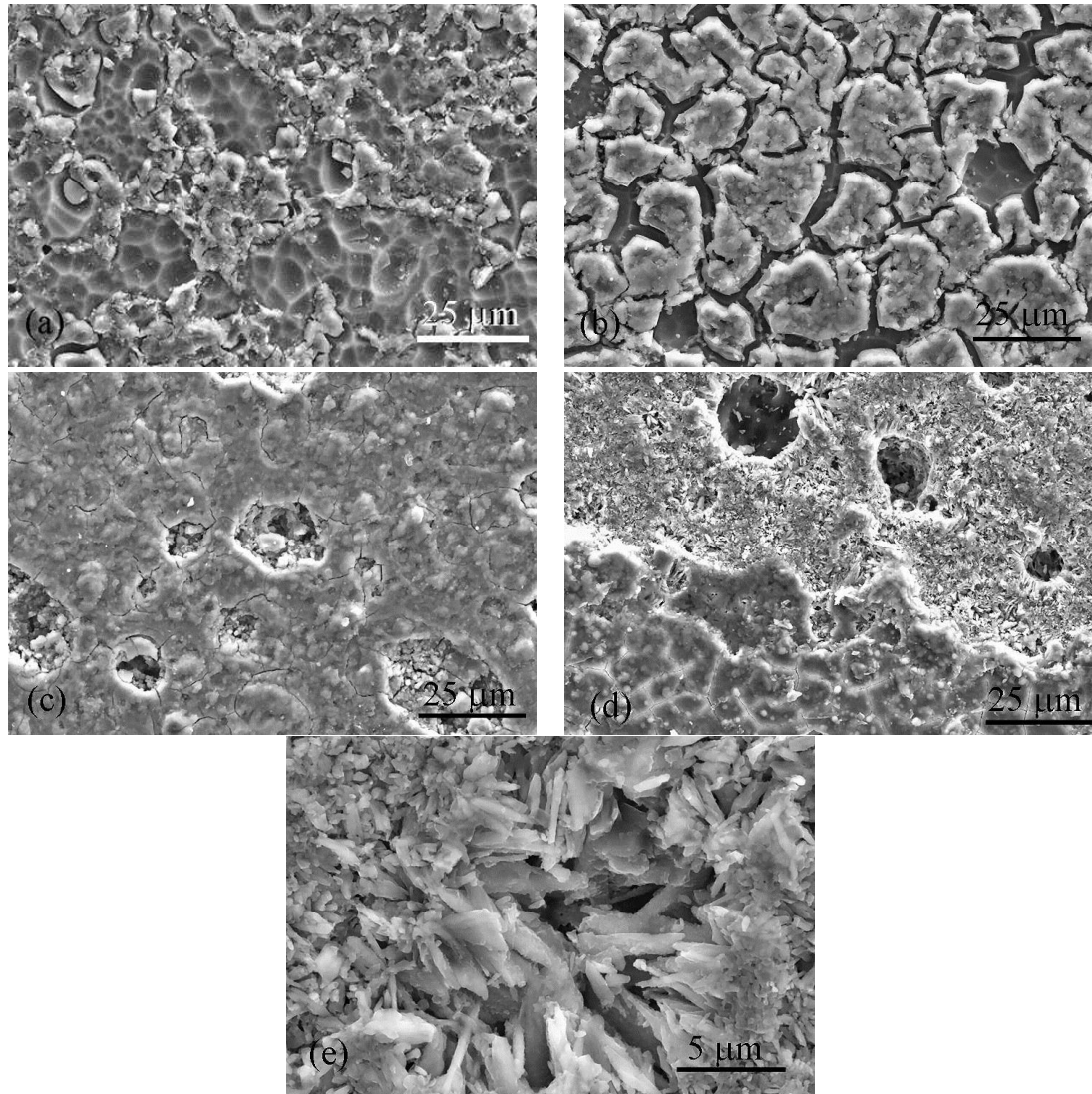


Figure 4.1.8. SEM images of glass powder compacts (a) TCP-10, (b) TCP-20, (c) TCP-30, after sintering at 800 °C for 1 h, respectively while (d) and (e) represent glass composition TCP-10 after sintering at 900 °C for 1 h.

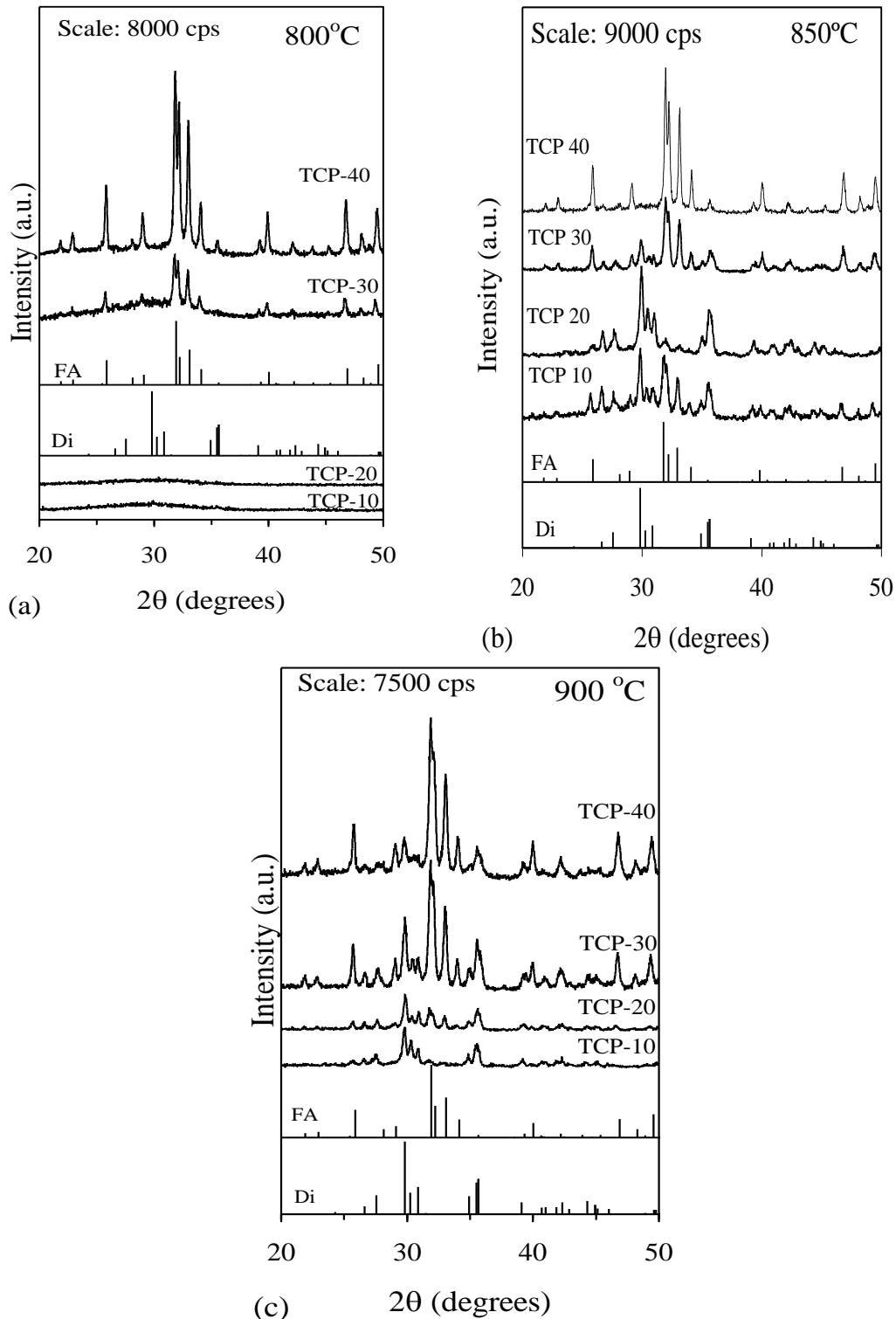


Figure 4.1.9 X-ray diffractograms of glass compositions after sintering at (a) 800 °C; (b) 900 °C and 1000 °C, respectively.

The flexural strength values as obtained for composition TCP-20 sintered at 800 and 850 °C are 85 ± 6 MPa and 135 ± 9 MPa, respectively. The qualitative crystalline phase analysis of sintered glass powders as presented in Figure 4.1.9 revealed that compositions

TCP-10 and TCP-20 were completely amorphous after sintering at 800 °C while FA (ICDD card: 71-880) precipitated as the major crystalline phase in compositions TCP-30 and TCP-40 along with Di (ICDD card: 78-1390) and the intensity of XRD peaks increased with increasing TCP content in glasses, thus, indicating an increase in crystallinity (Figure 4.1.9a). These results are in co-relation with the microstructural evolution of sintered glass-ceramics as studied through SEM. Figure 4.1.8c depicts the formation of crystals beneath the amorphous layer in composition TCP-30, thus depicting the presence of crystallinity. Further increase in sintering temperature to 850 °C (Figure 4.1.9b) and 900 °C (Figure 4.1.9c) resulted in appearance of crystallinity in all the investigated glass compositions with Di as the major crystalline phase in compositions TCP-10 and TCP-20, thus rendering them good sintering ability while FA dominated the crystalline phase assemblage in compositions TCP-30 and TCP-40, thus leading to their poor sintering ability. The SEM images (Figure 4.1.8d and 4.1.8e) obtained from glass-ceramics TCP-10 after sintering at 900 °C depict the presence of thin lamellar crystals typical for Di intermixed with needle like FA crystals (Figure 4.1.8e). The results obtained in the present study are different from those obtained by Kamitakahara et al. [103] in their study related with synthesis of glass-ceramics in Di-TCP binary system and also from the results of Magallanes-Perdomo et al. [152] where they investigated the devitrification behaviour of a eutectic glass-ceramic composition in wollastonite-TCP binary system as in both the earlier studies, TCP crystallized in glass-ceramics the form of α -TCP [152] or β -TCP [103] along with other crystalline phases. However, in the present study, no trace of crystallization of TCP has been observed as its growth seems to be masked by FA.

4.1.2.6 Cellular response to sintered glass powder compacts

The cell proliferation on the sintered glass powder compacts and control during culture for 3, 7 and 14 days is shown in Figure 4.1.10. For the control, cells proliferated actively for up to 7 days and showed a plateau with prolonged culture for 14 days.

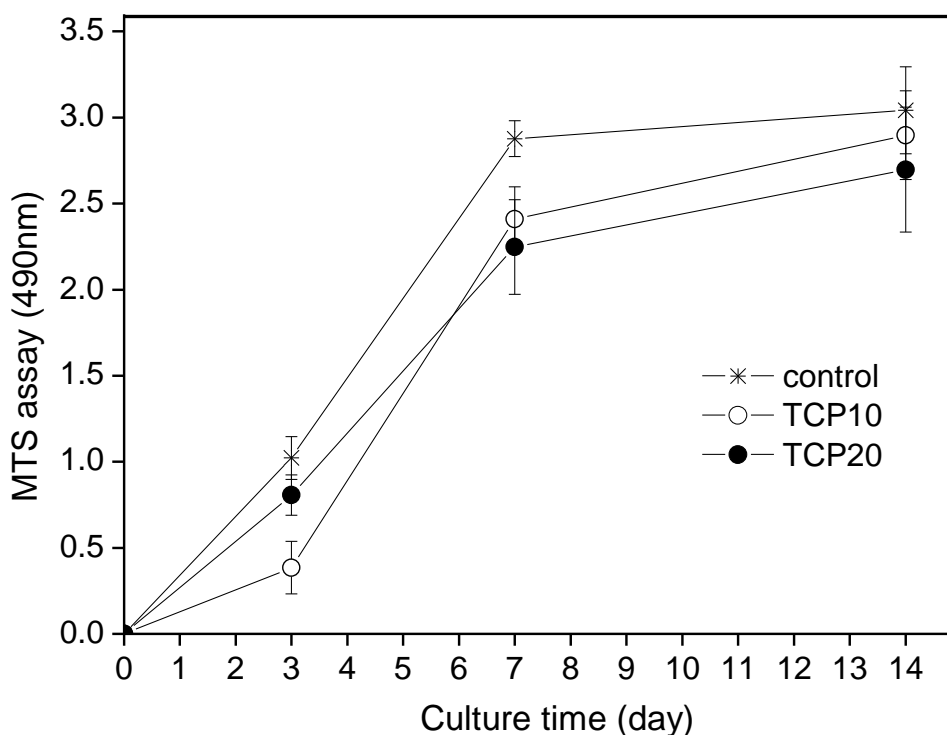
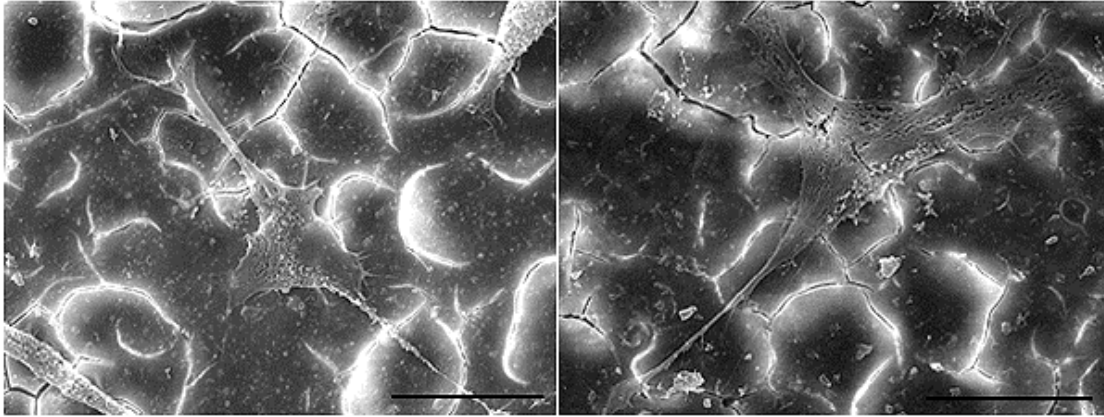


Figure 4.1.10 Proliferation behaviour of the MSCs cultured on the glass compacts (TCP-10 and TCP-20) and the tissue culture plastic used as a control during the periods for 3, 7 and 14 days. MSCs derived from rat bone marrow were used for the assay. Statistically significance difference was noticed between the groups; control vs. TCP-10 at day 3; control vs. TCP-10 or TCP-20 at day 7 ($p < 0.05$, ANOVA, $n = 3$)

On the other hand, the cell proliferation appeared to be relatively slower for investigated glass compositions in the culture for up to 7 days. However, cells continued to grow with prolonged culture period reaching to the proliferation level of the control at 14 days, featuring good proliferative potential of cells upon the glass disc substrates. The morphologies of cells grown on the glass disks for 7 days are shown in Figure 4.1.11.

TCP-10



TCP-20

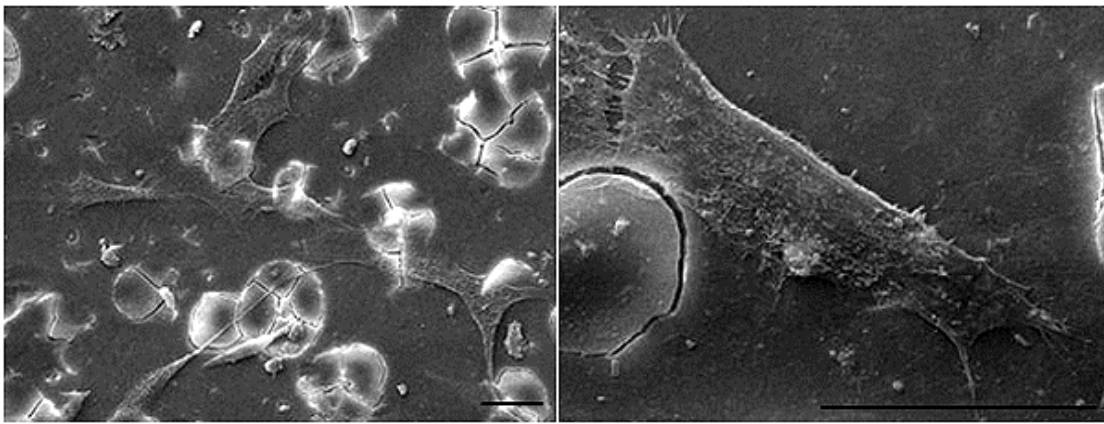


Figure 4.1.11 SEM images of the MSCs grown on the sintered glass powder compacts (TCP-10 and TCP-20) during culture for 7 days. Cells spread well on both glass samples in intimate contacts with the underlying substrates and have active cytoskeleton processes with highly elongated filopodia. Some surface cracks associated with the sample treatment for SEM are observed.

As is evident from the images, cells spread well on both the glass compositions in intimate contacts with the underlying substrates and have active cytoskeleton processes with highly elongated filopodia. The results on cell proliferation and growth morphology suggest that the developed glasses provide suitable substrate conditions for the MSCs to adhere and proliferate.

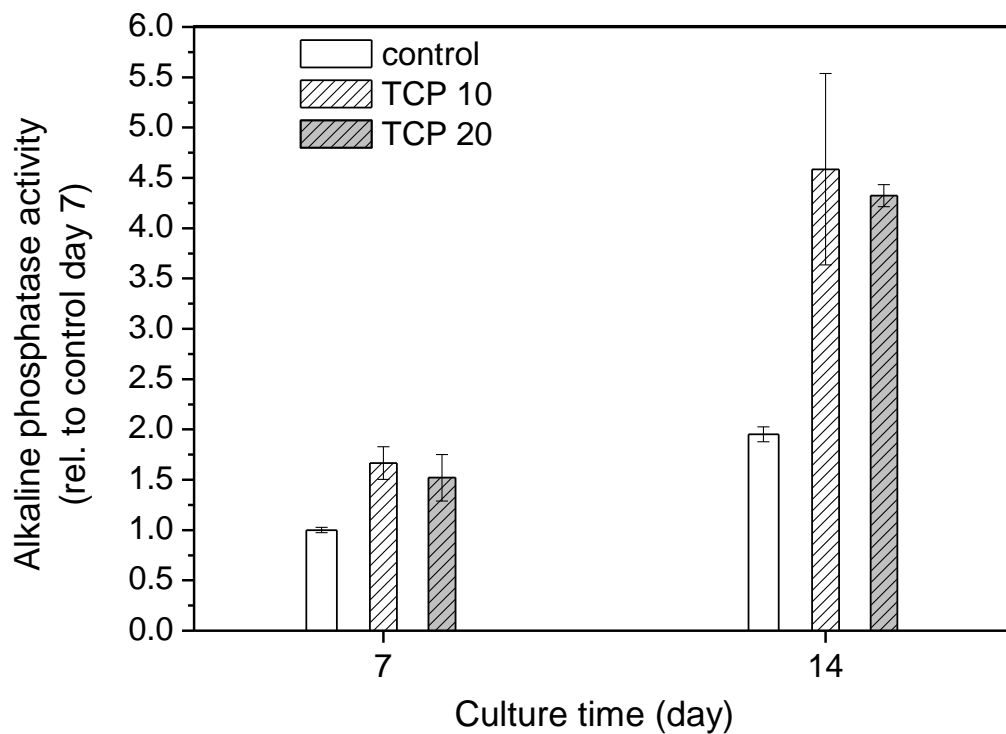


Figure 4.1.12 Alkaline phosphatase activity of the MSCs during culture for 7 and 14 days on the glass compacts (TCP-10 and TCP-20) and tissue culture plastic control. Statistically significant higher level was noticed on the glass samples with respect to control at both periods; * $p < 0.05$, ANOVA, $n = 3$.

The effect of the osteogenic differentiation was further investigated by the ALP activity of cells grown on the glass disks for 7 and 14 days. The data plotted in Figure 4.1.12 shows that ALP activity level was significantly higher on both types of glass compositions with respect to that on the control at all culture periods. In particular, the increase in the ALP level from 7 to 14 days was much higher in the glasses than in the control. ALP is known as one of the essential osteogenic markers of cells including MSCs, particularly at an early stage of osteogenic differentiation. Therefore, the significantly stimulated ALP level observed in the MSCs cultured on the glass-ceramics samples indicates that the materials developed herein are effective in modulating the functions of MSCs into the lineage of bone cells, consequently highlighting their potential usefulness for bone regeneration.

4.2.2 Conclusions

We have tried to shed some light on the influence of varying Di/TCP ratio on the structure, biodegradation, and sintering-crystallization behaviour of glasses in the Di-FA-TCP system has been presented. The as obtained results depict the potential of investigated glass compositions for their application in human biomedicine. The structure of the investigated glasses is dominated by Q2 (Si) units while phosphorus is predominantly in orthophosphate type environment. Some of the investigated glasses exhibited higher rate of bioactivity in vitro in comparison to 45S5 Bioglass® during initial 12 h of immersion in SBF solution. The glass with nominal composition Di50 – FA10 – TCP40 (wt%) (Labelled as TCP-40) exhibited hydroxyapatite formation on its surface within 1 h of its immersion in SBF while glass TCP-20 with composition Di70 – FA10 – TCP20 (wt%) exhibited apatite formation after 12 h of its immersion in SBF. All the glasses exhibited considerably lower weight loss in comparison to 45S5 Bioglass® in Tris-HCl. Sintering preceded crystallization in glass composition with TCP content varying between 10 – 30 wt.%. Further increase in TCP content in glasses deteriorated the sintering ability of glass powders considerably. The glass composition TCP-20 exhibited superior sintering ability in comparison to other investigated glasses. The resultant glass powder compacts were completely amorphous after sintering at 800 °C with a three-point flexural strength of ~85 MPa. Di crystallized as primary crystalline phase in compositions with TCP content 10 and 20 wt.%, respectively after sintering at 850 °C, while further increase in TCP content in glasses suppressed the formation of Di with FA being crystallized as the major phase. The sintered (but amorphous) glass powder compacts (TCP-10 and TCP-20) significantly increased the osteogenic differentiation of MSCs with respect to the culture plastic control, as assessed by the alkaline phosphatase activity.

4.2 Structural role of zinc in biodegradation of alkali-free bioactive glasses

4.2.1. Introduction

Zinc is an important element that plays a vital role in bone formation and resorption, which should be considered in the design of bone graft compositions aimed at bone regeneration and TE applications. Owing to the above-mentioned beneficial aspects of zinc in human metabolism in section 2.5.3, and considering the ion releasing ability of glasses in aqueous medium, bioactive glasses incorporated with zinc have gained considerable attention in the recent years for various TE applications. The increasing interest in Zn-containing bioactive glasses has resulted in a multiple-fold increase in the number of scientific publications in this area during last decade [82, 125, 153-160].

Despite the interesting studies, there exists a significant disparity among the results reported in literature with respect to influence of Zn^{2+} and its content on biodegradation, apatite forming ability, osteoblast activity, anti-inflammatory response and angiogenic behaviour in bioactive glasses [25, 161]. All these issues have been recently reviewed by Hoppe et al. [44] and therefore, will not be discussed in the present section. Apart from that, another major concern with most of the zinc-containing bioactive glass compositions studied until now is that they are either based on- or inspired by 45S5 Bioglass[®] [82, 120, 157, 162, 163] which contain significant amounts of alkali content.

In the light of above mentioned facts, it becomes necessary to investigate the influence of Zn^{2+} on different properties of bioactive glasses but with their chemical compositions completely different from that of 45S5 Bioglass[®] in order to obtain a comprehensive database highlighting the precise function and mechanism of zinc in regulating various biological processes in human body. Such an attempt has been made by Bini et al. [164] and Saino et al. [165] but on alkali-free sol-gel derived glass in the system $SiO_2-P_2O_5-CaO$. It is usually difficult to compare the results obtained on sol-gel glasses with those from melt-quenched glasses due to the high specific surface area and moisture content of the former along with the heterogeneous chemical environment of network modifier species in comparison to melt-quenched glasses [166].

The very promising glass composition TCP-20 discussed in section 4.1 was adopted as the starting point for synthesis new series of glasses and was developed by partial substitution ZnO for MgO in the same composition with the aim to study the effect of zinc on structure and biodegradation of melt-quenched alkali-free glasses designed in $CaO-MgO-SiO_2-P_2O_5-CaF_2$ glass system.

4.2.2 Results and discussion

4.2.2.1 Glass forming ability

For all the investigated glass compositions (mol%): 36.07 CaO – (19.24 – x) MgO – x ZnO – 5.61 P₂O₅ – 38.49 SiO₂ – 0.59 CaF₂, (x = 2–10) (Table 4.2.1), melting at 1570 °C for 1 h was sufficient to obtain bubble-free, transparent and XRD-amorphous glasses (Figure 4.2.1).

Table 4.2.1 Nominal composition of the as-designed glasses (mol%).

Glass	CaO	MgO	SiO ₂	P ₂ O ₅	ZnO	CaF ₂
Zn-0	36.07	19.24	38.49	5.61	0.00	0.59
Zn-2	36.07	17.24	38.49	5.61	2.00	0.59
Zn-4	36.07	15.24	38.49	5.61	4.00	0.59
Zn-6	36.07	13.24	38.49	5.61	6.00	0.59
Zn-8	36.07	11.24	38.49	5.61	8.00	0.59
Zn-10	36.07	9.24	38.49	5.61	10.00	0.59

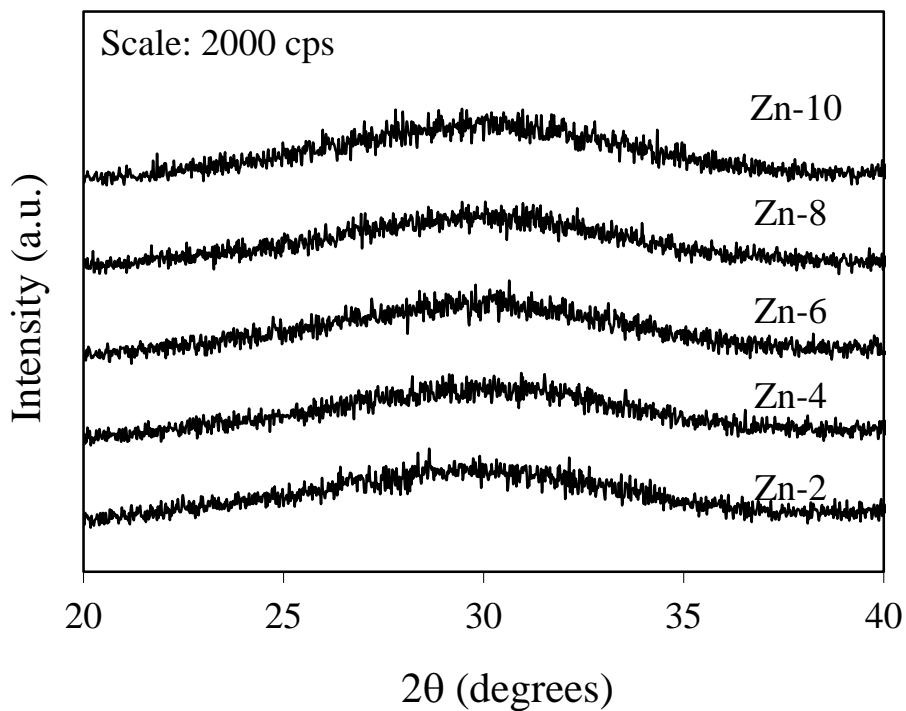


Figure 4.2.1 X-ray diffractograms of as-quenched glasses.

4.2.2.2 Glass structure

The MAS-NMR spectrum (Figure 4.2.2) shows that ZnO substitution for MgO does not affect the silicate network connectivity of these glasses. The ^{29}Si MAS-NMR results of all the glasses as presented in Figure 4.2.2a depict the dominance of Q^2 (Si) structural units in the glasses. Further, only slight shift in the peak positions of spectra could be observed and all the spectra are centred between -81 ppm and -82 ppm, thus depicting no significant changes in the silicon coordination in glass structure. The findings are further supported by the MD simulation studies performed on the glasses which show a predominance of Q^2 units ranging from 47 to 51 % from Zn-0 to Zn-10 [42].

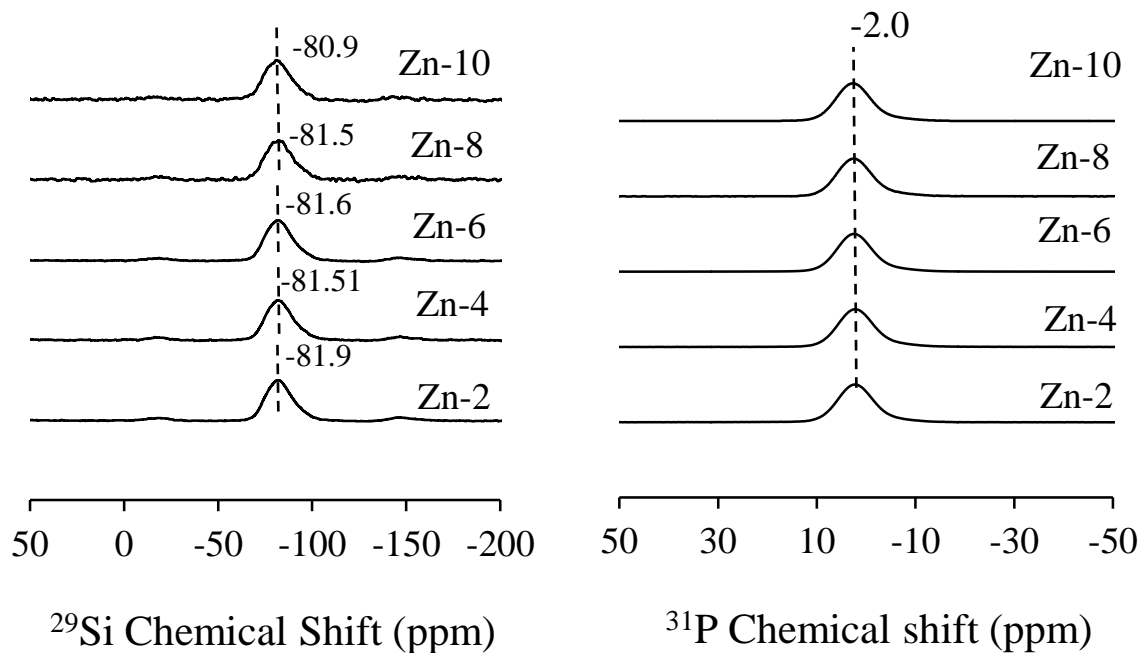


Figure 4.2.2 MAS NMR spectra of investigated glasses showing the peak positions of (a) ^{29}Si and (b) ^{31}P .

The ^{31}P MAS-NMR spectra of all the glasses show a predominance of an orthophosphate-type environment (Figure 4.2.2b), again in agreement with the MD results [42]. In fact, the observed chemical shifts, 1–3 ppm, are close to that of the calcium orthophosphate (3.1 ppm) and that of the amorphous magnesium orthophosphate (*ca.* 0.5 ppm) [137]. The phosphate environment is therefore similar to that of 45S5 Bioglass[®] [127, 167].

4.2.2.3 Apatite forming ability of glasses

The X-ray diffractograms of investigated glasses after soaking in SBF solution for time durations varying between 1 h – 7 days (Figure 4.2.3) showed considerable differences in comparison to the diffractograms of their respective parent glasses. A phase reflection at $2\theta = 31.77^\circ$ corresponding to the formation of crystalline hydroxyapatite [HA; $(\text{Ca}_5(\text{PO}_4)_3\text{OH}$; ICDD: 00-09-0432] is evident in the X-ray diffractograms of glasses with ZnO concentration varying between 4 – 10 mol% after their immersion in SBF for 1 h (Figure 4.2.3a). It should be noted that the HA formed in such experiments is carbonated HA and not stoichiometric crystalline HA. With further prolonging the immersion time, the intensity of the main XRD peak of HA increased particularly for the Zn-6 composition, while showed a fading trend for the other bioactive glasses (Figure 4.2.3b – 4.2.3d). Interestingly, at the conclusion of 7 days, HA formation was observed only for parent glass Zn-0 while no Zn-containing glass exhibited clear evidences for the formation of HA. Various reasons may be cited for such a trend observed from XRD data for bioactive glass dissolution and HA formation in SBF solution. The two main plausible factors behind this behaviour may include:

1. Influence of ZnO/MgO ratio on HA formation in bioactive glasses: Magnesium is known to delay the HA formation *in vitro* as well as *in vivo*. According to Pariente et al. [148], during *in vitro* SBF tests, magnesium tends to associate with phosphorus on the glass surface due to which apatite-like calcium phosphate domains are barely detected in magnesium containing glasses. Further, both Mg^{2+} and Zn^{2+} when present together also inhibit HA crystal growth.
2. Solution pH and degree of saturation: The pH of the SBF solution and its degree of saturation play crucial roles in deciding the nature of crystalline products as has been discussed in our study [23]. In the present study, the initial pH of SBF solution was 7.28 while the pH of SBF solution after 24 h of glass powder immersion varied between 7.7 – 7.95, irrespective of the ZnO concentration in glasses. It is now generally agreed that, both *in vitro* and *in vivo*, precipitation reactions at sufficiently high supersaturation and pH result in the initial formation of ACP with molar calcium/phosphate ratio of about 1.18 – 2.50 [168, 169]. The chemical composition of ACP is strongly dependent on the solution pH: ACP phases with Ca/P ratios in the range of 1.18:1 precipitated at pH 6.6 to 1.53:1 at pH 11.7 and even as high as 2.5:1 [170].

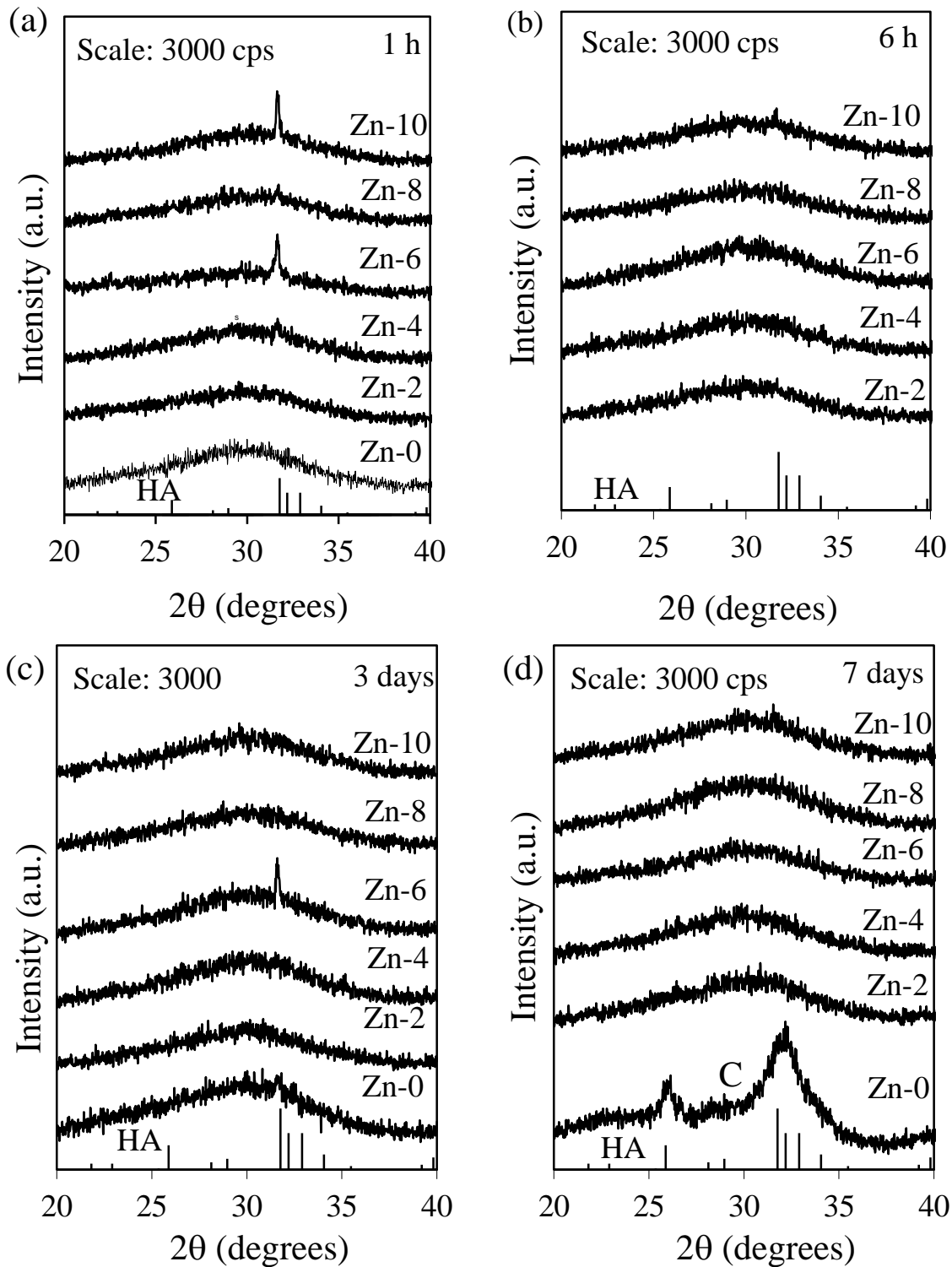


Figure 4.2.3 X-ray diffractograms of glass powders before and after immersion in SBF solution for (a) as quenched glasses (b) 1 h (c) 6 h (d) 3 days and (e) 7 days. HA refers to hydroxyapatite.

The FTIR spectra of glasses after immersion in SBF solution for 1 h (Figure 4.2.4a) depicts several changes in the glass structure that occurred due to the reaction between glass

powder and SBF. The strong low frequency band in the region $350 - 650 \text{ cm}^{-1}$ has been split into small bands at $\sim 480 \text{ cm}^{-1}$, $\sim 570 \text{ cm}^{-1}$ and $\sim 620 \text{ cm}^{-1}$ as is evident from Figure 4.2.4a. The band centred at 480 cm^{-1} can be ascribed to a deformation mode of silica layer that develops on the dissolving glass particles while small broad bands at 570 cm^{-1} and 620 cm^{-1} are characteristic for apatite and other phosphates as it corresponds to P–O bending vibrations in a PO_4^{3-} tetrahedron. A single peak in this region (570 cm^{-1}) suggests the presence of non-apatitic or ACP, which is usually taken as an indication of presence of precursors to HA. It is noteworthy that apatitic PO_4^{3-} groups have characteristic split bands at ~ 560 and 600 cm^{-1} , with a third signal at $\sim 575 \text{ cm}^{-1}$ observed for crystallites of small size [83, 87].

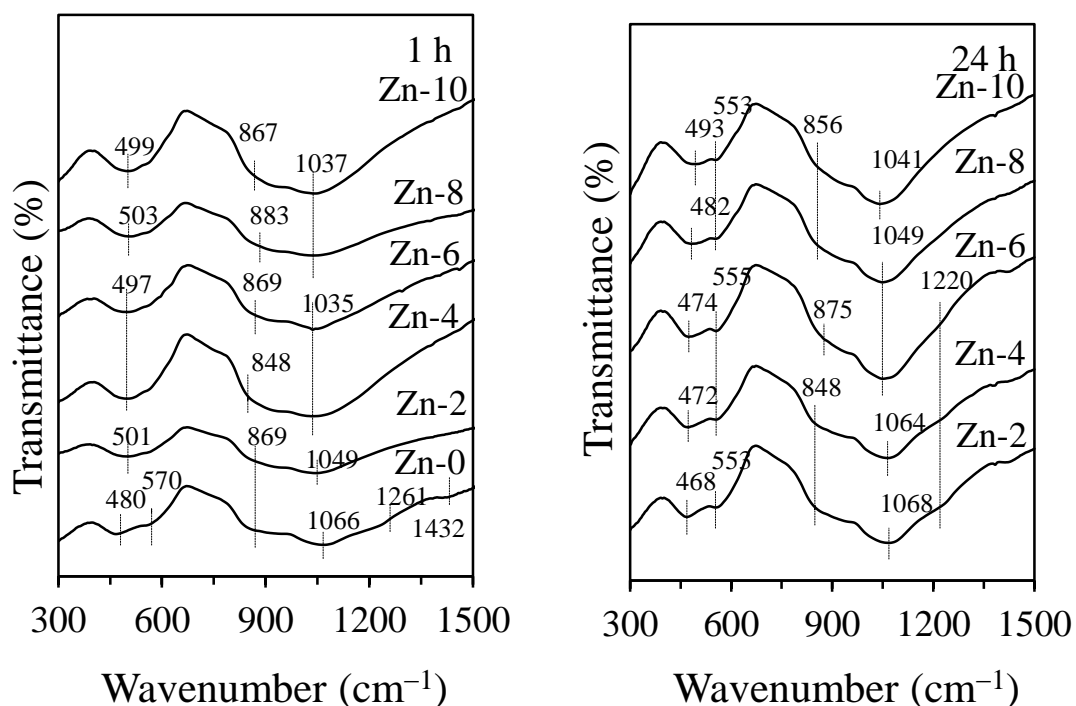


Figure 4.2.4 FTIR spectra of glass powders after immersion in SBF solution for (a) 1 h and (b) 24 h.

Further, a small band at $\sim 1440 \text{ cm}^{-1}$ along with a broad but intense band at $\sim 850 \text{ cm}^{-1}$ present in all glasses corresponds to incorporation of carbonate into the apatite, resulting in hydroxy carbonated apatite, rather than stoichiometric HA [83]. The most interesting feature of the FTIR data on zinc-containing glasses obtained after 1 h of immersion in SBF solution is the complete absence of the Si–O–Si vibration band in the region $1200-1270 \text{ cm}^{-1}$ which corresponds to the formation of silica gel layer, as postulated in Hench’s inorganic reaction set [20]. It is interesting due to the fact that this band is highly evident in the FTIR spectra of zinc-free parent glass, Zn-0. An increase in SBF immersion time to 24 h did lead to the

appearance of an absorption band at $\sim 1220\text{ cm}^{-1}$ in glasses with lower ZnO content (2–6 mol%) but this band was still absent in glasses with ZnO content varying between 8 and 10 mol% as shown in Figure 4.2.4b. Consequently, the increase in immersion time resulted in either sporadic or minimal apatite formation on glass surface during 7 days of immersion in SBF solution (Figure 4.2.3c – 4.2.3e). Similar observations regarding the absence of silica gel layer in bioactive glasses have been reported in zinc containing glasses by Oudadesse et al. [162], Kamitakahara et al. [158], Lusvardi et al. [82] and Ebisawa et al. [171].

4.2.2.4 Chemical degradation of glasses in Tris-HCl

The variation in pH of Tris–HCl with respect to ZnO content in glasses is presented in Figure 4.2.5. A slight decrease in pH from 7.4 to 7.2 was observed with increasing ZnO content in glasses. It is noteworthy that pH value of 9.7 has been reported for Tris-HCl during chemical degradation of 45S5 Bioglass[®] as reported in the section 4.1, thus exhibiting higher dissolution than the investigated glasses. The pH results are in good agreement with the weight loss data obtained for the investigated glasses as incorporation of ZnO in glasses reduced their dissolution which is evident from their weight loss (Figure 4.2.5).

All the glasses were amorphous after immersion in Tris-HCl for 120 h as shown in Figure 4.2.6, thus negating the possibility of any chemical reaction between the dissolution products

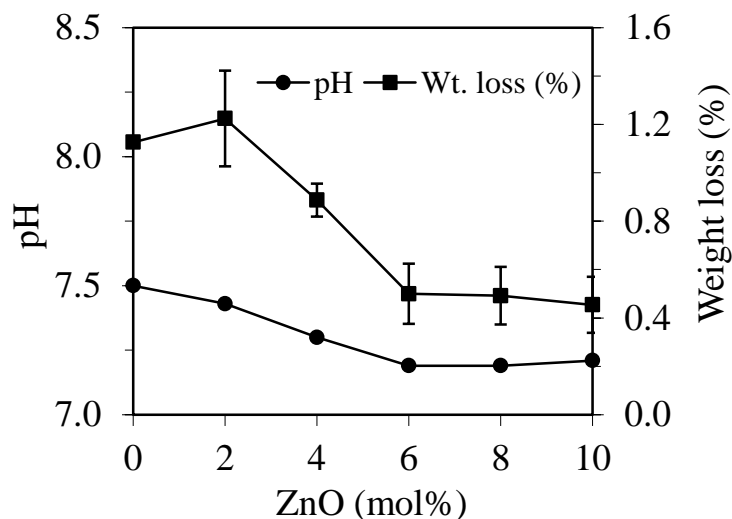


Figure 4.2.5 Graphs depicting the change in solution pH and weight loss of glass powders after immersion in Tris–HCl.

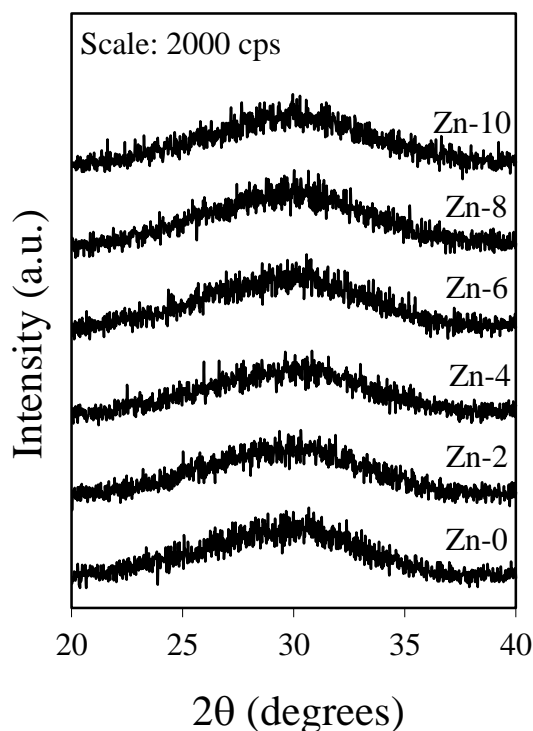


Figure 4.2.6 X-ray diffractograms of glass powder after 120 days of immersion in TRIS-HCL

The decrease in pH value of Tris-HCl with incorporation of ZnO is due to the low leaching of Mg and Ca ions from glasses as shown in Figure 4.2.7. The slower Ca release from the bioactive glasses with increasing ZnO content may be one of the reasons for slow HA formation on bioactive glass surface. The concentration of zinc ions leached out from glasses after 120 h of immersion in Tris-HCl increased with increase in ZnO content in glasses and varied between 0.06 ppm (for Zn-0) to 8 ppm (Zn-8). The zinc release profile of glasses is important from the fact that the role of major functional ions (Ca, Mg, Si, P) in bone regeneration and soft TE has been well established and documented [28, 104, 125, 172]. However, the influence of different functional ions which although present in trace quantities in human body are essential for good metabolism is still ambiguous. In particular case of zinc, its role in human metabolism has been shown to depend on its ionic release profile in body fluids and is therefore dose dependent [120, 157].

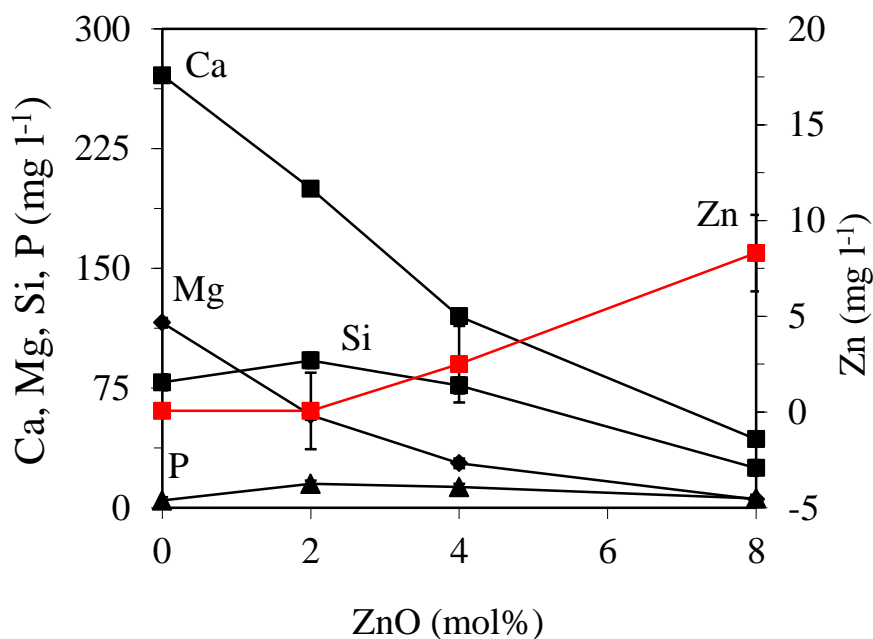


Figure 4.2.7 ICP-AES plots of elemental concentrations of Ca, Mg, P, Si and Zn in Tris-HCl after 120 h of immersion of glass powder. It should be noted that Si refers to SiO_4^{4-} and P refers to PO_4^{3-} species.

4.2.2.5 Discussion

The role of zinc on structure and bioactivity of glasses has been extensively studied in literature. For example, Aina et al. [120, 173] studied the influence of zinc on surface reactivity and cytotoxicity of 45S5-based glasses while Courthéoux et al. [174] investigated the influence of Zn^{2+} on alkali-free glasses in the $\text{CaO-P}_2\text{O}_5\text{-SiO}_2$ and CaO-SiO_2 systems, respectively. However, all the above mentioned studies have been focused upon sol-gel derived glass compositions which have high surface area due to inherent porosity, different surface chemistry in comparison to melt-quenched glasses. Therefore, a comparison between the results obtained on sol-gel derived and melt-quenched glasses is not plausible.

Some studies have also been reported on the influence of Zn^{2+} on the surface reactivity and biological activity of melt-quenched glasses. However, most of the results obtained in these studies are in contradiction with each other. For example: according to Aina et al. [120] and Lusvardi et al. [82], the incorporation of ZnO in 45S5 glass reduces its solubility but still apatite formation (when immersed in simulated body fluids) takes place within few hours to few days of time span. Also, they reported that ZnO enhances the biological activity of glasses *in vitro* as well as *in vivo*. On the other hand, according to Haimi et al. [175], zinc addition in bioactive glasses has no significant effect on the DNA content,

ALP activity and osteopontin concentration of human adipose stem cells. Similar results have also been reported by Popp et al. [176], who studied the influence of soluble zinc from ACP's on the proliferation of rat bone marrow stromal cells.

Despite the significant disparity in the results related with the biological behaviour of zinc, one result that is coherent among almost all the glass compositions reported in literature irrespective of their synthesis route is their decreasing solubility with increasing zinc content. A similar behaviour has been observed in the present investigation, as chemical degradation of glasses in Tris-HCl decreases with their increasing Zn^{2+} concentration. The implications of decreasing solubility with increasing zinc content in glasses may be interpreted on the basis of the solubility of parent glass, for example, according to Aina et al. [120], incorporation of Zn^{2+} in 45S5 glass is beneficial owing to the high solubility of the latter which leads to a significant increase in the pH of physiological fluid, thus affecting the proliferation of endothelial cells. However, the precise reason for decreasing solubility with zinc incorporation in glasses is still ambiguous as some studies explain it on the basis of influence of zinc on glass structure [162, 173] while others discuss it as a function of chemical composition and surface chemistry of glasses [177]. According to Aina et al. [173], the zinc species in alkali-free bioactive glasses are found in a tetrahedral environment, and can enhance the glass reticulation by forming Si–O–Zn inter-tetrahedral links. Similar results on the role of Zn in bioactive glasses irrespective of its concentration have also been reported by Linati et al. [110] on zinc-doped 45S5 Bioglass[®]. For the present compositions, the MD simulations studies [42] have shown that both Zn^{2+} and Mg^{2+} are primarily present in five-fold coordination, which appears reasonable considering the similar ionic radii of Mg^{2+} (0.65 Å) and Zn^{2+} (0.74 Å) [178]. The intermediate role of zinc is well documented in literature, and therefore depending on the glass composition and its local environment, Zn^{2+} can be a four-coordinated weak network former as has been suggested for traditional bioactive glasses or five-coordinated as has been observed in the present study [179]. In general, zinc has been shown to exhibit a marked preference for tetrahedral coordination in simple alkali silicate glasses [180] which has been the case with most of the studies based on Zn-doped 45S5 Bioglass[®] or its alkali-containing derivatives. However, with increasing Zn/modifier ratio, the ratio of six – to fourfold coordinate Zn species is reported to increase due to the availability of charge compensating modifier cations [180, 181]. Further lack of any significant changes in the silicate network connectivity glass by varying the Zn^{2+}/Mg^{2+} ratio indicates towards the similar co-ordination of Zinc to magnesium.

The decreasing glass degradation and reduced HA formation in the present case may be attributed to the ability of zinc to promote enhanced inter-tetrahedral cross-links as observed in MD simulations [42] which in combination with constant silicate network connectivity enhances the chemical durability of the glasses. The way in which a modifier or intermediate cation involved in inter-tetrahedral cross-links between adjacent silicate fragments can result in a more stable glass network (with a higher resistance to dissolution) even without actual changes in the silicate network connectivity has been recently discussed [110].

The importance of the silica-rich gel layer is usually attributed to the fact that its presence on the glass surface in SBF helps in inducing apatite formation while no apatite formation can be induced by silica glass or quartz crystal [182]. However, although carbonated-HA formation on glass surface during their immersion in biological fluids is considered to be a marker of bioactivity, recent evidence has indicated that formation of this HA layer is not critical for bone generation. The ionic dissolution products from bioactive glasses appear to stimulate the growth and differentiation of cells at the genetic level, an effect which has been considered to be dose dependent [28]. For example: Zn concentrations in the range of 2 – 8 ppm have been reported to cause damage to human osteoblasts via oxidative stress [157]. Similar results have been reported for endothelial cells where decrease in cell proliferation was observed due to toxic Zn concentration of 2.7 ppm released in the culture medium from a Zn-doped bioactive glass [120]. Therefore, special consideration should be given to the ZnO content in bioactive glasses and their release profile in body fluids while designing the compositions.

4.2.3 Conclusions

The effects of zinc in the biodegradation of alkali-free phosphosilicate glasses have been studied through a combination of MAS-NMR, FTIR, XRD and chemical degradation experiments. An increase in the Zn^{2+}/Mg^{2+} ratio did not induce any significant change in Q^n speciation and network connectivity, as revealed by MAS-NMR; however it did improve the chemical durability of investigated glasses (as observed from Tris-HCl studies) which consequently suppressed the apatite (carbonated) forming ability of glasses in simulated body fluid. The influence of zinc on suppressing the apatite forming ability of glasses has been explained on the basis of the constant silicate network connectivity of the combined with the previously suggested ability of Zn to strengthen the glass network through non-covalent Si-O---Zn---O-Si links. This results in a glass structure more resistant to dissolution in a

biological medium. An additional factor discussed is the potential influence of zinc on the surface chemistry of glasses when immersed in physiological fluids.

4.3 Influence of ZnO/MgO substitution on sintering, crystallization and bio-activity of alkali-free glass-ceramics

4.3.1 Introduction

Bioactive glasses and glass-ceramics are used in a wide range of applications: bulk implants to replace bones or teeth, coatings to anchor orthopaedic or dental devices, or in the form of powders, as bone grafts, to fill various types of bone defects [4, 183, 184]. The successful development of bioactive glasses for such applications requires suitable densification and crystallization behaviours along the heat treatment step. Such requirements are also of paramount importance in other advanced applications of bioactive glasses involving heat treatments aiming at obtaining products such as glass fibres.

The aim of the present section is to elucidate the effect of partial substitution of MgO by ZnO on the evolution of the glass structure and of the crystalline phases developed along the heat treatments using MAS-NMR and X-ray powder diffraction as complementary techniques and to study the sintering and crystallization behaviours of glass powders using hot-stage microscopy and differential thermal analysis, respectively. Understanding the sintering behaviour of the glass powders and the interactions between the sintering and crystallization events is of utmost importance for successfully fabricating porous scaffolds or coatings on metallic implants from bioactive glasses. Further, cell-culture tests using mesenchymal stem cells from rat bone marrow were used to investigate the *in vitro* behaviour of as designed glass-ceramics.

4.3.2 Results and discussion

4.3.2.1 Glass-forming ability

For all the investigated glass compositions presented in Table 4.2.1, melting at 1570 °C for 1 h was sufficient to obtain bubble-free, transparent and XRD-amorphous glasses.

4.3.2.2 Thermal analysis

The DTA thermographs of fine glass powders with $\beta = 20 \text{ K min}^{-1}$ are shown in Figure 4.3.1. All the glass compositions feature a single endothermic dip before the T_c corresponding to T_g , which is followed by the exothermic crystallization effect. The characteristic parameters obtained from DTA thermographs are summarized in the Table 4.3.1. In general, addition of ZnO resulted in gradually lowering T_g from 752 °C to 718 °C. The decrease in T_g can be attributed to the lower bond strength of Zn–O bond in comparison to the Mg–O bonds [185], which in turn reduces the rigidity of the glass network at high

temperature in comparison to magnesium, even though both possess similarities in size and charge. Further, structural rigidity of a glass network also depends on the field strength thus, the weak bond strength of Zn–O bond than Mg–O can be attributed to the weaker cation field strength of Zn in comparison to Mg [186]. This in turn translates in lowering the viscosity of the glasses [187] thus, decreasing their T_c values. Such changes could be observed in glass powder compacts sintered at 800 °C (not shown here) which remained amorphous for the lower zinc contents, and visible XRD peaks only appeared in the glasses with higher zinc contents. Hence, the results obtained in the present work for zinc-containing glass-ceramics are in good agreement with other literature reports [158, 186, 187].

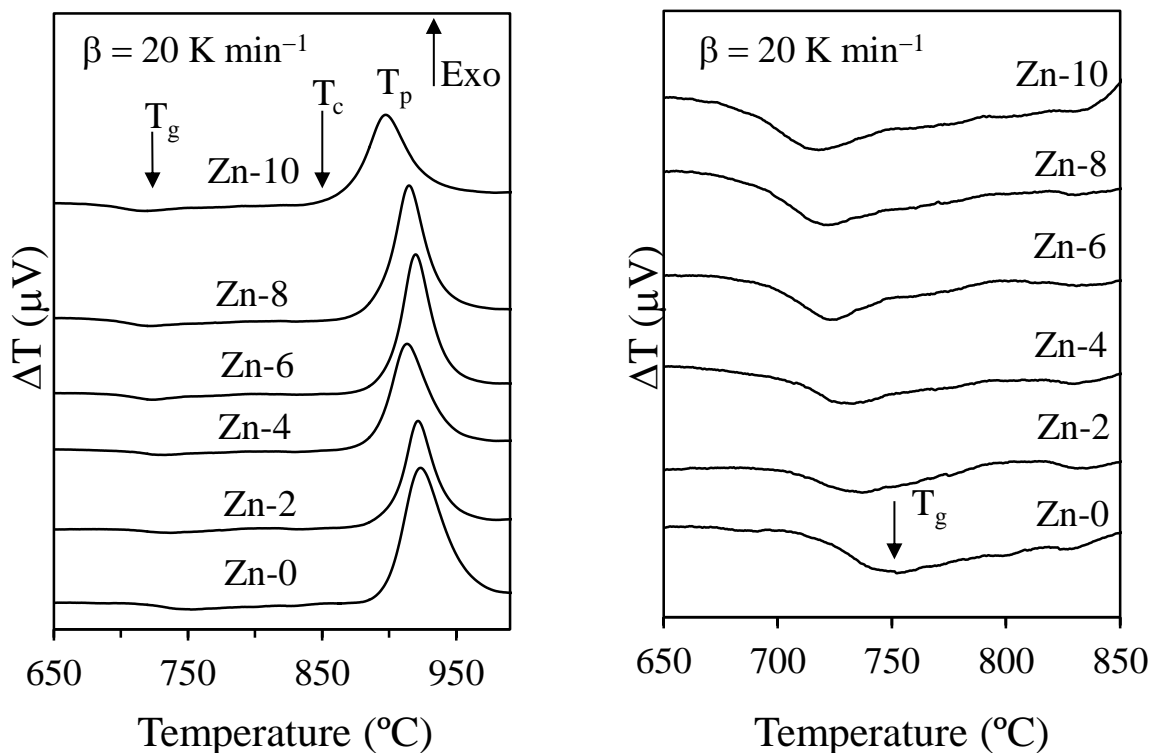


Figure 4.3.1 DTA thermographs of glasses at a heating rate of 20 K min⁻¹.

4.3.2.3 Sintering and Crystallization behaviour

A comparison between DTA and HSM results under the same heating conditions can be useful in investigating the effect of glass composition on sintering and devitrification phenomena. Figure 4.3.2 presents variation in the relative area and heat flow with respect to temperature as obtained from HSM and DTA, respectively, for all the investigated glasses at a similar heating rate of 5 K min⁻¹. Table 4.3.2 summarizes the values of the temperature of first shrinkage (T_{FS} ; $\log \eta = 9.1 \pm 0.1$, η is viscosity in dPa s), temperature for maximum shrinkage (T_{MS} ; $\log \eta = 7.8 \pm 0.1$) and ratio of the final area/initial area of the glass powder

compact (A/A_0) at T_{MS1} , as obtained from the HSM along with temperature for T_c and T_p , as obtained from the DTA of the glasses.

- (i) In general, T_{FS} values show a decreasing tendency with increasing content of ZnO.
- (ii) Two stage sintering was observed in glasses Zn-2, Zn-4 while a gradual shift to single stage shrinkage was observed for glasses thereafter (Figure 4.3.2). The conclusion of first sintering stage is characterized at T_{MS1} while end of second sintering stage is characterized by T_{MS2} . Interestingly, in all the glass compositions T_{MS1} was observed at temperatures lower than T_c (i.e., $T_{MS1} < T_c$). Thus sintering precedes crystallization in all the glasses. Therefore one can expect well sintered and mechanically strong glass powder compacts.
- (iii) The value for T_{MS2} was higher than T_c in the glasses exhibiting two stage sintering behaviour. Thus depicting that shrinkage continued in the glass powders even after onset of crystallization, probably due to the existence of residual glassy phase in the glass-ceramics.
- (iv) Table 4.3.1 lists the values of sinterability parameter (S_c), where $S_c = T_c - T_{MS}$. The parameter S_c is the measure of ability of sintering vs. crystallization: the greater this difference, the more independent are the kinetics of both processes. However, in the present study no particular trend could be observed for the variation of S_c . Nevertheless, all the investigated glasses show larger values of S_c (greater than 25 °C) (26 °C – 48 °C) indicating good sintering behaviour.
- (v) The values of T_p varied between 895 °C – 861 °C. As evident from Table 4.3.1, the highest T_p value was observed for Zn-0. Adding increasing amounts of ZnO to the parent glass at the expenses of MgO resulted in gradual decreases in T_p .
- (vi) Values of A/A_0 ranged from 0.63 to 0.67 (Table 4.3.1) for all the glasses implying towards good densification levels of 95–98%.

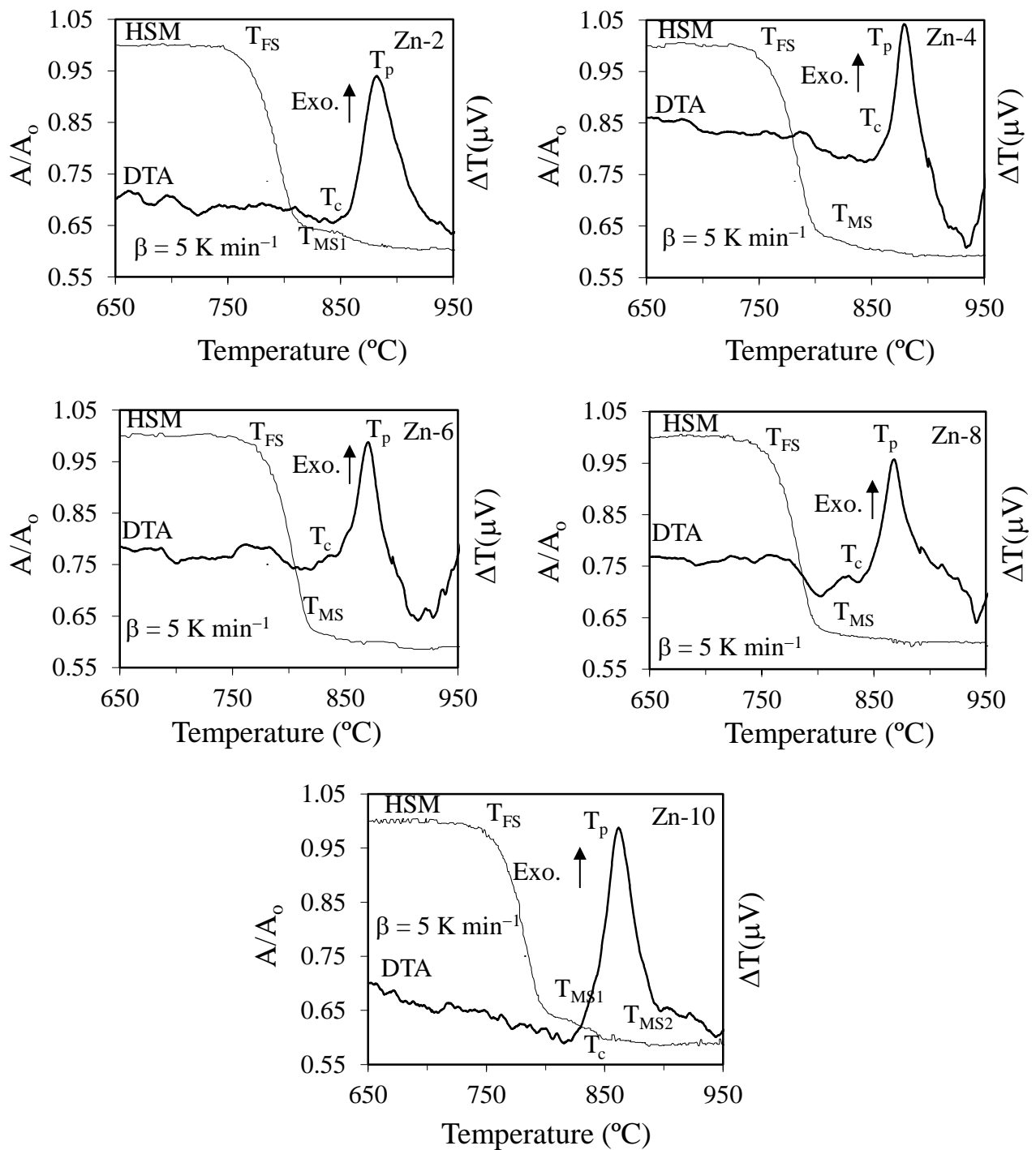


Figure 4.3.2 Comparison of DTA and HSM curves under the same heating rate (5 K min^{-1}) for compositions: (a) Zn-2, (b) Zn-4, (c) Zn-6, (d) Zn-8 and (e) Zn-10.

Table 4.3.1 Thermal parameters measured from DTA and HSM at 5 K min⁻¹ *β = 20 K min⁻¹.

	Zn-0	Zn-2	Zn-4	Zn-6	Zn-8	Zn-10
T _{FS} (±5 °C)	757	753	748	766	747	750
T _{MS1} (±5 °C)	820	809	797	817	797	795
T _{MS2} (±5 °C)	–	883	888	–	–	850
T _g [*] (±2 °C)	752	737	733	725	722	718
T _c (±2 °C)	850	843	852	843	837	822
T _p (±2 °C)	895	881	878	870	868	861
S _c (=T _c -T _{MS1})	30	48	55	26	41	27
A/A ₀ at T _{MS1}	0.66	0.67	0.66	0.63	0.65	0.67

4.3.2.4 Effect of heat treatment of the structure

4.3.2.4.1 Crystalline phase evolution by XRD

The exact nature of the phases produced during the heat treatment is of great interest in bioactive glasses as they are intended to be often exposed to high temperature when it is sintered for different biomedical application. Based on DTA thermographs, T_c was established for all the compositions and used as a criterion for selecting the heat treatment temperature to induce crystallization. In agreement with HSM and DTA, well sintered and dense glass-ceramics were obtained after heat treating the glass-powder compacts at 850 °C for 1 h. Figure 4.3.3 presents the qualitative crystalline phase analysis of the sintered glass-ceramics as depicted by XRD data. Thus heat treating at 850 °C for 1 h resulted in well-defined XRD phase reflections in all the compositions indicating their crystalline nature (Figure 4.3.3). Di (CaMgSi₂O₆; ICSD: 10223) and FA (Ca₅(PO₄)₃F; ICSD: 163790) were the two the primary crystalline phases formed in all the glass-ceramics, followed by rankinite (Ca₃Si₂O₇; ICSD: 2282) as secondary phase. Another phase named petedunnite (CaZnSi₂O₆; ICSD: 158143) crystallized in glass-ceramics with ZnO contents > 4 mol%. Consequently, with the addition of ZnO for MgO, Zn²⁺ replaced Mg²⁺ in the Di, thus forming the major crystalline phase with higher intensity than FA. The presence of FA phase is highly desirable as FA is more stable than HA. Therefore, materials containing FA would be recommended when coatings having low dissolution rate are required [136].

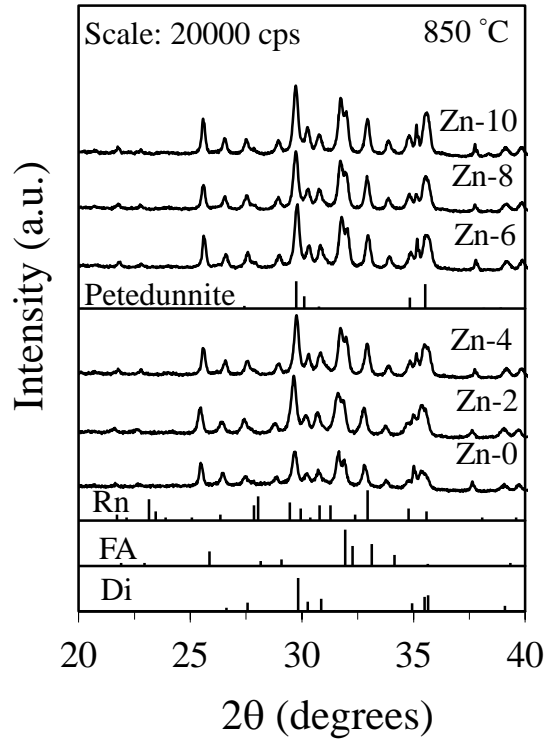


Figure 4.3.3 X-ray diffractograms of glass-ceramics heat treated at 850 °C for 1 h.

Hence, with the addition of ZnO to the parent composition the intensity of XRD peaks corresponding to Di increased whereas the intensity of FA peaks remained almost constant throughout the series.

4.3.2.4.2 MAS-NMR of glass-ceramics

The XRD data was further supported by MAS-NMR studies (Figure 4.3.4). The full width half maximum has reduced considerably in comparison to the original glasses (Figure 4.2.1). Further, as shown in Figure 4.3.4a, all the spectra have a sharp peak centred ~ -84.4 ppm and a small shoulder at -74.5 ppm, which becomes more pronounced with increase of zinc content in glasses, where the former is close to the pure Di [188] while the latter corresponds to the presence of minor phase rankinite [188]. In our study of XRD, a total of two silicate phases pertaining to chain silicates were observed in the glass-ceramics. However, discrimination between these phases is difficult due to the similarity in their silica connectivity. Therefore the resonance around -84 ppm can be due to the contribution from Di and petedunnite (inosilicates).

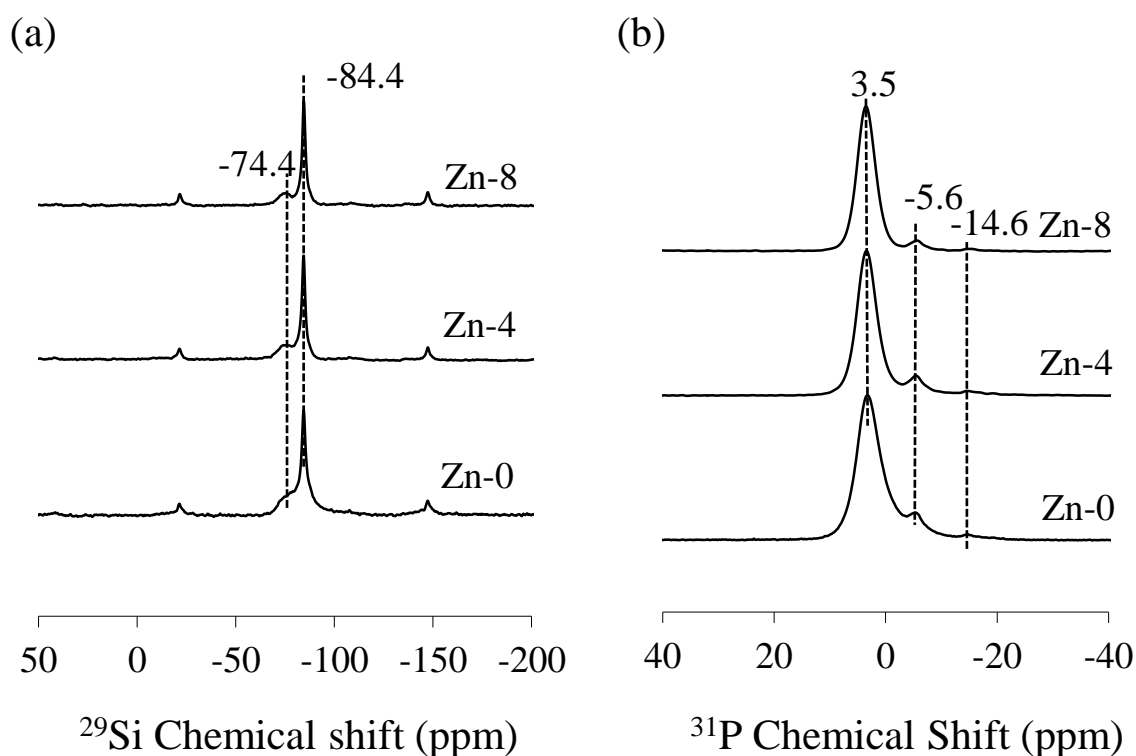


Figure 4.3.4 (a) ^{29}Si MAS-NMR and (b) ^{31}P MAS-NMR spectra of glass-ceramics heat treated at 850 °C for 1 h.

Figure 4.3.4b shows ^{31}P NMR spectra of glass-ceramics heat treated at 850 °C for 1 h. All the spectra have a sharp peak at 3.3 – 3.5 ppm corresponding to an orthophosphate environment and a small shoulder at around –5.3 and –14.6 ppm indicating the presence of pyrophosphate units. The band at 3.5 ppm is close to that reported for FA [136]. Further, the formation of pyrophosphate phase around –5.3 and –14.6 ppm may be due to the reduction in the charge balancing cations, which migrated towards their respective crystalline phases upon heat treatment. Further, Di being a mechanically strong phase renders high mechanical strength to the resultant glass-ceramics. It is worth noting that the presence of petedunnite as a minor phase indicates that zinc predominantly remains in the residual glassy phase.

4.3.2.5 Density and molar volume

The experimental results showed that substitution of MgO by ZnO caused an increase in the density (Table 4.3.2) of the glasses due to the higher density of ZnO (5.6 g cm^{-3}) in respect to MgO (3.6 g cm^{-3}). The molar volume of the glasses increased with increase in Zn content in glasses. The increase in molar volume can attributed to the small bond strength of

Zn–O bond in comparison to Mg–O bond which results in higher bond lengths thus causing an expansion in the network.

Table 4.3.2 Density and molar volume of the investigated glasses.

Glasses	Density (g cm ⁻³)	Molar volume (cm ⁻³ mol ⁻¹)
Zn-0	2.92	20.40
Zn-2	2.95	20.47
Zn-4	2.98	20.51
Zn-6	3.02	20.55
Zn-8	3.05	20.59
Zn-10	3.08	20.66

4.3.2.6 Mechanical Behaviour

Evaluating the mechanical strength of a biomaterial is very important while judging its suitability for a given intended application, such as scaffolds for bone regeneration. It is likely that mechanical strength of a given glass-ceramic will be dependent on the mechanical properties of the constituting crystalline phases, their volume fractions, the size/shape of the crystals formed, and on the interfacial bonding between the amorphous and crystalline phases. The flexural strength was calculated for powder compacts sintered at 850 °C. High flexural strength values were obtained for glass powder compacts, which can be attributed to the predominance of Di in all glass-ceramics (Figure 4.3.5). In general, an increase in mechanical strength with increasing Zn contents in glasses was observed, with the highest mechanical strength being measured for the GC Zn-8. As deduced from HSM and DTA analysis, this enhancement can be attributed to two complementary reasons: (i) an improved sintering ability due to a decrease in the viscosity of glasses translated by decreasing T_g values; (ii) a more extensive subsequent crystallization promoted by the enhanced diffusivity of ionic species in the glassy matrix.

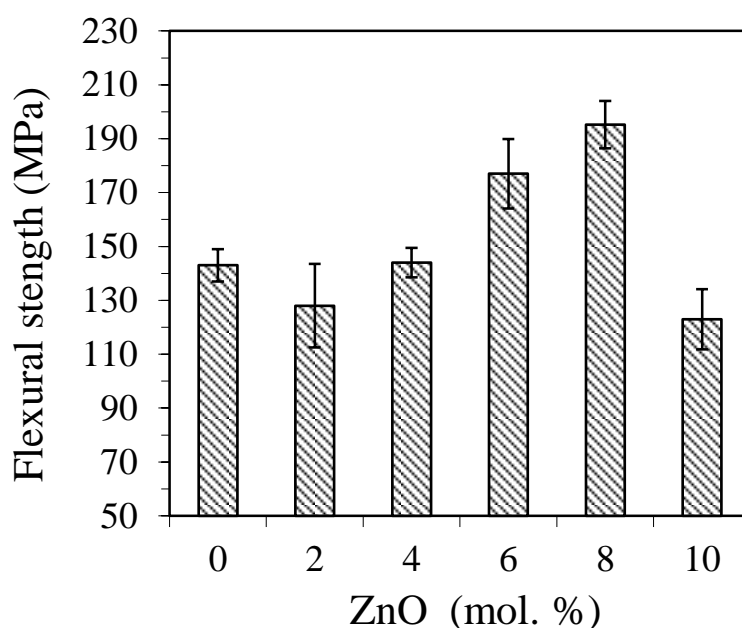


Figure 4.3.5 Flexural strength of the glass-ceramics heat treated at 850 °C for 1 h

4.3.2.7 Apatite forming ability of glass-ceramics

The SEM-EDS results of the glass-ceramic samples before and after immersion in SBF solution for different time periods are shown in Figure 4.3.6. The surface morphology of Zn-0, Zn-4 and Zn-8 samples before immersion in SBF (Figure 4.3.6a) is similar, a situation that was altered for the samples immersed in SBF (Figure 4.3.6b). The EDS data was gathered over the entire areas shown in the SEM micrographs to assure reliable averaging of the signals and the scale of all EDS spectra was always kept constant to enable a direct comparison. Although all the spectra reveal the presence of all glass-constituting elements, their relative intensities changed significantly after immersing the samples in SBF. It can be seen that the EDS spectrum of Zn-0 sample (Figure 4.3.6a) significantly differs from those obtained after immersing in SBF (Figure 4.3.6b). Namely, the intensities of Ca and P became more and more predominant with increasing immersion time. This constitutes an obvious evidence of apatite formation at the surface of the samples.

The formation of HA at the surface of ZnO-containing glass-ceramics is less obvious. Various reasons can be cited for this delayed bio-mineralization process in ZnO-containing glass-ceramics:

1. *Presence of ZnO*: The delayed formation of HA can be due to inter-tetrahedral non-covalent linkages in the residual glassy phase. Similar results have been reported in our previous section. Further, the concomitant presence of Mg^{2+} and

Zn^{2+} inhibits HA crystal growth. Literature reports suggest a Langmuir-type adsorption of these ionic species at active growth sites on the HA crystals [169]

2. *Low residual glassy phase:* The enhanced crystallization of ZnO-containing glass-ceramics (lower T_c values) and the consequent lower amount of residual glassy phase is also expected to decrease the apatite forming ability [189].

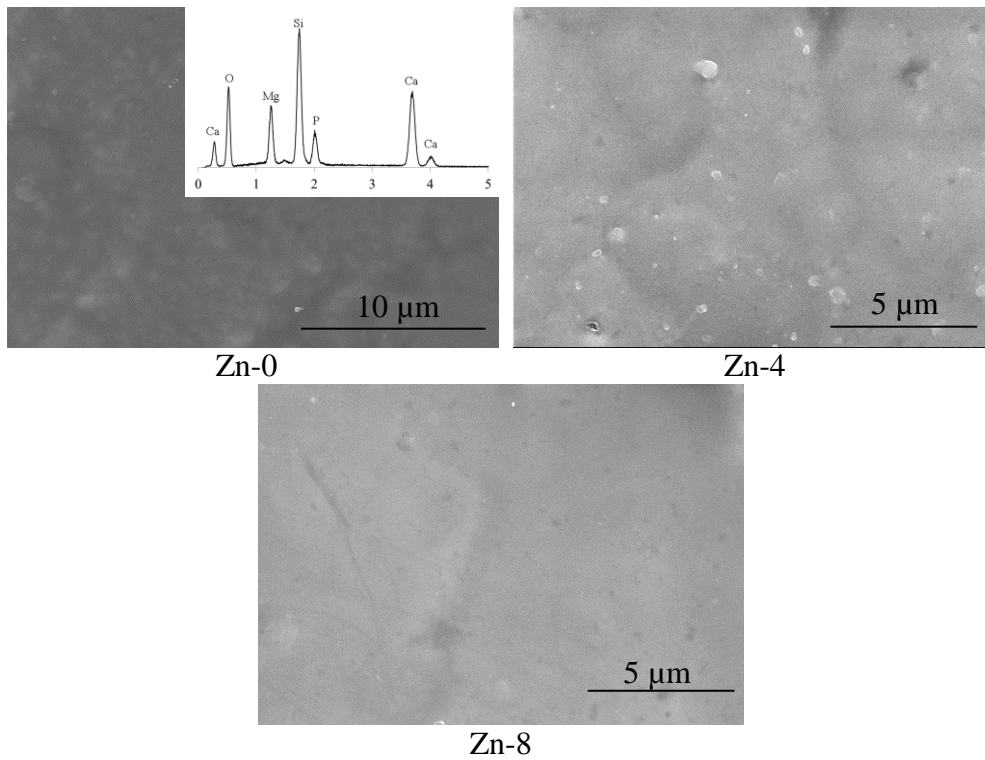


Figure 4.3.6a SEM/EDS micrographs images of unpolished and non-etched glass-ceramics samples before soaking in SBF: Zn-0, Zn-4, and Zn-8.

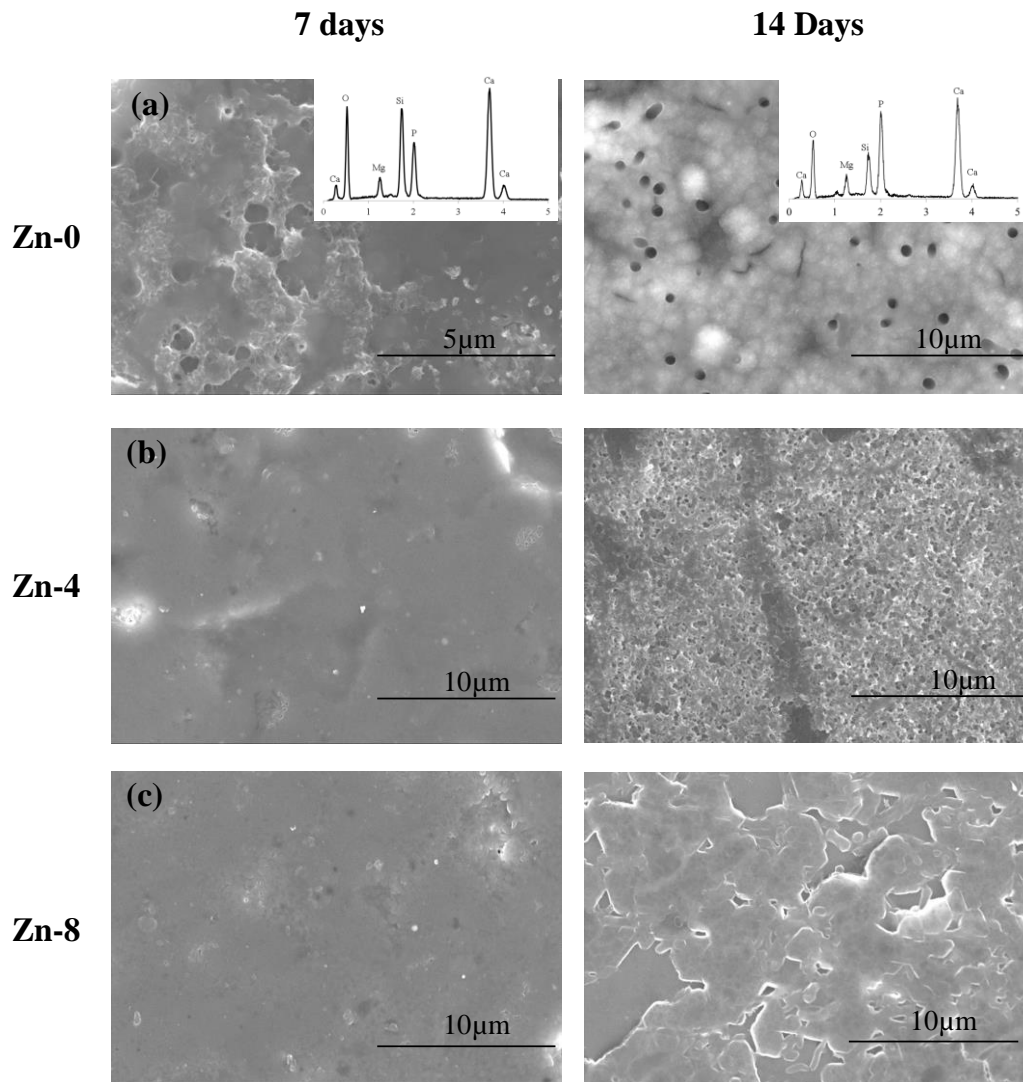


Figure 4.3.6b SEM/EDS micrographs images of unpolished and non-etched glass-ceramics samples after soaking in SBF for 7 and 14 days: (a) Zn-0, (b) Zn-4, and (c) Zn-8.

4.3.2.8 Mesenchymal cell activity and alkaline phosphatase activity

Figure 4.3.7 shows the cell viability on the glass-ceramics and control during culture for up to 7 days, as assessed by a CCK method. Apparently, the growth kinetics of glass-ceramics with 4 mol.% ZnO was significantly higher with respect to that of tissue culture plastic control as well as to that of other investigated glass-ceramics. Interestingly, all other zinc containing glass-ceramics showed lower cell viability in comparison to that for tissue culture plastic.

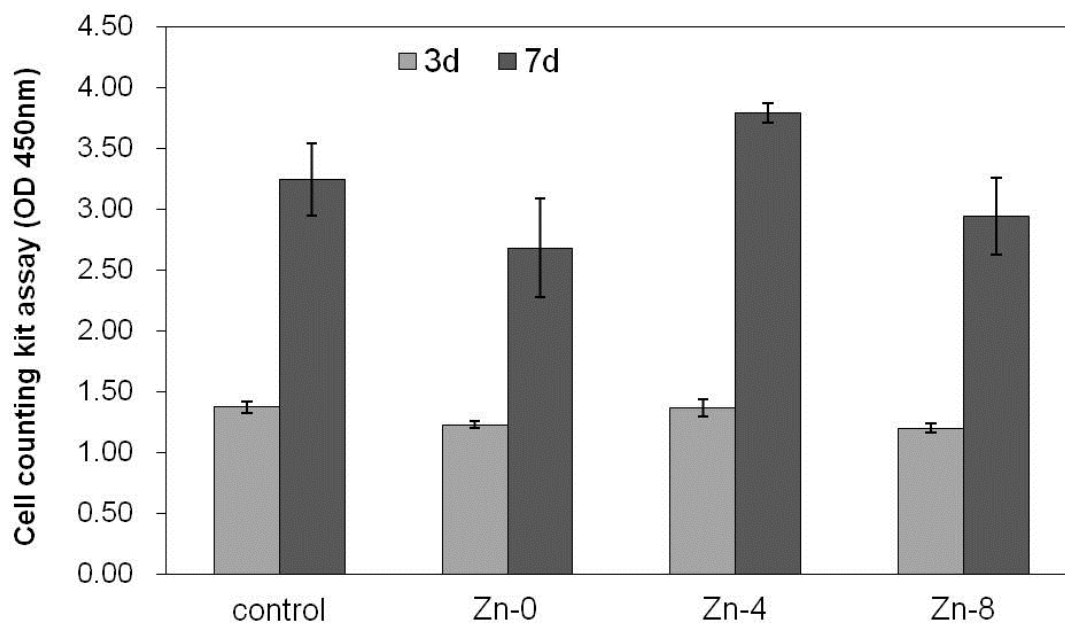


Figure 4.3.7 Influence of ZnO content in glass-ceramics on cell viability during culture for up to 7 days, as assessed by CCK method. Glass-ceramics with 4 mol% ZnO showed highest growth with respect to tissue culture plastic control as well as to that of other investigated glass-ceramics.

The representative cell growth images at day 3 and day 7 on the glass-ceramics samples are presented in Figure 4.3.8. The cells were not readily noticed on the Zn-0 glass-ceramic after 3 days while the cell proliferation was comparatively better on glass-ceramic Zn-8. On the other hand, when grown on Zn-4, the cells were readily observed covering the surface almost completely with active cytoskeletal processes and elongated filopodia indicating that glass-ceramic Zn-4 provides favourable conditions for adherence, spreading and proliferation of MSCs. After 7 days, although the cell proliferation on glass-ceramics other than Zn-4 was better in comparison to that observed after day 3 but still the glass-ceramic Zn-4 exhibited the highest rate of cell proliferation. The lower cell viability in the absence of zinc can be explained by the fact that after iron, zinc is the most abundant trace metal in human organisms and is essential for various metabolic activities as has been discussed above

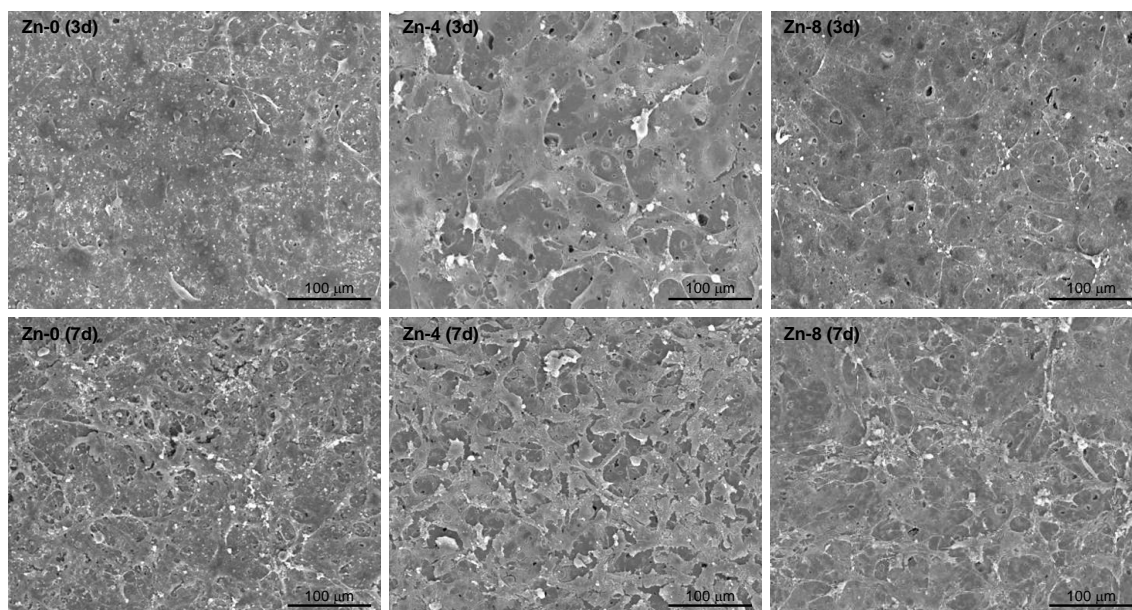


Figure 4.3.8 SEM images of the MSCs grown on the sintered glass powder compacts (Zn-0, Zn-4 and Zn-8) during culture for 3 and 7 days. After 7 days, cell proliferation on glass-ceramics was better in comparison to that observed after 3 days. Glass-ceramic Zn-4 exhibited the highest rate of cell proliferation.

However, the decreasing cell viability with increasing zinc concentration in glasses may be attributed to its dose-dependent effect. Zn^{2+} has been reported to play a dual role in affecting the cell death: although zinc seems to be inhibitor of many forms of apoptosis [190], exposure to excessive concentrations may contribute to neuronal cell death in acute neurological disorders and to apoptosis of human peripheral blood lymphocytes [191]. The mechanism by which Zn^{2+} induces cell death and oxidative stress is still unresolved. According to the available literature, an increase in Zn^{2+} concentration in cellular medium higher than ~2 ppm can lead to cytotoxicity and cell death [44]. Similar results with respect to proliferation of endothelial cells and osteoblasts have also been reported by Aina et al. [120, 157] where it has been shown that 45S5 Bioglass[®] doped with 5 wt% ZnO enhanced cell proliferation on its surface while increasing zinc concentration led to significant release of lactate dehydrogenase (index of cytotoxicity) thus, resulting in cell death. With respect to the bioactivity of glass-ceramic Zn-4, the cell growth kinetics in this sample is significantly higher in comparison to that reported for apatite-wollastonite [192] as well as for diopside-fluoroapatite [105] glass-ceramics, respectively.

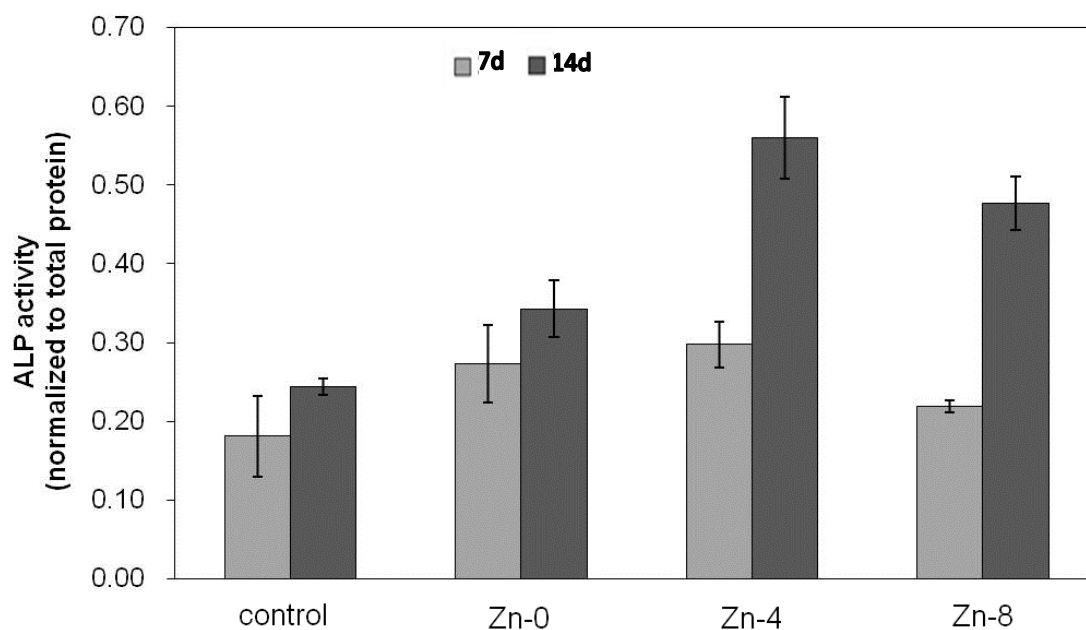


Figure 4.3.9 Alkaline phosphatase activity of the MSCs during culture for 7 and 14 days on the glass compacts (Zn-0 to Zn-8) and on tissue culture plastic control. For all the investigated glass-ceramics, irrespective of their ZnO content, ALP levels were always higher in comparison to that of control ($p < 0.05$, ANOVA, $n=3$)

The osteogenic differentiation of the MSCs cultured on the glass-ceramic samples was investigated in terms of ALP activity (Figure 4.3.9). Under the osteogenic medium used herein, rat bone marrow MSCs have been shown to switch to the lineage of osteoblastic cells [193]. When cultured on the control dish, MSCs showed an increased ALP level from days 7 to 14. The ALP levels for all the investigated glass-ceramics were higher in comparison to control irrespective of their zinc content. However, among all the investigated glass-ceramics, Zn-4 exhibited the highest ALP activity of cells during 7 and 14 days of culture. It should be noted that ALP is a homodimeric metalloenzyme that catalyses the hydrolysis of almost any phosphor monoester with the release of phosphate and alcohol. Its properties have been associated with the mineralization process and phosphate homeostasis in bone tissue [194]. ALP acts as a nucleation centre for hydroxyapatite as it is able to release phosphate and captures calcium ions. In this way, the presence of ALP and a solution rich in Ca^{2+} ions induces the deposition of hydroxyapatite (bone forming mineral) crystals and amorphous calcium phosphate.

4.3.3 Conclusions

A detailed investigation about the influence of adding increasing amounts of ZnO to partially replace MgO in a parent bioactive glass composition (TCP-20) was shown to have consequences in terms of sintering and crystallisation behaviours and on the relevant properties of the resulting glass-ceramics, including mechanical and biological responses. The glass forming ability of the glasses was unaffected by the level of MgO substitution. All the glass compositions investigated exhibited good sintering ability upon heat treating at 850 °C for 1 h thus, resulting in well sintered and mechanically strong glass-ceramics with diopside and fluorapatite as the primary crystalline phases. A minor crystalline phase (petedunnite) was also formed for ZnO > 4 mol%. The ZnO content also revealed to play an essential role on the *in vitro* bioactivity. The glass-ceramic composition with ZnO = 4 mol% exhibited the highest levels of mesenchymal cell proliferation and alkaline phosphatase activity, while further increasing ZnO contents led to a significant decrease in the *in vitro* performance of the investigated glass-ceramics.

4.4 Role of glass structure in defining the chemical dissolution behaviour, bioactivity and antioxidant properties of zinc- and strontium- co-doped alkali-free phosphosilicate glasses

4.4.1 Introduction

Since the chemical degradation of multi-component glasses is strictly related to their atomic and molecular structure [5] the design of bioactive glasses requires a thorough understanding of the relationship between their atomic/molecular structure and dissolution behaviour. In fact, it has been well established that the ionic dissolution products are key to understand the behaviour of their parent inorganic materials *in vitro* and *in vivo*, especially in the context of TE applications [195]. This relationship becomes more important when functional ions (for example: Sr^{2+} , Zn^{2+} , F^- , etc.) are incorporated in the glasses with an aim to enhance their biological efficacy because these ions interact with and modify the phosphosilicate glass matrix, thus, affecting the dissolution behaviour of resultant glass compositions. Therefore, it is of paramount importance to understand the influence of these functional ions on the structure and bioactivity of glasses so as to design glass compositions with controlled chemical dissolution and ion release rates.

Zinc and strontium are two such functional ions whose biological importance has been well documented in literature [42, 56, 59, 121]. Despite being present in trace amounts, both these ions play essential roles in the chemistry of bone [196, 197]. For this reason several studies describing the influence of zinc and/or strontium on various aspects of bioactive glasses and their properties have been reported in literature during the last few years [42, 58, 82, 114, 119-122, 198]. Further, most of the work on strontium and zinc co-doped bioactive glasses available in literature has been published by Boyd and co-authors [125, 154, 199-203] in the $\text{CaO-SrO-ZnO-Na}_2\text{O-SiO}_2$ glass system.

The present section aims at defining the structure-property relationships in a series of alkali-free phosphosilicate glass composition in Di-FA-TCP system co-doped with Zn^{2+} and Sr^{2+} . An attempt has been made to understand the structural role of Sr^{2+} and Zn^{2+} co-doping on the chemical dissolution behaviour of glasses and its impact on their apatite forming ability, osteoblast proliferation and antioxidant behaviour. The very promising glass composition TCP-20 discussed in section 2.1 was adopted as the starting point for synthesis of present series of glasses. The structure of the as-obtained glasses has been investigated by MAS-NMR while the biodegradation of glasses has been investigated by their immersion in Tris-HCl and SBF. Furthermore, the influence of glass structure and the

dissolution behaviour on osteoblast proliferation and oxidative stress levels has been discussed.

4.4.2 Results

4.4.2.1 Glass forming ability

For all the investigated glass compositions with varying Zn^{2+}/Mg^{2+} and Ca^{2+}/Sr^{2+} ratio: (mol%) (36.07-x) CaO – xSrO – (19.24-x) MgO – xZnO – 5.61P₂O₅ – 38.49SiO₂ – 0.59 CaF₂ (x = 0–10), melting at 1570 °C for 1 h was sufficient to obtain bubble-free, transparent and XRD-amorphous glasses (Figure 4.4.1). Table 4.4.1 presents the detailed compositions of the as-designed glasses.

Table 4.4.1 Nominal composition of the as-designed glasses (mol%).

Glass	CaO	MgO	SiO ₂	P ₂ O ₅	ZnO	SrO	CaF ₂
ZS-0	36.07	19.24	38.49	5.61	0.00	0.00	0.59
ZS-2	34.07	17.24	38.49	5.61	2.00	2.00	0.59
ZS-4	32.07	15.24	38.49	5.61	4.00	4.00	0.59
ZS-6	30.07	13.24	38.49	5.61	6.00	6.00	0.59
ZS-8	28.07	11.24	38.49	5.61	8.00	8.00	0.59
ZS-10	26.07	9.24	38.49	5.61	10.00	10.00	0.59

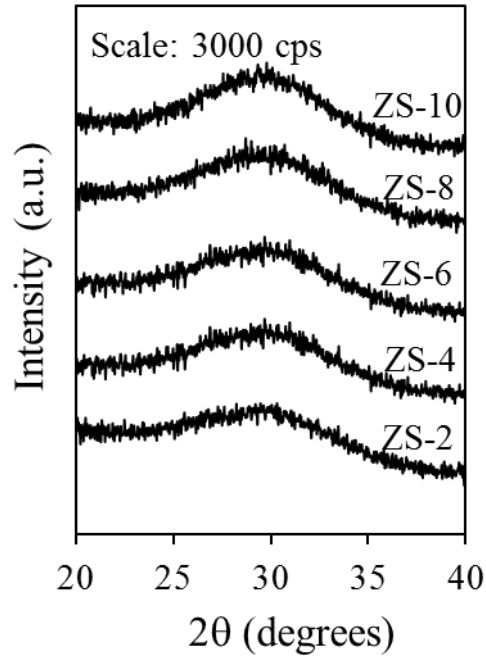


Figure 4.4.1 X-ray diffractograms of glass powders

4.4.2.2 Structure of glasses

The ^{29}Si MAS-NMR results of all the glasses as presented in Figure (4.4.2a, 4.4.3a), depict the dominance of Q^2 (Si) structural units in the glasses. Furthermore, the dominance of Q^2 structural units is confirmed by the quantitative analysis of deconvoluted NMR spectra (Table 4.4.2b). The Q^n distributions for the three compositions are rather close to each other, i.e. the silicate distribution is dominated by Q^2 chain species, with substantial amounts of chain-terminators Q^1 and branched Q^3 species. Further, only slight shift in the peak positions of spectra could be observed and all the spectra are centred between -81 ppm and -82 ppm, thus depicting no significant changes in the silica coordination in glass structure. The ^{31}P MAS-NMR spectra of all the glasses (Figure 4.4.2b) and the corresponding de-convolution (Table 4.4.3) show a predominance of orthophosphate-type species with chemical shifts centred at around 2–2.5 ppm, close to that of the calcium orthophosphate (3.1 ppm) [137]. Besides the dominant Q^0 orthophosphates, Table 4.4.3 also highlights the presence of non-negligible amounts of non-orthophosphate species, in agreement with the MD models, a phosphorus environment thus qualitatively similar to that found for the 45S5 glass [127, 167]. Similar results were obtained for alkali-free bioactive glasses doped with ZnO and SrO on independent basis where insignificant influence on silicate network connectivity was observed by varying SrO/CaO ratio [204] or ZnO/MgO [42] ratio in the glasses while most of the phosphorus component was found in orthophosphate environment.

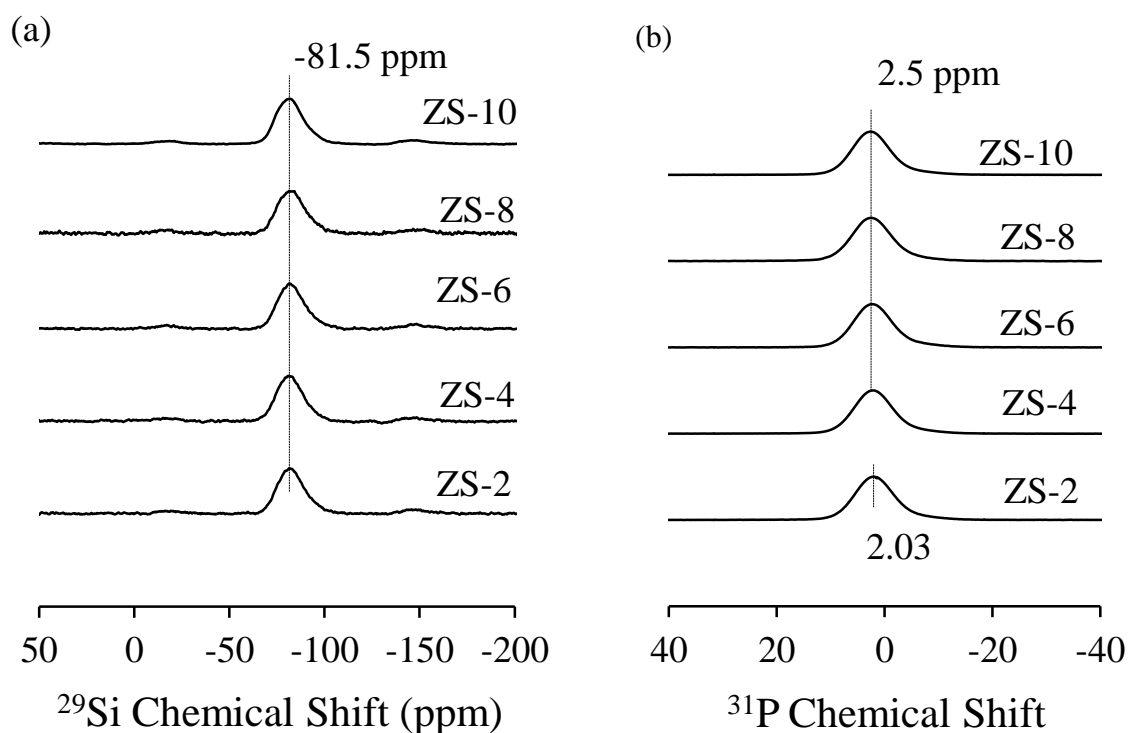


Figure 4.4.2 MAS NMR spectra of investigated glasses showing the peak positions of (a) ^{29}Si and (b) ^{31}P .

Thus NMR results shows that $\text{Zn}^{2+}/\text{Mg}^{2+}$ and $\text{Ca}^{2+}/\text{Sr}^{2+}$ substitutions do not affect the silicate network connectivity of these glasses.

Table 4.4.2 Q^n (Si) distribution for glasses ZS-4 and ZS-10 obtained by NMR deconvolution.

Q^n	ZS-4		ZS-10	
	peak position (ppm)	% integral	peak position (ppm)	% integral
Q^0	-66.5	0.3	-66.0	0.3
Q^1	-75.7	22.7	-75.8	28.8
Q^2	-81.7	50.6	-82.6	48.0
Q^3	-88.3	24.1	-90.5	22.7
Q^4	-96.7	2.2	-107.4	0.1

Table 4.4.3 Q^n (P) distribution for glasses ZS-4 and ZS-10 obtained by NMR deconvolution.

Q^n	ZS-4		ZS-10	
	peak position (ppm)	% integral	peak position (ppm)	% integral
Q^0 (Ca)	3.2	52.3	3.2	67.4
Q^0 (Mg)	0.5	27.5	0.8	17.3
Q^1	-1.0	20.3	-1.9	15.2
Q^2	-	-	-	-

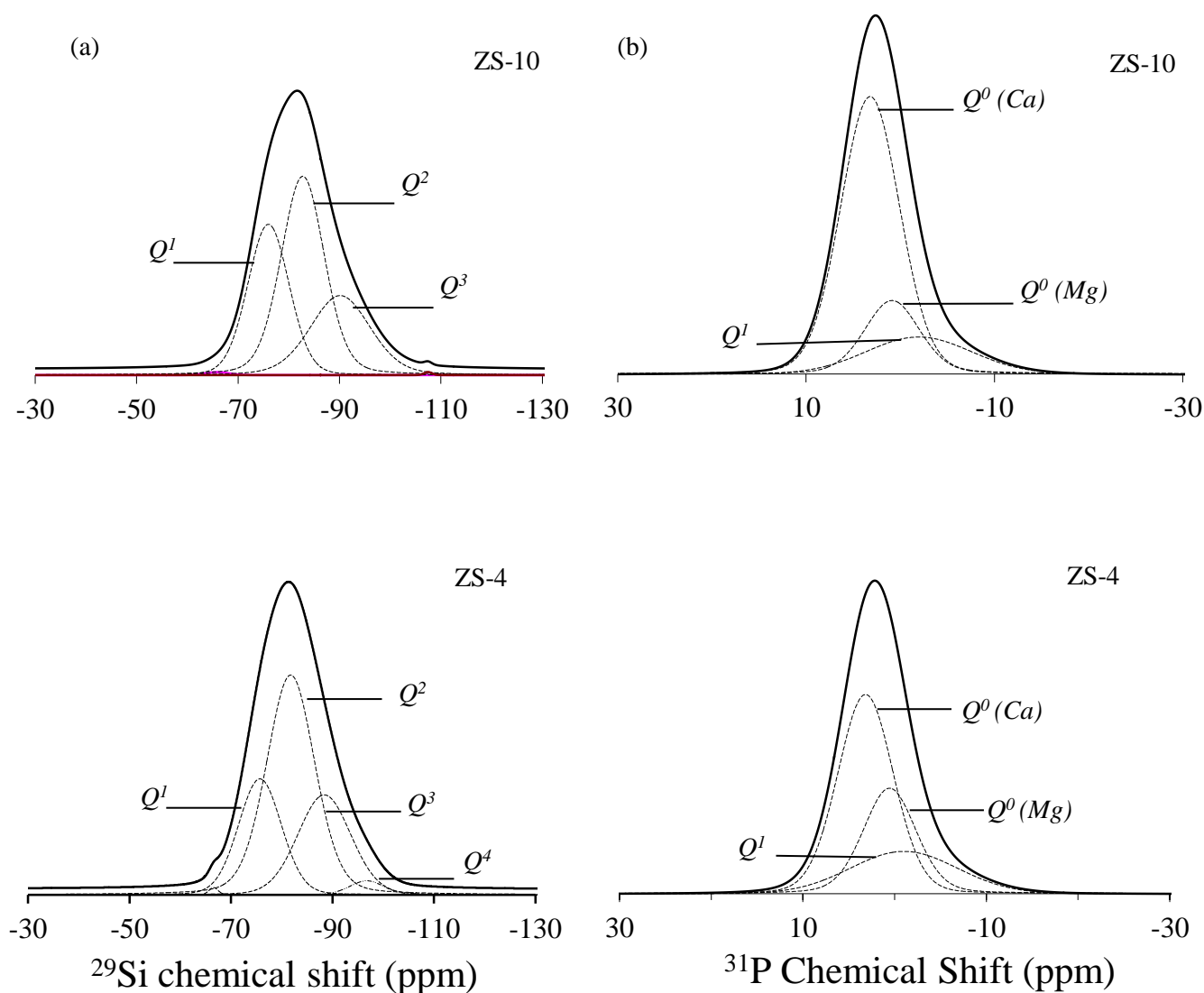


Figure 4.4.3 (a) ^{29}Si MAS NMR spectra and (b) ^{31}P MAS NMR spectra after deconvolution of investigated glasses.

4.4.2.3 SBF immersion studies

In the present case, FTIR spectra of all the glass powders before immersion in SBF solution are presented in Figure 4.4.4a. All the investigated glasses show three broad bands in 350–1300 cm^{-1} region. The broadness clearly shows the disorder in the glass structure with uneven distribution of Q^n units. The band ranging from 800–1300 cm^{-1} corresponds to presence of two optical modes of Si–O–Si groups: Si–O bending mode identified around 800 cm^{-1} and the asymmetric stretching mode Si–O (s) in 1000–1300 cm^{-1} region. The $\sim 500 \text{ cm}^{-1}$ band can be attributed to Si–O–Si bending modes, while the weak shoulder around $\sim 750 \text{ cm}^{-1}$ may be due to Si–O–Si symmetric stretching with simultaneous Si cations motion [205]. Further, the band centred around 559 cm^{-1} corresponds to P–O bending modes [206].

The immersion of glass powders in SBF for varying time durations led to a considerable change in the glass chemistry which is evident from the FTIR data presented in Figure 4.4.4b–4.4.4d. The soaking of glass powders in SBF for 1 h resulted in the appearance of a strong low frequency band around $\sim 503 \text{ cm}^{-1}$ (Figure 4.4.4b) typical for the deformation mode of silica gel-like layer. In addition to that the main IR band now appeared at 1051 cm^{-1} along with a weak shoulder at 1180 cm^{-1} which could be assigned to Si–O–Si stretching vibrations [206]. These bands indicate the development of interfacial high-area silica gel layer, as postulated in Hench's inorganic reactions set [20] and can be observed in all the glasses. The peaks around $\sim 560, 600, 1035 \text{ cm}^{-1}$ present in all the glasses are evidence for the formation of crystalline hydroxyapatite and other crystalline phosphate species as these bands correspond to P–O bending vibrations in a PO_4^{-3} tetrahedron. Further, the bands at 1296 cm^{-1} and 1461 cm^{-1} corresponding to the formation of complex carbonate species imply towards formation of carbonated HA. It is noteworthy that formation of any calcium carbonate (CaCO_3) polymorphs has been negated considering their absence in the XRD data obtained on glasses after immersion in SBF solution as shown in Figure 4.4.5.

The XRD data obtained on glass powders after immersion in SBF solution for varying time durations support the FTIR results as all the glasses exhibit well defined characteristic X-ray peak at $2\theta = 31.77^\circ$ corresponding to the formation of crystalline hydroxyapatite [HA; $(\text{Ca}_5(\text{PO}_4)_3\text{OH})$; ICDD: 00–09–0432] after 1 h of immersion (Figure 4.4.5).

The intensity of the XRD phase reflections for HA increased with increase in SBF immersion time, thus, depicting the high apatite forming ability of these glasses. Interestingly, the apatite forming ability of same parent glass (ZS–0) was observed to decrease considerably when doped with SrO (at the expense of CaO) or ZnO (at the expense of MgO) on individual basis as has been reported in our previous articles [42, 204].

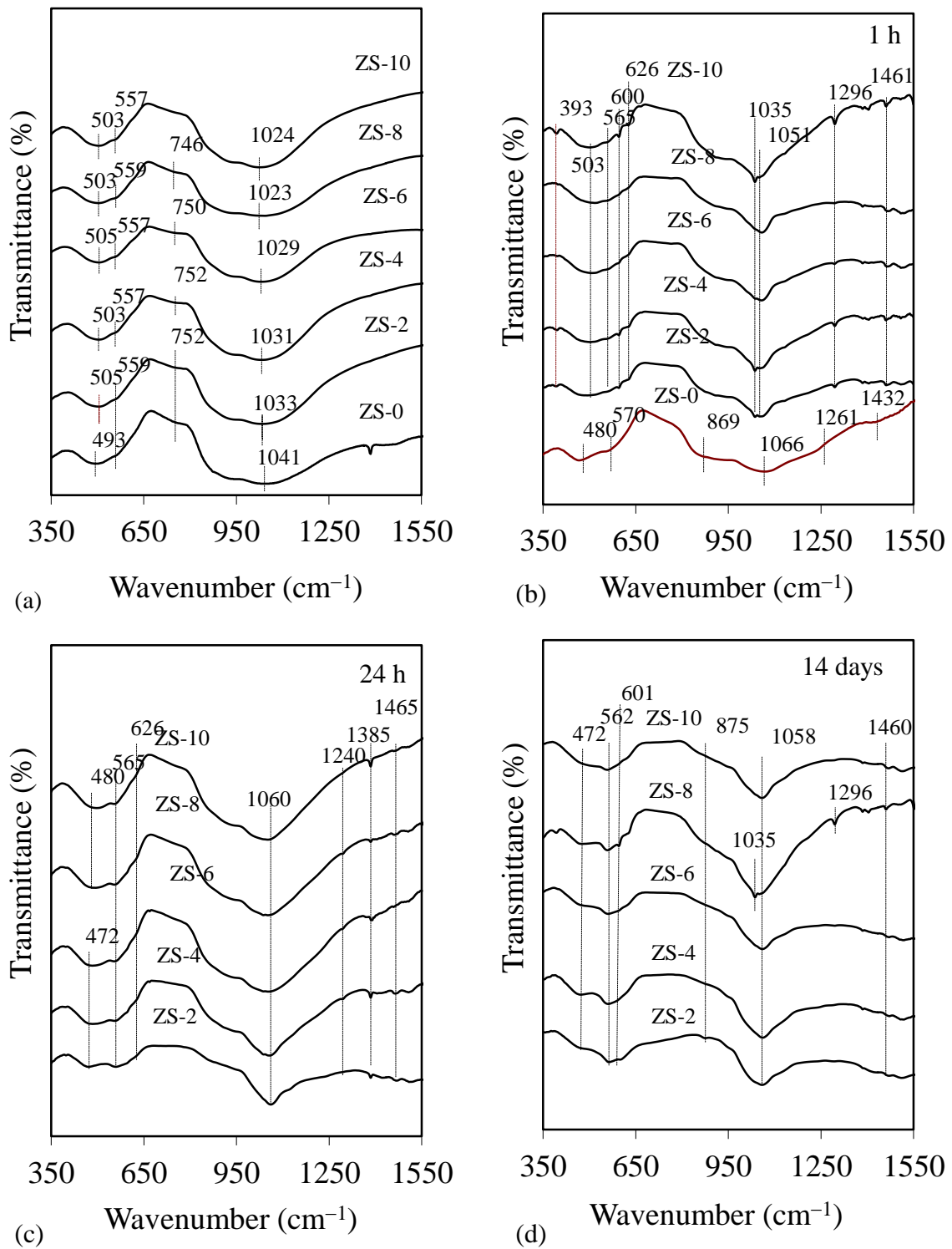


Figure 4.4.4 FTIR spectra of glass powders (a) before, after (b) 1h, (c) 24h, and (d) 14 days immersion in SBF.

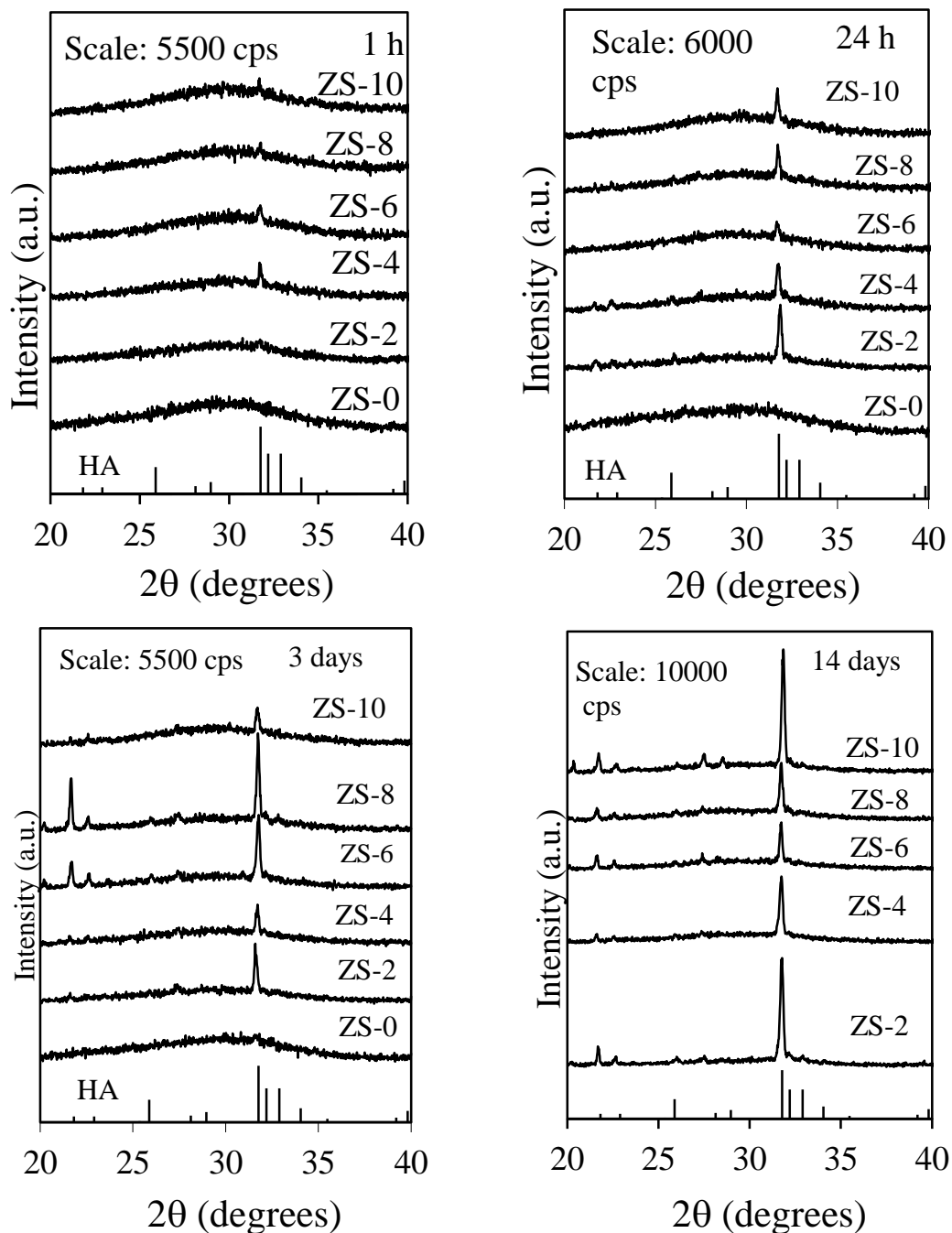


Figure 4.4.5 X-ray diffractograms of glass powders after immersing the glass powders in SBF solution for (a) 1 h (b) 3 h (c) 6 h (d) 24 h (e) 3 days and (e) 14 days.

In order to gain a better insight into the glass dissolution process and apatite forming ability of the investigated glasses, the elemental release profile of these glasses was studied when immersed in SBF solution for initial 24 h. The trends observed for variation in concentration (mg l^{-1}) of different ionic species (Ca^{2+} , Mg^{2+} , PO_4^{3-} , SiO_4^{4-} , Zn^{2+} , Sr^{2+}) in SBF detected during initial 24 h are presented in Figure 4.4.6. The results obtained have been summarized below:

- i) The trend of Ca^{2+} concentration after 1 h of immersion corresponds to an increase for all glasses which reaches its maximum within 12 h of immersion in SBF solution (Figure 4.4.6a). The increasing Ca^{2+} concentration in SBF during initial immersion for all glasses imply towards the initiation of the bio-mineralization process, where modifier cations in the glass exchange with hydronium ions in the external solution [20]. This increase in the Ca^{2+} concentration may be attributed to the exchange of Ca^{2+} with the hydronium ion present in the SBF solution due to disruption of the glass network. Thereafter, a kind of saturation plateau is reached for all the investigated glasses. The similar dissolution behaviour for all the glass compositions may be ascribed to the similar network connectivity exhibited by all the glasses. The release of Ca^{2+} seems to depend on their actual concentration in parent glasses as increasing SrO/CaO ratio in glasses decreased the Ca^{2+} ion release concentration in the SBF solution.
- ii) The concentration of PO_4^{3-} follows steadily decaying profiles, an indication that the dissolution rate from glasses is lower than the rate of surface deposition of such species.
- iii) The Mg^{2+} ion concentration profile is similar to that of Ca^{2+} in SBF solution and was detected to be highest after 12 h of immersion time for all the glass compositions while no significant variations were observed after prolonged SBF immersions (Figure 4.4.6c), possibly due to attainment of equilibrium between the Mg^{2+} concentration in glass and SBF. In general, the amount of Mg detected after any particular immersion time was highest for ZS-2 and lowest for ZS-8 possibly due to higher magnesium content in ZS-2 as compared to ZS-8.
- iv) Sr^{2+} can accumulate in bone by exchanging with Ca^{2+} in the hydroxyapatite crystal lattice due to the chemical analogy to Ca^{2+} . As shown in Figure 4.4.6d, glass compositions up to ZS-4 exhibit Sr release profiles that are similar to other alkaline earth ions for all compositions with a maximum after 12 h of immersion in SBF solution. With further increasing the ZnO and SrO content to ZS-8, the strontium release profile was observed to steadily increase beyond 12 h. Although we did not make elemental analysis of the SBF solution obtained after immersion of glass ZS-10 for varying time durations, a similar behaviour is expected from this glass too.
- v) In general SiO_4^{4-} ion concentration increases with increase in immersion time, thereafter reaching a saturation plateau after 6–12 h of immersion (Figure 4.4.6e). It is worth noting that Si concentrations reached highest values for ZS-2, an indication that the chemical resistance of glasses somewhat increased with increasing added amounts of doping ions.
- vi) The Zn ion release profiles for the investigated glasses over 24 h are shown in Figure 4.4.6f. In all the investigated glasses the Zn ion concentration in SBF increases with 1 h of immersion time, thereafter decreases to a saturation value. Zn^{2+} release from these

glasses appears to be independent from the Zn content in the glasses. Also it is worth noting that co-doping of glasses with SrO and ZnO does not prevent the formation of HA on the glasses.

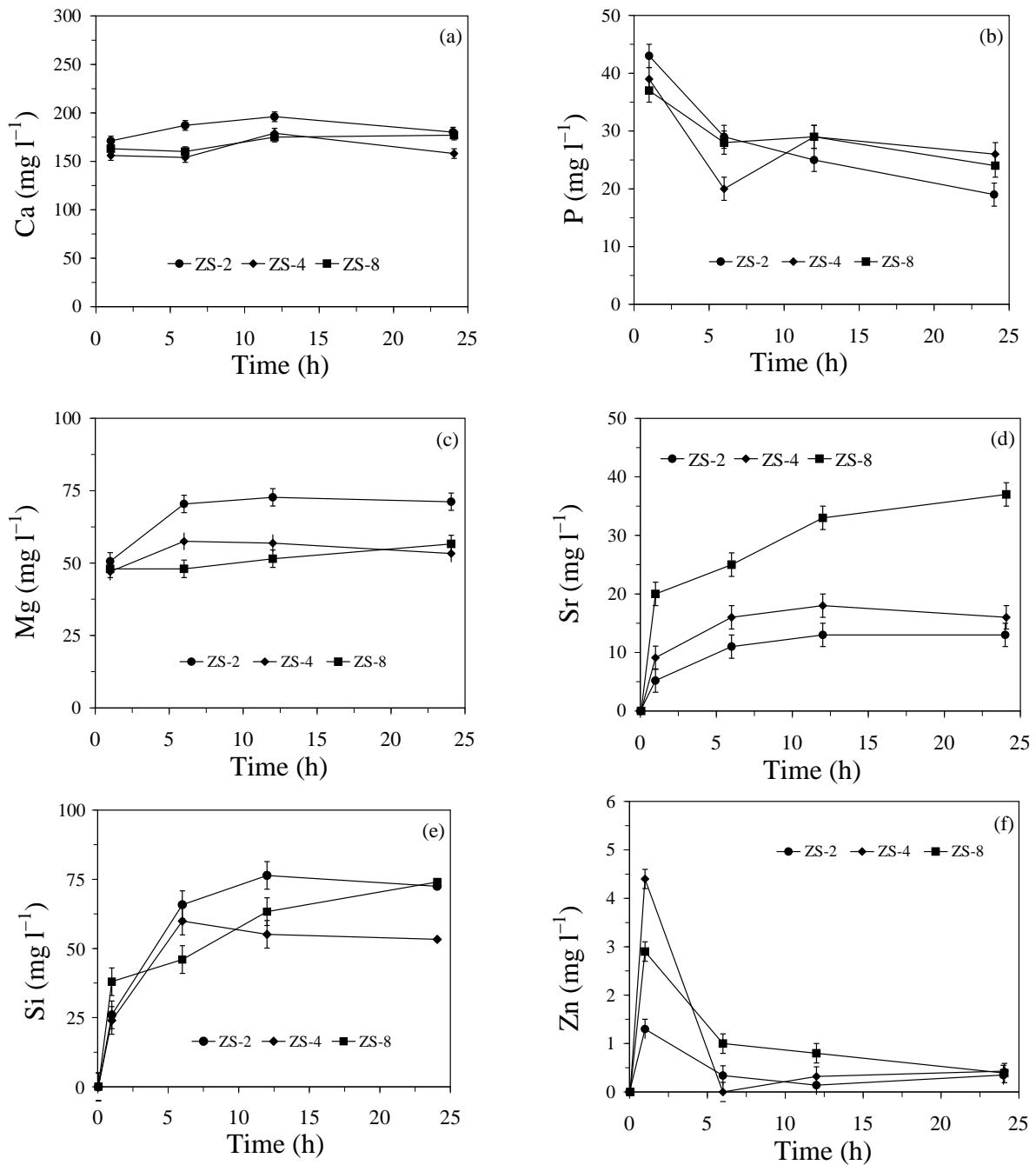


Figure 4.4.6 ICP plots of elemental concentration of (a) Ca, (b) P, (c) Mg, (d) Sr, (e) Si and (f) Zn, in SBF solution versus immersion time for the investigated glass powders.

4.4.2.4 Chemical degradation of glasses in Tris-HCl

All the glasses were XRD amorphous after immersion in Tris-HCl for 120 h, thus negating the possibility of any phase formation due to chemical reaction between the dissolution products (Figure 4.4.7).

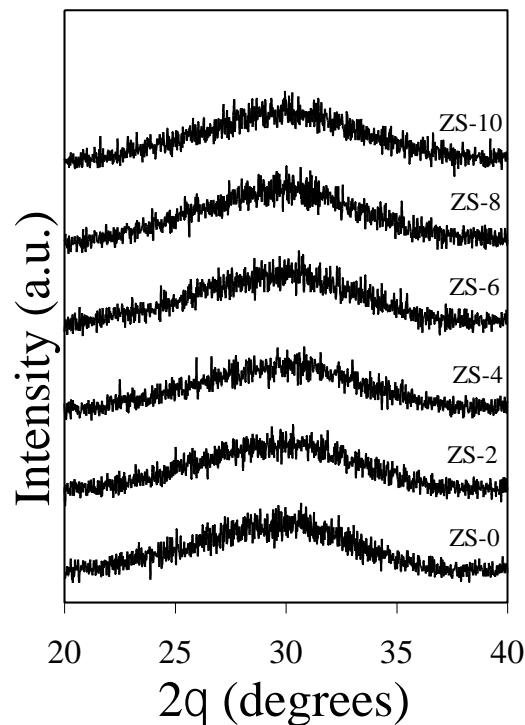


Figure 4.4.7 X-ray diffractograms of glass powder after 120 days of immersion in TRIS-HCL

The variation in pH of Tris-HCl along with weight loss of the glasses with respect to SrO and ZnO content in glasses is presented in Figure 4.4.8a. A slight change in pH of Tris-HCl from 7.54 to 7.24 was observed with increasing SrO and ZnO content in glasses after 120 h of immersion. This depicts good chemical stability of glasses which in turn should support cell viability due to the absence of sudden pH changes in the dissolution medium. A steep decrease in the weight loss of glass was observed with increasing equimolar concentrations of ZnO and SrO content up to 6 mol%. Further increase in ZnO and SrO content in glasses did not lead to any significant change in the weight loss of glasses.

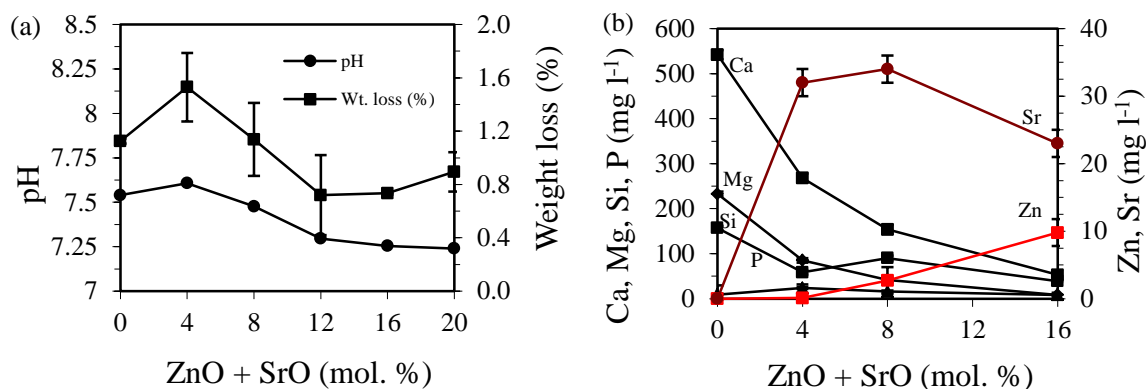


Figure 4.4.8 (a) Graphs depicting the change in solution pH and weight loss of glass powder samples (with respect to variation in ZnO and SrO content in glasses) after immersion in Tris-HCl; (b) ICP-AES plots of elemental concentrations of Ca, Mg, P, Si, Sr and Zn in Tris-HCl after 120 h of immersion of glass powder. It should be noted that Si refers to SiO_4^{4-} and P refers to PO_4^{3-} species.

With respect to the ion release profile the ICP-OES analysis revealed that studied glasses demonstrated SiO_4^{4-} ion release in the range of 39–157 ppm (1 ppm = 1 mg l⁻¹). Also increasing strontium and zinc content in the glasses decreased the release of SiO_4^{4-} species in Tris-HCl as shown in Figure 4.4.8b, thus explaining the lower chemical degradation of glasses. Previous studies have shown that SiO_4^{4-} release levels in the range 0.1–100 ppm from bioactive glass and other biomaterials show stimulatory effects on osteoblasts and the expression of TGF- β mRNA in human osteoblast-like cells [207]. Furthermore, gradual release of soluble silica over time enhances bone bonding due to the increased formation of Si-OH (silanol) groups. Therefore, it is apparent that any bioactive glass releasing SiO_4^{4-} within these ranges will have similar beneficial effects. Hence, all the glasses in the present study may possess beneficial properties towards various biological processes.

Phosphorus being a major component of the inorganic phase of human bone plays an important role in bone formation as mentioned in section 2. In the present study, the ionic concentration of phosphorus released (8.6–24 ppm; Figure 4.4.8b) from the glasses in Tris-HCl lies within the above mentioned limit required to promote favourable biological activity.

Further, Ca^{2+} ion release from experimental glasses in Tris-HCl solution decreased from 268–53 ppm (Figure 4.4.8b) probably owing to the decrease in CaO concentration in glasses. The significance of calcium in bone mineralization is well established and its gradual release over time is bound to enhance therapeutic efficacy of the glasses. Similarly, Magnesium concentration in the extracellular fluid ranges within 17–25.5 ppm. In the present

study the concentration of Mg^{2+} released from the investigated glasses in Tris–HCl solution is higher than the concentration vital for favourable biological properties. However, due to efficient excretion of Magnesium in the urine, incidences related to hyper–magnesium conditions are rare [60]. With respect to release of strontium and zinc from the studied glasses, all the glasses demonstrated a release of 23–32 ppm of strontium and 0.1–9.8 ppm of zinc over 5 days of immersion in Tris–HCl (Figure 4.4.8b). Although, the amount of strontium released from glasses is within the limits of its therapeutic efficacy, the amount of zinc released from glasses with ZnO content >4 mol% is slightly higher than required for biomedical purpose.

4.4.2.5 Cellular response on bioactive glasses

4.4.2.5.1 In vitro proliferation of MG63 cells

Figure 4.4.9 depicts the cell viability on glasses under investigation in comparison with commercially available culture plates, of ZS–2, ZS–4, and ZS–6 and ZS–8 bioactive glasses. MG-63 cells were used for the following reasons firstly, MG-63 cells display suitable integrin molecules required for cell adhesion making them a more appropriate model under the present study, secondly the response of MG-63 cells to 1,25(OH)₂D₃ administration has been shown to be similar to normal human osteoblast cells [208]. Additionally, human and MG63 cells produce cAMP in response to Parathyroid hormone therapy [209, 210]. Moreover, MG-63 cells provide an excellent model for studying the antioxidant properties of bioactive glasses as they have been used in variety of studies especially for their use in capsaicin induced apoptosis via the caspase cascade and the antioxidant enzyme system and Okadaic acid induced apoptosis through the PKR, NF- κ B and caspase pathway. These pathways are similar to the apoptotic death caused by H₂O₂ used and oxidizing agent in the present study which have earlier been used to studying protection of MG63 cells by Melatonin and Simvastatin [211, 212]. Apparently, the proliferation of MG63 cells was 89.0±4.2%, 86.7±3.9%, 80.25±3.6% and 72.8±3.1% on glasses ZS–2, ZS–4, ZS–6 and ZS–8, respectively (Figure 4.4.9a).

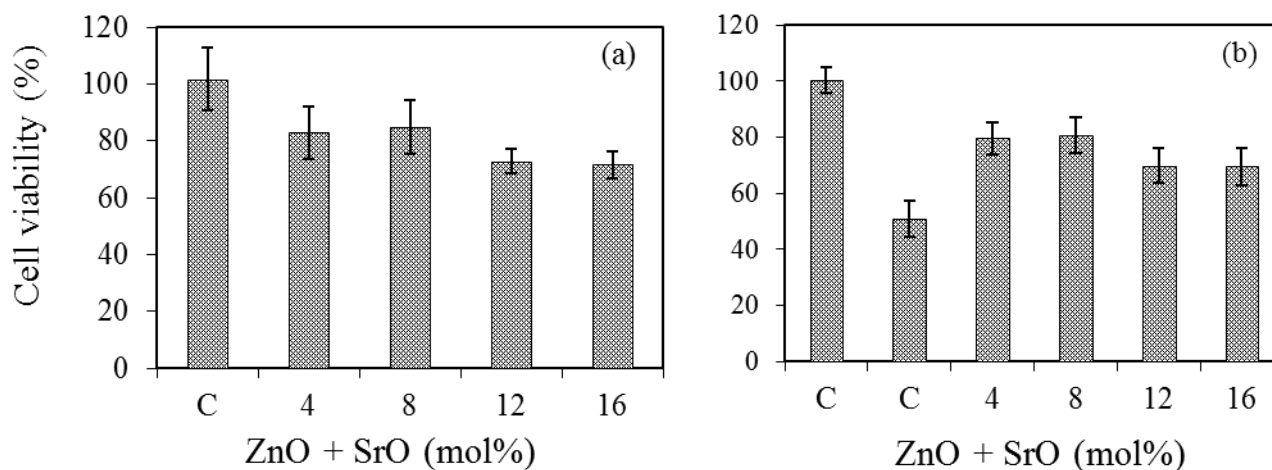


Figure 4.4.9 Plots showing the cell growth kinetics of the glasses (ZS-2, ZS-4, ZS-6, and ZS-8) (a) under normal condition during culture after 4 days under normal conditions (b) under H₂O₂ (250 μM) induced oxidative stress in MG63 cell after 3 days. *(C for control)

The antioxidant potential of investigated glasses was examined on H₂O₂ induced oxidative damage in MG63 cell line after 24 h of cell growth. H₂O₂ is one major contributor to the oxidative damage and leaks from mitochondria in the cells. According to Li et al. [213] H₂O₂ stops cells proliferation in MG63 cells by reducing the levels of cycline B1 and induction of G₂ cell cycle arrest. Although, the cell viability was higher (in comparison to control) in the presence of Sr- and Zn-doped bioactive glasses under investigation; interestingly, the cell viability decreased for SrO- and ZnO-concentration in glasses beyond ZS-4, as is evident from Figure 4.4.9b. Accordingly, the highest cell viability under oxidative stress was observed for glass ZS-2 (163%) followed by ZS-4 (151%), ZS-6 (138%) and ZS-8 (135%) when compared with control cultures at LD50 dose of H₂O₂ (Figure 4.4.9b).

4.4.3 Discussion

From MD simulation results [214], the network connectivity (NC) in the investigated glasses is ~1.95. Based on the qualitative interpretation of the correlation between solubility and NC, an empirical upper limit of NC~3 has been defined separating bioactive (NC <3) from bio-inert (NC >3) glasses [39]. According to O'Donnell and Hill [112], melt-quenched silicate glasses with NC = 2 are good candidates for bioactive materials as biological response and other properties of glasses rapidly change around this value. Inert glasses with NC below 2 usually exhibit very high dissolution rates (due to highly depolymerized glass structure), being considered less practical in biological systems [112]. However, this

empirical interpretation based on NC should be considered only as a qualitative guideline for designing bioactive glasses. As a matter of fact, our investigated glasses having a NC <2 would be expected to exhibit excessive dissolution rates and unsuitable bioactivity, which is at odds with their apatite forming ability in SBF (Figure 4.4.5) and very moderate weight loss in Tris–HCl shown in Figure 4.4.8a.

Further, the ^{29}Si MAS–NMR data reveal the predominance of Q^2 units along with considerable fraction of $Q^1(\text{Si})$ and $Q^3(\text{Si})$ in all the glasses (Table 4.4.2). The phosphate component in the glass is predominantly coordinated in orthophosphate environment thus, not contributing to the glass network backbone. This is again a desired feature because the low connectivity of phosphorus in the glass structure along with its ability to rip off the network modifying cations (mainly Ca^{2+}) from the silicate network not only facilitates the release of additional soluble phosphate species into the contact fluid which will increase the local supersaturation but also accelerate the bone bonding ability of glass by enhancing the HA deposition on the glass surface.

The network modifying role of SrO/CaO along with the intermediate role of ZnO/MgO seems to play the major role in deciding the biological efficacy of the investigated glasses. This is evident from the significant disparity in the leaching behaviour of ZnO and SrO from glasses in SBF solution or Tris–HCl despite the fact that both these oxides have been incorporated in the glasses in the equimolar concentrations. The slow release of zinc (due to its ability to enhance the strength of inter-tetrahedral cross-links) and the comparatively faster release of strontium along with other elements help in enhancing the osteoblast proliferation and anti-oxidative properties of the studied glass compositions. According to literature, strontium when released in concentrations of <10 ppm has the ability to inhibit H_2O_2 induced oxidative stress in osteoblasts (CRL-11372) within a duration of 6–12 h [215]. For concentrations >87.6 ppm, strontium becomes an apoptotic agent and induces the apoptotic effect of H_2O_2 [215]. The blood active Sr^{2+} concentration in postmenopausal osteoporotic patients treated with strontium ranelate (Protelos[®], Servier Laboratories, Ireland) has been measured to be 10.5 ppm [56]. On the other hand, zinc concentrations have been observed to follow a strict dose-dependent behaviour with their therapeutic efficacy being restricted to the dose limits of <2 ppm. According to Aina et al. [157], when the concentration of zinc released from bioactive glasses exceeds 2 ppm, it causes damage to the osteoblasts (MG63) *via* oxidative stress. In a similar study, Bergandi et al. [216] explained the role of fluoride ions released from F-doped 45S5 Bioglass[®] in inducing the oxidative stress when in contact with MG63 human osteoblast cell line due to inhibition of the pentose

phosphate oxidative pathway and, in particular, through the oxidative inhibition of glucose 6-phosphate dehydrogenase. A similar observation has been made in the present study as the glass ZS-2, which releases <1.5 ppm zinc and ~10 ppm strontium in SBF (Figure 4.4.6) exhibits antioxidant behaviour by enhancing the cell viability and negating the effect of oxidative stress induced by H₂O₂ addition in the cell culture medium. Further increasing the ZnO and SrO contents in glasses led to an increase in their released zinc and strontium concentrations. However, the decrease of their antioxidant behaviour could only be clearly noticed for the glass compositions with their respective ZnO and SrO content ≥ 6 mol%. Interestingly, although our glasses contain equimolar concentrations of ZnO and SrO, the release of Sr²⁺ into the SBF or Tris-HCl solutions is significantly higher than that of Zn²⁺. This depicts the importance of the structural coordination of zinc ions as intermediate in the glass structure (at variance with the stronger network modifying role of strontium, and its higher ionic field strength in comparison to strontium).

Oxidative stress plays a prominent role in bone healing and regeneration. It arises due to the formation of reactive oxygen species (ROS). ROS ($\bullet\text{O}_2^-$, $\bullet\text{OH}$, H₂O₂, OCl⁻, etc.), which are generally produced in cellular mechanisms during conversion of oxygen to water (in order to produce energy) by mitochondria or during an encounter between white blood cells (WBCs) and pathogens in our body [217]. In case of a bone fracture, oxidative stress injury may be caused by an ischemia-reperfusion mechanism. In such a scenario, tissue damage is caused due to oxidative stress when blood supply returns to the tissue after a period of lack of oxygen. These radicals may cause oxidative injury to the fractured bone as has been seen in other tissues with reperfusion injury [218, 219]. The protection of MG63 cell line from H₂O₂ induced oxidative stress in the present study by alkali-free bioactive glasses (mainly by glasses ZS-2 and ZS-4) may be attributed to the anti-apoptotic effect of zinc and strontium when released in a controlled manner. It has been recently reported that zinc is involved in direct inhibition of H₂O₂ induced apoptosis by activation of the P13K/Akt and MAPK/ERK pathways [220], while in case of strontium, a recent study by Jebahi et al. [221] reports an increase in the Superoxide Dismutase (SOD), Catalase (CAT) and Glutathione Peroxidase (GPx) *in vivo* as the prominent features providing antioxidant behaviour to the materials doped with these trace elements. In the overall context of bone healing and regeneration, the as designed glasses are potential candidates for applications in the treatment of osteoporosis.

4.4.4 Conclusions

The effects of co-doping of zinc and strontium on the structure, chemical dissolution behaviour of alkali-free phosphosilicate glasses and its impact on their apatite forming ability, osteoblast proliferation and antioxidant behaviour have been studied with NMR, FTIR, XRD, chemical degradation and cell culture experiments. An increase in the Zn^{2+}/Mg^{2+} and Sr^{2+}/Ca^{2+} ratio did not induce any significant change in Q^n speciation and network connectivity, as revealed by MAS-NMR. The chemical durability of investigated glass improved (as observed from Tris-HCl studies), however all the glasses exhibit good apatite forming ability. The glass ZS-2 which releases < 1.5 ppm zinc and ≤ 10 ppm strontium in SBF, is exhibiting good antioxidant behaviour by enhancing the cell viability and negating the effect of oxidative stress induced by H_2O_2 addition in the cell culture medium. However, further increase in ZnO and SrO content in glasses led to an increase in their released zinc and strontium concentrations, thus, decreasing their antioxidant behaviour. Thus zinc concentration < 1.5 ppm has an anti-oxidant effect. The anti-oxidant behaviour may be attributed to the anti-apoptotic effect of zinc and strontium when released in a controlled manner. Although promising results suggest possible clinical use of bioactive glass, further investigations of long-term outcomes are going on for the glass to be used in orthopaedic applications.

4.5 Thermo-mechanical behaviour of alkali-free bioactive glass-ceramics co-doped with strontium and zinc

4.5.1 Introduction

TE has emerged as an effective approach in response to the challenges in reconstructive and orthopaedic surgeries which involve restoring the diseased or damaged tissue by applying a combination of functional cells and scaffolds made of synthetic biomaterials. TE offers a feasible solution to the problems associated with the allograft and autograft [23]. This approach requires scaffolds with a well-defined architecture which not only provide temporary mechanical strength but also act as guiding channels for cell proliferation and tissue ingrowths [161]. The ideal scaffold should (i) be biocompatible (non-toxic) and should promote cell adhesion and proliferation; (ii) exhibit mechanical properties that are comparable to those of the tissue to be replaced; (iii) exhibit controlled degradation rate and should degrade into nontoxic products that can be easily resorbed or excreted by the body; and (iv) be capable of being machined easily into required shapes [161]. All these properties are highly dependent on the substrate material properties and it is due to this reason that the choice of the material plays an important role in designing a suitable scaffold.

In today's scenario, bioactive glass-ceramics are considered to be potential materials for bone TE because of a number of salient features not only in relation with their good bioactivity but also owing to their good sintering ability, high mechanical strength and controlled chemical degradability [141, 189, 206]. The aim of the present section is understand the influence of co-doping of Zn^{2+} and Sr^{2+} on the thermal and mechanical behaviour of TCP-20. Although, good amount of literature is available on the influence of these two ions on various properties of bioactive glasses on individual basis as mention in section 4.4, it is rare to find literature describing the influence of both these ions on thermal behaviour of glasses.

4.5.2. Results and Discussion

4.5.2.1 Glass-forming ability

For all the investigated glass compositions shown in Table 4.4.1, melting at 1570 °C for 1 h was sufficient to obtain bubble-free, transparent and XRD-amorphous glasses.

4.5.2.2 Thermal analysis

The DTA thermographs of fine glass powders with $\beta = 20 \text{ K min}^{-1}$ are shown in Figure 4.5.1. All the glass compositions feature a single endothermic dip which corresponds to T_g before T_c followed by an exothermic crystallization curve. The characteristic parameters obtained from DTA thermographs are summarized in the Table 4.5.1. In general, T_g decreases with increase in SrO and ZnO content in glasses. This decrease in T_g can be attributed to decrease in oxygen density (ρ_o) of glasses with addition of SrO and ZnO as shown in Figure 4.5.2. Oxygen density is a measure of compactness of the glass structure and can be calculated by using the following relation [114]:

$$\rho_o = \frac{M(O) \times (2x_{SiO_2} + 5x_{P_2O_5} + x_{SrO} + x_{CaO} + x_{ZnO} + x_{MgO})}{M_v}$$

Where, $M(O)$ is the molecular mass of oxygen atom and x corresponds to the molar concentration of the respective oxides and M_v corresponds to the molar volume of the glasses. In general, the decrease in oxygen density points towards the expansion of glass structure resulting in the weakening of the glass network and an associated decrease in T_g .

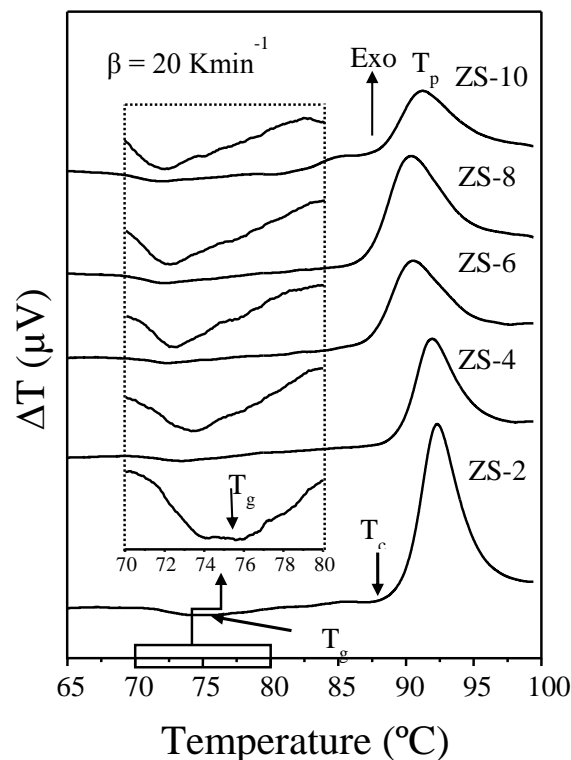


Figure 4.5.1 DTA thermographs of glasses at a heating rate of 20 K min^{-1} .

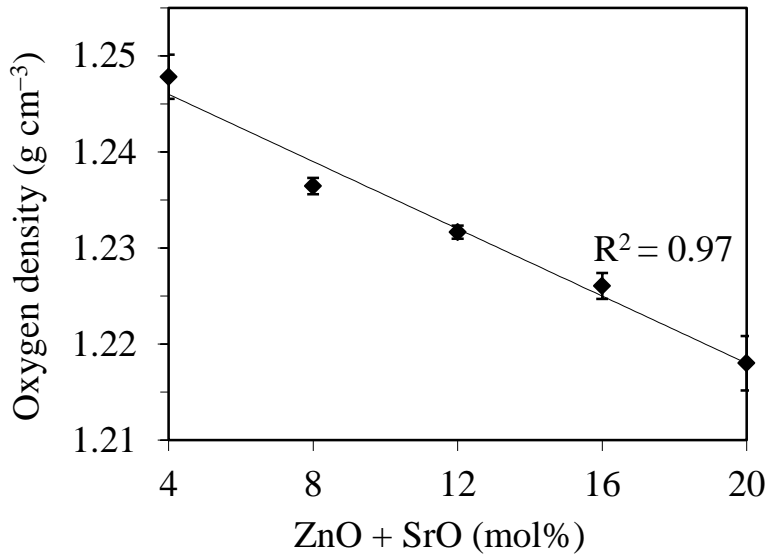


Figure 4.5.2 Oxygen density plotted against percentage zinc and strontium substitution.

Table 4.5.1 Thermal parameters measured from DTA at 20 K min⁻¹.

	ZS-2	ZS-4	ZS-6	ZS-8	ZS-10
T _c (±2 °C)	885	884	871	866	870
T _g (±2 °C)	756	734	725	721	720
ΔT(=T _c -T _g)	129	150	146	145	150

4.5.2.3 Sintering and Crystallization behaviour

Figure 4.5.3 presents variation in the relative area and heat flow with respect to temperature as obtained from HSM and DTA, respectively, for all the investigated glasses at a similar heating rate of 5 K min⁻¹. Table 4.5.2 summarizes the values of the temperature of first shrinkage (T_{FS}; log η = 9.1 ± 0.1, η is viscosity in dPa s), temperature for maximum shrinkage (T_{MS}; log η = 7.8 ± 0.1) and ratio of the final area/initial area of the glass powder compact (A/A₀) at T_{MS1}, as obtained from the HSM data along with temperature for T_c and T_p, as obtained from the DTA of the glasses.

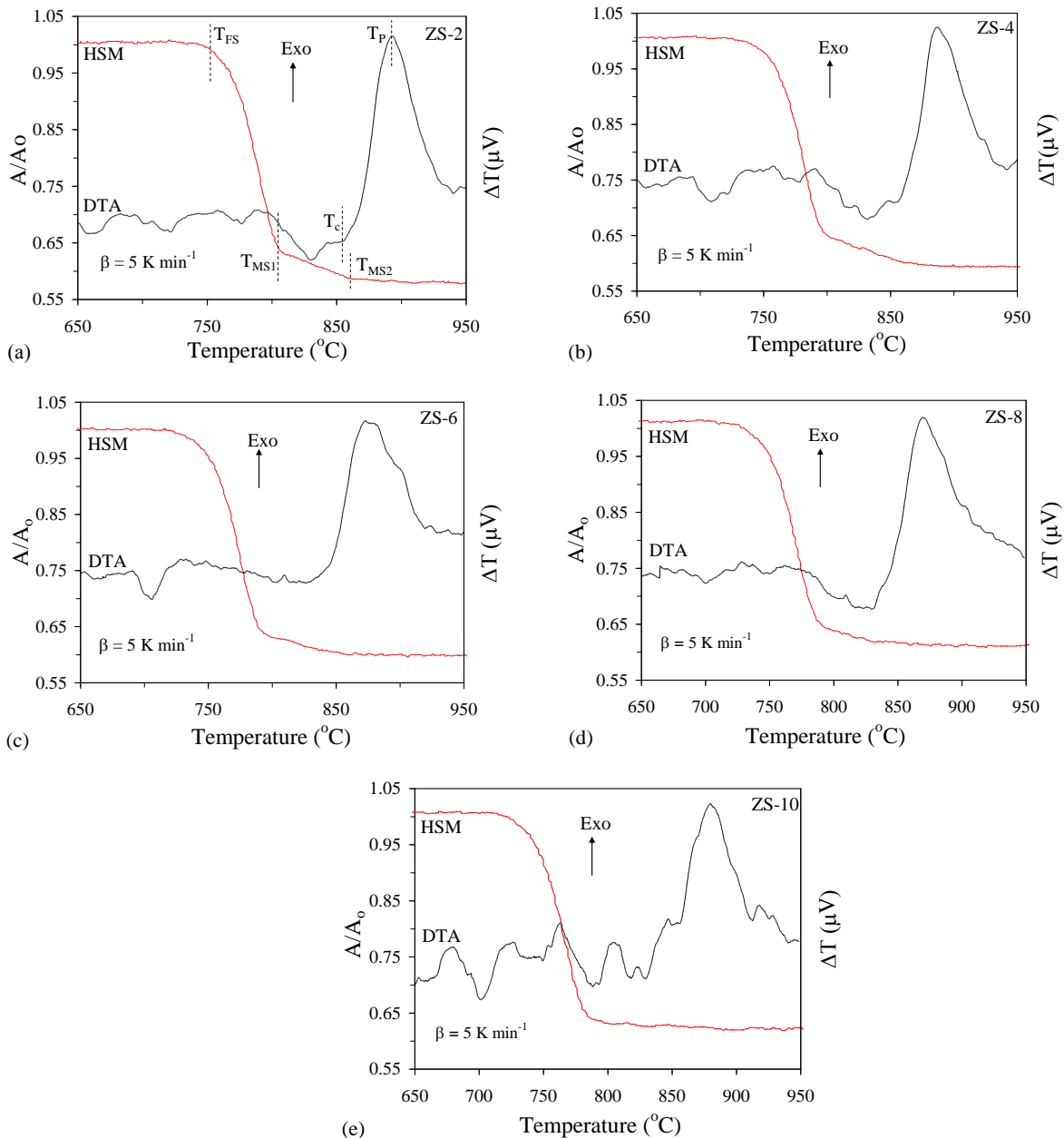


Figure 4.5.3 Comparison of DTA and HSM curves under the same heating rate (5 K min^{-1}) for compositions: (a) ZS-2, (b) ZS-4, (c) ZS-6, (d) ZS-8 and (e) ZS-10.

- (i) T_{FS} decreased monotonically from 765 to 740 °C with increasing SrO/CaO and ZnO/MgO ratios.
- (ii) Two stage sintering behaviours, with the main shrinkage occurring along the first step, were observed for glasses ZS-2, ZS-4 and ZS-6, while a gradual shift to single stage shrinkage was registered for glasses ZS-8 and ZS-10 (Figure 4.5.3). The first sintering stage is accomplished at T_{MS1} while the second one at T_{MS2} . In all the glass compositions T_{MS1} was observed at temperatures lower than T_c (i.e., $T_{MS1} < T_c$). This

feature will ensure the production of well sintered and mechanically strong glass powder compacts. The second stage of densification occurred in competition with crystallization and ended at temperatures higher than T_c . This depicts that shrinkage continued in the glass powders even after onset of crystallization, possibly due to the presence of residual glassy phase in the glass-ceramics.

- (iii) The thermal stability parameter, $\Delta T = T_c - T_g$ varied from 129 °C for ZS-2 to ~150 °C for the remaining compositions (ZS-4 to ZS-10), Table 4.5.1. This suggests that thermal stability was enhanced with the increasing amounts of ZnO and SrO within the composition range, thus favouring densification during sintering. On the other hand, no particular trend could be observed for the variation in S_c values reported in Table 4.5.2. However, all the glasses exhibited a comfortable $T_c - T_{MS}$ difference which enables delaying the nucleation events thus, providing a wide processing window for attaining maximum densification [23].
- (iv) The DTA thermographs of glasses (ZS-2 to ZS-8) exhibited single crystallization exothermic curves. This signifies that the obtained glass-ceramics are formed either as a result of single phase crystallization or of an almost simultaneous precipitation of more than one crystalline phase. The two distinct exothermic events observed for ZS-10 suggests the almost simultaneous precipitation of two crystalline phases
- (v) Values of A/A_0 ranged from 0.65 to 0.67 (Table 4.5.3) for all the glasses implying towards good densification levels of 95–98%.

Table 4.5.2 Thermal parameters measured from DTA and HSM at 5 K min⁻¹

	ZS-2	ZS-4	ZS-6	ZS-8	ZS-10
T_{FS} (± 5 °C)	765	752	748	746	740
T_{MS1} (± 5 °C)	803	794	790	789	782
T_{MS2} (± 5 °C)	862	865	854	–	–
T_c (± 2 °C)	855	856	831	829	855
T_p (± 2 °C)	892	887	872	869	879
$S_c (= T_c - T_{MS1})$	52	62	40	41	73
A/A_0 at T_{MS1} (± 0.02)	0.65	0.67	0.65	0.65	0.65

4.5.2.4 Structural transformation in glasses during heat treatment:

4.5.2.4.1 XRD

In agreement with HSM and DTA data, Figure 4.5.4a shows that amorphous glass powder compacts were obtained for the ZS-2 and ZS-4 samples after sintering for 1 h at 800 °C, while crystalline peaks corresponding to strontium-containing FA (Sr-fluorapatite) ($\text{Sr}_{0.59}\text{Ca}_{4.41}(\text{PO}_4)_3$) (ICDD card: 01-070-3522) with a maximum intensity at $2\theta = 31.75^\circ$ were observed for the other compositions (ZS-6 – ZS-10). Further increase in temperature to 850 and 900 °C led to the crystallization of strontium containing Di phase (Sr-Diopside), ($\text{Sr}_{0.15}\text{Ca}_{0.75}\text{Mg}_{1.1}(\text{Si}_2\text{O}_6)$) (ICDD card: 04-015-0688) in all the glass-ceramics. The XRD data revealed that solid solutions involving partial substitution of Ca^{2+} by Sr^{2+} in FA and Di crystal structures were formed. Considering the higher ionic radius of Sr^{2+} (132 Å) in comparison to that of Ca^{2+} (114 Å), variations in lattice parameters are likely to occur. As a matter of fact, Figure 4.5.4b-c shows slight shifts in the peak positions to lower 2θ angles, especially in case of Sr-FA. Concerning the evolution of the XRD peaks with increasing contents of SrO and ZnO in the glass-ceramics, Figure 4.5.4b-c also show two opposite trends for the two identified crystalline phases. Namely, the intensity of the XRD peaks increases for Sr-FA and decreases for Sr-Di.

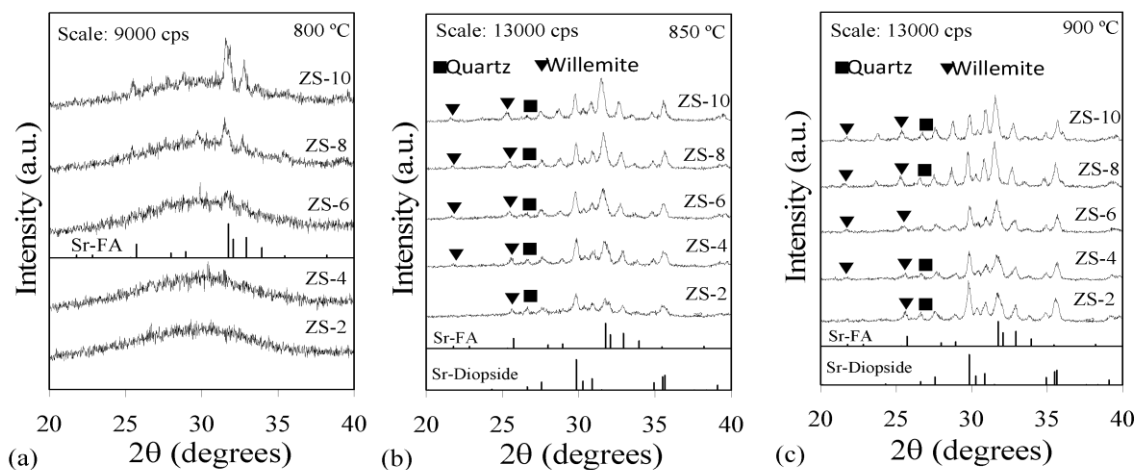


Figure 4

Figure 4.5.4 X-ray diffractograms of glass-ceramics heat treated for 1 h at: (a) 800 °C, (b) 850 °C and (c) 900 °C.

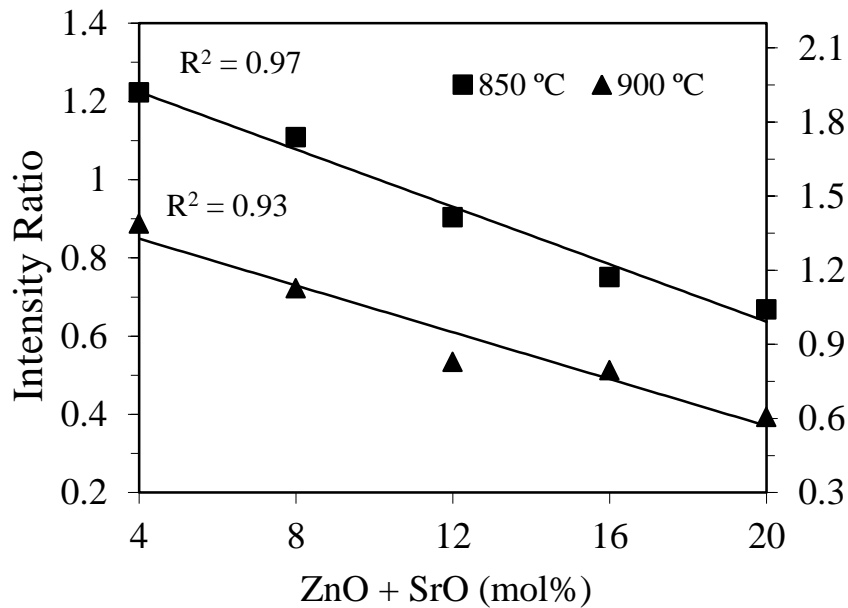


Figure 4.5.5 Intensity ratio of the main XRD intensity peaks of Sr-diopside to Sr-fluorapatite plotted against percentage of zinc and strontium substitution for glass-ceramics heat treated for 1 h at 850 °C and 900 °C.

Figure 4.5.5 shows the variation of the ratio between the highest intensity XRD peaks of Sr-Di / Sr-FA with respect to the ZnO + SrO content in the glass. Linear decreasing intensity trends are observed. The decrease in Sr-Di phase with increasing SrO/CaO and ZnO/MgO ratios can be attributed to the decrease in the Mg content in the glass network due to ZnO substitution. Along with the two major crystalline phases mentioned above, low-quartz (SiO_2) and willemite (Zn_2SiO_4) also precipitate out as minor phases in the glass-ceramics sintered at 850 and 900 °C. It is worth noting that the presence of willemite as minor phase indicates that zinc predominantly remains in the residual glassy phase.

Representative SEM images and EDS data collected in the areas indicated in the SEM micrographs are shown in Figure 4.5.6 for glass-ceramics ZS-8 samples sintered for 1 h at different temperatures. At 800 °C, the microstructure is essentially amorphous and the few FA crystals are still isometric. With increasing the sintering temperature, the typical elongated morphology of FA became evident. Although the results are informative, there are significant deviations in the measured atomic percentages of the different elements relatively to those planned for the starting glass compositions or relatively to their proportions in the crystalline phases. This is not surprising considering that the area being analysed is larger than a single crystal and the measured result is influenced by the surrounding area. In

contrast, there is a good agreement between the XRD results (Figure 4.5.4) and the SEM observations (Figure 4.5.6).

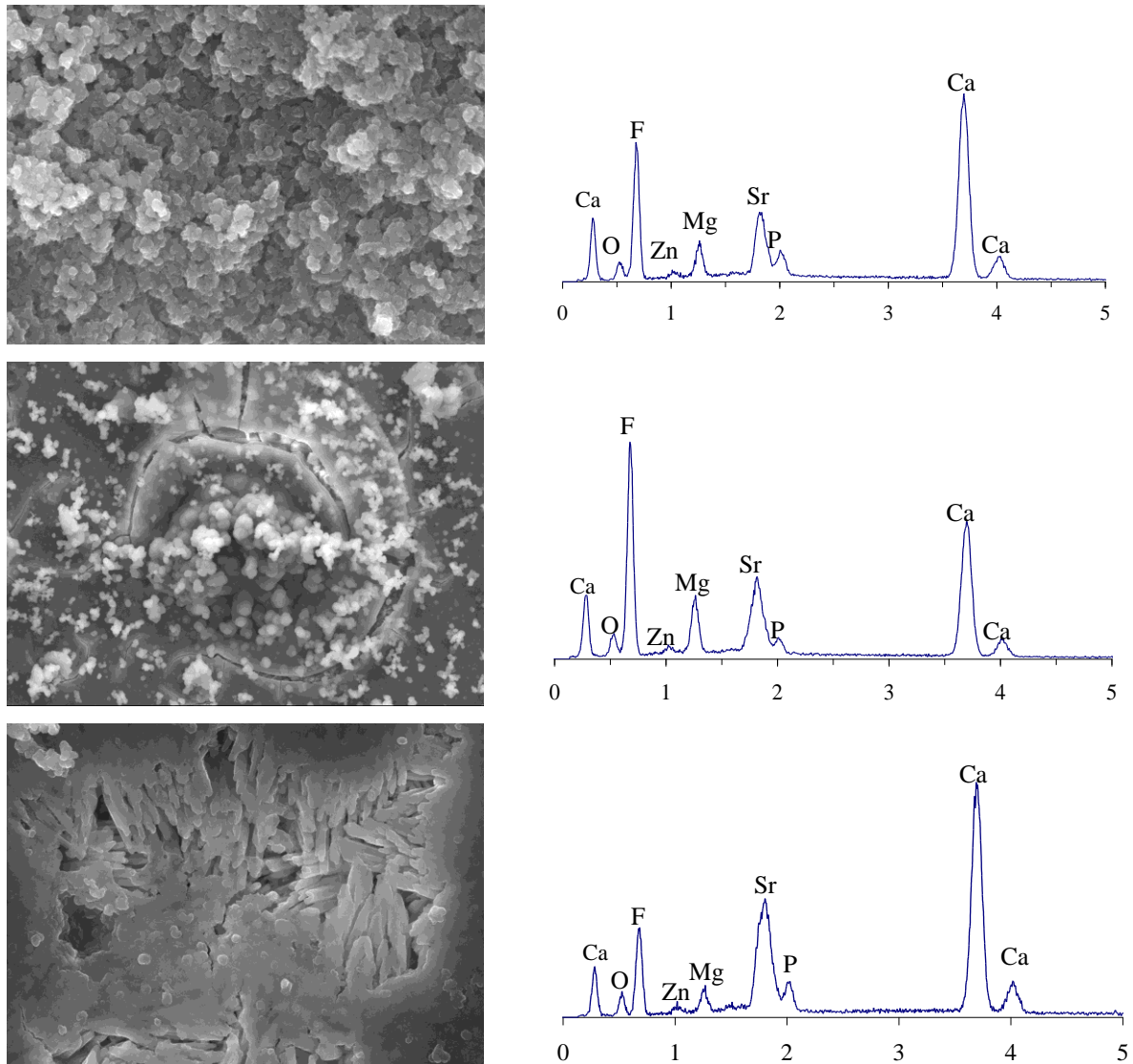


Figure 4.5.6 SEM images and EDS results of glass-ceramic ZS-8 sintered for 1 h at: (a) 800 °C, (b) 850 °C, (c) 900 °C, after a heating rate ramp of 5 K min⁻¹.

4.5.2.5 Mechanical Behaviour:

The flexural strength was calculated for powder compacts sintered at 800, 850 and 900 °C (Figure 4.5.7). Despite their highly amorphous nature, the glass powder compacts sintered at 800 °C exhibited flexural strength of ~ 60 – 70 MPa depicting their good sintering ability.

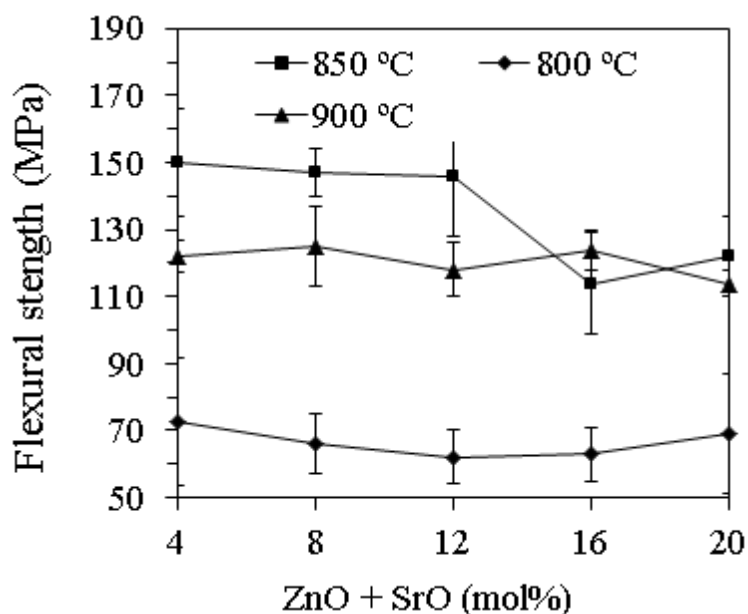


Figure 4.5.7 Flexural strength of glass-ceramics heat treated for 1 h at: (a) 800 °C, (b) 850 °C and (c) 900 °C, using a heating rate of 5 K min⁻¹.

Further, higher values of flexural strength were obtained for glass-ceramics sintered at 850 °C as sintering at 900 °C led to a decrease in their mechanical strength. The variation in mechanical strength with the sintering temperature can be explained on the basis of crystalline phase evolution, including the type of predominating phase and, eventually, the size of crystals formed in these glass-ceramics. The mechanical strength was firstly enhanced with the predominate formation of Di, a mechanically strong crystalline material. Therefore, the relatively higher intensity XRD peaks of Di in glass-ceramics sintered at 850 °C in comparison to their counterparts sintered at 800 and 900 °C suggests an enhanced fraction of this phase that confers to these samples higher mechanical strength. At 900 °C, FA became the dominant crystalline phase in glass-ceramics with higher SrO and ZnO content. This resulted in lower mechanical strength owing to the poor mechanical properties of FA in comparison to Di [131].

4.5.3 Discussions

We have investigated the influence of strontium and zinc oxides on the sintering and mechanical behaviour of alkali-free bioactive phosphosilicate glass-ceramics. The increase in SrO and ZnO concentration leads to the expansion of the glass structure and to concomitant decreases in T_g . all the investigated glasses exhibit good sintering behaviour and good flexural strength with Sr-diopside and Sr-fluorapatite evolved as the major crystalline phases

in the glass-ceramics along with willemite and quartz as minor phases. Due chemical similarity between strontium and calcium increase in concentration of SrO at the expense of CaO led to the partial replacement of Ca^{2+} by Sr^{2+} in the FA crystal structure whereas ZnO predominantly remained in the glassy phase.

4.6 Understanding the influence of composition on structure bioactive and thermal behaviour of Diopside – Tricalcium phosphate based glasses

4.6.1 Introduction

The present work aims at gaining an insight about the influence of composition on the structure, bioactivity and thermal behaviour in alkali-free bioactive glasses in the CaO–MgO–SiO₂–P₂O₅ system designed along Di–TCP binary join by varying Di/TCP ratio and These glass compositions are derived from the ternary Di–FA–TCP system which has been extensively studied in this thesis. Furthermore, the glass compositions derived from these binary and ternary systems have been regarded with much of interest to biomaterials community for their potential applications in bone regeneration and tissue engineering [131-134, 139, 140, 222].

Table 4.6.1 Nominal composition of the as-designed glasses (mol%).

Glasses	CaO	MgO	SiO ₂	P ₂ O ₅
Di-0	75	–	–	25
Di-10	68.13	3.43	6.87	21.57
Di-20	61.82	6.59	13.18	18.41
Di-30	55.99	9.5	19.02	15.49
Di-40	50.57	12.22	24.42	12.79
Di-50	45.55	14.73	29.44	10.28
Di-60	40.88	17.06	34.12	7.94
Di-70	36.52	19.24	38.48	5.76
Di-80	32.44	21.28	42.57	3.71
Di- 90	28.60	23.20	46.40	1.80
Di-100	25.00	25.00	50.00	–

4.6.2 Results

4.6.2.1 Glass forming ability

For all the investigated compositions (Table 4.6.1), we could obtain amorphous glasses only from compositions with Di \geq 50 wt%. The melting of compositions with Di content varying between 30–50 wt% at 1570 °C for 1 h resulted in a highly viscous liquid which was prone to spontaneous crystallization even after quenching in cold water, thus resulting in a white, opaque material. Decreasing further the Di content to 20 wt% led to the

formation of highly viscous, non-homogeneous melt under the same experimental conditions. Therefore, the present study will be dedicated towards the investigation of structure, bioactivity and chemical degradation of glasses with Di content varying between 50 – 100 wt%.

4.6.2.2 Structure of glasses by MAS-NMR

The ^{29}Si MAS-NMR spectra of the glasses are shown in Figure 4.6.1a. All glasses exhibit a broad peak with full width half maximum in the range of 16–17 ppm centred around -81 to -82 ppm indicative of both Q^2 and Q^3 silicate species along with very low amounts of Q^0 , Q^1 and Q^4 . There is a slight change in the peak position towards higher ppm up to Di-90; afterwards the peak shifts towards less negative ppm.

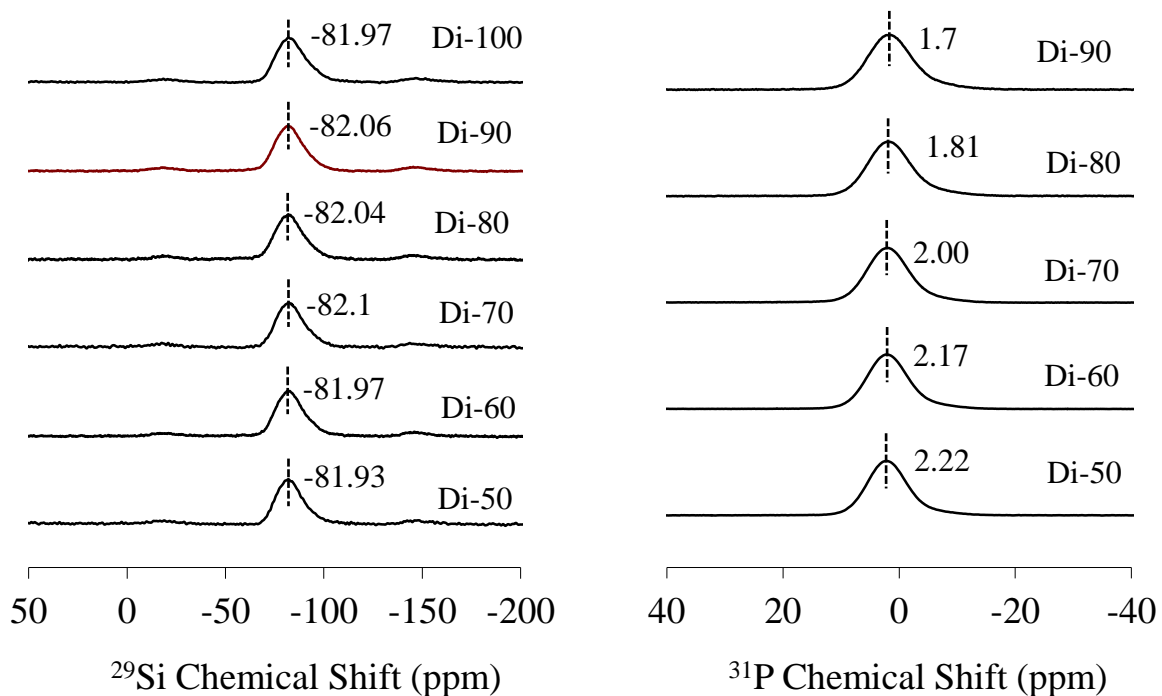


Figure 4.6.1 MAS NMR spectra of investigated glasses showing the peak positions of (a) ^{29}Si and (b) ^{31}P .

Figure 4.6.1b represents the ^{31}P spectra of the investigated glass samples. Irrespective of the content of the modifiers in the glasses, all the spectra are characterised by a relatively symmetric peak with chemical shift within the range of 1–3 ppm with an approximate line width of 8–9 ppm. The line width and the chemical shift values correspond to phosphorus in

orthophosphate environment (Ca–Mg orthophosphate). A downfield shift from 2.2–1.7 ppm was observed with the increments in Di content.

In general, infrared spectra of all investigated glasses exhibit three broad transmittance bands in the region of 300–1300 cm^{-1} (Figure 4.6.2). This lack of sharp features is indicative of the general disorder in the silicate and phosphate network mainly due to a wide distribution of Q^n units occurring in these glasses. The most intense bands in the 800–1300 cm^{-1} region correspond to the stretching vibrations of the SiO_4 tetrahedron with a different number of BO atoms [205]. In all the glasses this band further split in two transmittance bands, a low frequency band at 940 cm^{-1} and a second band in the range 1030–1038 cm^{-1} . The high frequency bands can be assigned to the Si–O asymmetric stretching mode of BOs, whereas the $\sim 940 \text{ cm}^{-1}$ may be attributed to the Si–O asymmetric stretching mode of the NBOs [205, 223]. While the weak 750 cm^{-1} shoulder may be due to Si–O–Si symmetric stretching with simultaneous Si cation motions. Further, a weak shoulder $\sim 600 \text{ cm}^{-1}$ corresponds to P–O bending modes [206].

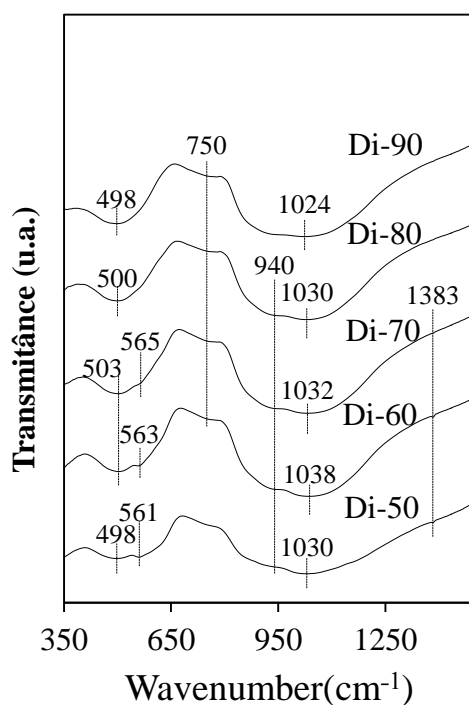


Figure 4.6.2 FTIR spectra of the investigated glasses

4.6.2.3 SBF immersion studies

The immersion of glass powders in SBF for varying time durations led to a considerable change in the glass chemistry that occurred due to the reaction between glass and SBF (Figure 4.6.3). The soaking of glass powders in SBF for 1 h resulted in the splitting

of a strong low frequency band in the region 350–650 cm^{-1} into two small bands at $\sim 470 \text{ cm}^{-1}$ and $\sim 563 \text{ cm}^{-1}$ (Figure 4.6.3a). The band centred around 470 cm^{-1} can be ascribed to a deformation mode of the silica gel layer that develops on the dissolution of glass particles [83], while small band at $\sim 563 \text{ cm}^{-1}$ characteristic phosphates as it corresponds to P–O bending vibrations in a $(\text{PO}_4)^{3-}$ tetrahedron. The band now occurring at $\sim 1060 \text{ cm}^{-1}$ and a nearby shoulder, centred at $\sim 1240 \text{ cm}^{-1}$ are attributed to Si–O–Si vibration [147]. These bands indicate the development of interfacial high–area silica gel layer, as postulated in Hench’s inorganic reactions set [20] and can be observed in all the glasses. After 6 h of immersion the bands pertaining to the formation of complex carbonates 875, 1430, 1485 cm^{-1} and silica gel layer ($\sim 1235 \text{ cm}^{-1}$) became more evident (not shown). Further, an increase in immersion time up to 24 h (Figure 4.6.3b), resulted in the sporadic appearance of new bands around 798 and 960 cm^{-1} , indicating towards silica gel layer, and also, band at $\sim 560 \text{ cm}^{-1}$ suggests the presence of non-apatitic or amorphous calcium phosphate, which is usually taken as an indication of the presence of precursors to HA. Immersion of glass powder for 3 days (Figure 4.6.3c) led to the formation of well-defined bands in all the glasses at ~ 563 and 604 cm^{-1} , attributed to crystalline apatite. After 14 days of immersion (Figure 4.6.3d), no new bands formation could be seen apart from the increase in intensity of the bands corresponding to crystalline apatite i.e., at ~ 563 and 604 cm^{-1} , indicating an increase in crystallinity. In addition, a small band at $\sim 1420 \text{ cm}^{-1}$ along with a broad but intense band at $\sim 850 \text{ cm}^{-1}$ present in all glasses.

In agreement with the FTIR results, the XRD patterns of the samples immersed in SBF for different time periods are displayed in Figure 4.6.4. Although there are a few sporadic peaks apparently related to hydroxyapatite (HA) even after 1 h of immersion (see Di–80), the indubitable formation of crystalline HA at the surface of the samples Di–50 – Di–90 only becomes clearly evident after 3 days of immersion. With the increase in immersion time to 14 days, the intensity of XRD peaks increased irrespective of the glass composition (Di–50 – Di–90). Further, the formation of any calcium carbonate (CaCO_3) polymorphs along the entire immersion period was not observed whereas, formation of calcite under similar testing conditions has been reported for pure Di glass [105].

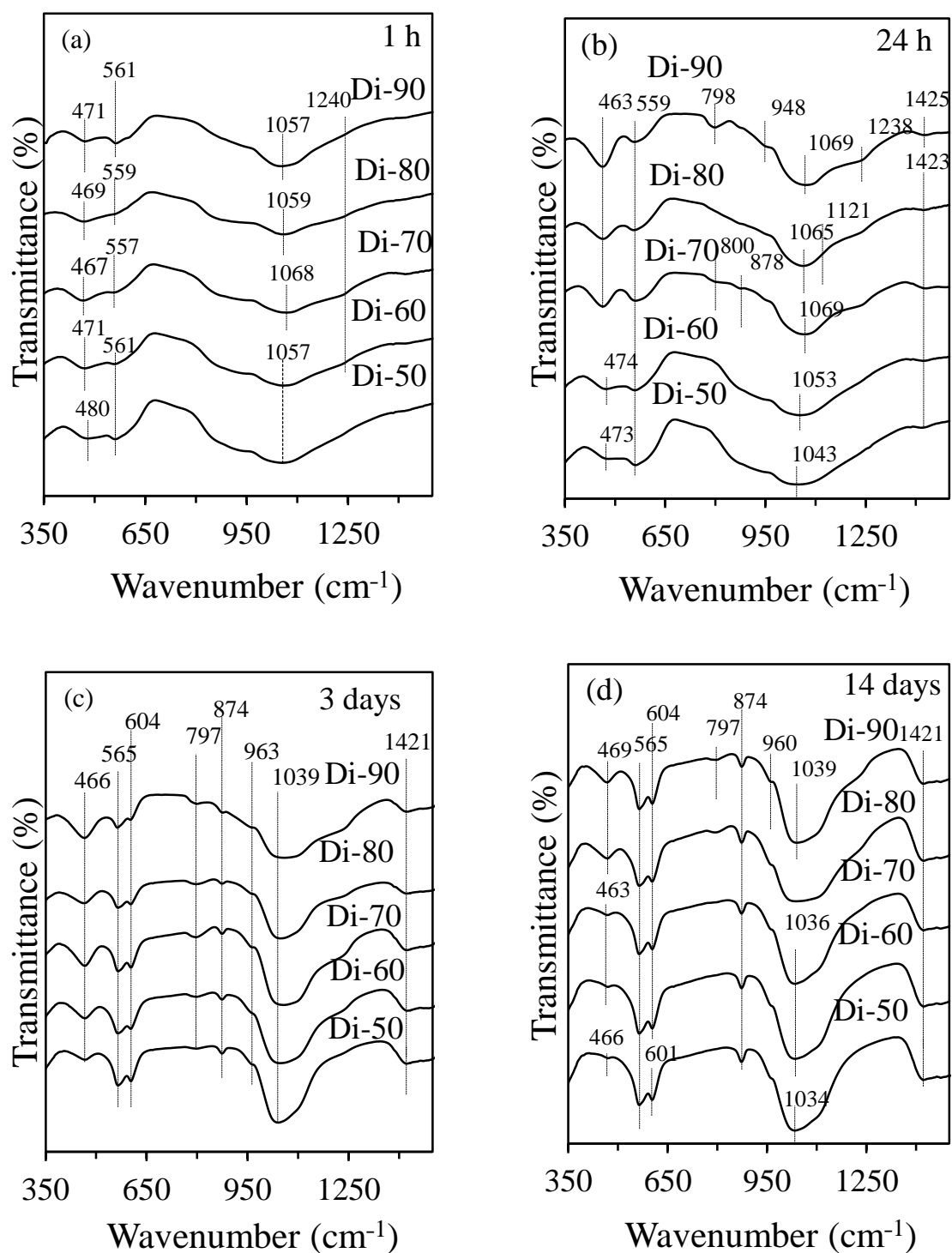


Figure 4.6.3 FTIR spectra of glasses powders after immersion in SBF solution for (a) 1 h, (b) 24 h, (c) 3 days, and (d) 14 h.

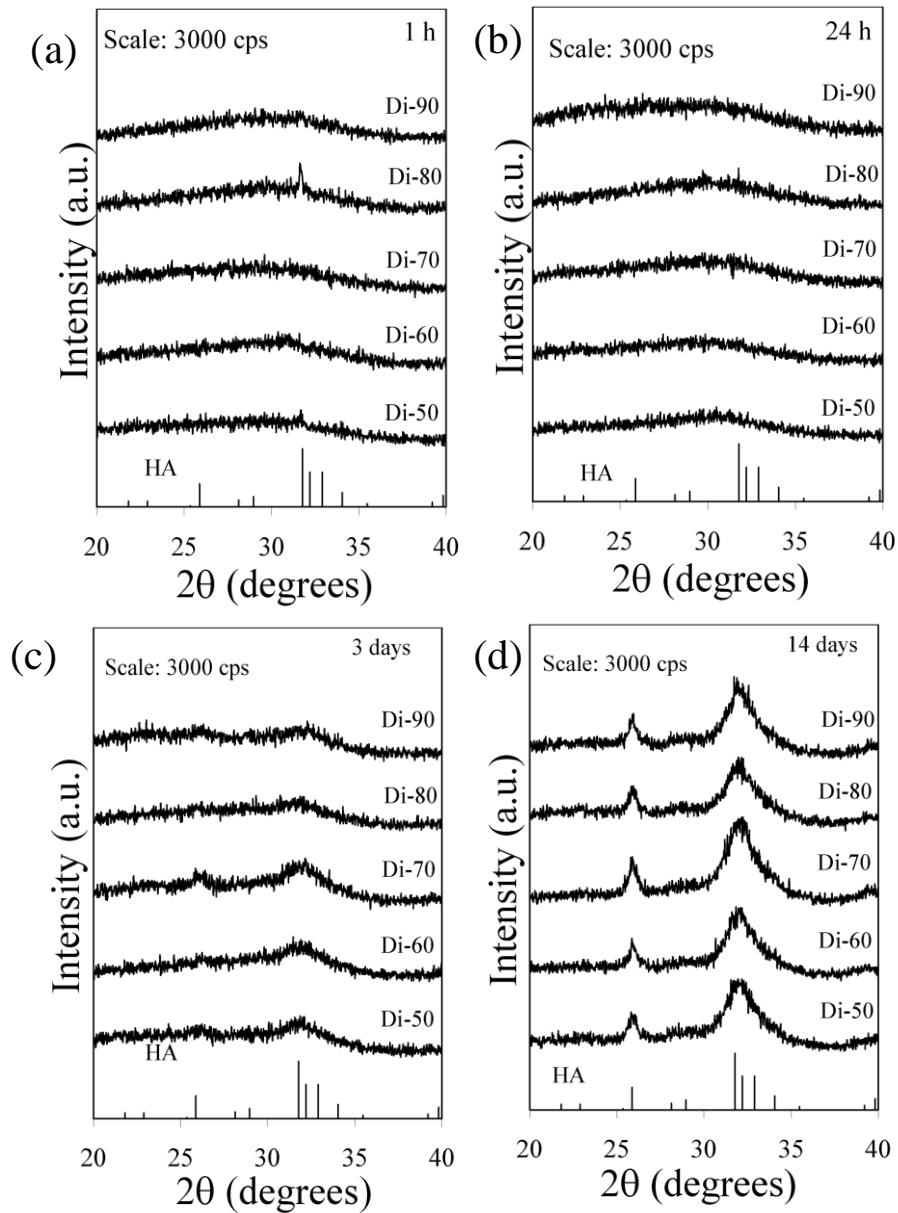


Figure 4.6.4 X-ray diffractograms of glass powders before and after immersion in SBF solution for (a) 1 h (b) 24 h (c) 3 days and (d) 14 days. HA refers to hydroxyapatite.

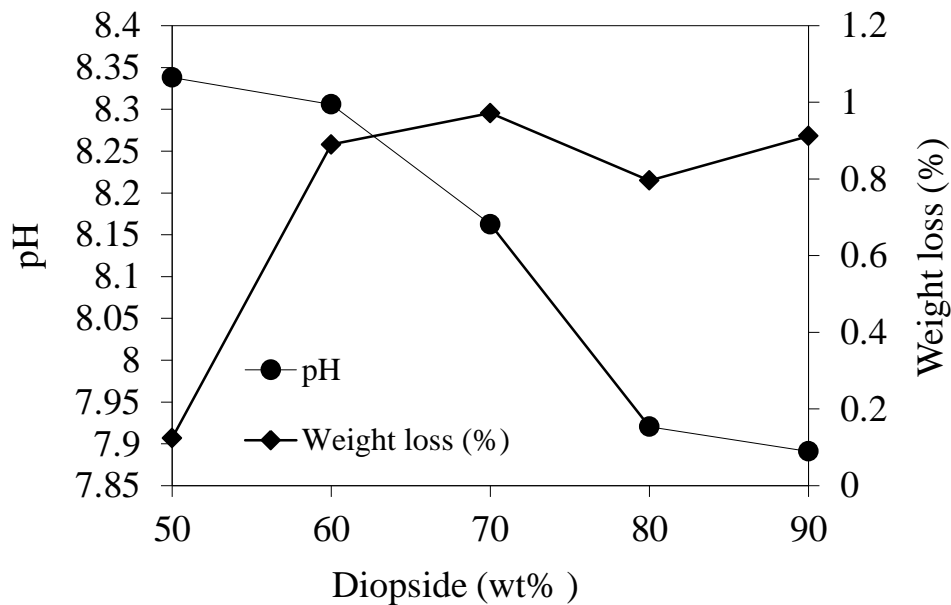


Figure 4.6.5 Variations in pH and weight loss of glass powders upon immersion in Tris-HCl solution for 7 days

4.6.2.4 Chemical degradation of glasses in Tris-HCl

Chemical durability of the glasses is a critically dependent on the pH and the nature of the solution. The leaching behaviour depends on the diffusability of the ions which determined by the ionic field strength of the ions and structure of the glasses. In the present case, a slight in pH of Tris-HCl solution from 7.8 to 8.33 was observed with increasing TCP content (Figure 4.6.5). The increase in the final pH value with increasing TCP content can be attributed to the increase in the CaO content in the glass. However, the weight loss of the analysed samples (Figure 4.6.5), does not reflect well the expected mass balance through the ion exchange, in particular less weight loss of the sample Di-50 (~0.12%).

Glasses with TCP content varying between 10 – 40 wt.% did show some stability in observed weight loss, thus approaching more the expected trend when one considers that the weight losses derived only from the passage of species from the solid to the solution. Further, all the glasses were XRD amorphous (Figure 4.6.6) after immersion in Tris-HCl solution for 7 days.

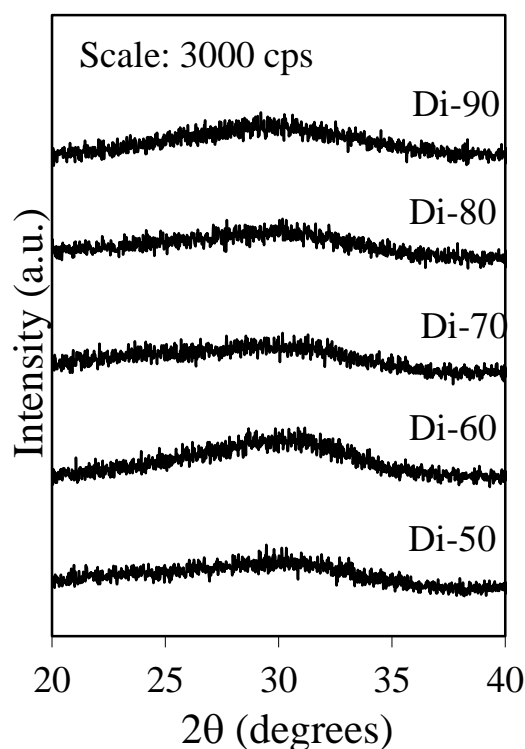


Figure 4.6.6 X-ray diffractograms of glass powder after 120 days of immersion in TRIS-HCL

Table 4.6.2 Thermal parameters measured from DTA at 20 K min⁻¹.

Glasses	T _g (±2)	T _c (±2)	ΔT
Di-50	747	825	78
Di-60	748	861	113
Di-70	748	881	133
Di-80	749	901	152
Di-90	736	880	144
Di-100	744	839	95

4.6.2.5 Thermal analysis

The DTA thermographs of fine glass powders with $\beta = 20 \text{ K min}^{-1}$ are shown in Figure 4.6.7. All the glass compositions feature a single endothermic dip between 748–736 °C before the T_c, corresponding to T_g, estimated from the inflection temperature in DTA curve where the first derivative is null [224]. This thermal event was then followed by a single exothermic crystallization peak/band for glasses Di-60 to Di-100, whereas two crystallization peaks points (T_{p1} and T_{p2}) were observed in glass Di-50. We could not observe any significant differences in the variation of T_g values with varying Di/TCP ratio in

the glasses. The characteristic thermal parameters, T_g , T_c and thermal stability, defined as $\Delta T (=T_c - T_g)$ obtained from DTA thermographs are summarized in the Table 4.6.2. The thermal stability parameter, $\Delta T = T_c - T_g$ varied from 78 °C for Di-50 to ~152 °C for Di-80.

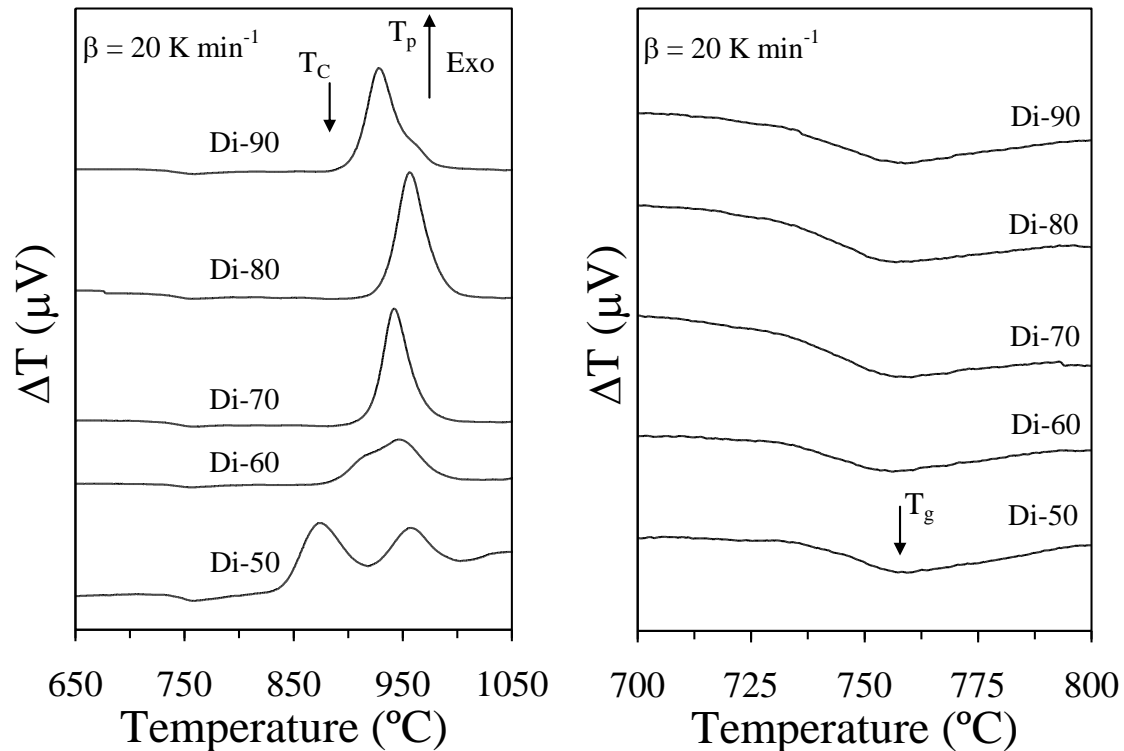


Figure 4.6.7 DTA thermographs of glasses at a heating rate of 20 K min⁻¹

4.6.2.6 Sintering and crystallization behaviours

The variations in the relative area and heat flow as functions of the heat treatment temperature as obtained from HSM and DTA, respectively, under a similar heating rate of 5 K min⁻¹ are presented in Figure 4.6.8a–f for all the investigated glasses. The DTA thermographs of glasses with Di contents varying between 60 and 100 wt.% exhibit single crystallization exothermic peaks Figure (4.6.8b–f), confirming the crystallization behaviour discussed above observed under a higher heating rate of 20 K min⁻¹. Table 3 summarizes the values of some relevant thermal parameters including the temperature of first shrinkage (T_{FS} ; $\log \eta = 9.1 \pm 0.1$, η is viscosity in dPa s), temperature for maximum shrinkage (T_{MS} ; $\log \eta = 7.8 \pm 0.1$) and ratio of the final area/initial area of the glass powder compact (A/A_0) at T_{MS1} , as obtained from the HSM data. The temperatures corresponding T_c , and T_p obtained from the DTA of the glasses are also reported. From these DTA and HSM results the following observations can be made:

1. The temperature of first shrinkage (T_{FS}) showed a slight increase with increasing TCP contents in the glasses before decreasing abruptly to at Di-50;
2. The first sintering stage is accomplished at T_{MS1} while the second one at T_{MS2} . In all the glass compositions (except the extreme ones Di-50 and Di-100), T_{MS1} was lower than T_c meaning that maximum shrinkage was reached before onset of crystallization. The second stage of densification T_{MS2} occurred in much smaller extent and in competition with crystallization, ending at temperatures around T_c . This general trend is more obvious in the intermediate glass compositions from Di-60 to Di-90.
3. The sintering parameter, defined as $S_c = T_c - T_{MS}$, reflects the extent of separation between the sintering and crystallization events in the temperature scale. The S_c values for all investigated glasses are reported in Table 4.6.3. Initially the sintering ability increased with increase in TCP content until glass Di-80, while further TCP increments led to its degradation. In case of Di-100, T_{MS} coinciding with T_c , $S_c (T_c - T_{MS}) = 0$ as shown in Figure 4.6.8f.
4. The values of the A/A_0 ratio between the area (A) of the sample at T_{MS} to its initial area (A_0) decreased from 0.94 in Di-50 (the less prone composition for sintering) to 0.66 in Di-90. Except for Di-50, all other glass-powder compacts exhibited good densification with A/A_0 ratios varying within the range of 0.72 – 0.66.

Table 4.6.3 Thermal parameters ($^{\circ}\text{C}$) and A/A_0 ratio derived from DTA and HSM at 5 K min^{-1} .

	$T_{FS} (\pm 5)$	$T_{MS1} (\pm 5)$	$T_{MS2} (\pm 5)$	$T_c (\pm 2)$	$T_p (\pm 2)$	$T_{p2} (\pm 2)$	S_c	A/A_0
Di-50	737	786	932	795	845	910	9	0.94
Di-60	786	826	–	831	881	903	5	0.72
Di-70	763	850	–	874	905	–	24	0.75
Di-80	774	812	–	899	955	–	87	0.68
Di-90	777	824	–	857	895	–	33	0.66
Di-100	756	823	–	823	853	–	0	0.69

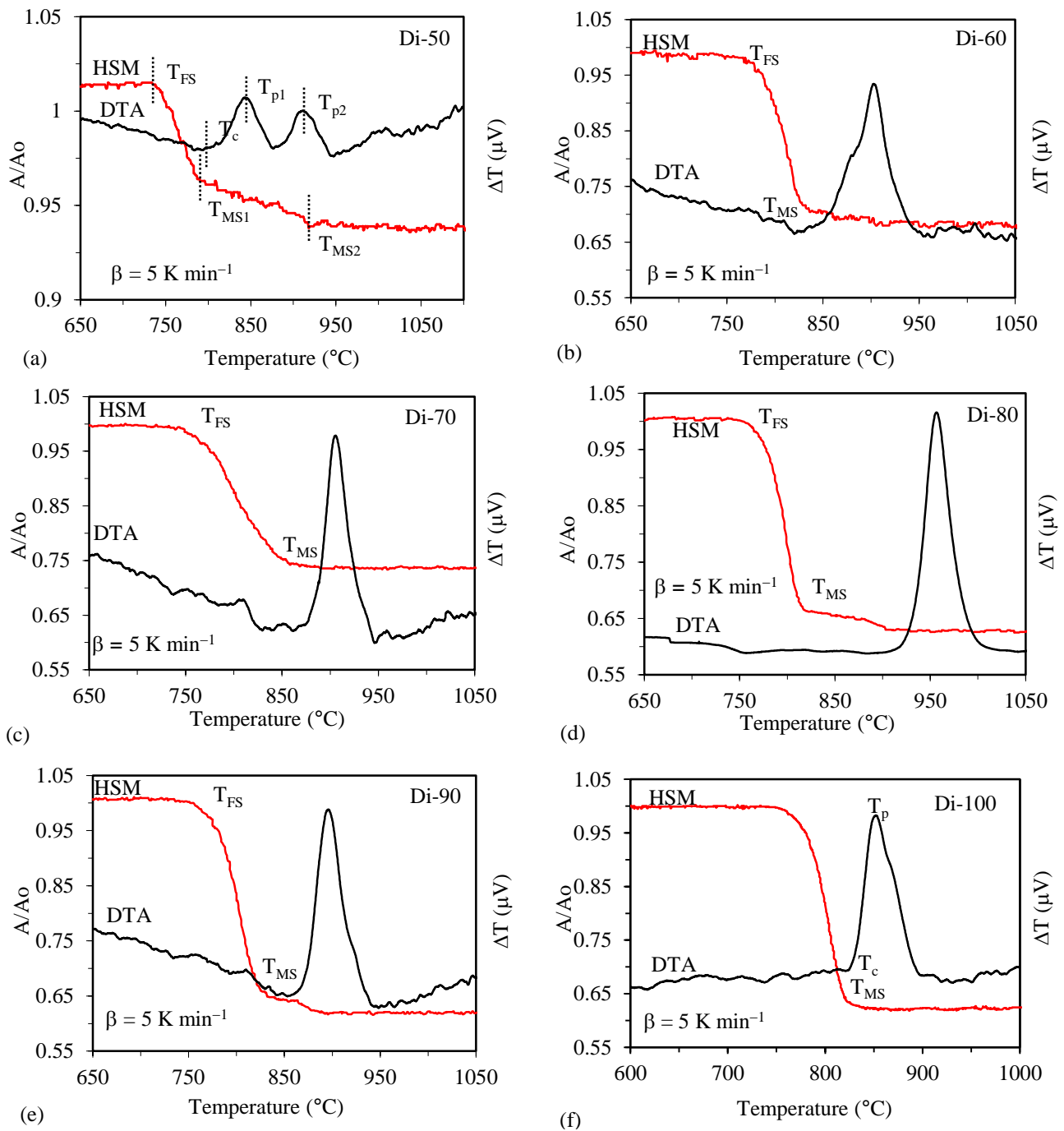


Figure 4.6.8 Comparison of DTA and HSM curves under the same heating rate (5 K min^{-1}) for compositions: (a) Di-50, (b) Di-60 (c) Di-70, (d) Di-80 (e) Di-90 and (f) Di-100

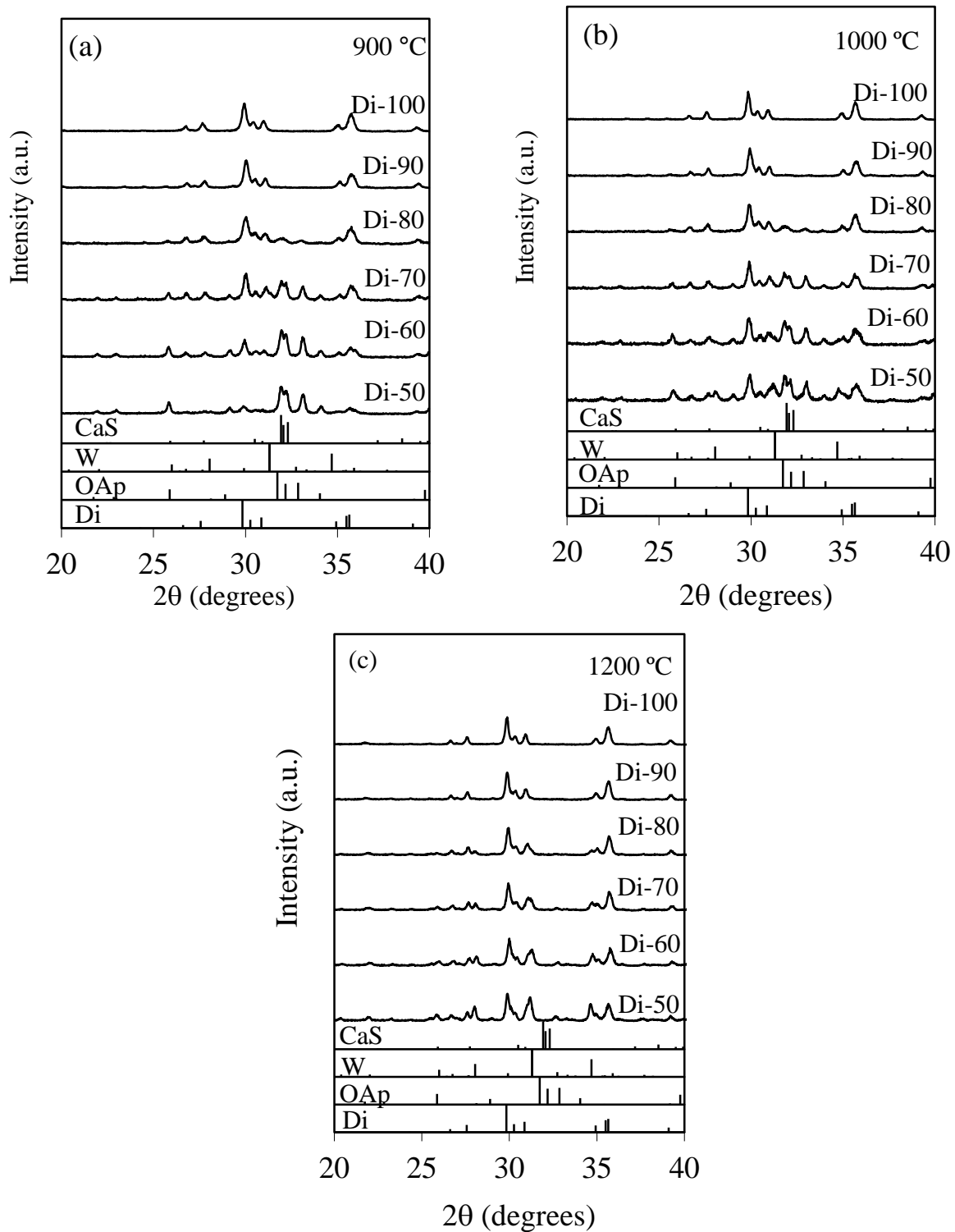


Figure 4.6.9 X-ray diffractograms of glass-ceramics heat treated at (a) 900 (b) 1000, and (c) 1200 °C for 1 h. (Di: Diopside, OAp: oxyapatite, W: Whitlockite, CaS: Calcium Silicate)

4.6.2.7 Structural transformations during heat treatment

Figure 4.6.9 shows the XRD patterns of the glass powder compacts heat treated for 1 h at 900, 1000 and 1200 °C. The peak at $2\theta = 29.83^\circ$ position appeared in all glasses and became more intense as the Di content is increased. The peak around of $2\theta = 31.74^\circ$ was restricted to the composition with higher TCP contents (Di-50 to Di-70). In addition, a number of low intensity peaks were also present as minor crystalline phase, being more prominent in these compositions (Di-50 to Di-70). The crystalline phase assemblage did not change much upon further increasing the heat treatment temperature to 1000 °C (Figure 4.6.9b), traces of new peaks at $2\theta = 31.30^\circ$ start appearing at this temperature especially for Di-50 to Di-70 compositions. Further, with the increase in the heat treatment temperature to 1200 °C peaks $\sim 2\theta = 31.74^\circ$ disappeared along with some minor phases and new peaks with maxima at $2\theta = 31.30^\circ$ appeared as the prominent phases (Figure 4.6.9c).

4.6.2.8 Density

The experimental density data measured for bulk glasses and glass-ceramics heat treated at different temperatures are reported in Table 2.6.4. The density of glass Di-50 was not measured due to its partial crystallization upon casting/slow cooling. It can be seen that density of the glass tends to decrease with increasing proportions of Di. All the glass-ceramics, except Di-50, exhibited good densification ability, achieving densities that are superior in comparison to those of bulk glasses. The density values show a general increasing trend with temperature increasing followed by its reversion with further augmenting the sintering temperature, with small composition dependent variations.

Table 4.6.4 Density (kg m^{-3}) of glasses and glass-ceramics.

Compositions	Bulk glass	Glass ceramics heat treated at		
		900 °C	1000 °C	1200 °C
Di-50*	-	2,819±47	2,863±60	2,893±16
Di-60	2.945	2,951±12	2,972±4	2,964±15
.Di-70	2.921	2,972±60	2,953±6	2,962±1
Di-80	2.897	2,933±1	2,973±6	2,924±3
Di-90	2.871	2,930±7	2,936±6	2,925±11
Di-100	2.852	2,897±3	2,936±17	2,892±4

* Partial crystallisation upon casting

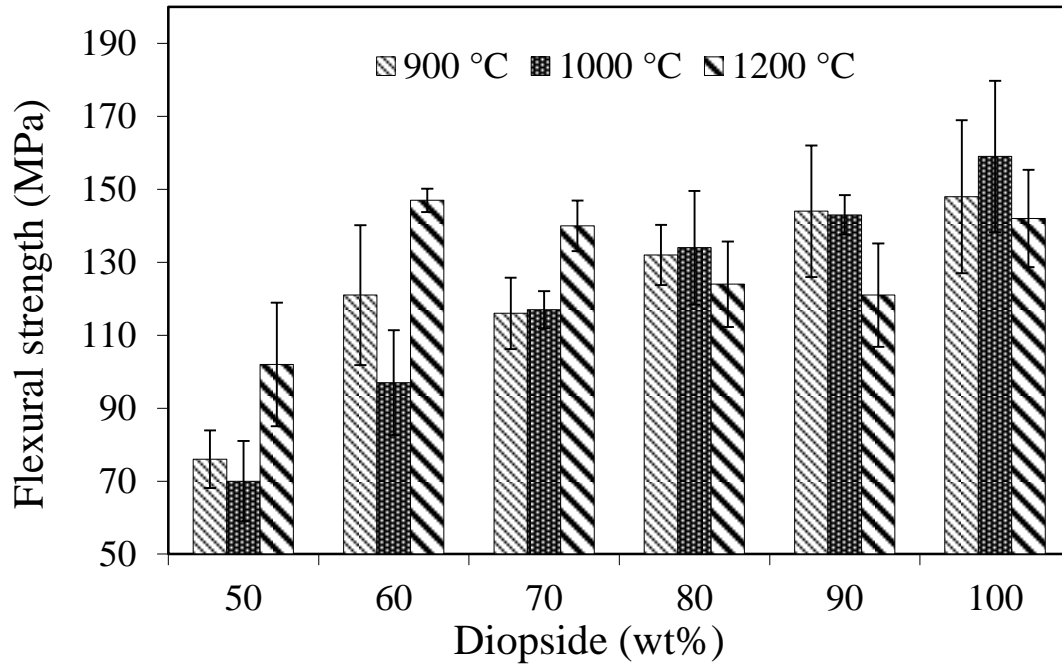


Figure 4.6.10 Flexural strength of glass-ceramics heat treated for 1 h at (a) 900 °C (b) 1000 °C, and (c) 1200 °C.

4.6.2.9 Mechanical properties

The 3-point bending strength was calculated for glass powder compacts sintered for 1 h at 900, 1000 and 1200 °C (Figure 4.6.10). In general, the flexural strength increased from Di-50 – Di-100 in all the glass powder compacts heat treated at 900 and 1000 °C. Interestingly, for the glass-ceramics sintered at 1200 °C a point of inflection was observed after Di-70, i.e., at 1200 °C there was a gradual decrease in the flexural strength of the glass-ceramics with increasing Di content.

4.6.2.10 Cell culture studies

hMSCs' metabolic activity on Di-60, Di-70 and Di-90 and Tissue culture polystyrene (TCPS) after 1, 3, 7, 14 and 21 days under both conditions are shown in Figure 4.6.11.

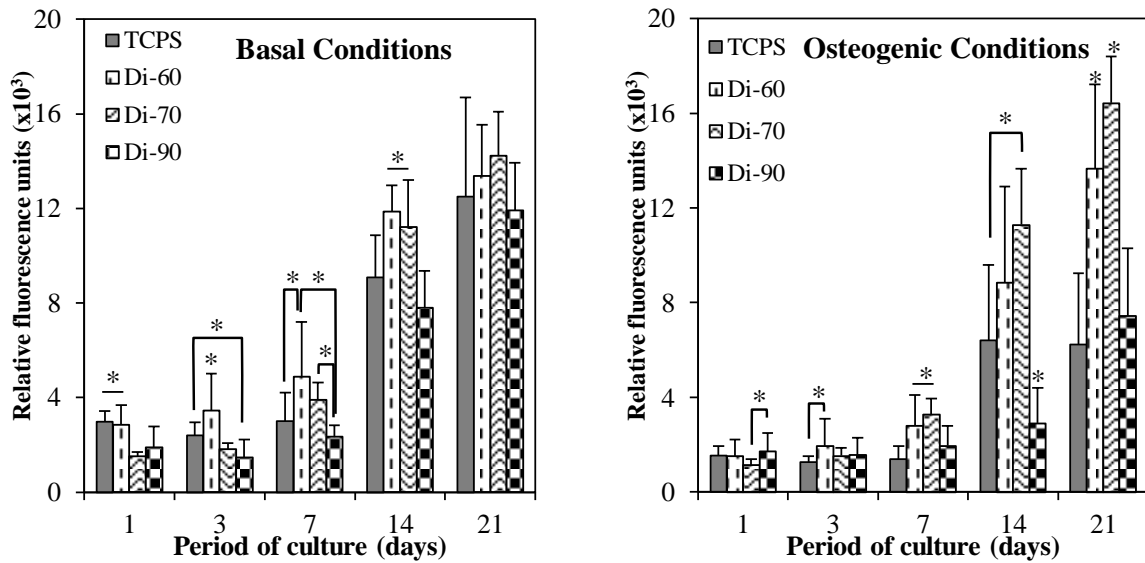


Figure 4.6.11 Metabolic activities of hMSCs on Di-60, Di-70 and Di-90 and TCPS after 1, 3, 7, 14 and 21 days.

An increase in cells' metabolic activity was observed under both basal and osteogenic conditions for the culture period tested. On day 14 of culture in a basal medium, the metabolic activity of cells on Di-60 and Di-70 showed superior and significant statistical difference when compared with the control. However, no statistically significant difference was found after 21 days. Under osteogenic conditions, by day 14, cells' metabolic activity was inferior and exhibited significant statistical difference with Di-90 in comparison with the control. On day 21, cell's on Di-70 presented a higher metabolic activity than cells on Di-60, D-90 and the control. At this time point, it was also possible to notice a potential recovery of cells' metabolic activity on Di-90.

4.6.3 Discussions

The gradual replacement of Di ($\text{CaO} \cdot \text{MgO} \cdot 2\text{SiO}_2$) by TCP ($3\text{CaO} \cdot \text{P}_2\text{O}_5$) changes the balance between glass formers and glass modifiers, implying structural variations that will influence the properties of glasses. The decreasing contents of Si lead to the formation of an increasing number of non-bridging oxygens in the glass structure. Further, no abrupt change in the glass structure was observed with increasing amounts of Di. However, the change in peak position towards more negative ppm values with increase in content of Di may be attributed to addition of silica and removal of phosphate from the glass network. On the

contrary, the up field peak shift in case of Di-100 can be attributed to complete removal of phosphate ion and simultaneous movement of modifier ions towards SiO₂ which were earlier attached to P₂O₅.

Figure 4.6.1b shows that ³¹P MAS-NMR continuously shifts for all the glasses lying predominantly in the range for calcium orthophosphate (1–3 ppm), and a small amount of magnesium orthophosphate (0.5 ppm) can be expected. This therefore suggests that phosphorus is present in mixed calcium and magnesium orthophosphate. The phosphate component in the glass is predominantly coordinated in orthophosphate environment thus, not contributing to the glass network backbone. This facilitates the release of additional soluble phosphate species into the surrounding fluid, increasing their local super-saturation levels and accelerating the bone bonding ability of glass by enhancing the HA deposition on the glass surface. Further Lockeyer et al. [225] attributed the presence of orthophosphate-like environment as a result of phase separation in glasses. All the glasses prepared by Lockeyer et al [225] were annealed for 6 h at 450 °C before slow cooling. However, the compositions under investigation were rapidly quenched in water, thus reducing the possibility of phase separation. Further, as the cation field strength and electronegativity of the modifiers significantly affect the ³¹P chemical shift in glasses. The peak shift observed in the spectra with increasing Di contents can be attributed to the increase in the Mg²⁺ (high field strength) and the concomitant decrease in the amount of Ca²⁺ content (low field strength).

In terms of bioactive behaviour, all the investigated glasses have shown good *in vitro* bio-mineralization activity in terms of the formation ability of an HCA surface layer over 14 days of soaking in SBF (Figure 4.6.3), except for pure Di (Di–100) [104]. The inability of Di–100 to form a HCA surface layer after 14 days of immersion can be attributed the relatively high amount of MgO which retards the formation of apatite-like calcium phosphate [148]. However, the presence of ACP could be detected for these glasses after 24 h of immersion (Figure 4.6.3). Further, despite the differences in P₂O₅ content, all the investigated alkali-free glasses show similar rate of biomineralisation in contrast to the results reported by O'Donnell et al. [226] and Mneimne et al. [227]. The possible reason behind these different behaviours could be attributed to high alkali content (22–29 mol%) of the bioglass compositions used by O'Donnell et al [228] and Mneimne et al. [227]. The eventual association of P with Na in the form Na-orthophosphate is likely to contribute to faster rates of dissolution and release of phosphates species from these glasses into the surrounding fluid in comparison to alkali-free counter parts. Interestingly, the presence of varying amounts of

magnesium did not apparently affect the rate of apatite formation in our alkali-free bioactive glasses, even though a suppressing role in apatite formation has been reported in literature for Mg [229]. However, the results obtained in this study are in line with findings reported elsewhere [99] about the negligible effects of Mg on the apatite forming ability of other bioactive glass compositions. Thus, it seems reasonable to conclude that the effects of MgO on the properties of bioactive glasses do not exclusively depend on the added amount of MgO but also on the presence and relative contents of other oxides in each glass composition [229].

The foremost requirement for optimizing the fabrication of glass–ceramics scaffolds is to understand the sintering and crystallization behaviours of the glass powder compacts and avoid the overlapping of these two thermal events. A thorough understanding of the transformations that occur during the thermal treatment of glasses and how they depend on the starting compositions is therefore essential for designing biomedical applications/devices based on bioactive glasses that have to undergo high temperature treatments. We could not observe any significant differences in the variation of T_g values with varying Di/TCP ratio in the glasses. Further, the presence of single crystallization exotherm anticipates that the glass–ceramics are formed as a result of either single phase crystallization (Di–100) or an almost simultaneous precipitation of different crystalline phases (Di–60 – Di–90), while the appearance of two crystallization peaks points (T_{p1} and T_{p2}) in Di–50 glass points towards the separate precipitation of two different crystalline phases. Further, good sintering behaviour was observed in the glasses as T_{MS1} was lower than T_c , meaning that maximum shrinkage was reached before onset of crystallization. Further, the higher values of the sintering parameter, $S_c = (T_c - T_{MS})$ for intermediate compositions (Table 4.6.3) clearly explain why these compositions perform better upon sintering. The observed decrease in the sintering ability for the higher added amounts of TCP is attributed to the formation of phosphate rich phases that degrade the sintering ability by enhancing the crystallization tendency of the glasses. In case of Di–100, T_{MS} coinciding with T_c ($T_c - T_{MS} = 0$), (Figure 4.6.8f). However, well sintered glass powder compacts were obtained as maximum shrinkage was achieved just before the onset of crystallization. This is confirmed by the density data reported in Table 4.6.4. The lowest density of Di–50 glass-ceramics is in good agreement with its poorer densification ability as deduced from the DTA-HSM results, with T_{MS2} coinciding with the onset of crystallization. Some bubbling was observed upon immersing the Di-50 glass-ceramics in diethyl phthalate due to the presence of some open pores, a tendency that decreased with increasing temperature, but was not completely eliminated. The absence of

bubbling for the remaining glass-ceramics samples and their higher sintered density values in comparison to the parent bulk glasses attest their good sintering ability, in good agreement with the predictions derived from DTA-HSM studies. Density data confirm that the compositions within the range of Di-60 to Di-80 exhibit the higher sintering ability, being the most interesting ones for scaffolds fabrication. The general tendency of density to decrease with heat treatment increasing can be attributed to the elimination of a few pores left at lower temperatures and or to the formation of increasing amounts of denser crystalline phases. The reversion of this trend with temperature further increasing might be due to partial re-melting of crystalline phases, crystalline phase transformations. Therefore, exact information about the nature of crystalline phases formed upon heat treating the bioactive glasses is of great interest as they determine the relevant final properties of the glass-ceramic materials. Besides being composition dependent, the phase assemblage might be also affected in a certain extent by the heat treatment schedule.

In the present study, Di ($\text{CaMgSi}_2\text{O}_6$) (ICDD: 01-072-1497) and oxyapatite (ICDD: 65-1659) were the principal crystalline phases formed at 900 °C (Figure 4.6.9a). The presence of oxyapatite was restricted to the composition with higher TCP contents (Di-50 to Di-70). Calcium silicate (Ca_2SiO_4) (ICDD: 01-086-0401) was also present as minor crystalline phase, being more prominent in these compositions (Di-50 to Di-70) as evident from the X-ray diffractograms. The crystalline phase assemblage did not change much upon further increasing the heat treatment temperature to 1000 °C, but traces of whitlockite ($\text{Ca}_{2.71}\text{Mg}_{0.29}(\text{PO}_4)_2$) (ICDD: 01-070-0682) start appearing at this temperature especially for Di-50 to Di-70 compositions. The absence of calcium silicate and whitlockite phases in the glass-ceramics with higher Di contents can be attributed to the gradual depletion in Ca required to form those phases and the concomitant increasing amounts of MgO that tend to enhance the viscosity of the melts. Further increasing the heat treatment temperature to 1200 °C led to the dissolution of oxyapatite and calcium silicate phases, favouring the formation of whitlockite along with Di as the prominent phases. The dissolution of oxyapatite and calcium silicate at 1200 °C can be attributed to increase in the amount of Di phase and the associated decrement of calcium content in the residual glassy phase available for apatite/ Ca_2SiO_4 formation.

Mechanical strength of the scaffolds is a very important aspect to take into consideration when designing glass-ceramics for bone tissue engineering applications. The mechanical strength of glass-ceramics is dependent on the mechanical properties of the

constituting crystalline phases and the densification ability of glass-powder compacts. In the present investigation the mechanical strength of the glass-ceramics (Di-60 – Di-100) exhibit good mechanical strength which can be attributed the mechanical properties of the constituting crystalline phases and high density obtained by the glass-ceramics (2,890–2,970 kg m⁻³). In case of Di-50, the poor sintering/densification ability and lower mechanical strength of the dominant phase can attributed to the lower mechanical strength upon sintering. Further glass-ceramics with higher amounts of Di (a mechanically stronger phase) [230] exhibit high mechanical strength values when heat treated up to 1000 °C. Further, the overall decrease in the mechanical strength of the resultant glass-ceramics heat treated at 1200 °C can be due to the decline in the densification ability of the glass-ceramics and formation of considerable volume fraction of whitlockite (a mechanically weaker phase), explaining the overall decrease in the mechanical strength of the resultant glass-ceramics.

The cell culture studies showed an excellent cellular response to the investigated glass compositions, with the exception of the cells tested with osteogenic supplements and Di-90. Under these conditions, cells had lower metabolic activity than control, Di-60 and Di-70. Since Di-90 has higher amount of silica and MgO than the other compositions, the release of the compounds to the culture medium may induce some levels of cytotoxicity towards the hMSCs. Previous studies have shown that high Si concentrations can be cytotoxic [231, 232]. However this behaviour was more prominent under osteogenic conditions, which might be attributed to the inhibition of the stimulatory effect of osteogenic supplements in the presence of high Si concentrations [233]. At the end of the culture period, these cells seem to recover from the imposed toxic levels as suggested by an increase in their metabolic activity. This behaviour has been reported by several authors [231, 234]. On the contrary, Di-60 and Di-70 promoted a good cell adhesion, metabolic activity into an osteoblastic phenotype, suggesting a potential stimulatory effect of these materials on hMSCs by the release of soluble factors or by the fastest formation of a CaP layer [235]. It has been reported the Si-, Ca- and Mg-containing bioactive ceramics can release soluble ionic products to stimulate the proliferation and osteogenic differentiation of osteoblasts and human mesenchymal stem cells [236-238].

4.6.4 Conclusions

An attempt has been made gain an insight into composition - structure - bioactivity relationships of alkali-free bioactive glasses in the CaO-MgO-SiO₂-P₂O₅ system. The glasses have been designed in the Di (CaO•MgO•2SiO₂) – TCP (3CaO•P₂O₅) binary join by

varying the Di/TCP ratio. We could obtain amorphous glasses only from compositions with $\text{Di} \geq 50$ wt%. The melting of compositions with Di contents varying between 30-50 wt% at 1570 °C for 1 h resulted in a highly viscous liquids which were prone to spontaneous crystallization even after quenching in cold water, thus resulting in a white, opaque material. Further decrease in Di content to 20 wt% led to the formation of highly viscous, non-homogeneous melts under the experimental conditions. Further, there was no significant change in the structure of the glass with decrease in Di content as investigated glasses have predominantly Q^2 (Si) units while phosphorus is mostly in orthophosphate type environment. As expected from the structure of the glasses, all other investigated glasses have shown good *in vitro* bio-mineralisation activity in terms of the formation ability of an HCA surface layer over 14 days of soaking in SBF. All the glasses exhibited considerably lower weight loss in comparison to 45S5 Bioglass[®] in Tris-HCl with Di-50 exhibiting lowest weight loss. The cell culture studies showed an excellent cellular response to the investigated glass compositions, with the exception of the Di-90. Further, all the glasses exhibit good thermal stability and processing window wide enough for the fabrication of scaffolds. TCP addition resulted in slight T_g variations. Good densification was achieved for the glass powder compacts at all investigated temperatures, resulting in well sintered and mechanically strong glass-ceramics. Diopside, oxyapatite were the major phases present at 900 °C and 1000 °C with calcium silicate and whitlockite as the minor phases. At 1200 °C, diopside and whitlockite were the major phases present with no other minor phase detected.

Chapter 5

General conclusions

5. General conclusions

The present work aimed at developing alkali-free bioactive glasses in the ternary system of Di-FA-TCP having high bioactivity, lower dissolution rate and good sintering behaviour for bone regeneration and tissue engineering applications. In this pursuit, an attempt was made to understand the structure-property relationships in alkali-free bioactive glasses. Further, the influence of various functional ions on the structure and their implications on the biodegradation, sintering and crystallization behaviour of bioactive glasses was studied. In terms of structure, the glasses are almost similar to 45S5 Bioglass®, while significantly differing in the properties that are relevant for the intended applications. The designed alkali-free bioactive glasses exhibit: (i) higher bioactivity and slower chemical degradation in comparison to 45S5 Bioglass®; (ii) enhanced sintering ability resulting in well sintered and mechanically strong glass-ceramics with high residual amorphous content; (iii) good ability to be dispersed in aqueous media and to fabricate scaffolds for bone regeneration and tissue engineering applications with good mechanical properties and high bioactivity; (iv) the pH of the media is kept at moderate values owing to the absence of alkali metals in the composition, making them non-cytotoxic.

Further, the addition of zinc to the parent glasses enhanced their chemical durability and the sintering ability without causing a substantial change in the structure. The flexural strength of 200 MPa achieved for Zn-8 We is comparable to that of the A-W glass-ceramics. Glasses doped with equimolar concentrations of ZnO and SrO showed excellent bioactivity despite of their very low degradation in comparison to 45S5 Bioglass®. In addition, the glass ZS-2 released doses of zinc and strontium into the SBF that are within the considered therapeutic ranges (< 1.5 ppm Zn and ≤ 10 ppm Sr), and exhibited good antioxidant behaviour by enhancing the cell viability and negating the effect of oxidative stress induced by H₂O₂ addition in the cell culture medium. Thus zinc concentration < 1.5 ppm has an anti-oxidant effect.

Moreover, we have elucidated that a straightforward correlation between the glass structure as evaluated by the network connectivity (Q_n units) and dissolution behaviour of alkali-free bioactive glasses is difficult to establish as the bulk molecular structure of glasses does not completely control the hydroxyapatite formation on the surface of bioactive glasses. The structural coordination of functional ions in the glass plays a crucial role in deciding their elemental release profile thus, affecting the bioactivity of glasses. In the investigated alkali-free bioactive glasses, all the glasses had almost similar molecular structure (Q_n and NC). However, the structural coordination of zinc (five-coordinated) and strontium (six

coordinated) played an important role in deciding their biodegradation and sintering and crystallization behaviour. Also, in order to obtain a comprehensive picture about the dissolution mechanism and surface reactivity of glasses, it is of utmost importance to explore the surface chemistry of bioactive glasses and correlate it with their molecular structure.

Chapter 6

Future works

6. Future works

During this research work, an attempt has been made to develop diopside based Alkali-free bioactive glasses for bone regeneration applications. We have succeeded in shedding some light on the composition-structure-property relationships in the glasses and the effect of various functional ions on the biodegradation, sintering, thermal and in vitro behaviour of bioactive glasses, which render them suitable for further experimentation as potential candidates in various bone regeneration applications. However, a lot work still needs to be accomplished in order to understand the biodegradation behaviour of the glasses. Therefore, in our opinion, the future work in this area may be addressed to the following issues:

1. Surface chemistry of the glasses is highly important aspect to study the bioactive phenomenon. It could be interesting to study the relation of surface chemistry of glasses with their biodegradation behaviour and compare them with alkali-containing counterparts.
2. In addition, biologically relevant additives (Co, Mn, Cu etc.) can be added to study their effect on bio-degradation behaviour in order to enhance the therapeutic efficacy of the glasses
3. Further in depth in vitro tests are required to see the interaction of bioglass with variety to cellular environments.
4. Also, in vivo tests of glasses/glass-ceramics are required to further establish its application in human biomedicine.

References

References

- [1] Shelby JE. Introduction to Glass Science and Technology : Edition 2. 2005.
- [2] Hench L. The story of Bioglass®. J Mater Sci: Mater Med 2006;17:967-78.
- [3] Hench LL. Bioceramics - from Concept to Clinic. J Am Ceram Soc 1991;74:1487-510.
- [4] Hench LL, Deegan HW, RVM. Glass and Medicine. Int J Appl Glass Sci;1:104--17.
- [5] Tilocca A. Structural models of bioactive glasses from molecular dynamics simulations. Proc R Soc A;2009;465:1003-27.
- [6] Tilocca A, Cormack AN, de Leeuw NH. The formation of nanoscale structures in soluble phosphosilicate glasses for biomedical applications: MD simulations. Faraday Discuss 2007;136:45-55.
- [7] Tilocca A, Cormack AN, de Leeuw NH. The structure of bioactive silicate glasses: New insight from molecular dynamics simulations. Chem Mater 2007;19:95-103.
- [8] Lefebvre L, Chevalier J, Gremillard L, Zenati R, Thollet G, Bernache-Assolant D, et al. Structural transformations of bioactive glass 45S5 with thermal treatments. Acta Materialia 2007;55:3305-13.
- [9] Bretcanu O, Chatzistavrou X, Paraskevopoulos K, Conradt R, Thompson I, Boccaccini AR. Sintering and crystallisation of 45S5 Bioglass® powder. J Eur Cer Soc 2009;29:3299-306.
- [10] Lefebvre L, Gremillard L, Chevalier J, Zenati R, Bernache-Assolant D. Sintering behaviour of 45S5 bioactive glass. Acta Biomater 2008;4:1894-903.
- [11] Wallace KE, Hill RG, Pembroke JT, Brown CJ, Hatton PV. Influence of sodium oxide content on bioactive glass properties. J Mater Sci: Mater Med 1999;10:697-701.
- [12] Jones JR, Hench LL. Regeneration of trabecular bone using porous ceramics. Curr Opin Solid St M 2003;7:301-7.
- [13] Johnell O, Kanis JA. An estimate of the worldwide prevalence and disability associated with osteoporotic fractures. Osteoporosis Int 2006;17:1726-33.
- [14] Gullberg B, Johnell O, Kanis JA. World-wide projections for hip fracture. Osteoporosis Int 1997;7:407-13.
- [15] Cooper C, Campion G, Melton LJ. Hip-Fractures in the Elderly - a Worldwide Projection. Osteoporosis Int 1992;2:285-9.
- [16] Nandi SK, Roy S, Mukherjee P, Kundu B, De DK, Basu D. Orthopaedic applications of bone graft & graft substitutes: a review. Indian J Med Res 2010;132:15-30.
- [17] Hench LL, Polak JM. Third-generation biomedical materials. Science 2002;295:1014.

- [18] Charnley J. Anchorage of the Femoral Head Prosthesis to the Shaft of the Femur. *J Bone Joint Surg Br* 1960;42:28-30.
- [19] Buddy D. Ratner ASH, Frederick J. Schoen and Jack E. Lemons 2012. 3 ed: Elsevier
- [20] Hench LL. Bioceramics. *J Am Ceram Soc* 1998;81:1705-28.
- [21] Hench LL, Paschall HA. Direct Chemical Bond of Bioactive Glass-Ceramic Materials to Bone and Muscle. *J Biomed Mater Res* 1973;7:25-42.
- [22] Kulkarni RK, Moore EG, Hegyeli AF, Leonard F. Biodegradable poly(lactic acid) polymers. *J Biomed Mater Res* 1971;5:169-81.
- [23] Goel A, Kapoor S, Rajagopal RR, Pascual MJ, Kim HW, Ferreira JMF. Alkali-free bioactive glasses for bone tissue engineering: A preliminary investigation. *Acta Biomater* 2012;8:361-72.
- [24] Shapoff CA, Alexander DC, Clark AE. Clinical use of a bioactive glass particulate in the treatment of human osseous defects. *Compendium of continuing education in dentistry (Jamesburg, NJ : 1995)* 1997;18:352-4, 6, 8 passim.
- [25] Jones JR. Review of bioactive glass: From Hench to hybrids. *Acta Biomater* 2013;9:4457-86.
- [26] Hench LL, Splinter RJ, Allen WC, Greenlee TK. Bonding mechanisms at the interface of ceramic prosthetic materials. *J Biomed Mater Res* 1971;5:117-41.
- [27] Xynos ID, Edgar AJ, Buttery LDK, Hench LL, Polak JM. Ionic products of bioactive glass dissolution increase proliferation of human osteoblasts and induce insulin-like growth factor II mRNA expression and protein synthesis. *Biochem Biophys Res Commun* 2000;276:461-5.
- [28] Xynos ID, Edgar AJ, Buttery LDK, Hench LL, Polak JM. Gene-expression profiling of human osteoblasts following treatment with the ionic products of Bioglass[®] 45S5 dissolution. *J Biomed Mater Res* 2001;55:151-7.
- [29] Leach JK, Kaigler D, Wang Z, Krebsbach PH, Mooney DJ. Coating of VEGF-releasing scaffolds with bioactive glass for angiogenesis and bone regeneration. *Biomaterials* 2006;27:3249-55.
- [30] Gorustovich AA, Roether JA, Boccaccini AR. Effect of Bioactive Glasses on Angiogenesis: A Review of In Vitro and In Vivo Evidences. *Tissue Eng Part B-Re* 2010;16:199-207.
- [31] Kaur G, Pandey OP, Singh K, Homa D, Scott B, Pickrell G. A review of bioactive glasses: Their structure, properties, fabrication, and apatite formation. *J Biomed Mater Res A* 2014;102:254-74.

- [32] Liu X, Rahaman MN, Fu QA. Oriented bioactive glass (13-93) scaffolds with controllable pore size by unidirectional freezing of camphene-based suspensions: Microstructure and mechanical response. *Acta Biomater* 2011;7:406-16.
- [33] Jung SB, Day DE, Day T, Stoecker W, Taylor P. Treatment of Non-Healing Diabetic Venous Stasis Ulcers with Bioactive Glass Nanofibers. *Wound Repair Regen* 2011;19:A30-A.
- [34] Abou Neel EA, Pickup DM, Valappil SP, Newport RJ, Knowles JC. Bioactive functional materials: a perspective on phosphate-based glasses. *J Mater Chem* 2009;19:690-701.
- [35] Li R, Clark AE, Hench LL. An investigation of bioactive glass powders by sol-gel processing. *J Appl Biomater* 1991;2:231-9.
- [36] Pereira MM, Clark AE, Hench LL. Calcium phosphate formation on sol-gel-derived bioactive glasses in vitro. *J Biomed Mater Res* 1994;28:693-8.
- [37] Martinez A, Izquierdo-Barba I, Vallet-Regi M. Bioactivity of a CaO - SiO₂ binary glasses system. *Chem Mater* 2000;12:3080-8.
- [38] Balamurugan A, Balossier G, Kannan S, Michel J, Rebelo AHS, Ferreira JMF. Development and in vitro characterization of sol-gel derived CaO-P₂O₅-SiO₂-ZnO bioglass. *Acta Biomater* 2007;3:255-62.
- [39] Hill R. An alternative view of the degradation of bioglass. *J Mater Sci Lett* 1996;15:1122-5.
- [40] Strnad Z. Role of the Glass Phase in Bioactive Glass-Ceramics. *Biomaterials* 1992;13:317-21.
- [41] Edén M. The split network analysis for exploring composition–structure correlations in multi-component glasses: I. Rationalizing bioactivity-composition trends of bioglasses. *J Non-Cryst Solids* 2011;357:1595-602.
- [42] Goel A, Kapoor S, Tilocca A, Rajagopal RR, Ferreira JMF. Structural role of zinc in biodegradation of alkali-free bioactive glasses. *J Mater Chem B* 2013;1:3073-82.
- [43] Sanders DM, Hench LL. Mechanisms of Glass Corrosion. *J Am Ceram Soc* 1973;56:373-7.
- [44] Hoppe A, Güldal NS, Boccaccini AR. A review of the biological response to ionic dissolution products from bioactive glasses and glass-ceramics. *Biomaterials* 2011;32:2757-74.
- [45] Hench LL, Boccaccini AR, Day RM, Gabe SM. Third-generation gene-activating biomaterials. *Mater Sci Forum* 2003;426-4:179-84.

- [46] Hench LL. Genetic design of bioactive glass. *Journal of the European Ceramic Society* 2009;29:1257-65.
- [47] Jugdaohsingh R. Silicon and bone health. *J Nutr Health Aging* 2007;11:99-110.
- [48] Carlisle EM. Silicon - a Requirement in Bone-Formation Independent of Vitamin-D1. *Calcified Tissue Int* 1981;33:27-34.
- [49] Carlisle EM. In vivo requirement for silicon in articular cartilage and connective tissue formation in the chick. *J Nutr* 1976;106:478-84.
- [50] Schwarz K. A bound form of silicon in glycosaminoglycans and polyuronides. *Proc Natl Acad Sci U S A* 1973;70:1608-12.
- [51] Reffitt DM, Ogston N, Jugdaohsingh R, Cheung HFJ, Evans BAJ, Thompson RPH, et al. Orthosilicic acid stimulates collagen type 1 synthesis and osteoblastic differentiation in human osteoblast-like cells in vitro. *Bone* 2003;32:127-35.
- [52] Hott M, De Pollak C, Modrowski D, Marie PJ. Short-term effects of organic silicon on trabecular bone in mature ovariectomized rats. *Calcified Tissue Int* 1993;53:174-9.
- [53] Seaborn CD, Nielsen FH. Dietary silicon and arginine affect mineral element composition of rat femur and vertebra. *Bio Trace Elem Res* 2002;89:239-50.
- [54] Seaborn CD, Nielsen FH. Dietary silicon affects acid and alkaline phosphatase and Calcium uptake in bone of rats. *J Trace Ele Exp Med* 1994;7:11-8.
- [55] Kim MH, Bae YJ, Choi MK, Chung YS. Silicon Supplementation Improves the Bone Mineral Density of Calcium-Deficient Ovariectomized Rats by Reducing Bone Resorption. *Bio Trace Elem Res* 2009;128:239-47.
- [56] Bonnelye E, Chabadel A, Saltel F, Jurdic P. Dual effect of strontium ranelate: Stimulation of osteoblast differentiation and inhibition of osteoclast formation and resorption in vitro. *Bone* 2008;42:129-38.
- [57] Marie PJ, Hott M, Modrowski D, Depollak C, Guillemain J, Deloffre P, et al. An Uncoupling Agent Containing Strontium Prevents Bone Loss by Depressing Bone-Resorption and Maintaining Bone-Formation in Estrogen-Deficient Rats. *J Bone Miner Res* 1993;8:607-15.
- [58] Gentleman E, Fredholm YC, Jell G, Lotfibakhshaiesh N, O'Donnell MD, Hill RG, et al. The effects of strontium-substituted bioactive glasses on osteoblasts and osteoclasts in vitro. *Biomaterials* 2010;31:3949-56.
- [59] Agren MS. Studies on zinc in wound healing. *Acta dermato-venereologica Supplementum* 1990;154:1-36.

- [60] Staiger MP, Pietak AM, Huadmai J, Dias G. Magnesium and its alloys as orthopedic biomaterials: A review. *Biomaterials* 2006;27:1728-34.
- [61] Zreiqat H, Howlett CR, Zannettino A, Evans P, Schulze-Tanzil G, Knabe C, et al. Mechanisms of magnesium-stimulated adhesion of osteoblastic cells to commonly used orthopaedic implants. *J Biomed Mater Res* 2002;62:175-84.
- [62] Rude RK, Gruber HE, Wei LY, Frausto A, Mills BG. Magnesium deficiency: Effect on bone and mineral metabolism in the mouse. *Calcified Tissue Int* 2003;72:32-41.
- [63] Rude RK, Gruber HE, Norton HJ, Wei LY, Frausto A, Kilburn J. Dietary magnesium reduction to 25% of nutrient requirement disrupts bone and mineral metabolism in the rat. *Bone* 2005;37:211-9.
- [64] Saris NEL, Mervaala E, Karppanen H, Khawaja JA, Lewenstam A. Magnesium - An update on physiological, clinical and analytical aspects. *Clinica Chimica Acta* 2000;294:1-26.
- [65] Vormann J. Magnesium: Nutrition and metabolism. *Mol Aspects Med* 2003;24:27-37.
- [66] Cashman KD. Calcium intake, calcium bioavailability and bone health. *Br J Nutr* 2002;87:S169-77.
- [67] Maeno S, Niki Y, Matsumoto H, Morioka H, Yatabe T, Funayama A, et al. The effect of calcium ion concentration on osteoblast viability, proliferation and differentiation in monolayer and 3D culture. *Biomaterials* 2005;26:4847-55.
- [68] Marie PJ. The calcium-sensing receptor in bone cells: A potential therapeutic target in osteoporosis. *Bone* 2010;46:571-6.
- [69] Valerio P, Pereira MM, Goes AM, Leite MF. Effects of extracellular calcium concentration on the glutamate release by bioactive glass (BG60S) preincubated osteoblasts. *Biomed Mater* 2009;4.
- [70] Hinoi E, Takarada T, Yoneda Y. Glutamate signaling system in bone. *J Pharmacol Sci* 2004;94:215-20.
- [71] Julien M, Khoshniat S, Lacreusette A, Gatius M, Bozec A, Wagner EF, et al. Phosphate-Dependent Regulation of MGP in Osteoblasts: Role of ERK1/2 and Fra-1. *J Bone Miner Res* 2009;24:1856-68.
- [72] Meleti Z, Shapiro IM, Adams CS. Inorganic phosphate induces apoptosis of osteoblast-like cells in culture. *Bone* 2000;27:359-66.
- [73] Sepulveda P, Jones JR, Hench LL. In vitro dissolution of melt-derived 45S5 and sol-gel derived 58S bioactive glasses. *J Biomed Mater Res* 2002;61:301-11.

- [74] Kansal I, Reddy A, Muñoz F, Choi S-J, Kim H-W, Tulyaganov DU, et al. Structure, biodegradation behavior and cytotoxicity of alkali-containing alkaline-earth phosphosilicate glasses. *Mater Sci Eng C* 2014;44:159-65.
- [75] Hench LL, Spilman DB, Hench JW. Fluoride-containing Bioglass™ compositions. Google Patents; 1988.
- [76] Andersson OH, Liu GZ, Karlsson KH, Niemi L, Miettinen J, Juhanoja J. In vivo Behavior of Glasses in the SiO₂-Na₂O-CaO-P₂O₅-Al₂O₃-B₂O₃ System. *J Mater Sci: Mater M* 1990;1:219-27.
- [77] Brink M, Turunen T, Happonen RP, YliUrpo A. Compositional dependence of bioactivity of glasses in the system Na₂O-K₂O-MgO-CaO-B₂O₃-P₂O₅-SiO₂. *J Biomed Mater Res* 1997;37:114-21.
- [78] Gomez-Vega JM, Saiz E, Tomsia AP, Oku T, Suganuma K, Marshall GW, et al. Novel Bioactive Functionally Graded Coatings on Ti6Al4V. *Adv Mater* 2000;12:894-8.
- [79] Kokubo TS, Masazumi; Nagashima, Yukihito; Tashiro, Megumi; Nakamura, Takashi; Yamamuro, Takao; Higashi, Shoichiro. Apatite- and Wollastonite-Containing Glass-Ceramics for Prosthetic Application. *Bull Inst Chem Res Kyoto Univ* 1982;60:260-8.
- [80] Elgayar I, Aliev AE, Boccaccini AR, Hill RG. Structural analysis of bioactive glasses. *J Non-Cryst Solids* 2005;351:173-83.
- [81] Vogel M, Voigt C, Gross UM, Muller-Mai CM. In vivo comparison of bioactive glass particles in rabbits. *Biomaterials* 2001;22:357-62.
- [82] Lusvardi G, Zaffe D, Menabue L, Bertoldi C, Malavasi G, Consolo U. In vitro and in vivo behaviour of zinc-doped phosphosilicate glasses. *Acta Biomater* 2009;5:419-28.
- [83] Lusvardi G, Malavasi G, Menabue L, Aina V, Morterra C. Fluoride-containing bioactive glasses: Surface reactivity in simulated body fluids solutions. *Acta Biomater* 2009;5:3548-62.
- [84] Zhang D, Hupa M, Hupa L. In situ pH within particle beds of bioactive glasses. *Acta Biomater* 2008;4:1498-505.
- [85] Chen QZ, Li YA, Jin LY, Quinn JMW, Komesaroff PA. A new sol-gel process for producing Na₂O-containing bioactive glass ceramics. *Acta Biomater* 2010;6:4143-53.
- [86] Waltimo T, Brunner TJ, Vollenweider M, Stark WJ, Zehnder M. Antimicrobial effect of nanometric bioactive glass 45S5. *J Dent Res* 2007;86:754-7.
- [87] Brauer DS, Karpukhina N, O'Donnell MD, Law RV, Hill RG. Fluoride-containing bioactive glasses: Effect of glass design and structure on degradation, pH and apatite formation in simulated body fluid. *Acta Biomater* 2010;6:3275-82.

- [88] Shibuya T, Morita Y, Matsui A. No alkali containing biocompatible glass ceramic with apatite, wollastonite and diopside crystals mixed. Google Patents; 1988.
- [89] Andersson OH, Peltola JK. Bioactive glass as a bone substitute. Google Patents; 1993.
- [90] Brink M, Karlsson K, Yli-Uro A. Novel bioactive glasses and their use. Google Patents; 1997.
- [91] Hill RG, Stevens MM. Bioactive glass. Google Patents; 2007.
- [92] O'donnell M, Hill RG. Multicomponent Glasses for use in Personal Care Products. Google Patents; 2011.
- [93] Brink M. The influence of alkali and alkaline earths on the working range for bioactive glasses. *J Biomed Mater Res* 1997;36:109-17.
- [94] Kokubo T, Hayashi T, Sakka S, Kitsugi T, Yamamuro T. Bonding between bioactive glasses, glass-ceramics or ceramics in a simulated body fluid. *Yogyo Kyokai Shi/J Cer Soc Japan* 1987;95:785-91.
- [95] Kitsugi T, Yamamuro T, Nakamura T, Kokubo T, Takagi M, Shibuya T, et al. Bonding behavior between two bioactive ceramics in vivo. *J Biomed Mater Res* 1987;2 1:1109-1123.
- [96] Kasuga T, Nakagawa K, Yoshida M, Miyade E. Compositional dependence of formation of an apatite layer on glass-ceramics in simulated physiological solution. *J Mater Sci* 1987;22:3721-4.
- [97] Ohura K, Nakamura T, Yamamuro T, Ebisawa Y, Kokubo T, Kotoura Y, et al. Bioactivity of $\text{CaO}\cdot\text{SiO}_2$ Glasses Added with Various Ions. *J Mater Sci: Mater M* 1992;3:95-100.
- [98] Galliano PG, Lopez JMP. Thermal-Behavior of Bioactive Alkaline-Earth Silicophosphate Glasses. *J Mater Sci: Mater M* 1995;6:353-9.
- [99] Salinas AJ, Román J, Vallet-Regi M, Oliveira JM, Correia RN, Fernandes MH. In vitro bioactivity of glass and glass-ceramics of the $3\text{CaO}\cdot\text{P}_2\text{O}_5\text{-CaO}\cdot\text{SiO}_2\text{-CaO}\cdot\text{MgO}\cdot 2\text{SiO}_2$ system. *Biomaterials* 2000;21:251-7.
- [100] Oliveira JM, Correia RN, Fernandes MH. Surface modifications of a glass and a glass-ceramic of the $\text{MgO}\cdot 3\text{CaO}\cdot\text{P}_2\text{O}_5\text{-SiO}_2$ system in a simulated body fluid. *Biomaterials* 1995;16:849-54.
- [101] Oliveira JM, Correia RN, Fernandes MH, Rocha J. Influence of the CaO/MgO ratio on the structure of phase-separated glasses: A solid state ^{29}Si and ^{31}P MAS NMR study. *J Non-Cryst Solids* 2000;265:221-9.
- [102] Oliveira JM, Correia RN, Fernandes MH. Effects of Si speciation on the in vitro bioactivity of glasses. *Biomaterials* 2002;23:371-9.

- [103] Kamitakahara M, Ohtsuki C, Kozaka Y, Ogata S, Tanihara M, Miyazaki T. Preparation of porous glass-ceramics containing whitlockite and diopside for bone repair. *J Ceram Soc Jpn* 2006;114:82-6.
- [104] Kansal I, Goel A, Tulyaganov DU, Santos LF, Ferreira JMF. Structure, surface reactivity and physico-chemical degradation of fluoride containing phospho-silicate glasses. *J Mater Chem* 2011;21:8074-84.
- [105] Kansal I, Goel A, Tulyaganov DU, Pascual MJ, Lee HY, Kim HW, et al. Diopside ($\text{CaO}\cdot\text{MgO}\cdot 2\text{SiO}_2$)-fluorapatite ($9\text{CaO}\cdot 3\text{P}_2\text{O}_5\cdot \text{CaF}_2$) glass-ceramics: potential materials for bone tissue engineering. *J Mater Chem* 2011;21:16247-56.
- [106] Kansal I, Goel A, Tulyaganov DU, Rajagopal RR, Ferreira JMF. Structural and thermal characterization of $\text{CaO-MgO-SiO}_2\text{-P}_2\text{O}_5\text{-CaF}_2$ glasses. *J Eur Cer Soc* 2012;32:2739-46.
- [107] Rawlings RD. Composition Dependence of the Bioactivity of Glasses. *J Mater Sci Lett* 1992;11:1340-3.
- [108] Hupa L, Hupa M. Recent Research on Composition Dependence of the Properties of Bioactive Glasses. *Advances in Bioceramics and Biotechnologies: John Wiley & Sons, Inc.;* 2010. p. 145-56.
- [109] Peitl O, Zanotto ED, Serbena FC, Hench LL. Compositional and microstructural design of highly bioactive $\text{P}_2\text{O}_5\text{-Na}_2\text{O-CaO-SiO}_2$ glass-ceramics. *Acta Biomater* 2012;8:321-32.
- [110] Linati L, Lusvardi G, Malavasi G, Menabue L, Menziani MC, Mustarelli P, et al. Qualitative and Quantitative Structure-Property Relationships Analysis of Multicomponent Potential Bioglasses. *J Phys Chem B* 2005;109:4989-98.
- [111] Lusvardi G, Malavasi G, Tarsitano F, Menabue L, Menziani MC, Pedone A. Quantitative Structure-Property Relationships of Potentially Bioactive Fluoro Phospho-silicate Glasses. *J Phys Chem B* 2009;113:10331-8.
- [112] O'Donnell MD, Hill RG. Influence of strontium and the importance of glass chemistry and structure when designing bioactive glasses for bone regeneration. *Acta Biomater* 2010;6:2382-5.
- [113] Lusvardi G, Malavasi G, Cortada M, Menabue L, Menziani MC, Pedone A, et al. Elucidation of the structural role of fluorine in potentially bioactive glasses by experimental and computational investigation. *J Phys Chem B* 2008;112:12730-9.
- [114] Fredholm YC, Karpukhina N, Law RV, Hill RG. Strontium containing bioactive glasses: Glass structure and physical properties. *J Non-Cryst Solids* 2010;356:2546-51.
- [115] Bonhomme C, Gervais C, Folliet N, Pourpoint F, Coelho Diogo C, Lao J, et al. ^{87}Sr Solid-State NMR as a Structurally Sensitive Tool for the Investigation of Materials:

Antiosteoporotic Pharmaceuticals and Bioactive Glasses. *J Am Chem Soc* 2012;134:12611-28.

[116] Martin RA, Twyman HL, Rees GJ, Smith JM, Barney ER, Smith ME, et al. A structural investigation of the alkali metal site distribution within bioactive glass using neutron diffraction and multinuclear solid state NMR. *Phys Chem Chem Phys* 2012;14:12105-13.

[117] Pedone A, Charpentier T, Menziani MC. The structure of fluoride-containing bioactive glasses: new insights from first-principles calculations and solid state NMR spectroscopy. *J Mater Chem* 2012;22:12599-608.

[118] Watts SJ, Hill RG, O'Donnell MD, Law RV. Influence of magnesia on the structure and properties of bioactive glasses. *J Non-Cryst Solids* 2010;356:517-24.

[119] Fredholm YC, Karpukhina N, Brauer DS, Jones JR, Law RV, Hill RG. Influence of strontium for calcium substitution in bioactive glasses on degradation, ion release and apatite formation. *J Roy Soc Interface* 2012;9:880-9.

[120] Aina V, Malavasi G, Fiorio Pla A, Munaron L, Morterra C. Zinc-containing bioactive glasses: Surface reactivity and behaviour towards endothelial cells. *Acta Biomater* 2009;5:1211-22.

[121] Lao J, Jallot E, Nedelec J-M. Strontium-Delivering Glasses with Enhanced Bioactivity: A New Biomaterial for Antiosteoporotic Applications? *Chem Mater* 2008;20:4969-73.

[122] Lao J, Nedelec JM, Jallot E. New strontium-based bioactive glasses: physicochemical reactivity and delivering capability of biologically active dissolution products. *J Mater Chem* 2009;19:2940-9.

[123] Navarro M, Ginebra M-P, Clément J, Salvador M, Gloria A, Planell JA. Physicochemical Degradation of Titania-Stabilized Soluble Phosphate Glasses for Medical Applications. *J Am Ceram Soc* 2003;86:1345-52.

[124] Dias AG, Gibson IR, Santos JD, Lopes MA. Physicochemical degradation studies of calcium phosphate glass ceramic in the CaO–P₂O₅–MgO–TiO₂ system. *Acta Biomater* 2007;3:263-9.

[125] Murphy S, Wren A, Towler M, Boyd D. The effect of ionic dissolution products of Ca–Sr–Na–Zn–Si bioactive glass on in vitro cytocompatibility. *J Mater Sci: Mater Med* 2010;21:2827-34.

[126] Serra J, González P, Liste S, Chiussi S, León B, Pérez-Amor M, et al. Influence of the non-bridging oxygen groups on the bioactivity of silicate glasses. *J Mater Sci: Mater Med* 2002;13:1221-5.

- [127] Tilocca A. Short- and medium-range structure of multicomponent bioactive glasses and melts: An assessment of the performances of shell-model and rigid-ion potentials. *J Chem Phys* 2008;129.
- [128] Tilocca A. Sodium migration pathways in multicomponent silicate glasses: Car-Parrinello molecular dynamics simulations. *J Chem Phys* 2010;133.
- [129] Hill RG, Brauer DS. Predicting the bioactivity of glasses using the network connectivity or split network models. *J Non-Cryst Solids* 2011;357:3884-7.
- [130] Tas AC. Synthesis of biomimetic Ca-hydroxyapatite powders at 37 degrees C in synthetic body fluids. *Biomaterials* 2000;21:1429-38.
- [131] Nonami T, Tsutsumi S. Study of diopside ceramics for biomaterials. *J Mater Sci: Mater Med* 1999;10:475-9.
- [132] De Aza PN, Luklinska ZB, Anseau M. Bioactivity of diopside ceramic in human parotid saliva. *Journal of biomedical materials research Part B, Appl Biomater* 2005;73:54-60.
- [133] Nakajima S, Harada Y, Kurihara Y, Wakatsuki T, Noma H. [Physicochemical characteristics of new reinforcement ceramic implant]. *Shika gakuho Dental science reports* 1989;89:1709-17.
- [134] Nakajima S. [Experimental studies of healing process on reinforcement ceramic implantation in rabbit mandible]. *Shika gakuho Dental science reports* 1990;90:525-53.
- [135] Yoganand C, Selvarajan V, Lusvarghi L, Goudouri OM, Paraskevopoulos KM, Rouabhia M. Bioactivity of CaO-MgO-SiO₂ glass ceramics synthesized using transferred arc plasma (TAP) process. *Mater Sci Eng C* 2009;29:1759-64.
- [136] Jana C, Braun M. ¹⁹F NMR spectroscopy of glass ceramics containing fluorapatites. *Biomaterials* 1996;17:2065-9.
- [137] Abo-Mosallam HA, Hill RG, Karpukhina N, Law RV. MAS-NMR studies of glasses and glass-ceramics based on a clinopyroxene-fluorapatite system. *J Mater Chem* 2010;20:790-7.
- [138] Tulyaganov DU, Agathopoulos S, Fernandes HR, Ventura JM, Ferreira JMF. Preparation and crystallization of glasses in the system tetrasilicic mica-fluorapatite-diopside. *J Eur Cer Soc* 2004;24:3521-8.
- [139] Wang Z, Guo Z, Bai H, Li J, Li X, Chen G, et al. Clinical evaluation of β -TCP in the treatment of lacunar bone defects: A prospective, randomized controlled study. *Mater Sci Eng C* 2013;33:1894-9.

- [140] Kotobuki N, Kawagoe D, Nomura D, Katou Y, Muraki K, Fujimori H, et al. Observation and quantitative analysis of rat bone marrow stromal cells cultured in vitro on newly formed transparent beta-tricalcium phosphate. *J Mater Sci: Mater Med* 2006;17:33-41.
- [141] Ashizuka M, Ishida E. Mechanical properties of silicate glass-ceramics containing tricalcium phosphate. *J Mater Sci* 1997;32:185-8.
- [142] Tilocca A. Structure and dynamics of bioactive phosphosilicate glasses and melts from ab initio molecular dynamics simulations. *Phys Rev B* 2007;76.
- [143] Tilocca A, Cormack AN. Structural effects of phosphorus inclusion in bioactive silicate glasses. *J Phys Chem B* 2007;111:14256-64.
- [144] Bohner M, Lemaître J. Can bioactivity be tested in vitro with SBF solution? *Biomaterials* 2009;30:2175-9.
- [145] Fujibayashi S, Neo M, Kim HM, Kokubo T, Nakamura T. A comparative study between in vivo bone ingrowth and in vitro apatite formation on Na₂O-CaO-SiO₂ glasses. *Biomaterials* 2003;24:1349-56.
- [146] Kokubo T, Takadama H. How useful is SBF in predicting in vivo bone bioactivity? *Biomaterials* 2006;27:2907-15.
- [147] Cerruti M, Morterra C. Carbonate formation on bioactive glasses. *Langmuir* 2004;20:6382-8.
- [148] Pérez-Pariente J, Balas F, Vallet-Regí M. Surface and Chemical Study of SiO₂·P₂O₅·CaO·(MgO) Bioactive Glasses. *Chem Mater* 2000;12:750-5.
- [149] Karlsson KH, Fröberg K, Ringbom T. A structural approach to bone adhering of bioactive glasses. *J Non-Cryst Solids* 1989;112:69-72.
- [150] Jones JR, Sepulveda P, Hench LL. Dose-dependent behavior of bioactive glass dissolution. *J Biomed Mater Res* 2001;58:720-6.
- [151] Lara C, Pascual MJ, Duran A. Glass-forming ability, sinterability and thermal properties in the systems RO-BaO-SiO₂ (R = Mg, Zn). *J Non-Cryst Solids* 2004;348:149-55.
- [152] Magallanes-Perdomo M, Pena P, De Aza PN, Carrodeguas RG, Rodriguez MA, Turrillas X, et al. Devitrification studies of wollastonite-tricalcium phosphate eutectic glass. *Acta Biomater* 2009;5:3057-66.
- [153] Lusvardi G, Malavasi G, Menabue L, Menziani MC, Pedone A, Segre U, et al. Properties of zinc releasing surfaces for clinical applications. *J Biomater Appl* 2008;22:505-26.
- [154] Murphy S, Boyd D, Moane S, Bennett M. The effect of composition on ion release from Ca-Sr-Na-Zn-Si glass bone grafts. *J Mater Sci: Mater Med* 2009;20:2207-14.

- [155] Du RL, Chang J. Preparation and characterization of Zn and Mg doped bioactive glasses. *J Inorg Mater* 2004;19:1353-8.
- [156] Du RL, Chang J, Ni SY, Zhai WY, Wang JY. Characterization and in vitro bioactivity of zinc-containing bioactive glass and glass-ceramics. *J Biomater Appl* 2006;20:341-60.
- [157] Aina V, Perardi A, Bergandi L, Malavasi G, Menabue L, Morterra C, et al. Cytotoxicity of zinc-containing bioactive glasses in contact with human osteoblasts. *Chem Biol Interact* 2007;167:207-18.
- [158] Kamitakahara M, Ohtsuki C, Inada H, Tanihara M, Miyazaki T. Effect of ZnO addition on bioactive CaO-SiO₂-P₂O₅-CaF₂ glass-ceramics containing apatite and wollastonite. *Acta Biomater* 2006;2:467-71.
- [159] Du RL, Chang J. The influence of Zn on the deposition of HA on sol-gel derived bioactive glass. *Bio Med Mater Eng* 2006;16:229-36.
- [160] Salinas AJ, Shruti S, Malavasi G, Menabue L, Vallet-Regi M. Substitutions of cerium, gallium and zinc in ordered mesoporous bioactive glasses. *Acta Biomater* 2011;7:3452-8.
- [161] Rahaman MN, Day DE, Bal BS, Fu Q, Jung SB, Bonewald LF, et al. Bioactive glass in tissue engineering. *Acta Biomater* 2011;7:2355-73.
- [162] Oudadesse H, Dietrich E, Gal YL, Pellen P, Bureau B, Mostafa AA, et al. Apatite forming ability and cytocompatibility of pure and Zn-doped bioactive glasses. *Biomed Mater* 2011;6.
- [163] Oudadesse H, Dietrich E, Lucas-Girot A, Le Gal Y, Jeanne S, Cathelineau G. Effects of Mg and Zn on the surface of doped melt-derived glass for biomaterials applications. *Appl Surf Sci* 2008;255:391-5.
- [164] Bini M, Grandi S, Capsoni D, Mustarelli P, Saino E, Visai L. SiO₂-P₂O₅-CaO Glasses and Glass-Ceramics with and without ZnO: Relationships among Composition, Microstructure, and Bioactivity. *J Phys Chem C* 2009;113:8821-8.
- [165] Saino E, Grandi S, Quartarone E, Maliardi V, Galli D, Bloise N, et al. In vitro calcified matrix deposition by human osteoblasts onto a zinc-containing bioactive glass. *Eur Cell Mater* 2011;21:59-72; discussion
- [166] Roy B, Jain H, Saha SK, Chakravorty D. Comparison of structure of alkali silicate glasses prepared by sol-gel and melt-quench methods. *J Non-Cryst Solids* 1995;183:268-76.
- [167] Linati L, Lusvardi G, Malavasi G, Menabue L, Menziani MC, Mustarelli P, et al. Medium-range order in phospho-silicate bioactive glasses: Insights from MAS-NMR spectra, chemical durability experiments and molecular dynamics simulations. *J Non-Cryst Solids* 2008;354:84-9.

- [168] Termine JD, Peckauskas RA, Posner AS. Calcium phosphate formation in vitro: II. Effects of environment on amorphous-crystalline transformation. *Arch Biochem Biophys* 1970;140:318-25.
- [169] Wang L, Nancollas GH. Calcium Orthophosphates: Crystallization and Dissolution. *Chem Rev* 2008;108:4628-69.
- [170] Dorozhkin SV, Epple M. Biological and Medical Significance of Calcium Phosphates. *Angew Chem Int Ed* 2002;41:3130-46.
- [171] Ebisawa Y, Kokubo T, Ohura K, Yamamuro T. Bioactivity of CaO•SiO₂-based glasses: in vitro evaluation. *J Mater Sci: Mater Med* 1990;1:239-44
- [172] Hoppe A, Guldal NS, Boccaccini AR. A review of the biological response to ionic dissolution products from bioactive glasses and glass-ceramics. *Biomaterials* 2011;32:2757-74.
- [173] Aina V, Bonino F, Morterra C, Miola M, Bianchi CL, Malavasi G, et al. Influence of the Chemical Composition on Nature and Activity of the Surface Layer of Zn-Substituted Sol-Gel (Bioactive) Glasses. *J Phys Chem C* 2011;115:2196-210.
- [174] Courtheoux L, Lao J, Nedelec JM, Jallot E. Controlled bioactivity in zinc-doped sol-gel-derived binary bioactive glasses. *J Phys Chem C* 2008;112:13663-7.
- [175] Haimi S, Gorianc G, Moimas L, Lindroos B, Huhtala H, Raty S, et al. Characterization of zinc-releasing three-dimensional bioactive glass scaffolds and their effect on human adipose stem cell proliferation and osteogenic differentiation. *Acta Biomater* 2009;5:3122-31.
- [176] Popp JR, Love BJ, Goldstein AS. Effect of soluble zinc on differentiation of osteoprogenitor cells. *J Biomed Mater Res A* 2007;81A:766-9.
- [177] Dellamea G, Gasparotto A, Bettinelli M, Montenero A, Scaglioni R. Chemical Durability of Zinc-Containing Glasses. *J Non-Cryst Solids* 1986;84:443-51.
- [178] Bock CW, Katz AK, Markham GD, Glusker JP. Manganese as a replacement for magnesium and zinc: Functional comparison of the divalent ions. *J Am Chem Soc* 1999;121:7360-72.
- [179] Cassingham NJ, Stennett MC, Bingham PA, Hyatt NC, Aquilanti G. The Structural Role of Zn in Nuclear Waste Glasses. *Int J Appl Glass Sci* 2011;2:343-53.
- [180] Le Grand M, Ramos AY, Calas G, Galois L, Ghaleb D, Pacaud F. Zinc environment in aluminoborosilicate glasses by ZnK-edge extended x-ray absorption fine structure spectroscopy. *J Mater Res* 2000;15:2015-9.
- [181] Calas G, Cormier L, Galois L, Jollivet P. Structure–property relationships in multicomponent oxide glasses. *Comptes Rendus Chimie* 2002;5:831-43.

- [182] Li P, Ohtsuki C, Kokubo T, Nakanishi K, Soga N, Nakamura T, et al. Apatite Formation Induced by Silica Gel in a Simulated Body Fluid. *J Am Ceram Soc* 1992;75:2094-7.
- [183] Fu Q, Saiz E, Rahaman MN, Tomsia AP. Bioactive glass scaffolds for bone tissue engineering: state of the art and future perspectives. *Mater Sci Eng C* 2011;31:1245-56.
- [184] Pawlowski L. *The Science and Engineering of Thermal Spray Coatings*. England: John Wiley & Sons Ltd; 2008.
- [185] Luo Y-R. *Comprehensive Handbook of Chemical Bond Energies*: CRC Press; 2010
- [186] Toyoda S, Fujino S, Morinaga K. Density, viscosity and surface tension of 50RO-50P(2)O(5) (R : Mg, Ca, Sr, Ba, and Zn) glass melts. *J Non-Cryst Solids* 2003;321:169-74.
- [187] Doremus RH. *Glass Science*. 2nd ed: John Wiley & Sons, Inc., New York; 1994. p. pp105.
- [188] Chapter 4 29Si NMR. In: Kenneth JDM, Mark ES, editors. *Pergamon Materials Series*: Pergamon; 2002. p. 201-68.
- [189] Li P, Yang Q, Zhang F, Kokubo T. The Effect of Residual Glassy Phase in a Bioactive Glass-Ceramic on the Formation of Its Surface Apatite Layer In vitro. *J Mater Sci: Mater Med* 1992;3:452-6.
- [190] Chai FG, Truong-Tran AQ, Ho LH, Zalewski PD. Regulation of caspase activation and apoptosis by cellular zinc fluxes and zinc deprivation: A review. *Immunol Cell Biol* 1999;77:272-8.
- [191] Choi DW, Koh JY. Zinc and brain injury. *Annu Rev Neurosci* 1998;21:347-75.
- [192] Zhang H, Ye XJ, Li JS. Preparation and biocompatibility evaluation of apatite/wollastonite-derived porous bioactive glass ceramic scaffolds. *Biomed Mater* 2009;4.
- [193] SA O, SH K, JE W, JJ K, US S, HW K. Effects on growth and osteogenic differentiation of mesenchymal stem cells by the zinc-added sol-gel bioactive glass granules. *Journal of Tissue Engineering* 2010;2010:475206.
- [194] Verne E, Ferraris S, Vitale-Brovarone C, Spriano S, Bianchi CL, Naldoni A, et al. Alkaline phosphatase grafting on bioactive glasses and glass ceramics. *Acta Biomater* 2010;6:229-40.
- [195] Hench LL, Xynos ID, Polak JM. Bioactive glasses for in situ tissue regeneration. *J Biomat Sci Polym E* 2004;15:543-62.
- [196] Nielsen SP. The biological role of strontium. *Bone* 2004;35:583-8.

- [197] Siccardi AJ, Padgett-Vasquez S, Garris HW, Nagy TR, D'Abramo LR, Watts SA. Dietary Strontium Increases Bone Mineral Density in Intact Zebrafish (*Danio rerio*): A Potential Model System for Bone Research. *Zebrafish* 2010;7:267-73.
- [198] Fujikura K, Karpukhina N, Kasuga T, Brauer DS, Hill RG, Law RV. Influence of strontium substitution on structure and crystallisation of Bioglass[®] 45S5. *J Mater Chem* 2012;22:7395-402.
- [199] Boyd D, Carroll G, Towler MR, Freeman C, Farthing P, Brook IM. Preliminary investigation of novel bone graft substitutes based on strontium-calcium-zinc-silicate glasses. *J Mater Sci-Mater M* 2009;20:413-20.
- [200] Boyd D, Towler MR, Watts S, Hill RG, Wren AW, Clarkin OM. The role of Sr²⁺ on the structure and reactivity of SrO-CaO-ZnO-SiO₂ ionomer glasses. *J Mater Sci: Mater Med* 2008;19:953-7.
- [201] Looney M, O'Shea H, Boyd D. Preliminary evaluation of therapeutic ion release from Sr-doped zinc-silicate glass ceramics. *J Biomater Appl* 2013;27:511-24.
- [202] Towler MR, Boyd D, Freeman C, Brook IM, Farthing P. Comparison of in vitro and in vivo Bioactivity of SrO-CaO-ZnO-SiO₂ Glass Grafts. *J Biomater Appl* 2009;23:561-72.
- [203] Xiang Y, Du JC, Skinner LB, Benmore CJ, Wren AW, Boydd DJ, et al. Structure and diffusion of ZnO-SrO-CaO-Na₂O-SiO₂ bioactive glasses: a combined high energy X-ray diffraction and molecular dynamics simulations study. *RSCAdvances* 2013;3:5966-78.
- [204] Goel A, Rajagopal RR, Ferreira JMF. Influence of strontium on structure, sintering and biodegradation behaviour of CaO-MgO-SrO-SiO₂-P₂O₅-CaF₂ glasses. *Acta Biomater* 2011;7:4071-80.
- [205] Omori K. Analysis of Infrared Absorption Spectrum of Diopside. *Am Mineral* 1971;56:1607.
- [206] Peitl O, Zanutto ED, Hench LL. Highly bioactive P₂O₅-Na₂O-CaO-SiO₂ glass-ceramics. *J Non-Cryst Solids* 2001;292:115-26.
- [207] Christodoulou I, Buttery LDK, Saravanapavan P, Tai GP, Hench LL, Polak JM. Dose- and time-dependent effect of bioactive gel-glass ionic-dissolution products on human fetal osteoblast-specific gene expression. *J Biomed Mater Res B* 2005;74B:529-37.
- [208] Clover J, Gowen M. Are Mg-63 and Hos Te85 Human Osteosarcoma Cell-Lines Representative Models of the Osteoblastic Phenotype. *Bone* 1994;15:585-91.
- [209] Lajeunesse D, Frondoza C, Schoffield B, Sacktor B. Osteocalcin Secretion by the Human Osteosarcoma Cell-Line Mg-63. *J Bone Miner Res* 1990;5:915-22.

- [210] Lajeunesse D, Kiebzak GM, Frondoza C, Sacktor B. Regulation of Osteocalcin Secretion by Human Primary Bone-Cells and by the Human Osteosarcoma Cell-Line Mg-63. *Bone Miner* 1991;14:237-50.
- [211] Chen L. Okadaic acid induces apoptosis through the PKR, NF-kappa B and caspase pathway in human osteoblastic osteosarcoma MG63 cells. *Toxicol in Vitro* 2011;25:1796-802.
- [212] Wang Y, Wei YD, Zhang HY, Shi YF, Li YL, Li RG. Arsenic trioxide induces apoptosis of p53 null osteosarcoma MG63 cells through the inhibition of catalase. *Med Oncol* 2012;29:1328-34.
- [213] Li M, Zhao L, Liu J, Liu A-L, Zeng W-S, Luo S-Q, et al. Hydrogen Peroxide Induces G2 Cell Cycle Arrest and Inhibits Cell Proliferation in Osteoblasts. *The Anat Rec: Adv Integ Anat Evol Biol* 2009;292:1107-13.
- [214] Kapoor S, Goel A, Tilocca A, Dhuna V, Bhatia G, Dhuna K, et al. Role of glass structure in defining the chemical dissolution behavior, bioactivity and antioxidant properties of zinc and strontium co-doped alkali-free phosphosilicate glasses. *Acta Biomater* 2014;10:3264-78.
- [215] Senkoylu A, Yilmaz A, Ergun M, İlhan M, Simsek A, Altun N, et al. Effect of Strontium Ranelate on Hydrogen Peroxide-Induced Apoptosis of CRL-11372 Cells. *Biochem Genet* 2008;46:197-205.
- [216] Bergandi L, Aina V, Garetto S, Malavasi G, Aldieri E, Laurenti E, et al. Fluoride-containing bioactive glasses inhibit pentose phosphate oxidative pathway and glucose 6-phosphate dehydrogenase activity in human osteoblasts. *Chem Biol Interact* 2010;183:405-15.
- [217] Rosenfeldt F, Wilson M, Lee G, Kure C, Ou R, Braun L, et al. Oxidative stress in surgery in an ageing population: Pathophysiology and therapy. *Exp Gerontol* 2013;48:45-54.
- [218] Cornell CN, Lane JM. Newest Factors in Fracture Healing. *Clinical Orthopaedics and Related Research* 1992;277:297-311.
- [219] Prasad G, Dhillon MS, Khullar M, Nagi ON. Evaluation of oxidative stress after fractures. A preliminary study. *Acta orthopaedica Belgica* 2003;69:546-51.
- [220] Liang D, Yang M, Guo B, Cao J, Yang L, Guo X, et al. Zinc Inhibits H₂O₂-Induced MC3T3-E1 Cells Apoptosis via MAPK and PI3K/AKT Pathways. *Bio Trace Elem Res* 2012;148:420-9.

- [221] Jebahi S, Oudadesse H, El Feki H, Rebai T, Keskes H, El Feki A. Antioxidative/oxidative status of muscular tissue surrounding strontium-substituted bioactive glass implanted in bone of ovariectomised rats. *Fund Clin Pharmacol* 2012;26:94-.
- [222] Wu C, Chang J. Degradation, bioactivity, and cytocompatibility of diopside, akermanite, and bredigite ceramics. *Journal of biomedical materials research Part B, Appl Biomater* 2007;83:153-60.
- [223] Aronne A, Sigaev VN, Champagnon B, Fanelli E, Califano V, Usmanova LZ, et al. The origin of nanostructuring in potassium niobiosilicate glasses by Raman and FTIR spectroscopy. *J Non-Cryst Solids* 2005;351:3610-8.
- [224] Fiore G, Ichim I, Battezzati L. Thermal analysis, fragility and viscosity of Au-based metallic glasses. *J Non-Cryst Solids* 2010;356:2218-22.
- [225] Lockyer MWG, Holland D, Dupree R. Nmr Investigation of the Structure of Some Bioactive and Related Glasses. *J Non-Cryst Solids* 1995;188:207-19.
- [226] O'Donnell MD, Watts SJ, Hill RG, Law RV. The effect of phosphate content on the bioactivity of soda-lime- phosphosilicate glasses. *J Mater Sci: Mater Med* 2009;20:1611-8.
- [227] Mneimne M, Hill RG, Bushby AJ, Brauer DS. High phosphate content significantly increases apatite formation of fluoride-containing bioactive glasses. *Acta Biomater* 2011;7:1827-34.
- [228] O'Donnell MD, Watts SJ, Law RV, Hill RG. Effect of P₂O₅ content in two series of soda lime phosphosilicate glasses on structure and properties – Part I: NMR. *J Non-Cryst Solids* 2008;354:3554-60.
- [229] Diba M, Tapia F, Boccaccini AR, Strobel LA. Magnesium-Containing Bioactive Glasses for Biomedical Applications. *Int J Appl Glass Sci* 2012;3:221-53.
- [230] Kapoor S, Goel A, Pascual MJ, Ferreira JMF. Thermo-mechanical behaviour of alkali free bioactive glass-ceramics co-doped with strontium and zinc. *J Non-Cryst Solids* 2013;375:74-82.
- [231] Zhang N, Molenda JA, Mankoci S, Zhou X, Murphy WL, Sahai N. Crystal structures of CaSiO₃ polymorphs control growth and osteogenic differentiation of human mesenchymal stem cells on bioceramic surfaces. *Biomater Sci* 2013;1:1101-10.
- [232] Han P, Wu C, Xiao Y. The effect of silicate ions on proliferation, osteogenic differentiation and cell signalling pathways (WNT and SHH) of bone marrow stromal cells. *Biomater Sci* 2013;1:379-92.

- [233] Zhang NL, Molenda JA, Fournelle JH, Murphy WL, Sahai N. Effects of pseudowollastonite (CaSiO₃) bioceramic on in vitro activity of human mesenchymal stem cells. *Biomaterials* 2010;31:7653-65.
- [234] Bidarra SJ, Barrias CC, Barbosa MA, Soares R, Granja PL. Immobilization of Human Mesenchymal Stem Cells within RGD-Grafted Alginate Microspheres and Assessment of Their Angiogenic Potential. *Biomacromolecules* 2010;11:1956-64.
- [235] Magallanes-Perdomo M, De Aza AH, Mateus AY, Teixeira S, Monteiro FJ, De Aza S, et al. In vitro study of the proliferation and growth of human bone marrow cells on apatite-wollastonite-2M glass ceramics. *Acta Biomater* 2010;6:2254-63.
- [236] Sun HL, Wu CT, Dai KR, Chang J, Tang TT. Proliferation and osteoblastic differentiation of human bone marrow-derived stromal cells on akermanite-bioactive ceramics. *Biomaterials* 2006;27:5651-7.
- [237] Huang Y, Jin XG, Zhang XL, Sun HL, Tu JW, Tang TT, et al. In vitro and in vivo evaluation of akermanite bioceramics for bone regeneration. *Biomaterials* 2009;30:5041-8.
- [238] Zhai WY, Lu HX, Wu CT, Chen L, Lin XT, Naoki K, et al. Stimulatory effects of the ionic products from Ca-Mg-Si bioceramics on both osteogenesis and angiogenesis in vitro. *Acta Biomater* 2013;9:8004-14.

Contents

List of figures.....	vii
List of tables.....	xiii
List of abbreviations	xv
List of publications	xvii
1. Introduction.....	3
2. State of the art.....	7
2.1 Need for Biomaterials for bone regeneration.....	7
2.2 Biomaterials for bone repair.....	8
2.3 Bioactive glasses	10
2.4 Glass structure and bioactivity	13
2.5 Mechanism of HCA layer deposition.....	15
2.6 Role of various functional ions	16
2.6.1 Silicon	16
2.6.2 Strontium.....	17
2.6.3 Zinc	18
2.6.4 Magnesium.....	18
2.6.5 Calcium	19
2.6.6 Phosphorus	19
2.7 Introduction to the present work	20
2.7.1 Aim of the thesis	23
3. Experimental.....	27
3.1 Glass synthesis	27
3.2 Density and Molar volume.....	27
3.3 Structural characterization of glasses.....	27
3.3.1 Magic angle spinning (MAS) – Nuclear magnetic resonance (NMR) spectroscopy.....	27
3.4 Biodegradation of glasses	28

3.5 Thermal analysis	29
3.6 Preparation of glass-ceramics	30
3.7 Characterization of glass-ceramics	30
3.7.1 Mechanical Properties of sintered glass-ceramics	30
3.7.2 Microstructural characterization- SEM and EDS	30
3.8 In vitro studies.....	31
3.8.1 Alkali-free glasses for bone tissue engineering: A preliminary investigation	31
3.8.1.1 Mesenchymal stem cell proliferation	31
3.8.2 Influence of ZnO/MgO substitution on sintering, crystallization, and bio-activity of alkali-free glass-ceramics.....	32
3.8.3 Role of glass structure in defining the chemical dissolution behaviour, bioactivity and antioxidant properties of zinc- and strontium- co-doped alkali-free phosphosilicate glasses	32
3.8.3.1 In vitro cellular tests.....	32
3.8.3.1 Cell Culture studies	32
3.8.4 An experimental approach towards understanding the composition-structure-bioactivity relationships in silicate glasses	34
3.8.4.1 Cell Culture Studies	34
3.8.4.2 Cell metabolic activity	34
4 Results and Discussion	37
4.1 Alkali-free glasses for bone tissue engineering: A preliminary investigation	37
4.1.1 Introduction	37
4.1.2 Results and discussions	38
4.1.2.1 Glass forming ability.....	38
4.1.2.2 Structure of glasses (MAS – NMR spectroscopy)	39
4.1.2.3 Apatite formation and chemical degradation of glasses	40
4.1.2.4 Differential thermal analysis	45

4.1.2.5 Sintering and crystallization behaviour of glasses	46
4.1.2.6 Cellular response to sintered glass powder compacts	51
4.2.2 Conclusions	55
4.2 Structural role of zinc in biodegradation of alkali-free bioactive glasses	57
4.2.1. Introduction	57
4.2.2 Results and discussion.....	58
4.2.2.1 Glass forming ability	58
4.2.2.2 Glass structure	59
4.2.2.3 Apatite forming ability of glasses	60
4.2.2.4 Chemical degradation of glasses in Tris-HCl	63
4.2.2.5 Discussion	65
4.2.3 Conclusions	67
4.3 Influence of ZnO/MgO substitution on sintering, crystallization and bio-activity of alkali-free glass-ceramics	69
4.3.1 Introduction	69
4.3.2 Results and discussion.....	69
4.3.2.1 Glass-forming ability	69
4.3.2.2 Thermal analysis	69
4.3.2.3 Sintering and Crystallization behaviour.....	70
4.3.2.4 Effect of heat treatment of the structure.....	73
4.3.2.4.1 Crystalline phase evolution by XRD.....	73
4.3.2.4.2 MAS-NMR of glass-ceramics	74
4.3.2.5 Density and molar volume	75
4.3.2.6 Mechanical Behaviour	76
4.3.2.7 Apatite forming ability of glass-ceramics	77
4.3.2.8 Mesenchymal cell activity and alkaline phosphatase activity.....	79
4.3.3 Conclusions	83

4.4 Role of glass structure in defining the chemical dissolution behaviour, bioactivity and antioxidant properties of zinc- and strontium- co-doped alkali-free phosphosilicate glasses	85
4.4.1 Introduction	85
4.4.2 Results	86
4.4.2.1 Glass forming ability	86
4.4.2.2 Structure of glasses	87
4.4.2.3 SBF immersion studies	90
4.4.2.4 Chemical degradation of glasses in Tris-HCl	95
4.4.2.5 Cellular response on bioactive glasses	97
4.4.2.5.1 In vitro proliferation of MG63 cells	97
4.4.3 Discussion	98
4.4.4 Conclusions	101
4.5 Thermo-mechanical behaviour of alkali-free bioactive glass-ceramics co-doped with strontium and zinc	103
4.5.1 Introduction	103
4.5.2. Results and Discussion.....	103
4.5.2.1 Glass-forming ability	103
4.5.2.2 Thermal analysis	104
4.5.2.3 Sintering and Crystallization behaviour	105
4.5.2.4 Structural transformation in glasses during heat treatment:	108
4.5.2.4.1 XRD	108
4.5.2.5 Mechanical Behaviour:	110
4.6 Understanding the influence of composition on structure bioactive and thermal behaviour of Diopside – Tricalcium phosphate based glasses	113
4.6.1 Introduction	113
4.6.2 Results	113

4.6.2.1 Glass forming ability.....	113
4.6.2.2 Structure of glasses by MAS-NMR	114
4.6.2.3 SBF immersion studies	115
4.6.2.4 Chemical degradation of glasses in Tris-HCl	119
4.6.2.5 Thermal analysis	120
4.6.2.6 Sintering and crystallization behaviours	121
4.6.2.7 Structural transformations during heat treatment.....	125
4.6.2.8 Density	125
4.6.2.9 Mechanical properties	126
4.6.2.10 Cell culture studies	126
4.6.3 Discussions.....	127
4.6.4 Conclusions	131
5. General conclusions	135
6. Future works	139
References.....	143

List of figures

Figure 2.1 Compositional dependence of bioactivity in Na ₂ O-CaO-SiO ₂ -P ₂ O ₅ glass system [2].....	11
Figure 2.2 2-dimensional representation of structure of silica glass [1].....	13
Figure 2.3 Number of papers published per year in the field of “bioactive glass” (compiled from a literature search SCOPUS carried out in November 2014).....	20
Figure 4.1.1 X-ray diffractograms of as-quenched glass frits.....	39
Figure 4.1.2 MAS NMR spectra of investigated glasses showing the peak positions of (a) ²⁹ Si and (b) ³¹ P.	40
Figure 4.1.3 X-ray diffractograms of glass powders after immersion in SBF solution for (a) 1 h; (c) 3 h; (c) 12 h, (d) 3 days and (e) 7 days. C refers to calcite while HA refers to hydroxyapatite.....	41
Figure 4.1.4 FTIR spectra of glass powder (TCP-20) before and after immersion in SBF solution for time durations varying between 1 h – 12 h.	43
Figure 4.1.5 Graph depicting changes in pH of solution and weight loss of glass powders after immersion in Tris-HCl for 120 h.....	45
Figure 4.1.6	46
Figure 4.1.7 Comparison of DTA and HSM curves under the same heating rate (5 K min ⁻¹) for compositions (a) TCP-20 and (b) TCP-40 at the heating rate of 5 K min ⁻¹ ; (c) influence of TCP content on different thermal parameters of glasses obtained from DTA and HSM, respectively	48
Figure 4.1.8. SEM images of glass powder compacts (a) TCP-10, (b) TCP-20, (c) TCP-30, after sintering at 800 °C for 1 h, respectively while (d) and (e) represent glass composition TCP-10 after sintering at 900 °C for 1 h.	49
Figure 4.1.9 X-ray diffractograms of glass compositions after sintering at (a) 800 °C; (b) 900 °C and 1000 °C, respectively.....	50
Figure 4.1.10 Proliferation behaviour of the MSCs cultured on the glass compacts (TCP-10 and TCP-20) and the tissue culture plastic used as a control during the periods for 3, 7 and 14 days. MSCs derived from rat bone marrow were used for the assay. Statistically significance difference was noticed between the groups; control vs. TCP-10 at day 3; control vs. TCP-10 or TCP-20 at day 7 (p < 0.05, ANOVA, n = 3)	52
Figure 4.1.11 SEM images of the MSCs grown on the sintered glass powder compacts (TCP-10 and TCP-20) during culture for 7 days. Cells spread well on both glass samples in intimate	

contacts with the underlying substrates and have active cytoskeleton processes with highly elongated filopodia. Some surface cracks associated with the sample treatment for SEM are observed.....	53
Figure 4.1.12 Alkaline phosphatase activity of the MSCs during culture for 7 and 14 days on the glass compacts (TCP-10 and TCP-20) and tissue culture plastic control. Statistically significant higher level was noticed on the glass samples with respect to control at both periods; *p < 0.05, ANOVA, n = 3.....	54
Figure 4.2.1 X-ray diffractograms of as-quenched glasses.....	58
Figure 4.2.2 MAS NMR spectra of investigated glasses showing the peak positions of (a) ²⁹ Si and (b) ³¹ P.....	59
Figure 4.2.3 X-ray diffractograms of glass powders before and after immersion in SBF solution for (a) as quenched glasses (b) 1 h (c) 6 h (d) 3 days and (e) 7 days. HA refers to hydroxyapatite.....	61
Figure 4.2.4 FTIR spectra of glass powders after immersion in SBF solution for (a) 1 h and (b) 24 h.....	62
Figure 4.2.5 Graphs depicting the change in solution pH and weight loss of glass powders after immersion in Tris–HCl.....	63
Figure 4.2.6 X-ray diffractograms of glass powder after 120 days of immersion in TRIS-HCL.....	64
Figure 4.2.7 ICP-AES plots of elemental concentrations of Ca, Mg, P, Si and Zn in Tris–HCl after 120 h of immersion of glass powder. It should be noted that Si refers to SiO ₄ ⁴⁻ and P refers to PO ₄ ³⁻ species.....	65
Figure 4.3.1 DTA thermographs of glasses at a heating rate of 20 K min ⁻¹	70
Figure 4.3.2 Comparison of DTA and HSM curves under the same heating rate (5 K min ⁻¹) for compositions: (a) Zn–2, (b) Zn–4, (c) Zn–6, (d) Zn–8 and (e) Zn–10.....	72
Figure 4.3.3 X-ray diffractograms of glass-ceramics heat treated at 850 °C for 1 h.	74
Figure 4.3.4 (a) ²⁹ Si MAS-NMR and (b) ³¹ P MAS-NMR spectra of glass-ceramics heat treated at 850 °C for 1 h.	75
Figure 4.3.5 Flexural strength of the glass-ceramics heat treated at 850 °C for 1 h.....	77
Figure 4.3.6a SEM/EDS micrographs images of unpolished and non-etched glass-ceramics samples before soaking in SBF: Zn-0, Zn-4, and Zn-8.....	78
Figure 4.3.6b SEM/EDS micrographs images of unpolished and non-etched glass-ceramics samples after soaking in SBF for 7 and 14 days: (a) Zn–0, (b) Zn–4, and (c) Zn–8.....	79

Figure 4.3.7 Influence of ZnO content in glass-ceramics on cell viability during culture for up to 7 days, as assessed by CCK method. Glass-ceramics with 4 mol% ZnO showed highest growth with respect to tissue culture plastic control as well as to that of other investigated glass-ceramics.	80
Figure 4.3.8 SEM images of the MSCs grown on the sintered glass powder compacts (Zn-0, Zn-4 and Zn-8) during culture for 3 and 7 days. After 7 days, cell proliferation on glass-ceramics was better in comparison to that observed after 3 days. Glass-ceramic Zn-4 exhibited the highest rate of cell proliferation.	81
Figure 4.3.9 Alkaline phosphatase activity of the MSCs during culture for 7 and 14 days on the glass compacts (Zn-0 to Zn-8) and on tissue culture plastic control. For all the investigated glass-ceramics, irrespective of their ZnO content, ALP levels were always higher in comparison to that of control ($p < 0.05$, ANOVA, $n=3$)	82
Figure 4.4.1 X-ray diffractograms of glass powders	87
Figure 4.4.2 MAS NMR spectra of investigated glasses showing the peak positions of (a) ^{29}Si and (b) ^{31}P	88
Thus NMR results shows that $\text{Zn}^{2+}/\text{Mg}^{2+}$ and $\text{Ca}^{2+}/\text{Sr}^{2+}$ substitutions do not affect the silicate network connectivity of these glasses.	88
Figure 4.4.3 (a) ^{29}Si MAS NMR spectra and (b) ^{31}P MAS NMR spectra after deconvolution of investigated glasses.	89
Figure 4.4.4 FTIR spectra of glass powders (a) before, after (b) 1h, (c) 24h, and (d)14 days immersion in SBF.	91
Figure 4.4.5 X-ray diffractograms of glass powders after immersing the glass powders in SBF solution for (a) 1 h (b) 3 h (c) 6 h (d) 24 h (e) 3 days and (e) 14 days.	92
Figure 4.4.6 ICP plots of elemental concentration of (a) Ca, (b) P, (c) Mg, (d) Sr, (e) Si and (f) Zn, in SBF solution versus immersion time for the investigated glass powders.	94
Figure 4.4.7 X-ray diffractograms of glass powder after 120 days of immersion in TRIS-HCL.....	95
Figure 4.4.8 (a) Graphs depicting the change in solution pH and weight loss of glass powder samples (with respect to variation in ZnO and SrO content in glasses) after immersion in Tris-HCl; (b) ICP-AES plots of elemental concentrations of Ca, Mg, P, Si, Sr and Zn in Tris-HCl after 120 h of immersion of glass powder. It should be noted that Si refers to SiO_4^{4-} and P refers to PO_4^{3-} species.....	96

Figure 4.4.9 Plots showing the cell growth kinetics of the glasses (ZS-2, ZS-4, ZS-6, and ZS-8) (a) under normal condition during culture after 4 days under normal conditions (b) under H ₂ O ₂ (250 μM) induced oxidative stress in MG63 cell after 3 days. *(C for control)..	98
Figure 4.5.1 DTA thermographs of glasses at a heating rate of 20 K min ⁻¹	104
Figure 4.5.2 Oxygen density plotted against percentage zinc and strontium substitution....	105
Figure 4.5.3 Comparison of DTA and HSM curves under the same heating rate (5 K min ⁻¹) for compositions: (a) ZS-2, (b) ZS-4, (c) ZS-6, (d) ZS-8 and (e) ZS-10.	106
Figure 4.5.4 X-ray diffractograms of glass-ceramics heat treated for 1 h at: (a) 800 °C, (b) 850 °C and (c) 900 °C.	108
Figure 4.5.5 Intensity ratio of the main XRD intensity peaks of Sr-diopside to Sr-fluorapatite plotted against percentage of zinc and strontium substitution for glass-ceramics heat treated for 1 h at 850 °C and 900 °C.	109
Figure 4.5.6 SEM images and EDS results of glass-ceramic ZS-8 sintered for 1 h at: (a) 800 °C, (b) 850 °C, (c) 900 °C, after a heating rate ramp of 5 K min ⁻¹	110
Figure 4.5.7 Flexural strength of glass-ceramics heat treated for 1 h at: (a) 800 °C, (b) 850 °C and (c) 900 °C, using a heating rate of 5 K min ⁻¹	111
Figure 4.6.1 MAS NMR spectra of investigated glasses showing the peak positions of (a) ²⁹ Si and (b) ³¹ P.	114
Figure 4.6.2 FTIR spectra of the investigated glasses	115
Figure 4.6.3 FTIR spectra of glasses powders after immersion in SBF solution for (a) 1 h, (b) 24 h, (c) 3 days, and (d) 14 h.	117
Figure 4.6.4 X-ray diffractograms of glass powders before and after immersion in SBF solution for (a) 1 h (b) 24 h (c) 3 days and (d) 14 days. HA refers to hydroxyapatite	118
Figure 4.6.5 Variations in pH and weight loss of glass powders upon immersion in Tris-HCl solution for 7 days.....	119
Figure 4.6.6 X-ray diffractograms of glass powder after 120 days of immersion in TRIS-HCL.....	120
Figure 4.6.7 DTA thermographs of glasses at a heating rate of 20 K min ⁻¹	121
Figure 4.6.8 Comparison of DTA and HSM curves under the same heating rate (5 K min ⁻¹) for compositions: (a) Di-50, (b) Di-60 (c) Di-70, (d) Di-80 (e) Di-90 and (f) Di-100.....	123
Figure 4.6.10 Flexural strength of glass-ceramics heat treated for 1 h at (a) 900 °C (b) 1000 °C, and (c) 1200 °C.	126

Figure 4.6.11 Metabolic activities of hMSCs on Di-60, Di-70 and Di-90 and TCPS after 1, 3, 7, 14 and 21 days.127

List of tables

Table 2.1 Selected bioactive glass compositions (mol%).	21
Table 3.1 Infrared bands of functional groups of bioactive glasses.	28
Table 4.1.1 Nominal composition of the as-designed glasses (mol%).	37
Table 4.2.1 Nominal composition of the as-designed glasses (mol%).	58
Table 4.3.1 Thermal parameters measured from DTA and HSM at 5 K min^{-1} * $\beta = 20 \text{ K min}^{-1}$.	73
Table 4.4.1 Nominal composition of the as-designed glasses (mol%).	86
Table 4.4.2 Q^n (Si) distribution for glasses ZS-4 and ZS-10 obtained by NMR deconvolution.	88
Table 4.4.3 Q^n (P) distribution for glasses ZS-4 and ZS-10 obtained by NMR deconvolution.	89
Table 4.5.1 Thermal parameters measured from DTA at 20 K min^{-1} .	105
Table 4.6.1 Nominal composition of the as-designed glasses (mol%).	113
Table 4.6.2 Thermal parameters measured from DTA at 20 K min^{-1} .	120
Table 4.6.3 Thermal parameters ($^{\circ}\text{C}$) and A/A_0 ratio derived from DTA and HSM at 5 K min^{-1} .	122
Table 4.6.4 Density (kg m^{-3}) of glasses and glass-ceramics.	125

List of abbreviations

A-W	Apatite-Wollastonite
ALP	Alkaline Phosphatase Activity
BO	Bridging Oxygen
BMD	Bone Mineral Density
CaSR	calcium-sensing receptor
CCK	Cell counting kit
Di	Diopside
DMEM	Dulbecco's Modified Eagle Medium
DMSO	Dimethyl Sulfoxide
DNA	Deoxyribonucleic acid
DTA	Differential Thermal Analysis
EthD-1	Ethidium Homodimer-1
EDTA	Ethylene diamine tetra acetic acid
EDS	Energy-Dispersive X-Ray Spectroscopy
ELISA	Enzyme-linked immunosorbent assay
FA	Fluorapatite
FBS	Foetal bovine serum
FTIR	Fourier Transform Infrared Spectroscopy
GPCR	G-protein coupled receptor
HA	Hydroxyapatite
hMSCs	Human Mesenchymal Stem Cells
HCA	Hydroxy Carbonate Apatite
ICP	Inductively Coupled Plasma
MAS-NMR	Magic Angle Spinning– Nuclear Magnetic Resonance
MSCs	Mesenchymal Stem Cells
NBO	Non-Bridging Oxygen
NC	Network connectivity
PBS	Phosphate Buffered Saline
PGA	Polyglycolic acid
PLA	Polylactic acid
SBF	Simulated Body Fluid
SEM	Scanning Electron Microscopy

Tris	Tris (Hydroxymethyl) Aminomethane
TE	Tissue Engineering
TCPS	Tissue Culture Polysterene
TCP	Tricalcium Phosphate
XRD	X-Ray Diffraction
v/v	Volume/volume

List of publications

1. **Saurabh Kapoor**, Ashutosh Goel, Antonio Tilocca Raghu, Vikram Dhuna, Gaurav Bhatia, Kshitija Dhuna, Jose M. F. Ferreira, *Role of glass structure in defining the chemical dissolution behaviour, bioactivity and antioxidant properties of zinc- and strontium- co-doped alkali-free phosphosilicate glasses*. **Acta Biomaterialia**, 2014; 10: 3264–78.
2. **Saurabh Kapoor**, Ashutosh Goel, Ana Filipa Correia, Maria J. Pascual, Hye-Young Lee, Hae-Won Kim, José M.F. Ferreira. *Synthesis and Characterization of Bioactive Glass-Ceramics* **Material Science and engineering C (accepted)**.
3. **Saurabh Kapoor**, Angela Semitela, Ashutosh Goel, YeXiang, Jincheng Du, Ana H Lourenço, Daniela M Sousa, Pedro L Ganja, José M. F. Ferreira. *Understanding the composition-structure-bioactivity relationships in diopside (CaO*MgO*2SiO₂) – tricalcium phosphate (3CaO*P₂O₅) glass system*, **Acta Bioamaterlia (accepted)**
4. **Saurabh Kapoor**, Ashutosh Goel, Maria J. Pascual, José M. F. Ferreira, *Thermo-mechanical behaviour of alkali free bioactive glass-ceramics co-doped with strontium and zinc*, **Journal of Non-crystalline Solids**, 2013; 375:74-82.
5. **Saurabh Kapoor**, Ashutosh Goel, Maria J. Pascual and José M. F. Ferreira, *Alkali-free bioactive Diopside – Tricalcium phosphate glass ceramics for scaffolds fabrication: sintering and crystallization behaviour*. **Journal of Non-crystalline Solids** (Invited paper for special issue on health care).
6. Ashutosh Goel, **Saurabh Kapoor**, Antonio Tilocca Raghu, Raman Rajagopal, Jose M. F. Ferreira, *Structural role of zinc in biodegradation of alkali-free bioactive glasses*, **Journal of Material Chemistry B**, 2013;1:3073-82.
7. Ashutosh Goel, **Saurabh Kapoor**, Raghu Raman Rajagopal, Maria J. Pascual, Hae-Won Kim, Jose M. F. Ferreira, *Alkali-Free bioactive glasses for bone tissue engineering: A preliminary investigation*, **Acta Biomaterialia**, 2012; 8: 361-72.

Other publications

1. Allu Amarnath Reddy, Dilshat U. Tulyaganov, Ashutosh Goel, **Saurabh Kapoor**, Maria J. Pascual, José M.F. Ferreira, *Sintering and devitrification of glass-powder compacts in the akermanite-gehlenite system*, **Journal of Materials Science**, 2013; 48:4128–36.
2. Allu Amarnath Reddy, Ashutosh Goel, Dilshat U. Tulyaganov, **Saurabh Kapoor**, K Pradeesh, Maria J. Pascual, José M.F. Ferreira, *Study of calcium-magnesium-aluminum-*

- silicate (CMAS) glass and glass-ceramic sealant for solid oxide fuel cell*, **Journal of Power Sources**, 2013;231:203–12.
3. Allu Amarnath Reddy, Dilshat U. Tulyaganov, **Saurabh Kapoor** , Ashutosh Goel , Maria J. Pascual Vladislav V. Kharton and José M. F. Ferreira, *Study of melilite based glasses and glass–ceramics nucleated by Bi₂O₃ for functional application*, **RSC Advance**, 2012;2: 10955–67.

Chapter 1

Introduction

1. Introduction

A glass can be defined as an amorphous solid completely lacking in long range, periodic atomic structure, and exhibiting a region of glass transformation behaviour. Any material, inorganic, organic, or metallic formed by any technique, which exhibits glass transformation behaviour is considered to be a glass [1].

Humans have been using glass for thousands of years, from the first uses of natural glass (e.g. obsidian, a volcanic glass) for tools and arrow heads, to the early man-made glass beads and drinking vessels of the Egyptians. Since then, glass has fascinated and attracted much interest both scientifically and technologically. The multiple forms and uses of glasses are becoming increasingly important in science, industry and in general daily life. During the last century, glasses and glass-ceramics became widely used for decorative articles, optics, architectural purposes (from windows to whole glass facades), and glassware for chemical reactions or fibres for telecommunication applications. The major advantage of glasses and glass-ceramics among its ceramic counterparts is their ability to accommodate various functional ions in their amorphous or crystalline phase, thus providing the flexibility to tailor and optimize their compositions with respect to different technological applications.

In particular bioactive glasses have been a relatively young group of materials discovered in 1970's by Larry Hench. Bioactive glasses and glass-ceramics constitute a class of bioactive materials, i.e. "Materials which elicit a special response on their surface when in contact with biological fluids, leading to strong bonding to living tissue". Since its discovery, 45S5 Bioglass[®] has been used in >650,000 human patients and is being marketed for various dental and orthopaedic applications under different commercial brand names [2-4]. Due to number of attractive properties for bone regeneration and tissue engineering (TE), increasing efforts have been made towards expanding the range of potential applications and understanding the fundamental science governing the physical, chemical and thermal properties of bioactive glasses in order to develop novel compositions with superior set of properties for biomedical applications [5-10]. Irrespective of this huge success, high alkali-containing glasses face some drawbacks which do restrict their application in some of the most advanced areas of human biomedicine. High alkali-content in glasses increase their crystallization tendency upon sintering, hindering the densification process and limiting the mechanical strength of sintered materials. Further, the relatively high chemical dissolution rates of such glasses in aqueous media decrease their *in vitro* and *in vivo* efficacy [11]. All these features constitute serious drawbacks in terms of fabrication of porous scaffolds or

porous coatings, and mitigate the potential benefits that could be drawn from their usage as biomedical devices for bone regeneration and TE.

Despite many comprehensive studies leading to the development of bioactive glasses from different systems, the majority of these studies were based on 45S5 Bioglass[®] or compositions inspired by it. Therefore, this work aims at designing new alkali-free bioactive glasses in the Diopside (Hereafter referred as Di) – Tricalcium phosphate (Hereafter referred as TCP) – Fluorapatite (Hereafter referred as FA) system having good bioactive properties and to understand the structure–property relationships in the as designed glasses.

In the light of the above mentioned perspective, this dissertation comprises of five chapters. The first chapter, i.e., the Introduction, provides an outlook of the content of each chapter; the second chapter will focus on the literature survey in the field of bioactive glasses for biomedical applications, with special emphasis on alkali-free silicate systems. The second chapter has been divided into different subsections; the first section aims at providing a historical background on the development and evolution of bioactive glasses in general, while the second section outlines the motivations and purpose behind the present work. The third chapter deals with the description of the general experimental procedures and methodologies used along the thesis. It provides details about all the experimental techniques and procedures employed in order to synthesise, characterize and test our samples. Chapter four is the most important part of this work as it presents all the experimental results obtained on alkali-free glasses and glass-ceramics during past 3 years along with the pertaining discussions. In chapter five we have tried to conclude all the results and achievements obtained during this work and chapter six provides future directions in this field of research.

Several experimental techniques were used throughout this investigation aiming at a better understanding of the glass structure, biodegradation behaviour and the sintering and crystallization behaviour of the corresponding glass powder compacts. Some properties of glasses and glass-ceramics such as density, mechanical strength, were also evaluated to achieve a better understanding concerning the structure-properties relations.

Chapter 2

State of the art

2. State of the art

2.1 Need for Biomaterials for bone regeneration

Human bone is a dynamic, highly vascularised connective tissue which provides structural support and act as a protective casing for the delicate internal organs of the body [12]. It is a tissue that is constantly remodelling to adapt to mechanical stresses imposed and repair minor injuries occurring during the lifetime. However, if the injuries suffered are extensive leading to very large bone defects, the use of bone grafts is required in order to repair the damaged part.

Worldwide, millions of people are affected by degenerative and inflammatory problems related to bone and joint. In fact, they account for half of all chronic diseases in people over 50 years of age in developed countries. Further, every year there are roughly 8.9 million cases of fractures, which occur due to osteoporosis only [13]. Also, approximately 1.6 million hip fractures occur worldwide each year, by 2050 this number could reach between 4.5 million [14] and 6.3 million [15]. Current treatments for filling bone defects and subsequent repair are based on autograft and allografts. Autologous grafts are the ones which contain essential elements for bone regeneration (osteogenic cells, osteoinductive growth factors and a matrix that supports adhesion and bone growth), are collected from the individual, minimizing the risk of rejection. Although autograft present relatively good percentages of success, however the range of applications is restricted, mainly due to the limited availability of living tissues and due to donor site morbidity [16]. Further, allograft bone introduces the possibilities of immune rejection and of pathogen transmission from donor to host. Although infrequent, infections could occur in the recipient's body after the transplantation [16]. Therefore there is a severe need to search for new bone regeneration strategies in order to meet the increasing medical and socioeconomic challenge of our aging population. Hence, materials that enhance bone regeneration have a wealth of potential clinical applications from the treatment of non-union fractures to spinal fusion. Synthetic biomaterials, developed in an effort to overcome the inherent limitations of autograft and allograft, represents an alternative strategy.

2.2 Biomaterials for bone repair

A biomaterial according to the American National Institute of Health is “*Any substance (other than a drug) or combination of substances, synthetic or natural in origin, which can be used for any period of time, as a whole or as a part of a system which treats, augments, or replaces any tissue, organ, or function of the body*”. The development of novel biomaterials is an iterative process that involves the creation of increasingly safer, more reliable, less expensive and more physiologically appropriate replacements for damaged or diseased human tissues. In the last 60 years, biomaterials for orthopaedic applications have evolved from materials available from different industrial applications into the materials with inherent capabilities to interact with the biological environment and to elicit specific biological responses. Most of the problems that orthopaedic surgery has to face have not basically changed, and are practically the same that orthopaedics had to face 50 years ago; however, the choice of possible solutions has been greatly expanded because new materials have allowed the design of innovative devices. Based on the evolution of biomaterials, these can be roughly divided into three broad categories depending upon the interaction mechanisms of the materials; namely inert materials (first generation biomaterials). Bioactive and biodegradable materials (second generation), and materials designed to stimulate specific cellular responses at the molecular level (third generation) [17]. This division represent the development in the field of biomaterials based on the requirements and properties of the materials involved. The present research is still devoted to the first or the second generation depending upon their properties and application. This means that the materials that each new generation brings in do not necessarily outweigh the existing materials.

First generation biomaterials: Developed in the early 1950s [18], the principle underlying the development of first generation biomaterials was that they should be as chemically inert as possible in order to minimize the immune response to the foreign body [17]. Initially, the first generation of biomaterials consisted of already functional materials which were being applied in industrial applications (for e.g. aerospace) where mechanical properties were the main benchmark for the selection of candidate materials for implant manufacture. These biomaterials are mainly metallic or alloys (Co–Cr–Mo alloys, Ti6Al4V, etc.), ceramics (alumina, zirconia, etc.) and polymers (silicone rubber, acrylic resins) [19]. Though bio-inert in nature, these tend to form a thin non-adherent fibrous capsule over their surface with the passage of time after implantation which inhibits further interaction with

tissue [20]. The thickness of the layer developed is a function of the level of reactivity of the implant. Formation of this thin layer is attributed to the absorption of unspecific proteins that results in unspecific signalling to the cellular environment. This thin layer leads to loosening and deterioration of the mechanical fit. Eventually, surgical removal of the device is required. Therefore the development of bioactive interfaces eliciting a specific biological response and avoiding any fibrous layer was one of the main driving forces behind the development of second generation biomaterials.

Second generation of biomaterials: Developed between the years 1970-1980. These biomaterials mainly include ceramics (bioactive glasses, glass-ceramics and calcium phosphates), biodegradable polymers (polylactic acid (PLA) and polyglycolic acid (PGA) etc.) [20]. Bioactive glasses discovered by Larry Hench in 1969-1971 [21] provided an alternative to the bio-inert materials used in orthopaedic applications. These second generation biomaterials were defined by their ability to interact with the biological environment in a controlled manner to enhance the biological response and the tissue/surface bonding. Further progress of the second generation biomaterials was the development of bioresorbable or bio-absorbable materials with the ability to undergo a progressive degradation while new tissue regenerates and heals [20, 22]. Bioactivity is defined as the ability of the material to bond to bone tissue via the formation of a bone-like hydroxyapatite (HA) layer on its surface [23]. The HA phase that forms on bioactive implants is equivalent chemically and structurally to the mineral phase in the bone, and is responsible for strong interfacial bonding, allowing for bone regeneration rather than replacement.

Second generation biomaterials have been in clinical use since 1980 in many orthopaedics and dental applications, including various compositions of bioactive glasses, ceramics, glass-ceramics, and composites. Synthetic calcium phosphate ceramics have been routinely used as bone cements and coatings over metallic prosthesis to facilitate bioactive fixation [20]. Different phases of calcium phosphate ceramics are used depending upon whether a bioresorbable or bioactive material is desired. Bioactive glasses and glass-ceramics are used as middle-ear prostheses to restore the ossicular chain and treat conductive hearing loss and as oral implants to preserve the alveolar ridge from the bone resorption that follows tooth extraction [20, 24, 25]. In comparison to the bioactive glasses and glass-ceramics, calcium phosphate based cements have been used in many orthopaedic applications such as

bone substitution, repair of bone fractures (including ligament fixation), cartilage, meniscus and intervertebral disc.

Third generation of biomaterials: Developed in the 21st century, third generation of biomaterials brought together separate concepts of bioresorbable and bioactive materials of second generation. The motive behind the design and development of these materials was to enhance the self-healing capabilities of the body, by the systematic stimulation of specific cellular responses at the molecular level [20]. Primarily, third generation biomaterials were developed by interchanging and intermixing of the properties of bioresorbable and bioactive materials. Consequently, these tailored biomaterials with new levels of bio-functionality have led to new approaches for the treatment of bone defects. Two main strategies have been followed during the last two decades with respect to tissue regeneration are TE and *in situ* tissue regeneration.

TE is one of the approaches in which cells planted in the scaffolds are made to proliferate and differentiate *in vitro*. These tissue-engineered constructs are then implanted into the patients to replace diseased or damaged tissues. Clinical applications include repair of articular cartilage, skin, and the vascular system, although stability of the repaired tissues needs improvement. Another method was *in situ* tissue regeneration which involved the use of biomaterials directly implanted into the body in the form of powders, solutions, or doped micro-particles to stimulate local tissue repair. These materials release controlled amount of ionic dissolution products or growth factors such as bone morphogenic protein (BMP) by diffusion or network breakdown.

2.3 Bioactive glasses

Bioactive glasses are amorphous materials, compatible with the human body; bond to bone and can stimulate new bone growth while dissolving over time. They therefore have the potential to restore diseased or damaged bone to its original state and function (bone regeneration). Bioactive glasses belong to class A of bioactive materials which are osteogenic and osteoconductive materials. The first bioactive glass (silicate based) was discovered by Larry Hench and colleagues in 1969 using melt-quench method, at the University of Florida [26]. The glass composition of the first bioactive glass was 46.1% SiO₂, 24.4% NaO, 26.9% CaO and 2.6% P₂O₅ (mol%), termed 45S5 Bioglass[®], which is now a trademarked name (Figure 2.1).

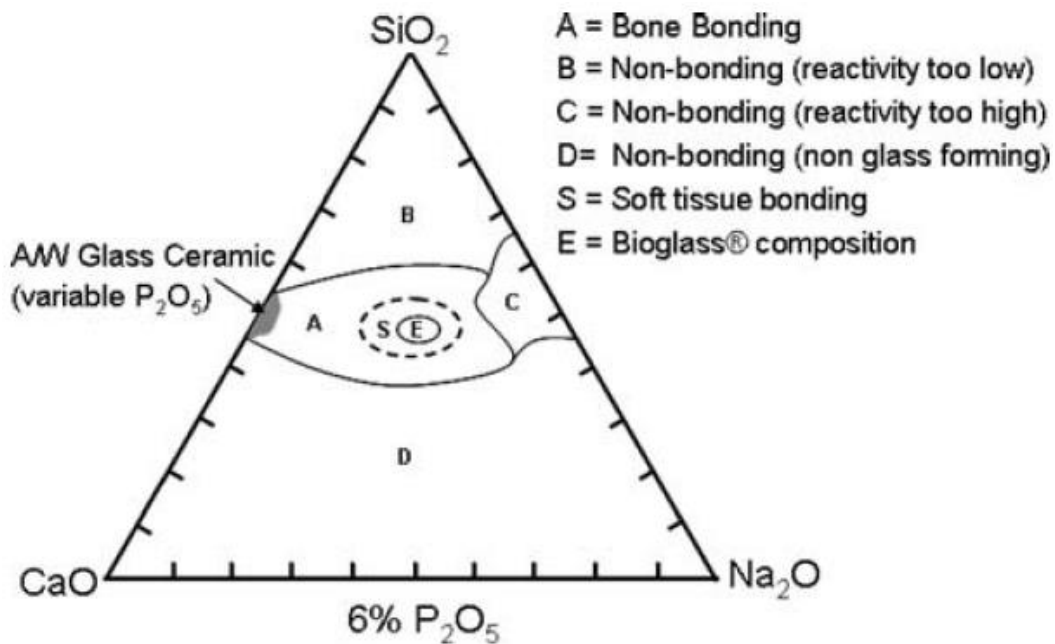


Figure 2.1 Compositional dependence of bioactivity in Na₂O-CaO-SiO₂-P₂O₅ glass system [2].

When in contact with a physiological fluid, bioactive glasses undergo a specific set of reactions, leading to the formation of an amorphous calcium phosphate (ACP) or crystalline HA phase on the surface of the glass, which is responsible for their strong bonding with the surrounding tissue [20]. Further, ionic dissolution products released from bioactive glasses (e.g. Si, Ca, P) are also reported to activate osteogenic gene expression [27, 28] and to stimulate angiogenesis [29, 30]. In addition to it, bioactive glasses offer remarkable advantages such as the ease of controlling chemical composition and, thus, the rate of degradation which make them attractive materials for orthopaedic applications. The structure and chemistry of glasses can be tailored over a wide range by changing either composition, or thermal or environmental processing history. Therefore, it is possible to design bioactive glasses with variable degradation rates to match that of bone ingrowth and remodelling.

Based on the type of glass former, there are mainly three types of bioactive glasses: the conventional silicate-based glasses; phosphate-based glasses; and borate-based glasses. Recently, there has been an increase in interest in borate based bioactive glasses [31, 32], largely due its potential ability to heal chronic wounds that would not heal under conventional treatment [33]. The soft tissue response may be due to their lower chemical durability (faster dissolution) in comparison to the silica-based counterparts [31]. Also phosphate-based glasses have shown great potential in regenerative medicine [31], as the

solubility of these glasses can be controlled by modifying their composition; therefore these glasses show additional clinical potential as resorbable materials. Thus, benefits of phosphate glasses are probably related to their very rapid solubility which is strongly composition dependent rather than bioactivity [34].

Oxide glasses are conventionally produced by melting the precursors (inorganic oxides, carbonates, fluorides and others) in precious metal or ceramic crucibles at high temperatures (for bioactive glasses typically above 1000 °C, depending on the composition). If the cooling is rapid enough (with the necessary cooling rates depending, again, on the composition) crystallization will be inhibited and an amorphous material, a glass, will result. Another common way of preparing bioactive glasses is by a polycondensation reaction from organic precursors, alkoxides such as tetraethyl orthosilicate [35]. Synthesized in the early 1990s [35], this new class of bioactive glasses displays higher compositional range of bioactivity: bioactive sol-gel glass compositions have been synthesized within the ternary $\text{SiO}_2\text{:CaO:P}_2\text{O}_5$ or even within the binary $\text{SiO}_2\text{:CaO}$ systems, and might contain between 60 and 90 mol% of silica [36, 37]. As the synthesis of glasses is highly dependent on composition and external conditions, sol-gel method gives better control over the surface and structural properties (such as surface area and porosity) of the resultant glass in comparison to melt-quenching method. The introduction of sol-gel synthesis technique has opened the research to new types of biomaterials. Many possible dopants can be introduced in a material synthesized via sol-gel. For example, it has been shown that sol-gel derived glasses containing 5 mol% ZnO resulted in increased alkaline phosphatase activity (ALP) activity and osteoblast proliferation [38].

However, in the frame of the present thesis, melt-quenching was used to prepare glasses and sol-gel derived glasses are beyond the scope of this PhD work program. Hence, the subsequent discussion will solely be based on the silicate based glasses prepared by melt-quenching.

2.4 Glass structure and bioactivity

Within the glass structure, three different components are usually described. *Network formers* are able to form amorphous materials without the need for additional components. The basic building unit of silicate glasses is the SiO_4 tetrahedron, which can be connected to neighbouring SiO_4 tetrahedra via Si—O—Si bonds, known as bridging oxygens (BO). Silicon possess a charge of 4^+ thus in the glasses when SiO_4 tetrahedral forms a network these building units can share all their four oxygen atoms to give the stoichiometry ($\text{SiO}_{4/2}$ or SiO_2 which is charge-balanced (assuming a charge of 2^- on the oxygen).

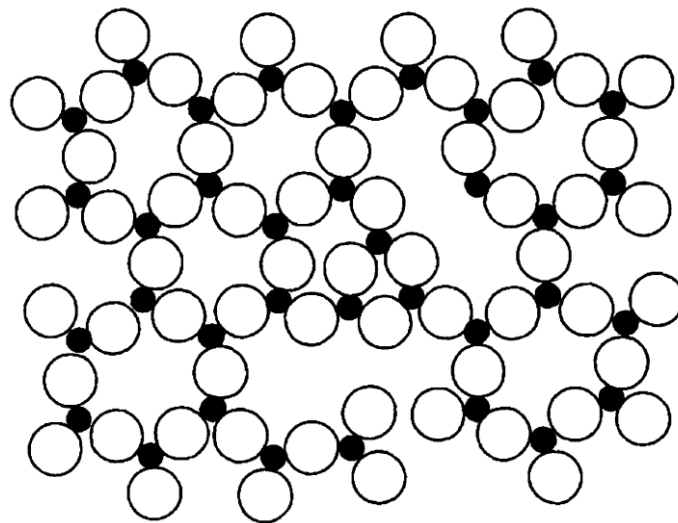


Figure 2.2 2-dimensional representation of structure of silica glass [1].

Each oxygen atom is shared between two silicon atoms, which occupy the centres of linked tetrahedra. Randomness in the structure is facilitated by the variability in the Si—O—Si angle connecting adjacent tetrahedra. Further rotation of adjacent tetrahedra around the point occupied by the oxygen atom linking the tetrahedra, and by rotation of the tetrahedra around the line connecting the linking oxygen with one of the silicon atoms results in augmentation in disorder in the structure. These tetrahedra are commonly referred to as Q^n ($n = 1, 2, 3, 4$) units, where n describes the number of BO connected to the tetrahedron. Silica glass therefore consists of Q^4 units only. A 2-dimensional representation of such a structure is shown in Figure 2.2, where the fourth oxygen, which would sit directly above the small silicon ion, is not shown.

Network modifiers, on the other hand, alter the glass structure by turning BO's (predominantly covalent in character) into non-bridging oxygens (NBO's) (Si—O- M⁺ linkages, predominantly ionic in character, where M⁺ is a modifier cation). Typical modifiers include the oxides of alkali or alkaline-earth metals having co-ordination number 6 or more. The more modifiers we have in the glass composition, lower is the average number of SiO₄ tetrahedra each tetrahedron is linked to. At the same time, the number of NBO's in the glass structure increases. In conventional silicate glasses, we find large concentrations of Q⁴ and Q³ units, i.e. SiO₄ tetrahedra connected to neighbouring ones in four or three directions, forming a silicate network. The relative concentrations of BO's and NBO's have an important influence on the structure and properties of the glasses. The rigidity of the glass network decreases gradually by replacing bridging atoms by non-bridging atoms.

Intermediates on the other hand can either act like typical network modifiers or enter the backbone of the glass structure, acting more like a network former. These have a co-ordination ranging from 4 to 6.

Bioactive glasses, by contrast, contain larger concentrations of network modifiers and smaller amounts of silica than conventional soda-lime silicate glasses, and they therefore consist of a more disrupted silicate network of mostly Q² units. According to Tilocca [5] maximum bioactivity for bioactive glasses is achieved if the structure is dominated by chains of Q² metasilicates, which are occasionally cross-linked through Q³ units, whereas the Q¹ species terminate the chain. Further, the structure of glass can also be estimated based on the glass composition. Different parameters have been suggested for describing the glass structure in the literature [39-41]. Strnad [40] introduced the concept of network connectivity (NC) model to describe the average number of bridging oxygens per network forming element and to correlate the molecular structure of silicate glasses with their bioactivity (apatite forming ability). In a pure silica glass (containing no network modifiers) we have only Q⁴ units, thus has a NC = 4. With the introduction of the network modifiers the NC decreases as the BO's are converted into NBO's. Bioactive glasses with NC value in the range of 2 and 3 are believed to show good bioactive properties (45S5 Bioglass[®] has a NC of 1.90 [39], corresponding to a structure consisting of silicate).

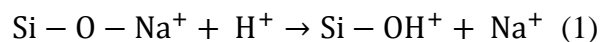
However, while NC may be a useful as a qualitative and a preliminary tool to predict the bioactivity of glasses, its predictive power rapidly decreases when: (i) a wider range of glass compositions are considered; (ii) cations of similar charge are partially substituted in the glass compositions. It has been shown that there is no straightforward correlation between

the NC and the degradation behaviour bioactive glasses. For example, glass compositions with NC similar to that of 45S5 Bioglass® (NC = ~1.95) have been shown to exhibit slower chemical dissolution behaviour in aqueous solutions than the latter while partial substitution of Zn²⁺ in bioactive glasses at the expense of Mg²⁺ retards the apatite forming ability of bioactive glasses despite their NC being unchanged [42].

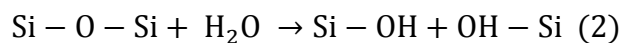
2.5 Mechanism of HCA layer deposition

Even though all the composition of silicate based bioactive glasses synthesized till date are quite different, the mechanism of HA or HCA (hydroxycarbonate apatite) formation are analogous for all of them. The apatite layer forms following solution-mediated dissolution of the glass with a mechanism very similar to conventional glass corrosion [43]. Accumulation of dissolution products causes both the chemical composition and the pH of the solution to change, providing surface sites and a pH conducive to apatite nucleation. There are five proposed stages for apatite formation in body fluid *in vivo* or in SBF *in vitro* [20].

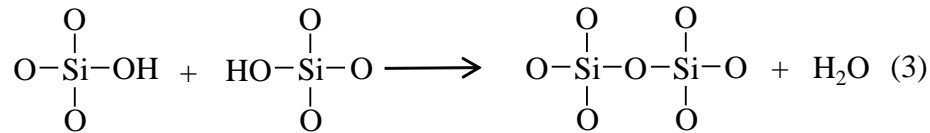
STEP 1 – Reactions for the rapid exchange of ions between the modifiers in the glass network (Na⁺ and Ca²⁺) with H⁺ ions or H₃O⁺ in solution, leading to hydrolysis of the groups of silica and creating silanol groups (Si–OH) on the glass surface. This process results in a net increase of pH of the solution due to the increasing OH ions.



STEP 2 – The increase of pH leads to attack on the glass network, breaking Si–O–Si bonds. Soluble silica is lost in the form of Si–OH to the solution, leaving more Si–OH (silanol) at the glass–solution interface. These silanol groups play a vital role as the nucleation centres of the apatite formation.



STEP 3 – Condensation and repolymerization of SiO₂-rich layer on the glass surface depleted in alkali and alkaline earth cations.



STEP 4 – Migration of Ca^{2+} and PO_4^{3-} groups to the surface through the silica-rich layer, forming a film rich in amorphous $\text{CaO-P}_2\text{O}_5$ on the silica-rich layer.

STEP 5 – Incorporation of hydroxyls and carbonate from solution and crystallization of the $\text{CaO-P}_2\text{O}_5$ film to form apatite. After the apatite layer is formed the adsorption of growth factors, attachment, proliferation and differentiation of osteoprogenitor cells are the biological mechanisms of bonding to bone. In addition to this, adsorption of adhesion proteins (e.g., fibronectin, vitronectin, etc.) is necessary condition for cellular attachment.

2.6 Role of various functional ions

The processes of bone formation and bone resorption (bone remodelling) are regulated by variety of systematic and local regulated agents including growth factors and hormones. Single inorganic ions are known to be involved in the bone formation and bone resorption (bone remodelling) and play a physiological role in angiogenesis, growth and mineralization of bone tissues. In particular, some metal ions act as enzyme co-factors and therefore influence signalling pathways and stimulate metabolic effects during tissue formation [44]. These properties make metal ions attractive for use as therapeutic agents in the fields of hard and soft TE.

Further, bioactive glasses have the ability to exhibit surface reactivity when in contact with body fluids leading to the release of ionic dissolution products (example: Si, Ca, P, Mg, F) which further stimulate the various vital mechanisms in human body like gene expression, osteoblast proliferation, angiogenesis and also provide anti-bacterial as well as anti-inflammatory effects [28, 30, 45]. In fact, it has been well established that ionic dissolution products are key to understand the behaviour of parent inorganic materials in vitro and in vivo, especially in context of TE applications [46].

2.6.1 Silicon

Silicon (Si) is a non-metallic element with an atomic weight of 28. It is the second most abundant element in the Earth's crust at 28 wt%. Si is known to be an essential element

for metabolic processes related with the formation and calcification of bone tissue [44]. Silicon is present in all body tissues, but the tissues with the highest concentrations of silicon are bone and other connective tissue including skin, hair, arteries, and nails [47]. Silicon plays an important role in the formation of cross-links between collagen and proteoglycans [48-50]. *In vitro* studies have demonstrated that silicon stimulates type I collagen synthesis and osteoblast differentiation [51]. Studies in rats have demonstrated that silicon at physiological levels improves calcium incorporation in bone when compared to rats that are deficient in silicon [52-54]. Additionally, dietary Si intake was shown to increase the bone mineral density (BMD) in men and premenopausal women. Further Si intake has shown to improve BMD by bone resorption in case of calcium deficiency in rats [55]. Moreover, it has been reported that Si has a biochemical function in bone growth processes affecting bone collagen turn over and sialic acid-containing ECM proteins like osteopontin. Moreover, orthosilicate acid (Si(OH)_4) at physiological concentration of 10 mmol has been shown to stimulate collagen I formation in human osteoblast cells (HOC) and to stimulate osteoblastic differentiation [44].

2.6.2 Strontium

Strontium (Sr) is an abundant and widely distributed element in the geosphere, natural water and human tissues. The amount of Sr in the skeleton is only 0.335% of its Ca content [56]. The biological properties of strontium are related to its chemical similarity to calcium. Sr can accumulate in bone by exchanging with Ca in the HA crystal lattice. Thus strontium accumulates to a high degree in bone, can displace calcium in hard tissue metabolic processes and at high concentrations interferes with normal bone development. Low levels of Sr have been known to be associated with low energy fracture sites. Presence of strontium lactate enhances Ca deposition in the bone and reduces bone pain in osteoporosis patients. Sr ions have been shown to stimulate osteoblastic bone formation and to inhibit osteoclastic bone resorption both *in vitro* and *in vivo* [56, 57]. Sr drew attention as a drug for the management of osteoporosis in the 1950s. Indeed, strontium ranelate (Protelos) is a drug approved for treatment and prevention of osteoporosis. Owing to the above-mentioned beneficial aspects of Sr in bone regeneration and considering the ion releasing ability of glasses in aqueous medium, bioactive glasses incorporated with Sr have gained considerable attention in the recent past for various orthopaedic applications. Sr-containing bioactive glasses were shown

to combine the known bone regenerative properties of bioactive glasses with the anabolic and anti-catabolic effects of Sr cations *in vitro* [58].

2.6.3 Zinc

Zinc (Zn) plays a vital role in bone formation, resorption and TE as it directly activates aminoacyl-tRNA synthetase (a rate-limiting enzyme at translational process of protein synthesis) in osteoblastic cells and stimulates cellular protein synthesis [42]. Zn has also been shown to stimulate gene expression of the transcription factors: runt-related transcription factor 2 (Runx2) that is related to differentiation into osteoblastic cells. Moreover, Zn inhibits osteoclastic bone resorption by inhibiting osteoclast-like cell formation from bone marrow cells and stimulating apoptotic cell death of mature osteoclasts [42].

In case of soft tissue regeneration, Zn has been proved to be an essential element for wound healing [30, 44, 45]. It is an essential trace mineral for DNA synthesis, cell division and protein synthesis during the proliferative phase of wound healing [42]. Zn deficiency has been associated with poor wound healing and decreased breaking strength of animal wounds [44] which can result from decreased protein and collagen synthesis during healing found in Zn deficient animals. Agren et al [59] demonstrated the beneficial aspect of topically applied Zn on leg ulcer healing and wound healing in animal models. It was shown that topical zinc oxide promotes cleansing, re-epithelialisation and inhibits bacterial growth.

2.6.4 Magnesium

Magnesium (Mg) is the fourth most abundant cation in human body with approximately half of the total physiological Mg stored in bone tissue [60]. It is essential to bone metabolism and has been shown to have stimulating effects on new bone formation [61]. Mg is a co-factor for many enzymes, and stabilizes the structures of DNA and RNA. Depletion of Mg in body results in impaired bone growth, increased bone resorption and loss in trabecular bone [62, 63]. The level of Mg in the extracellular fluid ranges between 17 ppm and 25.5 ppm, where homeostasis is maintained by the kidneys and intestine [60, 64]. Although Mg levels exceeding 25.5 ppm can lead to muscular paralysis, hypotension and respiratory distress and cardiac arrest occurs for severely high serum levels of 145–170 ppm, the incidence of hyper-Mg is rare due to the efficient excretion of the element in the urine [60, 64, 65].

2.6.5 Calcium

Calcium (Ca) accounts for 1-2 % of the adult human body weight [66], and a major component of mineralized tissues, approximately 99% of body Ca is found in bone, where it serves a key role as a component of HA. Ca plays an important role in osteoblast proliferation and bone remodelling by directly activating intracellular mechanisms by affecting Ca-sensing receptors in osteoblastic cells. The influence of Ca in the body is highly concentration dependent. Maeno et al. [67] found that Ca concentrations in blood varying within the range of 4–8 mmol are suitable for osteoblast proliferation, differentiation and extracellular matrix (ECM) mineralization, whereas higher Ca concentrations (>10 mmol) are cytotoxic. Extracellular Ca also plays an important role in the control of bone remodelling by directly regulating parathyroid cells through activation of the seven-transmembrane-spanning extracellular calcium-sensing receptor (CaSR), a member of the G-protein coupled receptor (GPCR) family [68]. Similar results were observed by Valério et al. [69], who found that extracellular Ca increases the glutamate release of osteoblastic cells. Since glutamate signalling pathways are known to play an important role for bone mechano sensitivity [70], extracellular Ca concentration must be considered as an important regulating agent in bone metabolism

2.6.6 Phosphorus

Phosphorus (P) is an essential nutrient for human and animal life. It is fundamental to growth, maintenance, and repair of all body tissues, and is necessary, along with calcium and magnesium, for proper growth and formation of bones in infants and children. P being a major component of the inorganic phase of human bone plays an important role in bone formation as it stimulates expression of matrix Gla protein (MGP), a key regulator for bone formation, in osteoblastic cells when added (10 mmol) to cell culture medium in concentration of <30 ppm [71, 72]. This release in controlled amounts has been shown to favour biomineralisation and induce expression of osteogenic messenger RNA transcripts while an increase in concentration of P beyond 30 ppm results in decrease in cell viability [72].

2.7 Introduction to the present work

Since the discovery of 45S5 Bioglass[®] in 1971 there has been a heightened interest in the science and biomedical application of bioactive glass over the last two decades, as evidenced by the growing number of publications in the field (Figure 2.3). Many artificial biomaterials based on, or inspired by Hench's glass have been developed and successfully employed in clinical applications for repairing and replacing parts of a human body

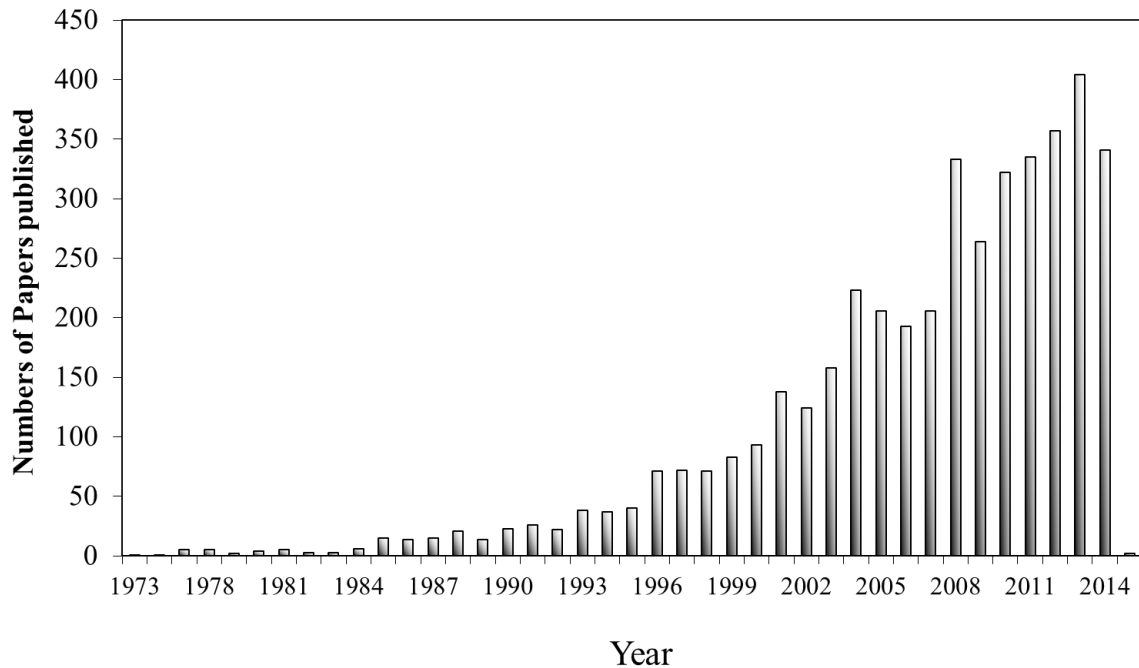


Figure 2.3 Number of papers published per year in the field of “bioactive glass” (compiled from a literature search SCOPUS carried out in November 2014).

. This field is continuously expanding: new processing routes have extended the range of applications towards new exciting directions in biomedicine [17], many of which still rely on the original Hench's base formulation, which is now considered a benchmark for the bioactive materials. Table 2.1 lists some bioactive glass compositions compiled from literature. Although the use of 45S5 Bioglass[®] in numerous clinical programs has exhibited favourable healing capability, one of the main problems associated with this glass is its high dissolution rate [73], mainly owing to its high alkali content. Our recent studies have shown that alkali-incorporation in bioactive glasses decreased their apatite forming ability during initial 72 hours of reaction with body fluids due to excessive release of sodium from the glasses [74], thus leading to apoptosis.

Table 2.1 Selected bioactive glass compositions (mol%).

	SiO ₂	P ₂ O ₅	Na ₂ O	CaO	K ₂ O	MgO	CaF ₂
45S5 [26]	46.1	2.6	24.4	26.9			
45S5F [75]	46.1	2.6	24.4	16.9			10
S53P4 [76]	53.9	1.7	22.7	21.8			
13-93 [77]	54.6	1.7	6.0	22.1	7.9	7.7	
6P61 [78]	61	2.5	10	13.5	2.4	10.7	
6P55 [78]	54.1	2.5	11.5	15.9	3.4	12.6	
A-W [79]	35.4	7.2	-	49.9	-	7.1	0.4
ICIE1[80]	49.46	1.07	26.38	23.08			
ICIE16 [80]	49.46	1.07	6.6	36.27	6.6		

With reference to the use of 45S5 Bioglass[®] *in vivo*, Vogel et al. [81] showed that this glass has good biological efficacy in cases where shorter healing periods are required (~1 month). However, this glass may not be a good option for serious injuries requiring prolonged treatment. Similarly, most of the bioactive glass compositions investigated so far and reported in papers [75-80, 82-87] and registered in a number of patents [75, 88-92] contain significant amounts of alkali oxides (Na₂O, K₂O). Although the incorporation of alkali oxides in bioactive glass is advantageous for their production, as they reduce their melting temperature, their presence in bioactive glass can reduce the usefulness of the glass *in vivo*. Often bioactive glasses for certain biomedical applications require heat treatments (coatings, sintering of porous scaffolds). When intended for coatings metal prosthesis the coefficient of thermal expansion has to match that of the metallic substrate. On the other hand, a good sintering ability is essential for achieving the required mechanical stability. These essential requirements are not fulfilled by alkali-rich bioactive glass compositions. As a matter of fact, high alkali contents degrade the working range of bioactive glasses by increasing the crystallization tendency of glass, thus rendering them unfit for use as bioactive porous scaffolds or porous coatings [93]. For example, in the case of 45S5 Bioglass[®], owing to its poor sintering ability, there have been problems with the manufacture of highly porous scaffolds possessing good mechanical. Hence, these drawbacks related to the alkali content of the bioactive glasses can be overcome by reducing the alkali contents or even by adopting alkali-free bioactive glass compositions.

The initial work for the development of alkali-free bioactive was made by Kukubo et al. in the year 1982, who designed a series of alkali-free glasses in the $3\text{CaO}\cdot\text{P}_2\text{O}_5 - \text{CaO}\cdot\text{SiO}_2 - \text{MgO}\cdot\text{CaO}\cdot 2\text{SiO}_2$ system [79]. The Apatite-Wollastonite (A-W) glass-ceramics designed by Kukubo et al. [94, 95] exhibit excellent mechanical properties as well as good *in vitro* and *in vivo* behaviour. Kasuga et al. [96] studied the effect of magnesium and aluminium on the bioactivity of the alkali-free glasses. Results indicated that Al_2O_3 tends to inhibit the apatite forming ability of the glasses and magnesium tends to slow down (but not hinder) the apatite forming ability of glasses when immersed in SBF solution. K. Ohura et al. [97] incorporated various ions into CaO-SiO_2 based glasses and studied their effect on the *in vivo* performance. The formation of a calcium phosphate layer was achieved in the all the glasses except for the ones containing Fe_2O_3 . In the mid 1990 Galliano et al. [98] investigated the influence of Mg^{2+} and Sr^{2+} on the structure and thermal behaviour of glasses in the $\text{CaO-SiO}_2\text{-P}_2\text{O}_5\text{-CaF}_2$ system. To the best of our knowledge, this is one of the foremost studies on Sr-containing bioactive glasses.

In another study, Salinas et al. [99] reported on the influence of Mg on the *in vitro* bioactivity of slightly modified A-W glasses and glass-ceramics. The results showed negligible changes in bioactivity of glasses; however, presence of Mg led to the appearance of new crystalline phases in the glass-ceramics which were able to suppress the *in vitro* bioactivity. Further, an extensive work has been done by Oliveira et al. [100-102] using ^{29}Si and ^{31}P MAS-NMR to investigate the structure *versus* bioactivity (assessed through immersing the glass samples in SBF) relationship of bioactive glasses compositions without alkali content. In 2006 Kamitakahara et al. [103] designed alkali-free Di based glass-ceramics and investigated their mechanical strength and bioactivity. They found that the flexural strength of an eutectic glass-ceramic composition 38 TCP-62 Di (wt.%) was higher than 200 MPa. However, no further studies dealing with this system have been reported since that, and our attempts to reproduce these results were unsuccessful. Recently, Kansal et al. [104-106] investigated the structure, thermal and dissolution behaviours of alkali-free glasses and glass-ceramics in Di-based glasses using MAS-NMR and ICP-AES. The as developed glasses exhibited better sintering ability than 45S5 Bioglass[®] and good *in vitro* bioactive properties.

2.7.1 Aim of the thesis

Despite of extensive amount of work done by scientists all over the world, literature survey reveals that since the earnest 1970s, most of the work in the field of bioactive glasses has been mainly focused upon understanding the compositional dependence of glass dissolution for 45S5 Bioglass[®] (46.1% SiO₂, 24.4% Na₂O, 26.9% CaO and 2.6% P₂O₅ in mole percent) or other silicate glasses with similar compositions [77, 107-109]. Further, last few years have witnessed a consistent upsurge of studies attempting correlating the atomic and molecular structure of silicate glasses with their chemical dissolution and bioactivity behaviours [5, 80, 110-112]. Simultaneously, significant efforts have been made either to unearth the influence of functional ions on the structure of bioactive glasses [113-118] or to study their influence on the chemical dissolution behaviour of glasses [119-125]. However, few attempts have been made to elucidate about the correlation between the structural role of these functional ions and the chemical degradation and bioactivity of glasses [23, 42, 87, 104, 126] especially in case of alkali-free bioactive glasses. Despite significant progress made in the pursuit of establishing relationships between chemical composition, molecular structure and bioactivity of silicate glasses, we are still not in a position to develop scientifically robust and statistically accurate models to predict the chemical dissolution and bioactivity of glasses mainly because most of the studies available in scientific literature still revolve around structure-property relationships of glasses based on or inspired by 45S5 Bioglass[®] [5, 110, 111, 127-129].

Therefore, in the present doctoral work we have tried to design and characterize glasses covering far from region of high alkali-content in an attempt to find a possible solution for the above discussed long-standing problem of alkali-containing glasses. Accordingly, the work reported in this dissertation has been directed towards fulfilment of the following aims:

1. To design alkali-free bioactive glasses having high bioactivity, lower dissolution rate and good sintering behaviour so as to prove their efficacy for bone regeneration and TE applications.
2. To understand on the structure-property relationships in alkali-free bioactive glasses
3. To understand effect of various functional ions on the structure and its implications on the biodegradation behaviour of the glasses and its impact on *in vitro* behaviour of glasses.

4. To understand the effect of these functional ions on sintering, crystallization behaviour of bioactive glasses and glass-ceramic.

We hope that the work reported in this dissertation will be a good contribution to the growing literature in the field of bioactive glasses, that will enable us to create a succinct database which can be further used to develop models for designing bioactive glasses with controlled chemical degradation rate and high bioactivity with novel applications in the field of human biomedicine.

Chapter 3

Experimental

3. Experimental

3.1 Glass synthesis

High purity powders of SiO₂ (BDH Chemicals Ltd., UK, purity >99.0%), CaCO₃ (BDH Chemicals Ltd., UK, purity >99.0%), MgCO₃ (BDH Chemicals Ltd., UK, purity >99.0%), NH₆PO₄ (Sigma Aldrich, Germany, >99.0%), ZnO (Sigma Aldrich, Germany, >99.9%), SrCO₃ (Sigma Aldrich, Germany, >99.9%) and CaF₂ (Sigma Aldrich, Germany, 325 mesh, >99.9%) were used. All the glass compositions have been prepared by melt-quenching technique. Homogeneous mixtures of batches (~100 g) obtained by ball milling, were preheated at 900 °C for 1 h for calcinations and then melted in platinum (Pt) crucibles at 1570-1590 °C for 1 h. The glasses were obtained in bulk form by casting the glass melt on a metallic mould and then annealing the glass at 500-700 °C for 1 h. The glasses were obtained in frit form by quenching of glass melts in cold water. The frits were dried and then milled in a high-speed agate mill resulting in fine glass powders with mean particle sizes of ~ 10–20 µm (determined by light scattering technique; Coulter LS 230, Beckman Coulter, Fullerton CA; Fraunhofer optical model). The amorphous/crystalline nature of frits was confirmed by X-ray diffraction (XRD) analysis (Rigaku GeigerflexD/Max, Tokyo, Japan; C Series; Cu Kα radiation; 2θ angle range 10°–60°; step 0.02° s⁻¹).

3.2 Density and Molar volume

Archimedes' method [i.e. immersion in diethyl phthalate (C₁₂H₁₄O₄) (molar mass: 222.24 g mol⁻¹; density: 1.12 g cm⁻³)] was employed to measure the apparent density of the bulk annealed glasses and glass-ceramics. Molar volume (V_m), was calculated using the density data for the bulk glasses using following relations:

$$V_m = \frac{M}{\rho}$$

Where M is the molar mass of the glass and ρ is the apparent density of the bulk glasses.

3.3 Structural characterization of glasses

3.3.1 Magic angle spinning (MAS) – Nuclear magnetic resonance (NMR) spectroscopy

The ²⁹Si MAS-NMR spectra were recorded on a Bruker ASX 400 spectrometer operating at 79.52 MHz (9.4 T) using a 7 mm probe at a spinning rate of 5 kHz and 60 seconds delay time was used. Kaolinite was used as the chemical shift reference. The ³¹P MAS-NMR spectra of glasses were recorded using 4 mm probe on a Bruker ASX 400

spectrometer operating at 161.97 MHz with 45° pulses, spinning rates of 12 kHz, a 60 s recycle delay and the chemical shift was quoted in ppm from phosphoric acid (85%).

3.3.2 Infra-red spectroscopy.

Fourier transform infrared (FTIR) spectra of the glasses (before and after immersion in SBF) were obtained using an Infrared Fourier spectrometer (FTIR, model Mattson Galaxy S-7000, USA). For this purpose glass powders were mixed with KBr in the proportion of 1/150 (by weight) and pressed into a pellet using a hand press. 64 scans for background and 64 scans per sample were made with signal gain 1. The resolution was 4 cm⁻¹. The bands were assigned as per the Table 3.1 [119, 208].

Table 3.1 Infrared bands of functional groups of bioactive glasses.

Vibration mode	Wavenumber (cm ⁻¹)
Si-O-Si	415-540
P-O bend crystal	515-530
P-O bend crystal	550-560
P-O bend amorphous	570-600
P-O bend crystal	600-610
C-O stretch	800-890
Si-O-Si tetrahedral	860-1175
Si-O stretch	1000-1100
P-O stretch	910-1040
P=O stretch	1180-1350

3.4 Biodegradation of glasses

The *in vitro* bioactivity of glasses, reflected in their capability of inducing HA-formation onto their surfaces, was investigated by immersion of glass powders in simulated body fluids (SBF) (0.10 g glass powder in 50 ml SBF solution) at 37 °C. SBF had an ionic concentration (Na⁺ 142.0, K⁺ 5.0, Ca²⁺ 2.5, Mg²⁺ 1.5, Cl⁻ 125.0, HPO₄⁻ 1.0, HCO₃²⁻ 27.0, SO₄²⁻ 0.5 mmol l⁻¹) nearly equivalent to human plasma, as discussed by Tas [130]. The powder-SBF mixtures were immediately sealed into sterilized plastic flasks and were placed in an oven at 37 °C (± 0.5 °C). The SBF solution was replaced every 48 h and sampling took place at variable times ranging from days to weeks. The experiments were performed in

duplicate in order to ensure the accuracy of results. The apatite forming ability on glass powders was followed by XRD and FTIR analysis.

The degradation tests were performed according to the standard ISO 10993–14 “Biological evaluation of medical devices – Part 14: Identification and quantification of degradation products from ceramics”. The test simulates the more frequently encountered *in vivo* pH (7.4 ± 0.1) and therefore investigates the degradation of glasses/ceramics in freshly prepared Tris–HCl buffered solution. The glass powder with particle size varying between 300 – 400 μm was added to the Tris–HCl solution (2.5 g glass powder in 50ml Tris–HCl solution). The tests were carried out without solution replacement at 37 °C and with a mixing speed of 120 rpm. The sampling was done after 120 h, when the solid and liquid phases were separated by filtering (0.22 μm , Millex GP, Millipore Corporation, USA). The solid samples were then washed in deionised water and dried in an oven to a constant weight. The structural changes (if any) in the glasses after immersion in Tris–HCl were analysed by XRD and FTIR analysis. The pH and elemental concentrations (Ca^{2+} , Sr^{2+} , Mg^{2+} , PO_5^{5-} , SiO_4^{4+}) (ICP-AES; JobinYvon, JY 70 plus, France) of the soaking solutions were measured. The relative weight loss percentage (W_L) of the glass samples after 120 h of immersion in the solutions was calculated from the following equation:

$$W_L = \left(\frac{W_0 - W_t}{W_0} \right) \times 100$$

Where W_0 refers to the weight of the glasses before immersion and W_t refers to their weight after immersion in Tris-HCl.

3.5 Thermal analysis

3.5.1 Sintering behaviour- hot stage microscope (HSM)

The sintering behaviour of the glass powders was investigated using a side-view hot stage microscope (HSM) EM 201 equipped with image analysis system and 1750/15 Leica electrical furnace. The cylindrical shaped samples with height and diameter of ~ 3 mm were prepared by cold-pressing the glass powders. The cylindrical samples were placed on a $10 \times 15 \times 1$ mm alumina (>99.5 wt% Al_2O_3) support. The temperature was measured with a Pt/Rh (6/30) thermocouple contacted under the alumina support. The microscope projects the image of the sample through a quartz window and onto the recording device. The computerized image analysis system automatically records and analyses the geometry changes of the sample during heating. The image analyser takes into account the thermal expansion of the

alumina substrate while measuring the height of the sample during firing, with the base as a reference. The HSM software calculates the percentage of decrease in height, width and area of the sample images. The measurements were conducted in air with a heating rate (β) of 5 K min⁻¹.

3.5.2 Differential thermal analysis

The values of the glass transition temperature (T_g), crystallization onset temperature (T_c) and peak temperature of crystallization (T_p) were obtained by differential thermal analysis (DTA) using a Setaram LabSys TG-DTA16 instrument (Setaram Instrumentation, France) calibrated in the temperature range 25–1000 °C. The measurements were performed using powdered glass samples (50 mg) in an alumina crucible and α -alumina powder as reference at a heating rate (β) of 5 K min⁻¹ and 20 K min⁻¹.

3.6 Preparation of glass-ceramics

Glass-ceramics can be prepared either by nucleation and crystallization through suitable heat treatments given to monolithic glasses, or by sintering and crystallization of glass powder compacts. Rectangular bars with dimensions 4 × 5 × 50 mm³ and circular disc shaped pellets with diameter 20 mm and thickness ~3 mm were prepared from fine glass powders by uniaxial pressing (80 MPa). The glass powder compacts were sintered under isothermal conditions for 1 h at the different temperatures. A slow heating rate (β) of 5 K min⁻¹ was maintained in order to prevent deformation of the samples.

3.7 Characterization of glass-ceramics

3.7.1 Mechanical Properties of sintered glass-ceramics

The mechanical properties were evaluated by measuring the three-point bending strength of rectified parallelepiped bars (3 × 4 × 50 mm³) of sintered glass-ceramics (Shimadzu Autograph AG 25 TA, Columbia, MD; 0.5 mm min⁻¹ displacement). The mean values and the standard deviation presented for shrinkage and density were obtained from (at least) ten different samples.

3.7.2 Microstructural characterization- SEM and EDS

Microstructural observations were made on polished surfaces of the sintered and heat treated glass powder compacts (chemically etched by immersion in 2 vol% HF solution for

duration of 2 min) by scanning electron microscopy (SEM; SU-70, Hitachi). In addition, energy dispersive spectroscopy (EDS; Bruker Quantax, Germany) has been utilized to study the distribution of elements.

3.8 In vitro studies

3.8.1 Alkali-free glasses for bone tissue engineering: A preliminary investigation

3.8.1.1 Mesenchymal stem cell proliferation

The biological performance of the as developed glass-ceramics was addressed by the *in vitro* cellular responses, including cell proliferation and osteoblastic differentiation. The results were compared with the tissue culture plastic used as a control. For the cellular study, mesenchymal stem cells (MSCs) derived from rat bone marrow were used. MSCs have been a potential source for the regenerative therapy of tissues including bone, because of their multipotent and self-renewal capacity without the concern of ethical issues. The experimental procedures were based on their previous work [28] and followed by the guidelines approved by the Animal Ethics Committee of Dankook University. MSCs gathered from the bone marrow of rats were maintained in a normal culture medium containing α -minimal essential medium (MEM) supplemented with 10% foetal bovine serum (FBS), 100 U ml⁻¹ penicillin and 100 mg ml⁻¹ streptomycin in a humidified atmosphere of 5% CO₂ in air at 37 °C.

MSCs maintained up to 3-4 passages were used for cellular study. The glass-ceramics were sterilized with 70% ethanol for 1 h prior to seeding cells. For the cell growth study, MSCs were seeded on each sample (15 mm × 2 mm disc type) and then cultured in the normal culture medium condition as described above. After culture for 3, 7 and 14 days, the cell growth level was analysed by the cell counting kit (CCK) assay. At each time of culturing (3 and 7 days), the CCK-8 reagent was added to each sample and incubated for 3 h at 37 °C. The absorbance was measured at a wavelength of 450 nm using a microplate reader (Molecular Devices, USA). The cell growth morphology was observed by SEM (Hitachi) after fixation the cells with 2.5% glutaraldehyde, dehydration with a graded series of ethanol (50, 70, 90 and 100%) and coating with gold.

3.8.1.2 Alkaline phosphatase activity

The osteoblastic differentiation of the MSCs on the glass-ceramics was determined by measuring the ALP activity. Cells were seeded on each sample (15 mm × 2 mm disc type), and cultured in the osteogenic medium containing 50 µg ml⁻¹ sodium ascorbate, 10 mM β -

glycerol phosphate, and 10 nM dexamethasone. After culture for 7 and 14 days, cellular samples were gathered and added to the ALP reaction media to allow an enzymatic reaction according to the manufacturer's instruction (Sigma). The quantity of samples used for the reaction was determined based on the total protein content which was determined by using a commercial DC protein assay kit (BioRad). As a result of the reaction, the product *p*-nitrophenol appears as the colour change which was then measured at an absorbance of 405 nm using a spectrophotometer.

The CCK and ALP assays were performed on three replicate samples ($n = 3$). Data were represented as means \pm standard deviations. Statistical analysis was carried out by analysis of variance (ANOVA) and significance level was considered at $p < 0.05$.

3.8.2 Influence of ZnO/MgO substitution on sintering, crystallization, and bio-activity of alkali-free glass-ceramics

Similar procedure as mention in section 3.8.1 was used.

3.8.3 Role of glass structure in defining the chemical dissolution behaviour, bioactivity and antioxidant properties of zinc- and strontium- co-doped alkali-free phosphosilicate glasses

3.8.3.1 In vitro cellular tests

For investigating the cellular responses and antioxidative effect for the developed glass compositions (ZS-2 to ZS-8), thin slices of glasses measuring ~ 1 mm of thickness were prepared by cutting and polishing the bulk annealed glasses. Tissue culture plastic was used as a control.

3.8.3.1 Cell Culture studies

Human osteosarcoma cell line MG63 was obtained from National Centre for Cell Science (NCCS), Pune, India and maintained on Dulbecco's Modified Eagle's Medium (DMEM) supplemented with streptomycin (100 U ml^{-1}), gentamycin ($100 \mu\text{g ml}^{-1}$), 10% FBS (Sigma-Aldrich) at 37°C and humid environment containing 5% CO_2 . MTT was used to assess cell integrity and potential cytotoxicity of the plant extract by monitoring the uptake of the vital mitochondrial dye, 3-[4,5-dimethylthiazol-2-yl]- 2,5-diphenyl tetrazolium bromide (MTT) by cell mitochondria.

Binding of MG63 cells to glass samples was carried out in 24 well plates. Rectangular shaped, sterilized glass slices were kept in triplicates in the 24 well plates. The wells without glass samples were considered as control. 500 μl of lymphocyte suspension at a concentration of 2×10^4 cells ml^{-1} was added to each well. The plate was then incubated at 37 °C, 5% CO_2 in air and 90% relative humidity in CO_2 incubator for 96 h. Four hours before the termination of cultures, 500 μl of MTT (2 mg ml^{-1}) prepared in serum free medium was added to each well. After 4 h, 500 μl of DMSO (Dimethyl sulfoxide) was added to each well. The blue colored formazan formed was read at 570 nm with Labsystems Multiskan EX ELISA reader against a reagent blank.

The cells on disks were fixed with freshly prepared Karnovsky's fixative (2% paraformaldehyde; 2.5% glutaraldehyde in 0.1 M phosphate buffer pH 7.4.) at 4 °C for 90 min. After fixation, the fixative was removed and cells were washed for 2 min with 0.1 M phosphate buffer. Further, cells were fixed in 1% buffered osmium tetroxide (prepared in phosphate buffer) for 90 min at 4 °C. The cells were further dehydrated with various concentrations of ethanol starting with 30% for 5 min twice and repeating the same with 50, 75, 95% and absolute ethanol. After critical point drying, cells were photographed with EVO[®] LS10 Life Science SEM.

3.8.3.2 Cytoprotective assay

Cytoprotective effect of bioactive glasses was carried out on hydrogen peroxide (H_2O_2) induced oxidative stress in human MG63 cells. The H_2O_2 dose (LD50) for cytoprotection studies was calculated by treating cells at 50% confluency with H_2O_2 (7.5 μM to 1000 μM diluted in medium) for 12 h in serum free medium. The glass slices were kept in triplicates in the 24 well plates. The wells without glass samples and H_2O_2 were considered as negative control and cells with H_2O_2 along with glass samples were kept as positive controls. 500 μl of cell suspension at a concentration of 2×10^4 cells ml^{-1} was added to each well. The plate was then incubated at 37 °C, 5% CO_2 in air and 90% relative humidity in CO_2 incubator for 72 h. The LD50 dose of H_2O_2 was given at this point to induce the oxidative stress for 12 h in the wells with and without glass samples except negative control. Four hours before the termination of cultures, 500 μl of MTT (2 mg ml^{-1}) prepared in serum free medium was added to each well. After 4 h, 500 μl of DMSO was added to each well. The blue colored formazan formed was read at 570 nm with Labsystems Multiskan EX ELISA reader against a reagent blank.

3.8.4 An experimental approach towards understanding the composition-structure-bioactivity relationships in silicate glasses

3.8.4.1 Cell Culture Studies

Human mesenchymal stem cells (hMSC, Lonza) were thawed and then cultured in 175 cm² tissue culture flasks containing DMEM (Gibco), supplemented with 10% v/v inactivated FBS (Gibco), and 1% v/v penicillin/streptomycin (P/S, Gibco). Cells were maintained at 37 °C under a 5% CO₂ humidified atmosphere. The medium was changed every third day until confluence, when cells were sub-cultured in order to prevent cell death. In order to sub-culture, the cell monolayer was washed with phosphate buffered saline (PBS) (Sigma) and incubated with a trypsin/ethylene diamine tetra acetic acid (EDTA) solution for 8 min at 37 °C to detach the cells. The effect of trypsin was then inhibited by adding culture medium at room temperature. Cells were used in the passage six.

The glass samples were autoclaved (120 °C, 20 min) and placed in untreated 48-well plates (~ 1 cm² surface area) (Cellstar[®]) to avoid cell adhesion to the bottom of the wells. The controls were wells treated with poly-D-lysine. The cells were seeded at 2×10⁴ cells per well and fresh medium was added, followed by incubation at 37 °C for 4 h to allow cell adhesion. Afterwards, fresh medium was added until it reached a final volume of 400 µl per well. To induce the hMSCs differentiation along the osteoblastic lineage, cells were also cultured with osteogenic medium: basal medium supplemented with 10 µl ml⁻¹ glycerophosphate (Sigma), 10 µl ml⁻¹ dexamethasone (Sigma), and 10 µl ml⁻¹ ascorbic acid (1.61 mg ml⁻¹) (Fluka). hMSCs were cultured on samples of the glass for periods of 1, 3, 7, 14 and 21 days. At each time point, the samples were evaluated for cell metabolic activity, viability, morphology and differentiation.

3.8.4.2 Cell metabolic activity

A resazurin method was used to assess metabolic activity at days 1, 3, 7, 14 and 21. A resazurin solution (Sigma) was added to fresh medium at a final concentration of 10% (v/v). Cells were incubated in this solution at 37 °C for 3 h, after which, 100 µl per well were transferred to a 96-well black plate and fluorescence was measured (530 nmEx/590 nmEm) in a Spectra Max Gemini XS (Molecular Devices).

Chapter 4

Results and Discussion

4 Results and Discussion

4.1 Alkali-free glasses for bone tissue engineering: A preliminary investigation

4.1.1 Introduction

The present chapter reports on a preliminary attempt to find a feasible solution for the above discussed long-standing problem of designing alkali-free bioactive glasses. In this pursuit, the alkali-free glass compositions have been designed in the system Di-FA-TCP with a general formula (Di) (90-x)-(FA)10-(TCP)x (x = 10-40 wt%). Table 4.1.1 presents the detailed compositions of the glasses. The present composition has been selected due to following reasons:

Table 4.1.1 Nominal composition of the as-designed glasses (mol%).

Glass	SiO ₂	P ₂ O ₅	CaO	MgO	CaF ₂
TCP-10	42.57	3.57	32	21.29	0.57
TCP-20	38.49	5.61	36.07	19.24	0.59
TCP-30	34.12	7.79	40.42	17.06	0.61
TCP-40	29.44	10.12	45.08	14.73	0.63

Di belongs to the group of inosilicates and is an important member of clinopyroxene group with composition CaMgSi₂O₆. The structure of amorphous Di is dominated by Q^2 unit which is a positive attribute for bioactivity in glasses. Also, it has been demonstrated that Di-based ceramics and glass-ceramics have no general toxicity in cell cultures and help in bone regeneration [131, 132]. Nakajima et al. [133, 134] found that Di possessed ability to form apatite in SBF and could closely bond to bone tissue when implanted in rabbits. Aza et al. [132] investigated the reactivity of the material in a natural medium of high protein content by soaking Di based ceramic pellets in human parotid saliva (HPS) over various time intervals. Also Yoganand et al. [135] synthesized bioactive glass-ceramics with the help of transferred arc plasma technique in the system CaO-MgO-SiO₂ with Di as the major crystalline phase.

In addition to the biocompatibility aspect of Di based ceramics and glass-ceramics; they are known to exhibit superior mechanical properties in comparison to many of their ceramic counterparts. Nonami et al. [131] reported significantly improved fracture toughness values for pure sintered HA with added Di. It was reported that the bending strength and

fracture toughness of Di-HA composite was 2 to 3 times higher in comparison to that of sintered HA. Therefore, owing to the presence of Di, we can expect superior mechanical properties for the glass-ceramics without compromising their biomedical characteristics.

Further, the presence of hydroxy-, oxy- or fluoro- apatite is highly favourable for biomedical applications. In particular, FA based glasses and glass-ceramics have gained attention [104, 105, 136, 137] due to their structural and chemical similarities with bone forming mineral, HA [87]. Also, fluoride is known to increase bone density and also has anti-carcinogenic properties [104]. Further, intracellular or plaque-associated enzymes have been reported to be affected by fluoride ions [104]. Alkali-free Di-FA-W bioactive glass-ceramics for replacement materials for tooth roots, dental crowns were developed by Shibuya et al. [88], while Tulyaganov et al. [138] developed glass-ceramics in ternary system tetrasilicic mica-FA-Di. Recently Kansal et al. [104, 105] reported the biodegradation behaviour of the Di-FA based glasses.

Similar to Di-FA join, glass-ceramics along Di-TCP join have been a subject of interest due to their potential biomedical applications. TCP is a typical bioresorbable material which is widely used in bone repair [139]. Also TCP ceramics bear excellent properties for bone marrow stromal cells culture towards osteogenic differentiation [140]. Therefore, the addition of TCP at the expense of Di in the glass compositions is expected to enhance their solubility as well as their bioactivity in physiological fluids. Also, the addition of TCP to Di is expected to improve its sintering ability as it has been reported that the flexural strength of eutectic glass-ceramic composition 38TCP-62Di (wt%) is higher than 200 MPa [103]. Kamitakahara et al. [103] studied the bioactivity and mechanical properties of bioactive scaffolds. Also, Ashizuka et al. [141] reported on the mechanical properties of Di-TCP based glass-ceramics. Thus it's expected that the combination of Di, FA and TCP phases is expected to result in the development of glasses with excellent bioactive properties, low chemical degradation and good sintering ability.

4.1.2 Results and discussions

4.1.2.1 Glass forming ability

For all the investigated glass compositions ($x = 10 - 40$ wt%), melting at 1570 °C for 1 h was sufficient to obtain bubble-free, transparent and amorphous glasses (Figure 4.1.1). The glass forming ability diminished with further increase in TCP content in glasses ($x > 40$ wt%) as resultant glass frits were prone to spontaneous crystallization even after super-

cooling in cold water thus, resulting in white, opaque material with FA as the only crystalline phase, as revealed by XRD analysis (not shown).

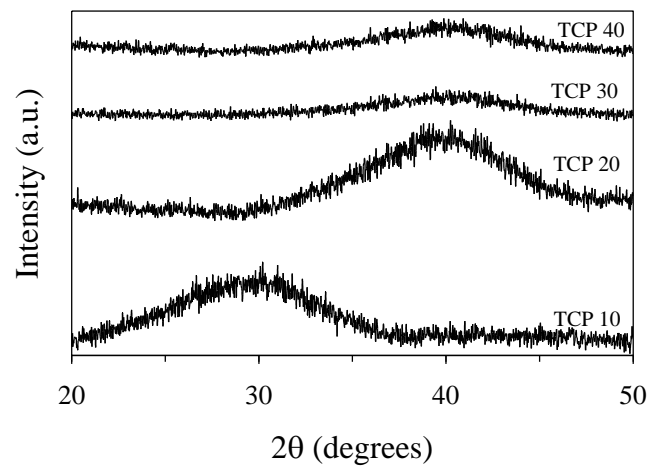


Figure 4.1.1 X-ray diffractograms of as-quenched glass frits.

4.1.2.2 Structure of glasses (MAS – NMR spectroscopy)

The molecular structure of glasses plays a crucial role in deciding their bioactivity. Therefore, understanding their structural features allows designing new glasses with improved chemical durability and tailored biodegradability for specific applications. In the present study, MAS-NMR results are presented in Figure 4.1.2, the ^{29}Si spectra (Figure 4.1.2a) for all the investigated glasses depict the dominance of Q^2 (Si) structural units in the glasses. In particular, the broad ^{29}Si spectra centred around -81 to -82 ppm indicative of Q^2 as predominant silicate species [188]. Further, with decrease in the amount of SiO_2 no change in structure was observed (TCP: 10 – 40 wt%), however a slight chemical peak shift towards more negative ppm was observed.

Further, we could not observe any significant change in peak maxima for spectra of ^{31}P nucleus with predominance of an orthophosphate-type environment (Figure 4.1.2b). In fact, the observed chemical shifts, 1–2 ppm, are close to that of the calcium orthophosphate (3.1 ppm) and that of the amorphous magnesium orthophosphate (*ca.* 0.5 ppm) [137]. However, it should be noticed that bioactivity is not solely a function of glass structure and also depends on their chemical nature [142]. According to Tilocca and Cormack [143], low contents of P_2O_5 in glasses (~ 10 mol%) enhance their bioactivity while further increase in P_2O_5 amount affects the bioactive nature of glasses in a negative manner.

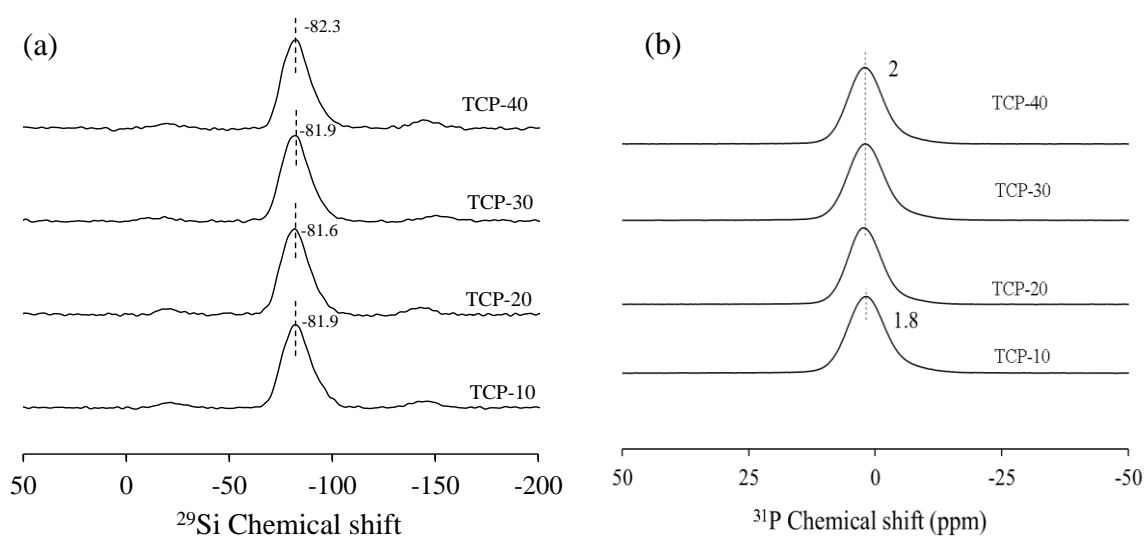


Figure 4.1.2 MAS NMR spectra of investigated glasses showing the peak positions of (a) ^{29}Si and (b) ^{31}P .

4.1.2.3 Apatite formation and chemical degradation of glasses

Immersing the materials in SBF is a relatively simple technique to evaluate the biomineralization activity and this method can be regarded as a first approach to assess bioactivity *in vitro*. However, even the preparation conditions of the SBF solution are tricky and there exist a lack of consensus regarding the usefulness of SBF tests in the literature [144]. But there are a large number of evidences about the good correlation between the biomineralization ability a given bioactive material (understood as the ability to form a carbonated apatite layer onto its surface) in SBF and its performance *in vivo* [145, 146].

The *in vitro* bioactivity analysis by immersion in SBF solution revealed the presence of apatite formation in all the glass powders. The results presented here have been mainly explained with an emphasis on glasses TCP-20 and TCP-40 due to their high potential for use in human biomedicine. The XRD patterns observed for all as-quenched glasses (Figure 4.1.1) exhibit an amorphous halo, thus depicting the absence of any crystallinity. However, the X-ray diffractograms of investigated glasses (including 45S5 Bioglass[®]) after soaking in SBF solution for time durations varying between 1 – 12 h (Figure 4.1.3) showed considerable differences in comparison to the diffractograms of their respective parent glasses. A small X-ray peak at $2\theta = 31.77^\circ$ corresponding to the formation of crystalline HA [$(\text{Ca}_5(\text{PO}_4)_3\text{OH}$; ICDD: 00-09-0432] can be seen for glass TCP-40 after immersion in SBF for 1 h, while 45S5 Bioglass[®] suggests that calcite (CaCO_3 ; ICDD: 01-083-0577) formation under similar conditions (Figure 4.1.3a). The XRD pattern for glass TCP-20 depicted a broad amorphous halo after 1 h immersion in SBF (Fig. 4.1.3a) while the infrared spectra of this glass (Figure 4.1.4)

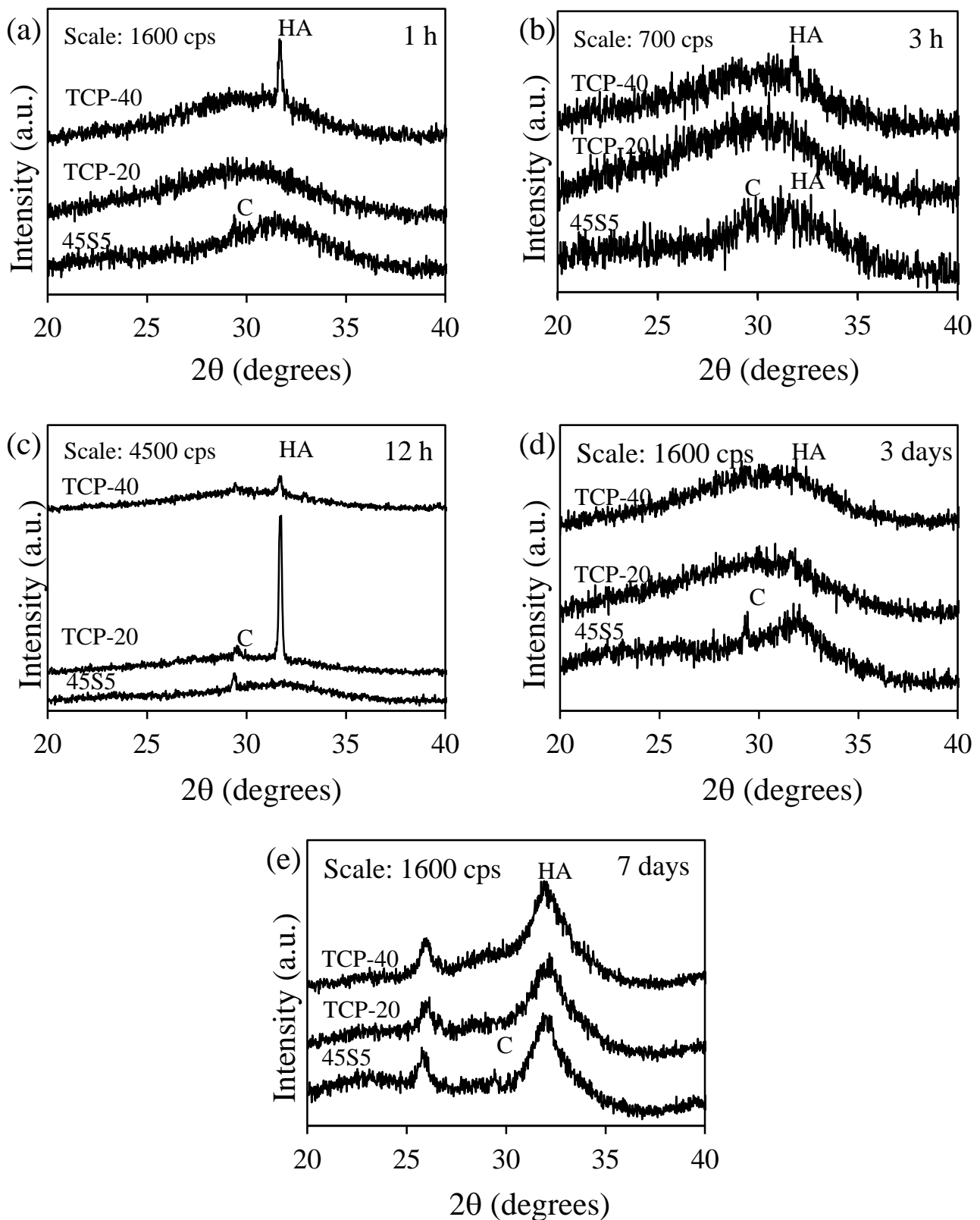


Figure 4.1.3 X-ray diffractograms of glass powders after immersion in SBF solution for (a) 1 h; (c) 3 h; (c) 12 h, (d) 3 days and (e) 7 days. C refers to calcite while HA refers to hydroxyapatite.

exhibited significant structural differences before and after immersion in SBF. As is evident from Figure 4.1.4, a strong low frequency band centred at $\sim 480 \text{ cm}^{-1}$, ascribed to a deformation mode of silica layer that develops on the dissolving glass particles could be seen in glass TCP-20 after immersion in SBF solution for 1 h [83]. The main IR band now occurs at 1080 cm^{-1} and a nearby shoulder, centred at $\sim 1235 \text{ cm}^{-1}$ attributed to Si-O-Si vibration can be observed [147], owing to the interfacial formation of high-area silica gel layer, as postulated in Hench's inorganic reaction set [20]. These features were common for all the glasses investigated in present study. Further, band at $\sim 1440 \text{ cm}^{-1}$ along with another one at $\sim 880 \text{ cm}^{-1}$ present in all glasses corresponds to incorporation of carbonate into the apatite, resulting in hydroxyl carbonated apatite, rather than stoichiometric HA [83].

Furthermore, a small broad band was observed in case of glass TCP-20 (Figure 4.1.4) at $\sim 565 \text{ cm}^{-1}$ after immersion in SBF solution for 1 h. This is the most characteristic region for apatite and other phosphates as it corresponds to P-O bending vibrations in a PO_4^{3-} tetrahedron. A single peak in this region suggests the presence of non-apatitic or ACP, which is usually taken as an indication of presence of precursors to HA. Apatitic PO_4^{3-} groups have characteristic split bands at ~ 560 and 600 cm^{-1} , with a third signal at $\sim 575 \text{ cm}^{-1}$ observed for crystallites of small size [83, 87]. However, apart from a band at $\sim 565 \text{ cm}^{-1}$ as is evident in Figure 4.1.4, no other bands in this region could be observed for glass TCP-20 even after 12 h of immersion in SBF solution while the XRD data of the same sample as presented in Figure 4.1.3c reveals the presence of sharp peak corresponding to formation of HA along with minor amounts of calcite. It is noteworthy that no HA formation could be observed instead a small X-ray peak at $2\theta = 29.41^\circ$ corresponding to the presence of calcite was observed in 45S5 Bioglass[®] even after 12 h of immersion in SBF solution (Fig. 4.1.3c)

The increasing tendency towards development of ACP rich layer leading to formation of crystalline HA with increasing TCP content in glasses may be explained on the basis of decreasing Mg concentration in glasses. It has been reported that Mg tends to associate preferentially with phosphorus at glass surface, which consequently leads to the decrease in concentration of apatite like-calcium phosphate domains on the glass surface that are supposed to act as nucleation centres for apatite formation [148]. Also, glass compositions containing phosphorus are known to be more soluble and exhibit faster release of silica in solution. Further, isolated orthophosphate groups can be directly released without breaking

any chemical bond; thus high rate of formation of HA in TCP containing glasses is likely related to the high availability of this species [149].

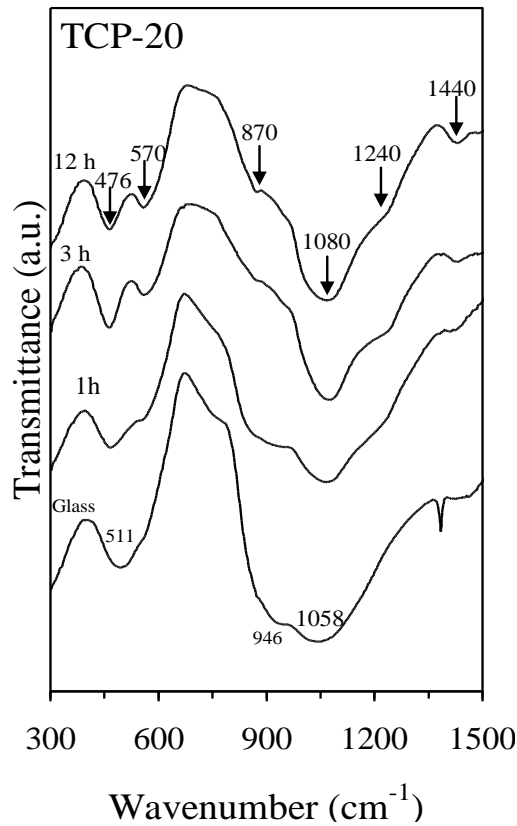


Figure 4.1.4 FTIR spectra of glass powder (TCP-20) before and after immersion in SBF solution for time durations varying between 1 h – 12 h.

The XRD data after 3 days of immersion in SBF solution (Figure 4.1.3d) depicts the highly amorphous character of glasses with a small phase reflection corresponding to HA in composition TCP-20 and TCP-40. Similar structural features could be observed in all the investigated glasses. Since intense ionic exchanges occur at the bioactive glass surface that cause major changes in the degree of super-saturation for HA formation in biological fluids, the potential for each glass to form an apatite layer can be extrapolated from the corresponding evolution of the degree of super-saturation. According to Lao et al. [122], the degree of super-saturation may be defined as: $SD = Q/K_{sp}$, where K_{sp} is the solubility product of HA in aqueous solution while Q is the ionic activity product for the formation of HA. Therefore, the solution and HA mineral phase reach equilibrium when $SD = 1$. For $SD < 1$, the dissolution of HA mineral phase is favoured, while the solution is supersaturated with

respect to HA mineral and its precipitation is favoured when $SD > 1$. In the present scenario, during the initial hours of immersion of the glass in SBF, the SD increases because of dealkalinization of the glass surface, while the formation of a silica-rich layer provides regions of low interfacial energy, thus providing favourable sites for the nucleation of HA. However, the decreasing intensity of the XRD phase reflections for the HA phase in investigated glasses after 72 h of immersion in SBF may be attributed to the changing degree of super-saturation owing to the refreshing of the SBF solution after every 48 h.

An increase in immersion time of glasses in SBF solution led to complete disappearance of calcite from the investigated glasses and depicted the formation of HA as the only crystalline phase as shown in Figure 4.1.3d. However, calcite still persisted in 45S5 glass as a minor phase along with HA even after 7 days of immersion in SBF. According to Jones et al. [150], the *in vitro* apatite forming ability of 45S5 glass decreases with increasing glass powder / SBF ratio beyond 0.002 g ml^{-1} as further increase in this value will favour the formation of calcite at the expense of HA on the glass surface. In the present study, the calcite formation in 45S5 glass may be attributed to the fact that we are exactly at this threshold value of glass powder / SBF ratio. It is noteworthy that Ca-carbonate phases present a higher solubility product ($K_{ps} \text{ calcite} = 1.7 \times 10^{-8}$) with respect to HA ($K_{ps} \text{ HA} = 1.6 \times 10^{-58}$) at pH 7.4 [83] and this should favour the precipitation of the latter. Nevertheless, Ca-carbonate phases are likely to present a higher rate of crystallization because of the presence of basic surface species (for instance: O^{2-} ions, OH^- ions or coordinatively unsaturated cation-anion pairs), which can coordinate with CO_2 , thus giving rise to many possible types of carbonate like species. According to Cerruti and Morterra [147], the carbonate formation in silica-based bioactive glasses occurs only if both CO_2 and an excess of water are present at the same time as it is believed that the gas-phase admission of both CO_2 and an excess of water mimics the long-lasting process of carbonate formation.

One of the relevant parameters in the study of glass dissolution is the kind of medium used. The pH and ionic strength of the medium play an important role in the rate at which the glasses dissolve. The variation in pH of Tris-HCl with respect to TCP content in glasses is presented in Figure 4.1.5. A slight increase in pH from 7.4 to 8.4 was observed in case of Tris-HCl with increasing TCP content in glasses while highest pH value of 9.7 was observed for the 45S5 glass, which exhibited higher dissolution rate than the investigated glasses. In the present study, an increasing pH of simulated solution with increasing TCP content in the glasses may be attributed to the increasing dissolution of Ca and Mg ions from glasses due to

the dissolution of charged ion pairs $(\text{Ca-F})^+$ or $(\text{Mg-F})^+$. 45S5 glass exhibited the highest weight loss in Tris-HCl (3.7%).

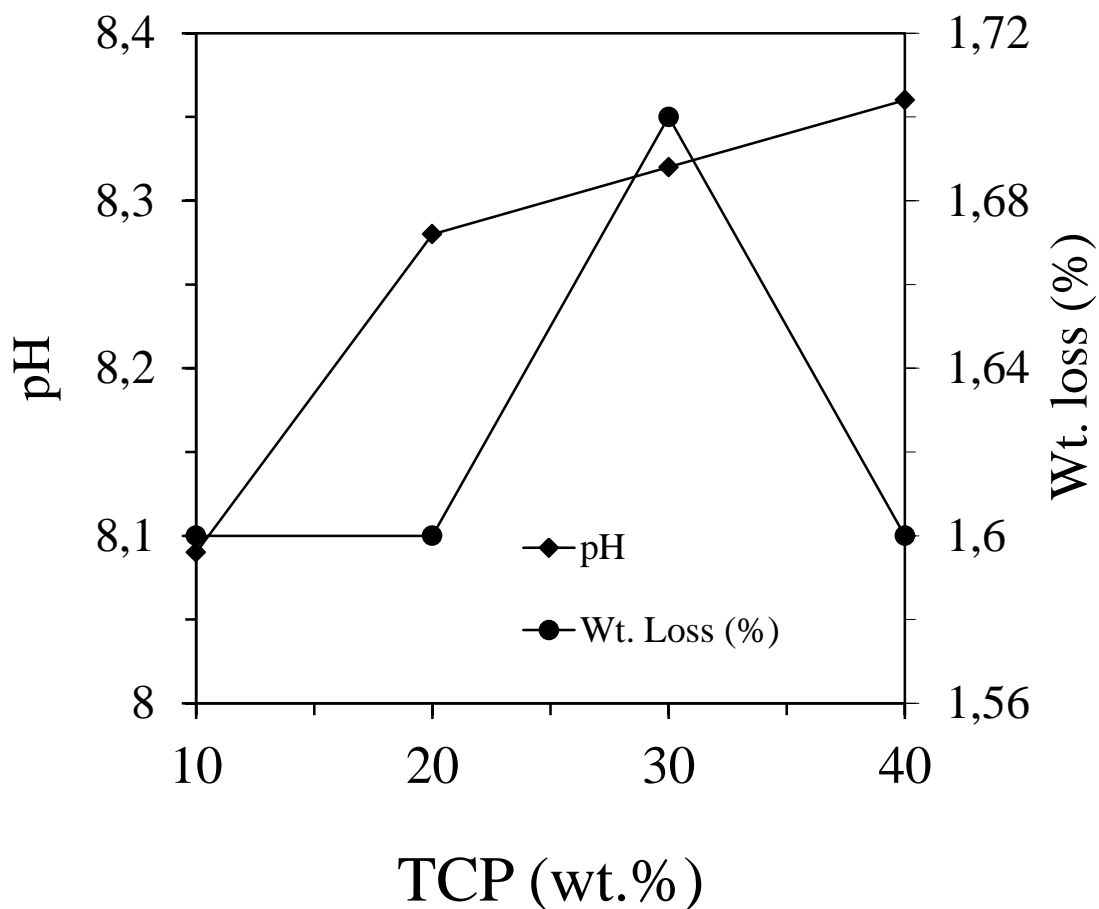


Figure 4.1.5 Graph depicting changes in pH of solution and weight loss of glass powders after immersion in Tris-HCl for 120 h.

Among all the investigated glasses, an increment in TCP content in glasses did not affect the weight loss significantly as it varied between 1.6–1.7% (Fig. 4.1.5).

4.1.2.4 Differential thermal analysis

The DTA plots of fine powders with a heating rate (β) of 20 K min^{-1} , shown in Figure 4.1.6, feature an endothermic dip in the temperature interval of $750 - 755 \text{ }^\circ\text{C}$ corresponding to T_g before T_c followed by a well-defined single exothermic crystallization curve for glasses TCP-10, TCP-20 and TCP-30. We could not observe any significant differences in the variation of T_g values with varying Di/TCP ratio in the glasses.

Further, the presence of a single crystallization exothermic peak in TCP-10 and TCP-20 samples anticipates that the resulting glass-ceramics are formed either by single crystalline phase, or derived from an almost simultaneous precipitation of different crystalline phases (TCP-30); while the appearance of two distinct crystallization peaks (Tp1 and Tp2) in glass TCP-40 points towards the formation of two different crystalline phases. The Tp values for glasses TCP-10 and TCP-20 are almost similar (i.e. 932 °C) while further decrease in Di/TCP ratio resulted in shifting of Tp to 907 °C for glass TCP-30 and 843 °C (Tp1) for glass TCP-40.

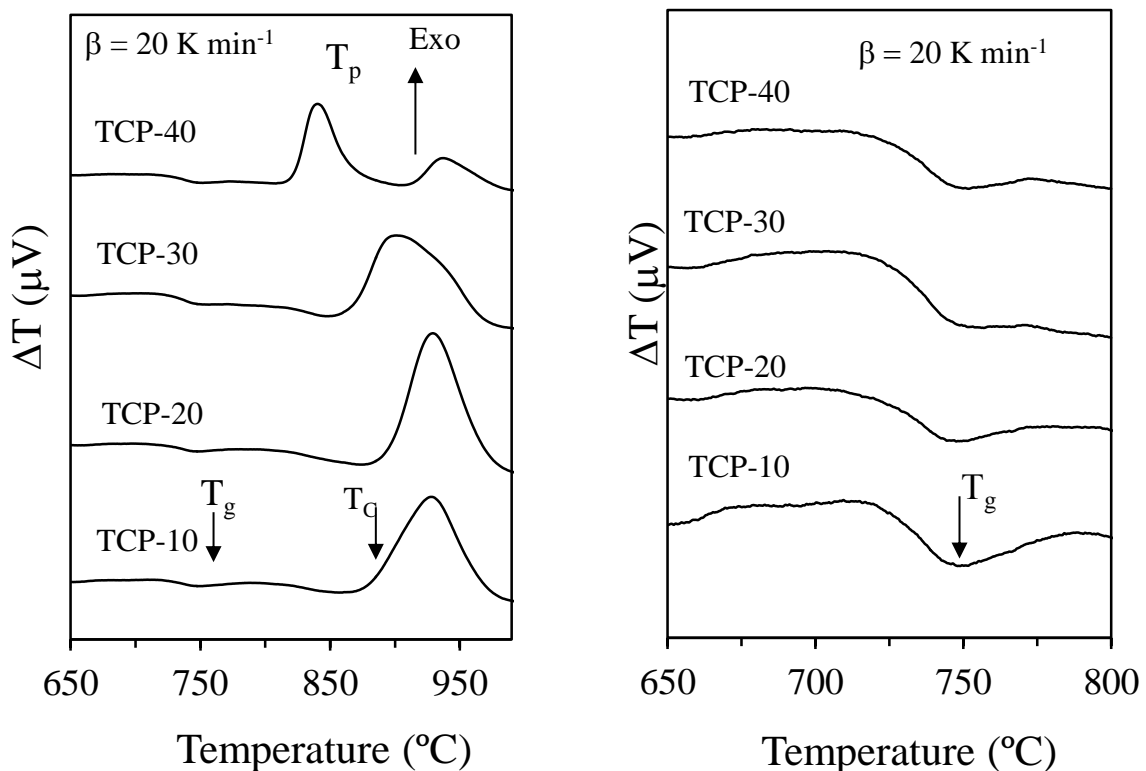


Figure 4.1.6 DTA thermographs of glasses at a heating rate of 20 K min⁻¹.

This decrease in T_p values with increasing TCP content in glasses may be attributed to their increasing crystallization tendency as will be shown further in section 4.1.6.

4.1.2.5 Sintering and crystallization behaviour of glasses

The prerequisite for optimizing the fabrication of glass-ceramics scaffolds is to understand the sintering conditions of glass powders and the interaction between sintering and crystallization of the material. By knowing the structural transformations which occur during the heat treatment of glasses, the scaffold fabrication process can be tailored, like in

terms of achieving the highest possible density of the sintered scaffolds and the required crystallinity which itself controls the material's bioactivity. It is due to this reason that a comparison between DTA and HSM thermographs obtained under the same heating conditions can reveal a great deal of information in this regard. In general, two different trends can be observed related to the sintering and crystallization behaviours of the glasses: (i) T_c occur after the final sintering stage. Therefore, under such circumstances, sintering and crystallization are independent processes. This is the required trait to obtain well sintered glass-ceramic scaffolds with good mechanical properties; (ii) T_c appears before maximum density has been reached. In this case, the crystallization process starts before complete densification, thus, preventing sintering.

In the present study both of the above mentioned trends related with sintering and crystallization behaviour of glasses have been observed depending on the glass compositions. Figure 4.1.7 presents the DTA and HSM thermographs of glasses TCP-20 (Figure 4.1.7a) and TCP-40 (Figure 4.1.7b), respectively at $\beta = 5 \text{ K min}^{-1}$ depicting a single stage sintering behaviour for the investigated glass compositions while Figure 4.1.7c presents the changes in different thermal parameters with respect to variation in TCP content in glasses. As is evident from Figure 4.1.7c, the values for temperature of first shrinkage (T_{FS} ; $\log \eta = 9.1 \pm 0.1$, where η is viscosity; dPa.s) and temperature of maximum shrinkage (T_{MS} ; $\log \eta = 7.8 \pm 0.1$) exhibited a slight decrease with increasing TCP content in glasses while values for T_c showed an initial increase and then a steep decrease with decreasing Di/TCP ratio.

With respect to T_{MS} and T_c , different trends were observed for the investigated glass compositions which can be explained with the aid of sinterability parameter (S_c), where $S_c = T_c - T_{MS}$. The parameter S_c is the measure of ability of sintering versus crystallization: the greater this difference, the more independent are the kinetics of both processes [151]. The estimated error for data points is smaller than $\pm 10\%$, approximately equal to the size of the data symbols. As can be seen from Figure 4.1.7c, the value of parameter S_c increased with increasing TCP content in the glasses until 20 wt%. However, further decrease in Di/TCP ratio led to a gradual decrease in the value of S_c with glass TCP-40 ($S_c = -24 \text{ }^\circ\text{C}$) exhibiting the lowest value for S_c . These results imply that sintering precedes crystallization in glass compositions TCP-10, TCP-20 and TCP-30 with glass composition TCP-20 exhibiting better sintering ability in comparison to the other investigated compositions.

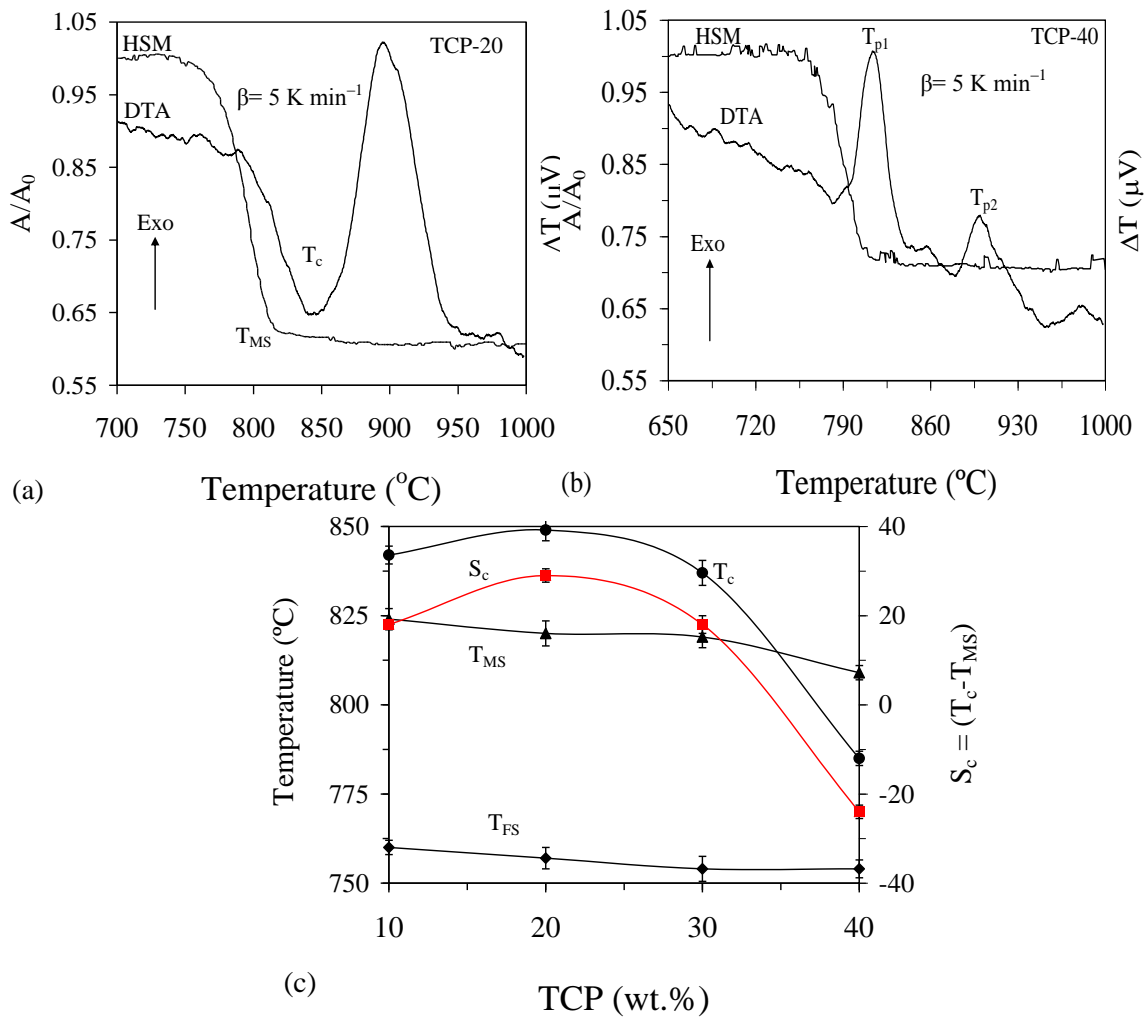


Figure 4.1.7 Comparison of DTA and HSM curves under the same heating rate (5 K min^{-1}) for compositions (a) TCP-20 and (b) TCP-40 at the heating rate of 5 K min^{-1} ; (c) influence of TCP content on different thermal parameters of glasses obtained from DTA and HSM, respectively

Therefore, we can expect well sintered, dense and mechanically stronger glass-ceramics from composition TCP-20 in comparison to its counterparts. On the other hand, crystallization precedes sintering in glass TCP-40 which should result in a poorly sintered and mechanically weak glass-ceramic material. The decreasing/poor sintering ability for glasses TCP-30 and TCP-40 is mainly due to predominance of FA in these glasses (as has been presented ahead in XRD results) which masks the influence of Di which is a crystalline phase with good mechanical strength.

Figure 4.1.8 presents the SEM images of the glass powder compacts after sintering in temperature interval of 800–900 °C for 1 h. In agreement with HSM and DTA results, the

sintering of glass powder compacts at 800 °C resulted in well sintered and dense glass-powder compacts for compositions TCP-10 (Figure 4.1.8a), TCP-20 (Figure 4.1.8b) and TCP-30 (Figure 4.1.8c), respectively, while TCP-40 resulted in a poorly sintered and mechanically weak glass powder compact.

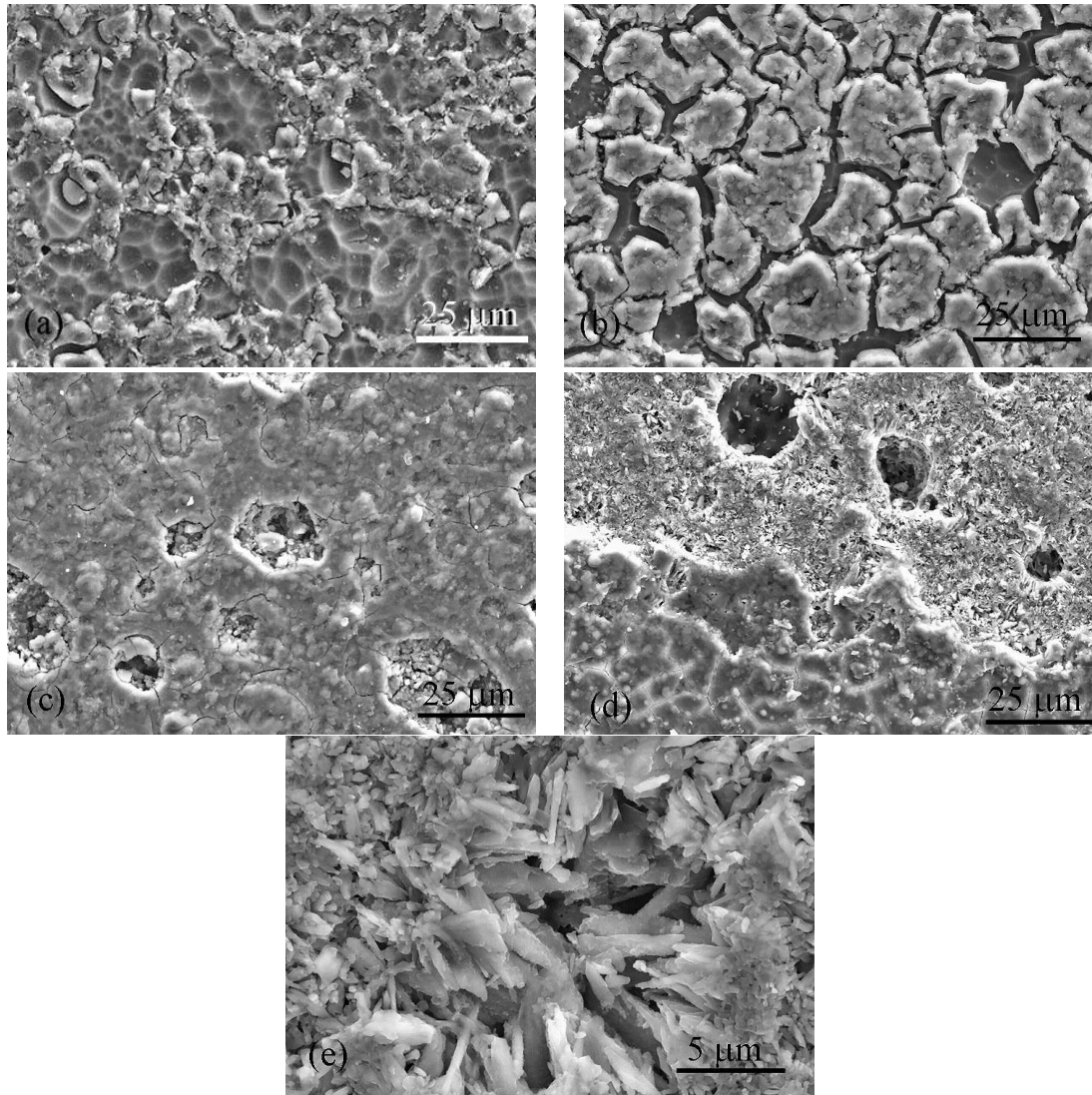


Figure 4.1.8. SEM images of glass powder compacts (a) TCP-10, (b) TCP-20, (c) TCP-30, after sintering at 800 °C for 1 h, respectively while (d) and (e) represent glass composition TCP-10 after sintering at 900 °C for 1 h.

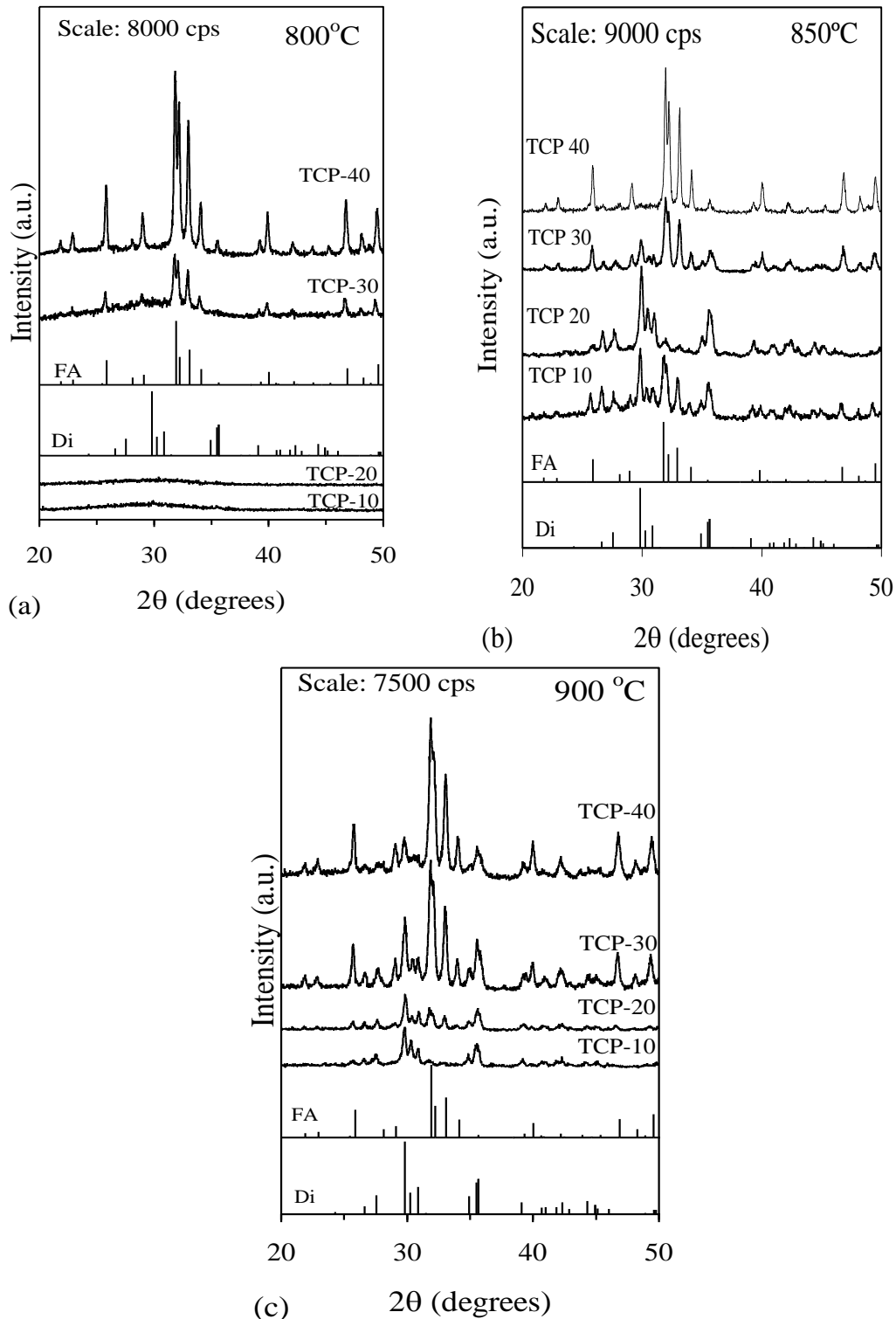


Figure 4.1.9 X-ray diffractograms of glass compositions after sintering at (a) 800 °C; (b) 900 °C and 1000 °C, respectively.

The flexural strength values as obtained for composition TCP-20 sintered at 800 and 850 °C are 85 ± 6 MPa and 135 ± 9 MPa, respectively. The qualitative crystalline phase analysis of sintered glass powders as presented in Figure 4.1.9 revealed that compositions

TCP-10 and TCP-20 were completely amorphous after sintering at 800 °C while FA (ICDD card: 71-880) precipitated as the major crystalline phase in compositions TCP-30 and TCP-40 along with Di (ICDD card: 78-1390) and the intensity of XRD peaks increased with increasing TCP content in glasses, thus, indicating an increase in crystallinity (Figure 4.1.9a). These results are in co-relation with the microstructural evolution of sintered glass-ceramics as studied through SEM. Figure 4.1.8c depicts the formation of crystals beneath the amorphous layer in composition TCP-30, thus depicting the presence of crystallinity. Further increase in sintering temperature to 850 °C (Figure 4.1.9b) and 900 °C (Figure 4.1.9c) resulted in appearance of crystallinity in all the investigated glass compositions with Di as the major crystalline phase in compositions TCP-10 and TCP-20, thus rendering them good sintering ability while FA dominated the crystalline phase assemblage in compositions TCP-30 and TCP-40, thus leading to their poor sintering ability. The SEM images (Figure 4.1.8d and 4.1.8e) obtained from glass-ceramics TCP-10 after sintering at 900 °C depict the presence of thin lamellar crystals typical for Di intermixed with needle like FA crystals (Figure 4.1.8e). The results obtained in the present study are different from those obtained by Kamitakahara et al. [103] in their study related with synthesis of glass-ceramics in Di-TCP binary system and also from the results of Magallanes-Perdomo et al. [152] where they investigated the devitrification behaviour of a eutectic glass-ceramic composition in wollastonite-TCP binary system as in both the earlier studies, TCP crystallized in glass-ceramics the form of α -TCP [152] or β -TCP [103] along with other crystalline phases. However, in the present study, no trace of crystallization of TCP has been observed as its growth seems to be masked by FA.

4.1.2.6 Cellular response to sintered glass powder compacts

The cell proliferation on the sintered glass powder compacts and control during culture for 3, 7 and 14 days is shown in Figure 4.1.10. For the control, cells proliferated actively for up to 7 days and showed a plateau with prolonged culture for 14 days.

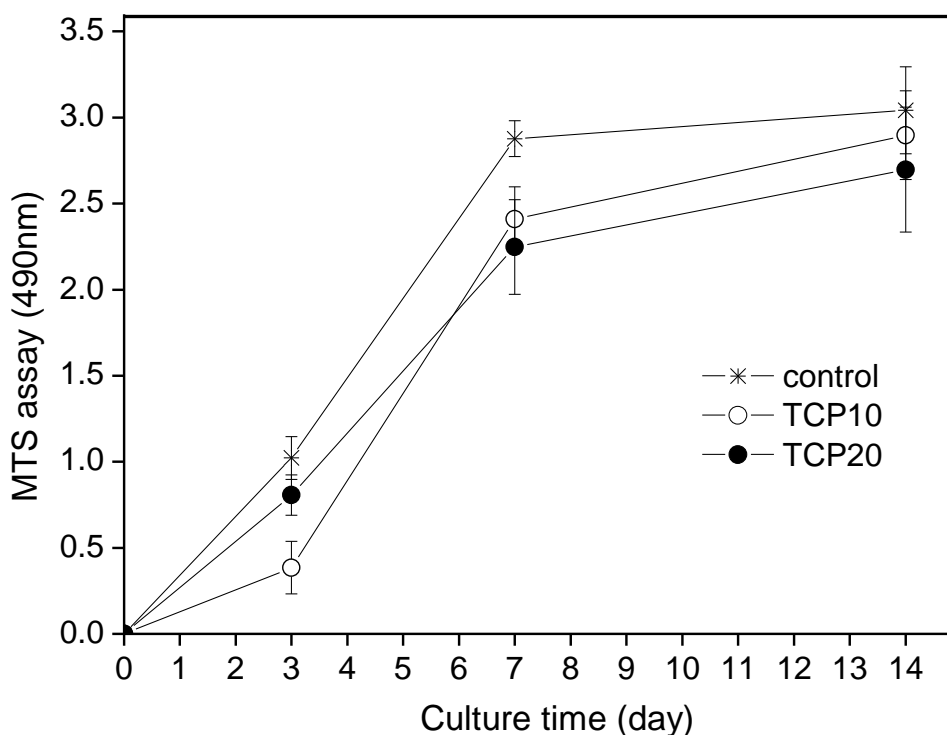
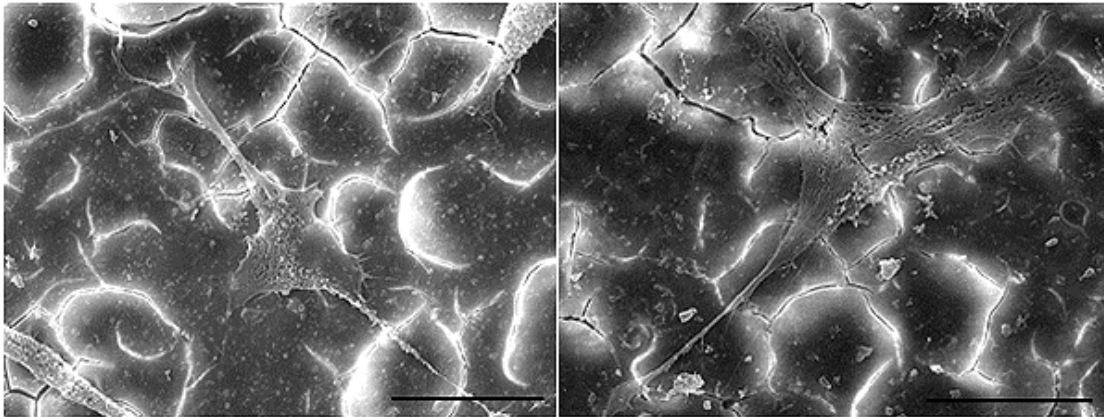


Figure 4.1.10 Proliferation behaviour of the MSCs cultured on the glass compacts (TCP-10 and TCP-20) and the tissue culture plastic used as a control during the periods for 3, 7 and 14 days. MSCs derived from rat bone marrow were used for the assay. Statistically significance difference was noticed between the groups; control vs. TCP-10 at day 3; control vs. TCP-10 or TCP-20 at day 7 ($p < 0.05$, ANOVA, $n = 3$)

On the other hand, the cell proliferation appeared to be relatively slower for investigated glass compositions in the culture for up to 7 days. However, cells continued to grow with prolonged culture period reaching to the proliferation level of the control at 14 days, featuring good proliferative potential of cells upon the glass disc substrates. The morphologies of cells grown on the glass disks for 7 days are shown in Figure 4.1.11.

TCP-10



TCP-20

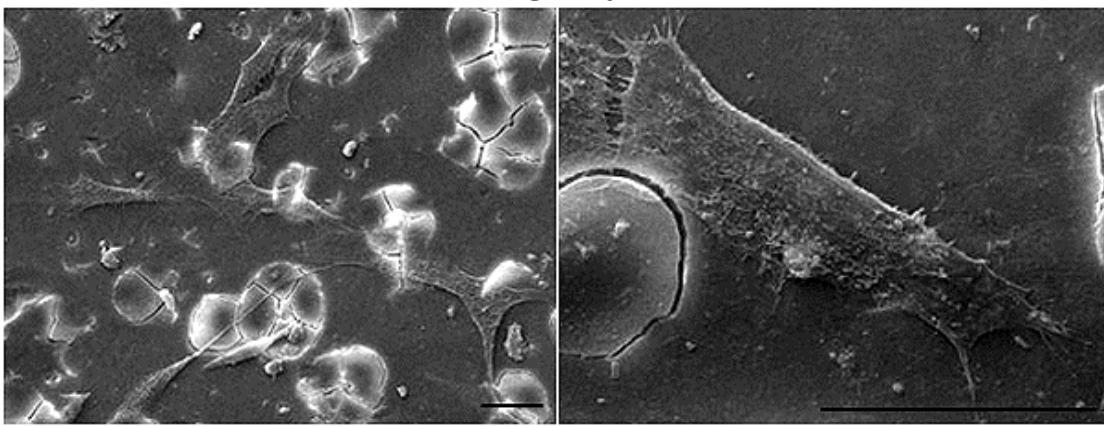


Figure 4.1.11 SEM images of the MSCs grown on the sintered glass powder compacts (TCP-10 and TCP-20) during culture for 7 days. Cells spread well on both glass samples in intimate contacts with the underlying substrates and have active cytoskeleton processes with highly elongated filopodia. Some surface cracks associated with the sample treatment for SEM are observed.

As is evident from the images, cells spread well on both the glass compositions in intimate contacts with the underlying substrates and have active cytoskeleton processes with highly elongated filopodia. The results on cell proliferation and growth morphology suggest that the developed glasses provide suitable substrate conditions for the MSCs to adhere and proliferate.

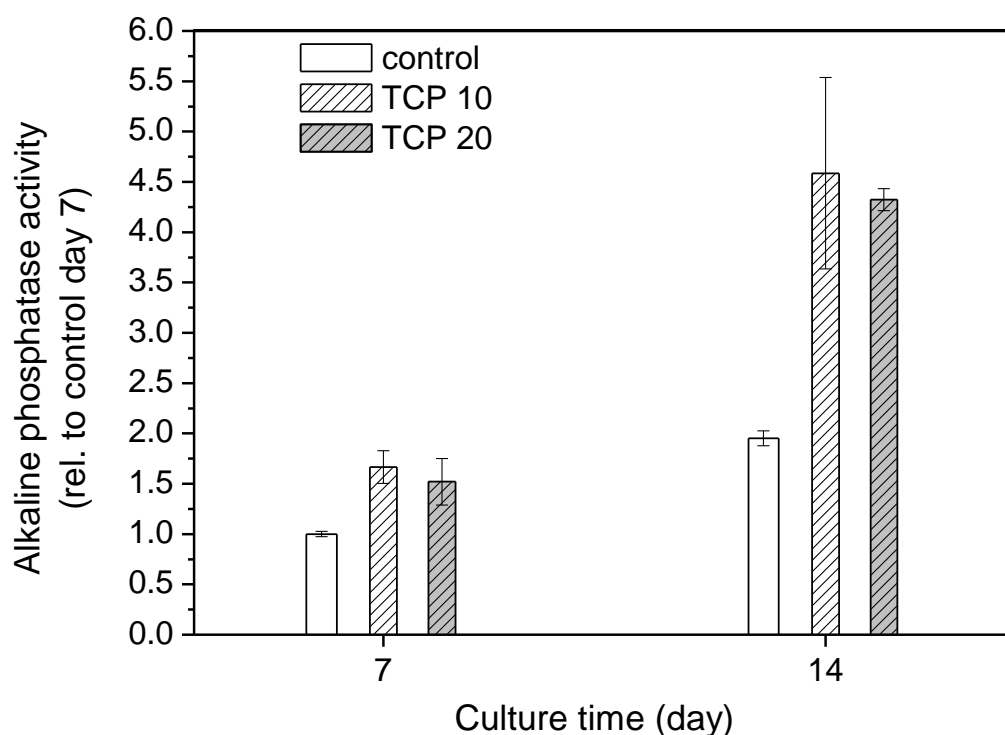


Figure 4.1.12 Alkaline phosphatase activity of the MSCs during culture for 7 and 14 days on the glass compacts (TCP-10 and TCP-20) and tissue culture plastic control. Statistically significant higher level was noticed on the glass samples with respect to control at both periods; * $p < 0.05$, ANOVA, $n = 3$.

The effect of the osteogenic differentiation was further investigated by the ALP activity of cells grown on the glass disks for 7 and 14 days. The data plotted in Figure 4.1.12 shows that ALP activity level was significantly higher on both types of glass compositions with respect to that on the control at all culture periods. In particular, the increase in the ALP level from 7 to 14 days was much higher in the glasses than in the control. ALP is known as one of the essential osteogenic markers of cells including MSCs, particularly at an early stage of osteogenic differentiation. Therefore, the significantly stimulated ALP level observed in the MSCs cultured on the glass-ceramics samples indicates that the materials developed herein are effective in modulating the functions of MSCs into the lineage of bone cells, consequently highlighting their potential usefulness for bone regeneration.

4.2.2 Conclusions

We have tried to shed some light on the influence of varying Di/TCP ratio on the structure, biodegradation, and sintering-crystallization behaviour of glasses in the Di-FA-TCP system has been presented. The as obtained results depict the potential of investigated glass compositions for their application in human biomedicine. The structure of the investigated glasses is dominated by Q2 (Si) units while phosphorus is predominantly in orthophosphate type environment. Some of the investigated glasses exhibited higher rate of bioactivity in vitro in comparison to 45S5 Bioglass® during initial 12 h of immersion in SBF solution. The glass with nominal composition Di50 – FA10 – TCP40 (wt%) (Labelled as TCP-40) exhibited hydroxyapatite formation on its surface within 1 h of its immersion in SBF while glass TCP-20 with composition Di70 – FA10 – TCP20 (wt%) exhibited apatite formation after 12 h of its immersion in SBF. All the glasses exhibited considerably lower weight loss in comparison to 45S5 Bioglass® in Tris-HCl. Sintering preceded crystallization in glass composition with TCP content varying between 10 – 30 wt.%. Further increase in TCP content in glasses deteriorated the sintering ability of glass powders considerably. The glass composition TCP-20 exhibited superior sintering ability in comparison to other investigated glasses. The resultant glass powder compacts were completely amorphous after sintering at 800 °C with a three-point flexural strength of ~85 MPa. Di crystallized as primary crystalline phase in compositions with TCP content 10 and 20 wt.%, respectively after sintering at 850 °C, while further increase in TCP content in glasses suppressed the formation of Di with FA being crystallized as the major phase. The sintered (but amorphous) glass powder compacts (TCP-10 and TCP-20) significantly increased the osteogenic differentiation of MSCs with respect to the culture plastic control, as assessed by the alkaline phosphatase activity.

4.2 Structural role of zinc in biodegradation of alkali-free bioactive glasses

4.2.1. Introduction

Zinc is an important element that plays a vital role in bone formation and resorption, which should be considered in the design of bone graft compositions aimed at bone regeneration and TE applications. Owing to the above-mentioned beneficial aspects of zinc in human metabolism in section 2.5.3, and considering the ion releasing ability of glasses in aqueous medium, bioactive glasses incorporated with zinc have gained considerable attention in the recent years for various TE applications. The increasing interest in Zn-containing bioactive glasses has resulted in a multiple-fold increase in the number of scientific publications in this area during last decade [82, 125, 153-160].

Despite the interesting studies, there exists a significant disparity among the results reported in literature with respect to influence of Zn^{2+} and its content on biodegradation, apatite forming ability, osteoblast activity, anti-inflammatory response and angiogenic behaviour in bioactive glasses [25, 161]. All these issues have been recently reviewed by Hoppe et al. [44] and therefore, will not be discussed in the present section. Apart from that, another major concern with most of the zinc-containing bioactive glass compositions studied until now is that they are either based on- or inspired by 45S5 Bioglass[®] [82, 120, 157, 162, 163] which contain significant amounts of alkali content.

In the light of above mentioned facts, it becomes necessary to investigate the influence of Zn^{2+} on different properties of bioactive glasses but with their chemical compositions completely different from that of 45S5 Bioglass[®] in order to obtain a comprehensive database highlighting the precise function and mechanism of zinc in regulating various biological processes in human body. Such an attempt has been made by Bini et al. [164] and Saino et al. [165] but on alkali-free sol-gel derived glass in the system $SiO_2-P_2O_5-CaO$. It is usually difficult to compare the results obtained on sol-gel glasses with those from melt-quenched glasses due to the high specific surface area and moisture content of the former along with the heterogeneous chemical environment of network modifier species in comparison to melt-quenched glasses [166].

The very promising glass composition TCP-20 discussed in section 4.1 was adopted as the starting point for synthesis new series of glasses and was developed by partial substitution ZnO for MgO in the same composition with the aim to study the effect of zinc on structure and biodegradation of melt-quenched alkali-free glasses designed in $CaO-MgO-SiO_2-P_2O_5-CaF_2$ glass system.

4.2.2 Results and discussion

4.2.2.1 Glass forming ability

For all the investigated glass compositions (mol%): 36.07 CaO – (19.24 – x) MgO – x ZnO – 5.61 P₂O₅ – 38.49 SiO₂ – 0.59 CaF₂, (x = 2–10) (Table 4.2.1), melting at 1570 °C for 1 h was sufficient to obtain bubble-free, transparent and XRD-amorphous glasses (Figure 4.2.1).

Table 4.2.1 Nominal composition of the as-designed glasses (mol%).

Glass	CaO	MgO	SiO ₂	P ₂ O ₅	ZnO	CaF ₂
Zn-0	36.07	19.24	38.49	5.61	0.00	0.59
Zn-2	36.07	17.24	38.49	5.61	2.00	0.59
Zn-4	36.07	15.24	38.49	5.61	4.00	0.59
Zn-6	36.07	13.24	38.49	5.61	6.00	0.59
Zn-8	36.07	11.24	38.49	5.61	8.00	0.59
Zn-10	36.07	9.24	38.49	5.61	10.00	0.59

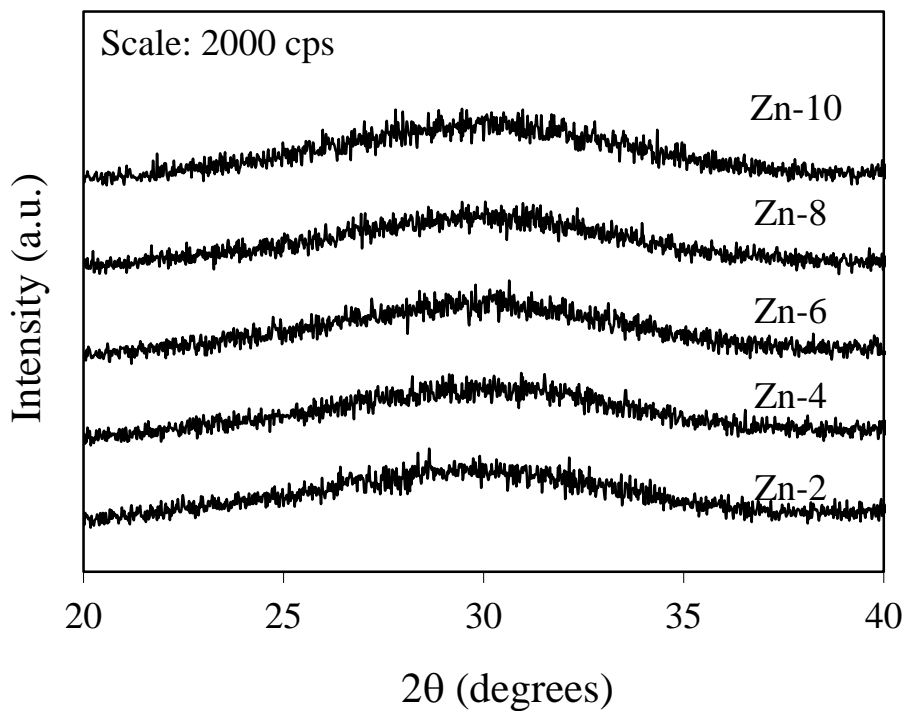


Figure 4.2.1 X-ray diffractograms of as-quenched glasses.

4.2.2.2 Glass structure

The MAS-NMR spectrum (Figure 4.2.2) shows that ZnO substitution for MgO does not affect the silicate network connectivity of these glasses. The ^{29}Si MAS-NMR results of all the glasses as presented in Figure 4.2.2a depict the dominance of Q^2 (Si) structural units in the glasses. Further, only slight shift in the peak positions of spectra could be observed and all the spectra are centred between -81 ppm and -82 ppm, thus depicting no significant changes in the silicon coordination in glass structure. The findings are further supported by the MD simulation studies performed on the glasses which show a predominance of Q^2 units ranging from 47 to 51 % from Zn-0 to Zn-10 [42].

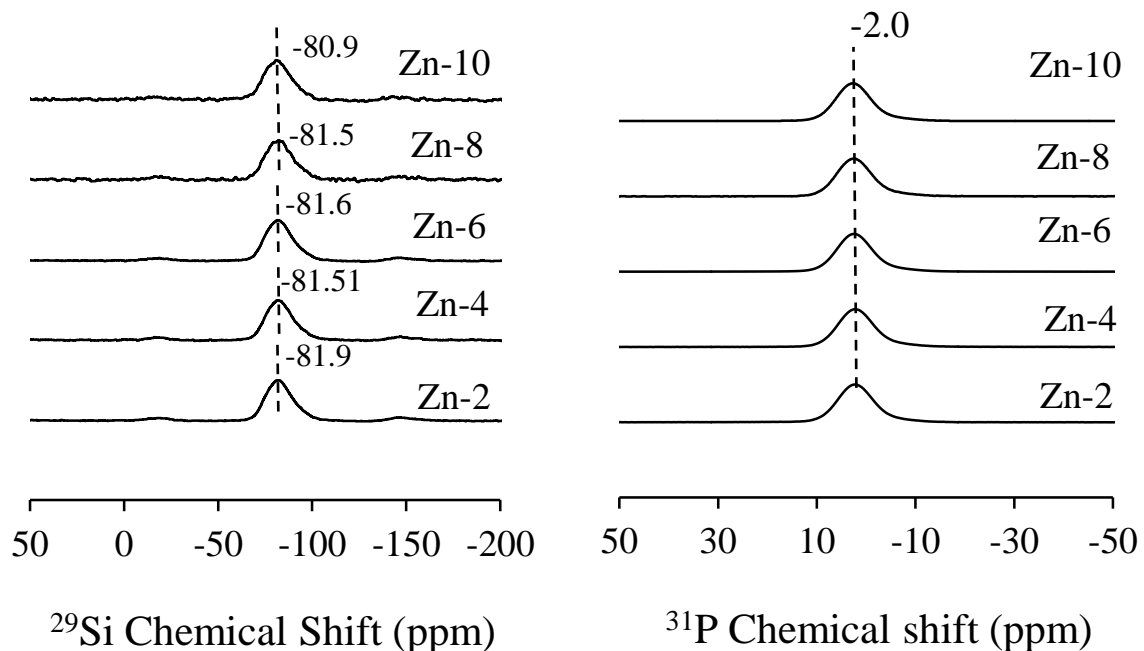


Figure 4.2.2 MAS NMR spectra of investigated glasses showing the peak positions of (a) ^{29}Si and (b) ^{31}P .

The ^{31}P MAS-NMR spectra of all the glasses show a predominance of an orthophosphate-type environment (Figure 4.2.2b), again in agreement with the MD results [42]. In fact, the observed chemical shifts, 1–3 ppm, are close to that of the calcium orthophosphate (3.1 ppm) and that of the amorphous magnesium orthophosphate (*ca.* 0.5 ppm) [137]. The phosphate environment is therefore similar to that of 45S5 Bioglass[®] [127, 167].

4.2.2.3 Apatite forming ability of glasses

The X-ray diffractograms of investigated glasses after soaking in SBF solution for time durations varying between 1 h – 7 days (Figure 4.2.3) showed considerable differences in comparison to the diffractograms of their respective parent glasses. A phase reflection at $2\theta = 31.77^\circ$ corresponding to the formation of crystalline hydroxyapatite [HA; $(\text{Ca}_5(\text{PO}_4)_3\text{OH}$; ICDD: 00-09-0432] is evident in the X-ray diffractograms of glasses with ZnO concentration varying between 4 – 10 mol% after their immersion in SBF for 1 h (Figure 4.2.3a). It should be noted that the HA formed in such experiments is carbonated HA and not stoichiometric crystalline HA. With further prolonging the immersion time, the intensity of the main XRD peak of HA increased particularly for the Zn-6 composition, while showed a fading trend for the other bioactive glasses (Figure 4.2.3b – 4.2.3d). Interestingly, at the conclusion of 7 days, HA formation was observed only for parent glass Zn-0 while no Zn-containing glass exhibited clear evidences for the formation of HA. Various reasons may be cited for such a trend observed from XRD data for bioactive glass dissolution and HA formation in SBF solution. The two main plausible factors behind this behaviour may include:

1. Influence of ZnO/MgO ratio on HA formation in bioactive glasses: Magnesium is known to delay the HA formation *in vitro* as well as *in vivo*. According to Pariente et al. [148], during *in vitro* SBF tests, magnesium tends to associate with phosphorus on the glass surface due to which apatite-like calcium phosphate domains are barely detected in magnesium containing glasses. Further, both Mg^{2+} and Zn^{2+} when present together also inhibit HA crystal growth.
2. Solution pH and degree of saturation: The pH of the SBF solution and its degree of saturation play crucial roles in deciding the nature of crystalline products as has been discussed in our study [23]. In the present study, the initial pH of SBF solution was 7.28 while the pH of SBF solution after 24 h of glass powder immersion varied between 7.7 – 7.95, irrespective of the ZnO concentration in glasses. It is now generally agreed that, both *in vitro* and *in vivo*, precipitation reactions at sufficiently high supersaturation and pH result in the initial formation of ACP with molar calcium/phosphate ratio of about 1.18 – 2.50 [168, 169]. The chemical composition of ACP is strongly dependent on the solution pH: ACP phases with Ca/P ratios in the

range of 1.18:1 precipitated at pH 6.6 to 1.53:1 at pH 11.7 and even as high as 2.5:1 [170].

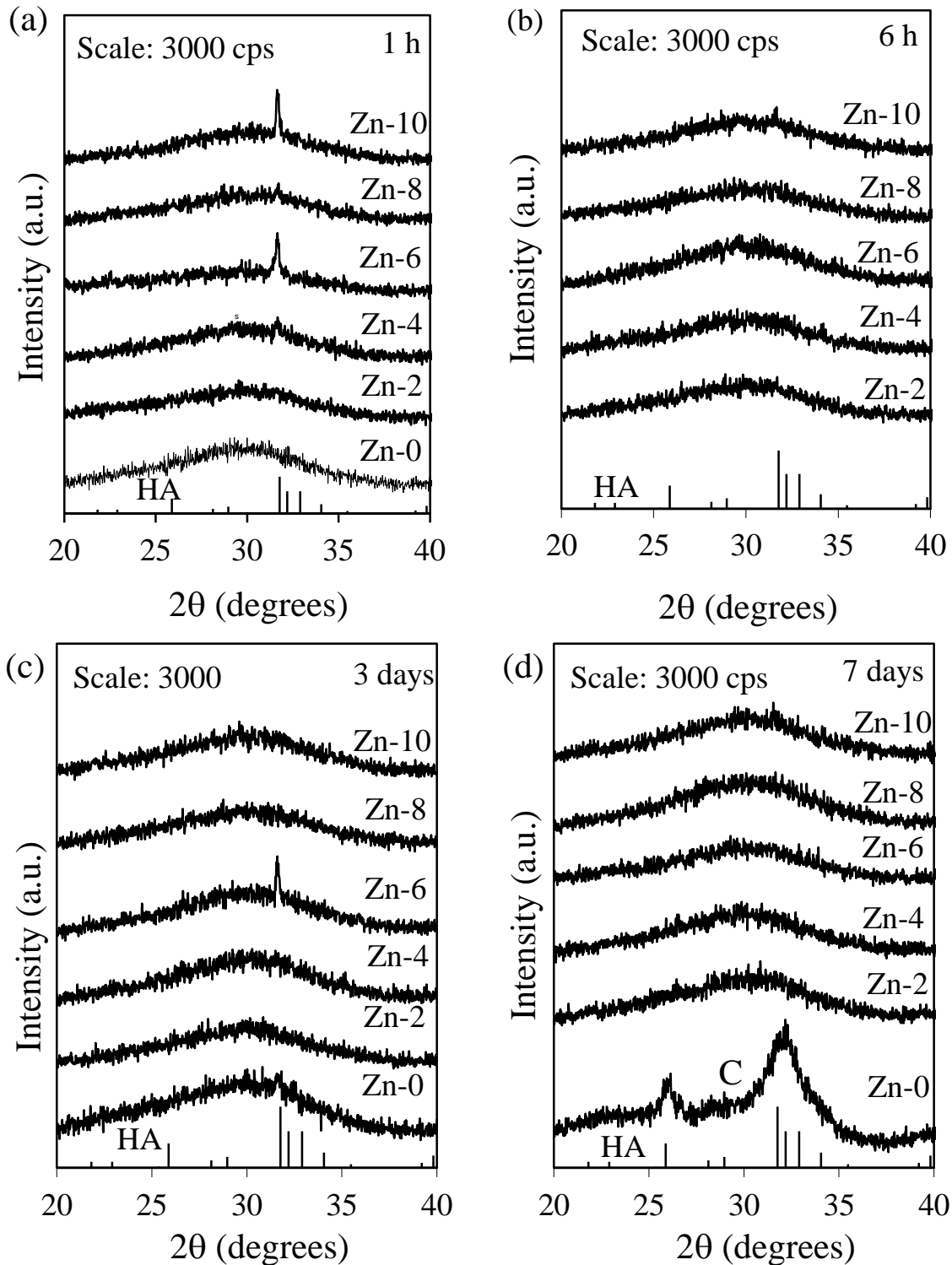


Figure 4.2.3 X-ray diffractograms of glass powders before and after immersion in SBF solution for (a) as quenched glasses (b) 1 h (c) 6 h (d) 3 days and (e) 7 days. HA refers to hydroxyapatite.

The FTIR spectra of glasses after immersion in SBF solution for 1 h (Figure 4.2.4a) depicts several changes in the glass structure that occurred due to the reaction between glass powder and SBF. The strong low frequency band in the region $350 - 650 \text{ cm}^{-1}$ has been split into small bands at $\sim 480 \text{ cm}^{-1}$, $\sim 570 \text{ cm}^{-1}$ and $\sim 620 \text{ cm}^{-1}$ as is evident from Figure 4.2.4a. The band centred at 480 cm^{-1} can be ascribed to a deformation mode of silica layer that develops on the dissolving glass particles while small broad bands at 570 cm^{-1} and 620 cm^{-1} are characteristic for apatite and other phosphates as it corresponds to P–O bending vibrations in a PO_4^{3-} tetrahedron. A single peak in this region (570 cm^{-1}) suggests the presence of non-apatitic or ACP, which is usually taken as an indication of presence of precursors to HA. It is noteworthy that apatitic PO_4^{3-} groups have characteristic split bands at ~ 560 and 600 cm^{-1} , with a third signal at $\sim 575 \text{ cm}^{-1}$ observed for crystallites of small size [83, 87].

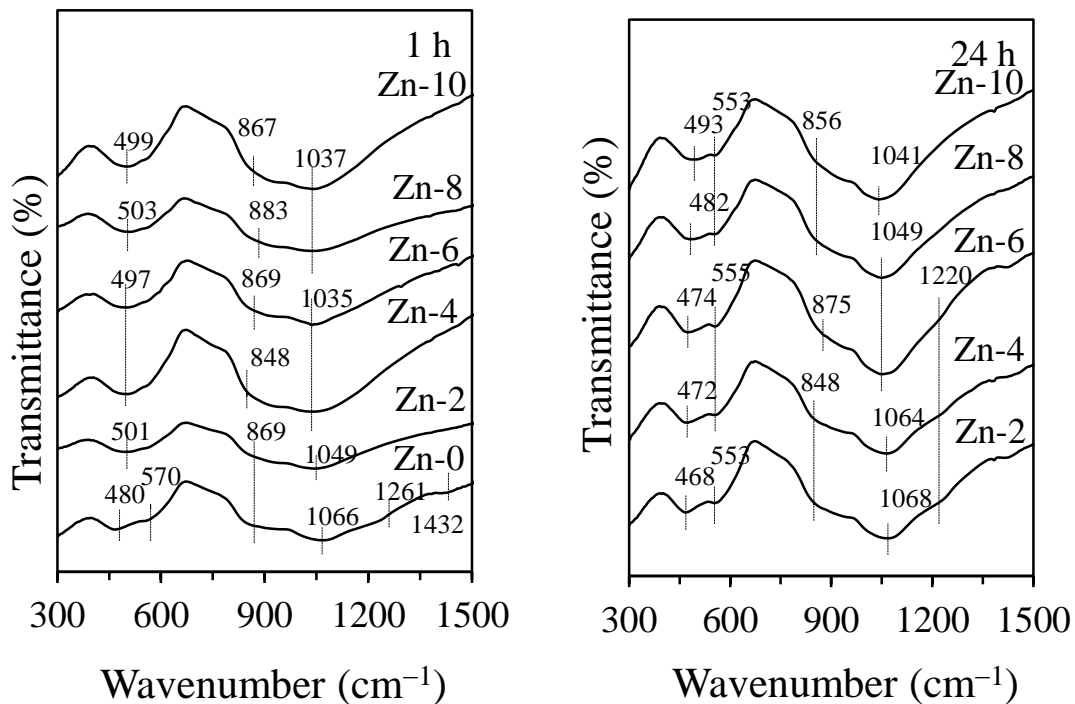


Figure 4.2.4 FTIR spectra of glass powders after immersion in SBF solution for (a) 1 h and (b) 24 h.

Further, a small band at $\sim 1440 \text{ cm}^{-1}$ along with a broad but intense band at $\sim 850 \text{ cm}^{-1}$ present in all glasses corresponds to incorporation of carbonate into the apatite, resulting in hydroxy carbonated apatite, rather than stoichiometric HA [83]. The most interesting feature of the FTIR data on zinc-containing glasses obtained after 1 h of immersion in SBF solution is the complete absence of the Si–O–Si vibration band in the region $1200 - 1270 \text{ cm}^{-1}$ which

corresponds to the formation of silica gel layer, as postulated in Hench's inorganic reaction set [20]. It is interesting due to the fact that this band is highly evident in the FTIR spectra of zinc-free parent glass, Zn-0. An increase in SBF immersion time to 24 h did lead to the appearance of an absorption band at $\sim 1220\text{ cm}^{-1}$ in glasses with lower ZnO content (2–6 mol%) but this band was still absent in glasses with ZnO content varying between 8 and 10 mol% as shown in Figure 4.2.4b. Consequently, the increase in immersion time resulted in either sporadic or minimal apatite formation on glass surface during 7 days of immersion in SBF solution (Figure 4.2.3c – 4.2.3e). Similar observations regarding the absence of silica gel layer in bioactive glasses have been reported in zinc containing glasses by Oudadesse et al. [162], Kamitakahara et al. [158], Lusvardi et al. [82] and Ebisawa et al. [171].

4.2.2.4 Chemical degradation of glasses in Tris-HCl

The variation in pH of Tris-HCl with respect to ZnO content in glasses is presented in Figure 4.2.5. A slight decrease in pH from 7.4 to 7.2 was observed with increasing ZnO content in glasses. It is noteworthy that pH value of 9.7 has been reported for Tris-HCl during chemical degradation of 45S5 Bioglass[®] as reported in the section 4.1, thus exhibiting higher dissolution than the investigated glasses. The pH results are in good agreement with the weight loss data obtained for the investigated glasses as incorporation of ZnO in glasses reduced their dissolution which is evident from their weight loss (Figure 4.2.5).

All the glasses were amorphous after immersion in Tris-HCl for 120 h as shown in Figure 4.2.6, thus negating the possibility of any chemical reaction between the dissolution products

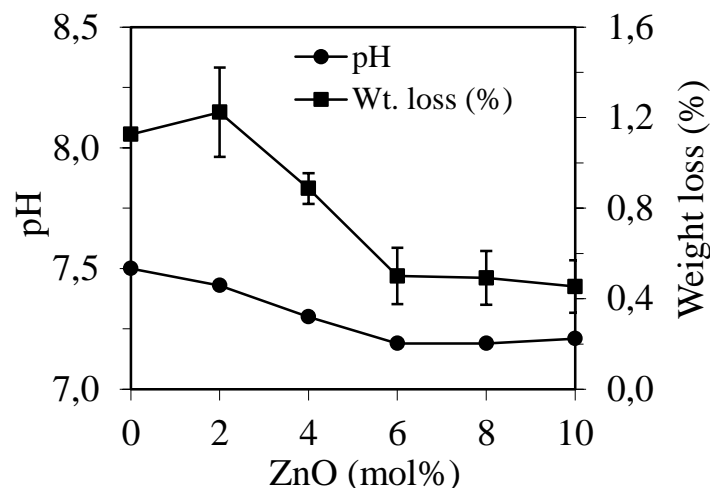


Figure 4.2.5 Graphs depicting the change in solution pH and weight loss of glass powders after immersion in Tris-HCl.

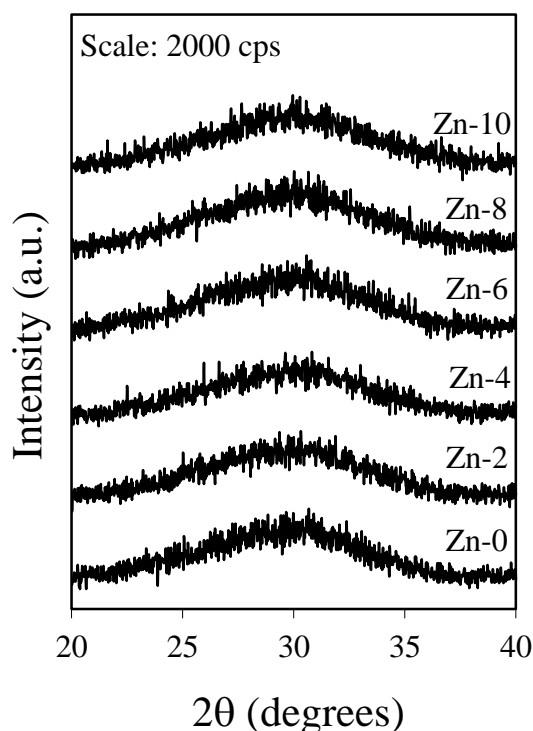


Figure 4.2.6 X-ray diffractograms of glass powder after 120 days of immersion in TRIS-HCL

The decrease in pH value of Tris-HCl with incorporation of ZnO is due to the low leaching of Mg and Ca ions from glasses as shown in Figure 4.2.7. The slower Ca release from the bioactive glasses with increasing ZnO content may be one of the reasons for slow HA formation on bioactive glass surface. The concentration of zinc ions leached out from glasses after 120 h of immersion in Tris-HCl increased with increase in ZnO content in glasses and varied between 0.06 ppm (for Zn-0) to 8 ppm (Zn-8). The zinc release profile of glasses is important from the fact that the role of major functional ions (Ca, Mg, Si, P) in bone regeneration and soft TE has been well established and documented [28, 104, 125, 172]. However, the influence of different functional ions which although present in trace quantities in human body are essential for good metabolism is still ambiguous. In particular case of zinc, its role in human metabolism has been shown to depend on its ionic release profile in body fluids and is therefore dose dependent [120, 157].

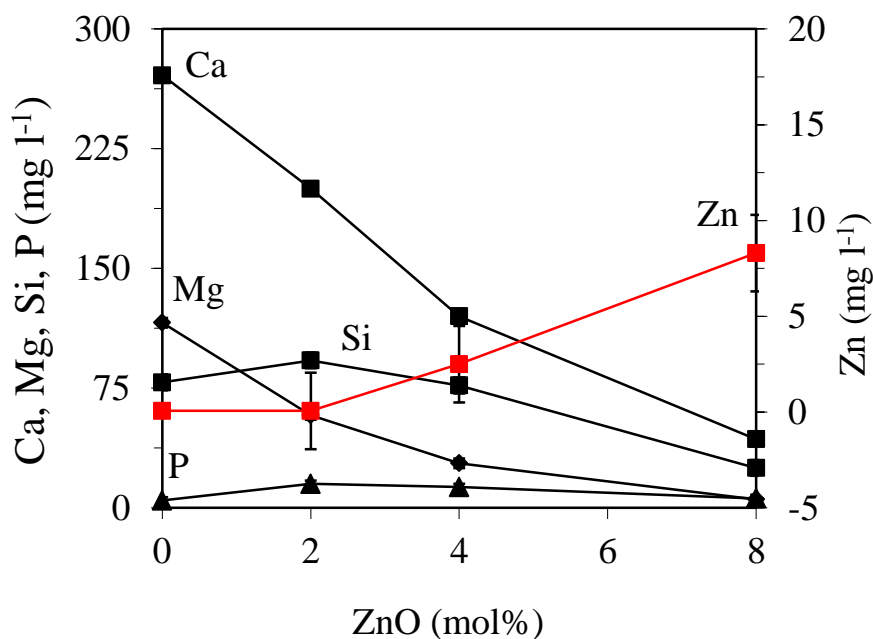


Figure 4.2.7 ICP-AES plots of elemental concentrations of Ca, Mg, P, Si and Zn in Tris-HCl after 120 h of immersion of glass powder. It should be noted that Si refers to SiO_4^{4-} and P refers to PO_4^{3-} species.

4.2.2.5 Discussion

The role of zinc on structure and bioactivity of glasses has been extensively studied in literature. For example, Aina et al. [120, 173] studied the influence of zinc on surface reactivity and cytotoxicity of 45S5-based glasses while Courthéoux et al. [174] investigated the influence of Zn^{2+} on alkali-free glasses in the $\text{CaO-P}_2\text{O}_5\text{-SiO}_2$ and CaO-SiO_2 systems, respectively. However, all the above mentioned studies have been focused upon sol-gel derived glass compositions which have high surface area due to inherent porosity, different surface chemistry in comparison to melt-quenched glasses. Therefore, a comparison between the results obtained on sol-gel derived and melt-quenched glasses is not plausible.

Some studies have also been reported on the influence of Zn^{2+} on the surface reactivity and biological activity of melt-quenched glasses. However, most of the results obtained in these studies are in contradiction with each other. For example: according to Aina et al. [120] and Lusvardi et al. [82], the incorporation of ZnO in 45S5 glass reduces its solubility but still apatite formation (when immersed in simulated body fluids) takes place within few hours to few days of time span. Also, they reported that ZnO enhances the biological activity of glasses *in vitro* as well as *in vivo*. On the other hand, according to Haimi

et al. [175], zinc addition in bioactive glasses has no significant effect on the DNA content, ALP activity and osteopontin concentration of human adipose stem cells. Similar results have also been reported by Popp et al. [176], who studied the influence of soluble zinc from ACP's on the proliferation of rat bone marrow stromal cells.

Despite the significant disparity in the results related with the biological behaviour of zinc, one result that is coherent among almost all the glass compositions reported in literature irrespective of their synthesis route is their decreasing solubility with increasing zinc content. A similar behaviour has been observed in the present investigation, as chemical degradation of glasses in Tris-HCl decreases with their increasing Zn^{2+} concentration. The implications of decreasing solubility with increasing zinc content in glasses may be interpreted on the basis of the solubility of parent glass, for example, according to Aina et al. [120], incorporation of Zn^{2+} in 45S5 glass is beneficial owing to the high solubility of the latter which leads to a significant increase in the pH of physiological fluid, thus affecting the proliferation of endothelial cells. However, the precise reason for decreasing solubility with zinc incorporation in glasses is still ambiguous as some studies explain it on the basis of influence of zinc on glass structure [162, 173] while others discuss it as a function of chemical composition and surface chemistry of glasses [177]. According to Aina et al. [173], the zinc species in alkali-free bioactive glasses are found in a tetrahedral environment, and can enhance the glass reticulation by forming Si–O–Zn inter-tetrahedral links. Similar results on the role of Zn in bioactive glasses irrespective of its concentration have also been reported by Linati et al. [110] on zinc-doped 45S5 Bioglass[®]. For the present compositions, the MD simulations studies [42] have shown that both Zn^{2+} and Mg^{2+} are primarily present in five-fold coordination, which appears reasonable considering the similar ionic radii of Mg^{2+} (0.65 Å) and Zn^{2+} (0.74 Å) [178]. The intermediate role of zinc is well documented in literature, and therefore depending on the glass composition and its local environment, Zn^{2+} can be a four-coordinated weak network former as has been suggested for traditional bioactive glasses or five-coordinated as has been observed in the present study [179]. In general, zinc has been shown to exhibit a marked preference for tetrahedral coordination in simple alkali silicate glasses [180] which has been the case with most of the studies based on Zn-doped 45S5 Bioglass[®] or its alkali-containing derivatives. However, with increasing Zn/modifier ratio, the ratio of six – to fourfold coordinate Zn species is reported to increase due to the availability of charge compensating modifier cations [180, 181]. Further lack of any significant changes

in the silicate network connectivity glass by varying the Zn^{2+}/Mg^{2+} ratio indicates towards the similar co-ordination of Zinc to magnesium.

The decreasing glass degradation and reduced HA formation in the present case may be attributed to the ability of zinc to promote enhanced inter-tetrahedral cross-links as observed in MD simulations [42] which in combination with constant silicate network connectivity enhances the chemical durability of the glasses. The way in which a modifier or intermediate cation involved in inter-tetrahedral cross-links between adjacent silicate fragments can result in a more stable glass network (with a higher resistance to dissolution) even without actual changes in the silicate network connectivity has been recently discussed [110].

The importance of the silica-rich gel layer is usually attributed to the fact that its presence on the glass surface in SBF helps in inducing apatite formation while no apatite formation can be induced by silica glass or quartz crystal [182]. However, although carbonated-HA formation on glass surface during their immersion in biological fluids is considered to be a marker of bioactivity, recent evidence has indicated that formation of this HA layer is not critical for bone generation. The ionic dissolution products from bioactive glasses appear to stimulate the growth and differentiation of cells at the genetic level, an effect which has been considered to be dose dependent [28]. For example: Zn concentrations in the range of 2 – 8 ppm have been reported to cause damage to human osteoblasts via oxidative stress [157]. Similar results have been reported for endothelial cells where decrease in cell proliferation was observed due to toxic Zn concentration of 2.7 ppm released in the culture medium from a Zn-doped bioactive glass [120]. Therefore, special consideration should be given to the ZnO content in bioactive glasses and their release profile in body fluids while designing the compositions.

4.2.3 Conclusions

The effects of zinc in the biodegradation of alkali-free phosphosilicate glasses have been studied through a combination of MAS-NMR, FTIR, XRD and chemical degradation experiments. An increase in the Zn^{2+}/Mg^{2+} ratio did not induce any significant change in Q^n speciation and network connectivity, as revealed by MAS-NMR; however it did improve the chemical durability of investigated glasses (as observed from Tris-HCl studies) which consequently suppressed the apatite (carbonated) forming ability of glasses in simulated body fluid. The influence of zinc on suppressing the apatite forming ability of glasses has been

explained on the basis of the constant silicate network connectivity of the combined with the previously suggested ability of Zn to strengthen the glass network through non-covalent Si-O---Zn---O-Si links. This results in a glass structure more resistant to dissolution in a biological medium. An additional factor discussed is the potential influence of zinc on the surface chemistry of glasses when immersed in physiological fluids.

4.3 Influence of ZnO/MgO substitution on sintering, crystallization and bio-activity of alkali-free glass-ceramics

4.3.1 Introduction

Bioactive glasses and glass-ceramics are used in a wide range of applications: bulk implants to replace bones or teeth, coatings to anchor orthopaedic or dental devices, or in the form of powders, as bone grafts, to fill various types of bone defects [4, 183, 184]. The successful development of bioactive glasses for such applications requires suitable densification and crystallization behaviours along the heat treatment step. Such requirements are also of paramount importance in other advanced applications of bioactive glasses involving heat treatments aiming at obtaining products such as glass fibres.

The aim of the present section is to elucidate the effect of partial substitution of MgO by ZnO on the evolution of the glass structure and of the crystalline phases developed along the heat treatments using MAS-NMR and X-ray powder diffraction as complementary techniques and to study the sintering and crystallization behaviours of glass powders using hot-stage microscopy and differential thermal analysis, respectively. Understanding the sintering behaviour of the glass powders and the interactions between the sintering and crystallization events is of utmost importance for successfully fabricating porous scaffolds or coatings on metallic implants from bioactive glasses. Further, cell-culture tests using mesenchymal stem cells from rat bone marrow were used to investigate the *in vitro* behaviour of as designed glass-ceramics.

4.3.2 Results and discussion

4.3.2.1 Glass-forming ability

For all the investigated glass compositions presented in Table 4.2.1, melting at 1570 °C for 1 h was sufficient to obtain bubble-free, transparent and XRD-amorphous glasses.

4.3.2.2 Thermal analysis

The DTA thermographs of fine glass powders with $\beta = 20 \text{ K min}^{-1}$ are shown in Figure 4.3.1. All the glass compositions feature a single endothermic dip before the T_c corresponding to T_g , which is followed by the exothermic crystallization effect. The characteristic parameters obtained from DTA thermographs are summarized in the Table 4.3.1. In general, addition of ZnO resulted in gradually lowering T_g from 752 °C to 718 °C. The decrease in T_g can be attributed to the lower bond strength of Zn–O bond in comparison to the Mg–O bonds [185], which in turn reduces the rigidity of the glass network at high

temperature in comparison to magnesium, even though both possess similarities in size and charge. Further, structural rigidity of a glass network also depends on the field strength thus, the weak bond strength of Zn–O bond than Mg–O can be attributed to the weaker cation field strength of Zn in comparison to Mg [186]. This in turn translates in lowering the viscosity of the glasses [187] thus, decreasing their T_c values. Such changes could be observed in glass powder compacts sintered at 800 °C (not shown here) which remained amorphous for the lower zinc contents, and visible XRD peaks only appeared in the glasses with higher zinc contents. Hence, the results obtained in the present work for zinc-containing glass-ceramics are in good agreement with other literature reports [158, 186, 187].

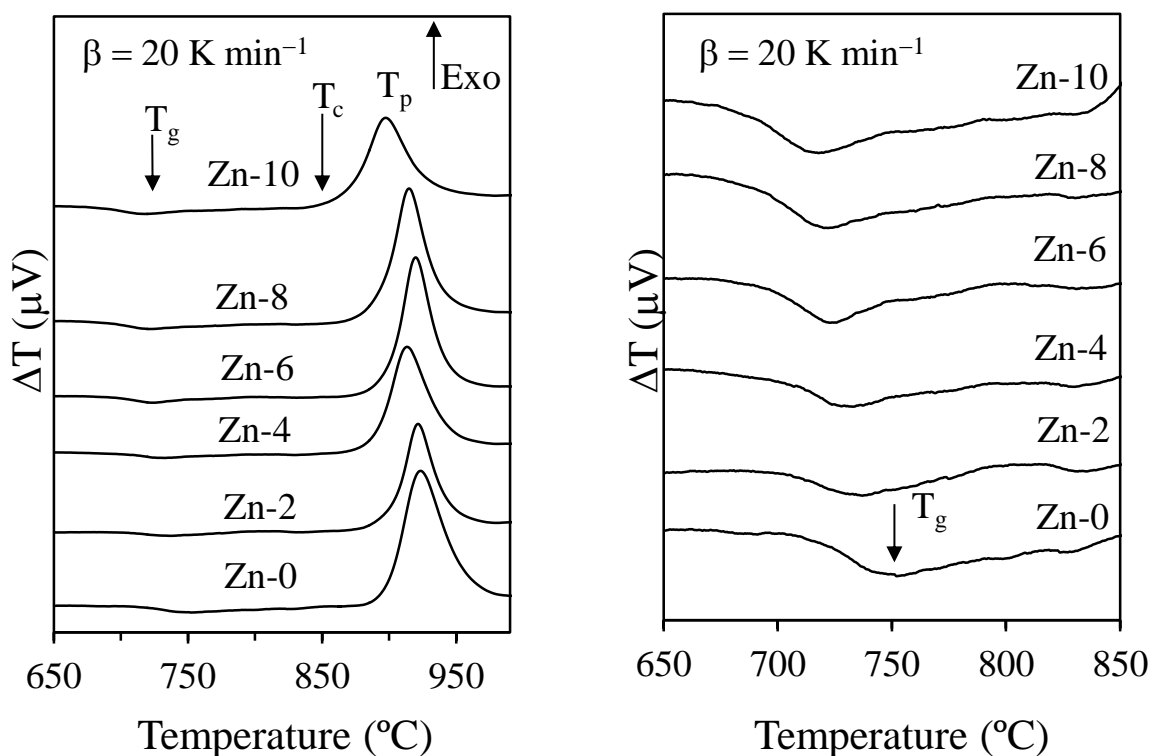


Figure 4.3.1 DTA thermographs of glasses at a heating rate of 20 K min⁻¹.

4.3.2.3 Sintering and Crystallization behaviour

A comparison between DTA and HSM results under the same heating conditions can be useful in investigating the effect of glass composition on sintering and devitrification phenomena. Figure 4.3.2 presents variation in the relative area and heat flow with respect to temperature as obtained from HSM and DTA, respectively, for all the investigated glasses at a similar heating rate of 5 K min⁻¹. Table 4.3.2 summarizes the values of the temperature of first shrinkage (T_{FS} ; $\log \eta = 9.1 \pm 0.1$, η is viscosity in dPa s), temperature for maximum

shrinkage (T_{MS} ; $\log \eta = 7.8 \pm 0.1$) and ratio of the final area/initial area of the glass powder compact (A/A_0) at T_{MS1} , as obtained from the HSM along with temperature for T_c and T_p , as obtained from the DTA of the glasses.

- (i) In general, T_{FS} values show a decreasing tendency with increasing content of ZnO.
- (ii) Two stage sintering was observed in glasses Zn-2, Zn-4 while a gradual shift to single stage shrinkage was observed for glasses thereafter (Figure 4.3.2). The conclusion of first sintering stage is characterized at T_{MS1} while end of second sintering stage is characterized by T_{MS2} . Interestingly, in all the glass compositions T_{MS1} was observed at temperatures lower than T_c (i.e., $T_{MS1} < T_c$). Thus sintering precedes crystallization in all the glasses. Therefore one can expect well sintered and mechanically strong glass powder compacts.
- (iii) The value for T_{MS2} was higher than T_c in the glasses exhibiting two stage sintering behaviour. Thus depicting that shrinkage continued in the glass powders even after onset of crystallization, probably due to the existence of residual glassy phase in the glass-ceramics.
- (iv) Table 4.3.1 lists the values of sinterability parameter (S_c), where $S_c = T_c - T_{MS}$. The parameter S_c is the measure of ability of sintering vs. crystallization: the greater this difference, the more independent are the kinetics of both processes. However, in the present study no particular trend could be observed for the variation of S_c . Nevertheless, all the investigated glasses show larger values of S_c (greater than 25 °C) (26 °C – 48 °C) indicating good sintering behaviour.
- (v) The values of T_p varied between 895 °C – 861 °C. As evident from Table 4.3.1, the highest T_p value was observed for Zn-0. Adding increasing amounts of ZnO to the parent glass at the expenses of MgO resulted in gradual decreases in T_p .
- (vi) Values of A/A_0 ranged from 0.63 to 0.67 (Table 4.3.1) for all the glasses implying towards good densification levels of 95–98%.

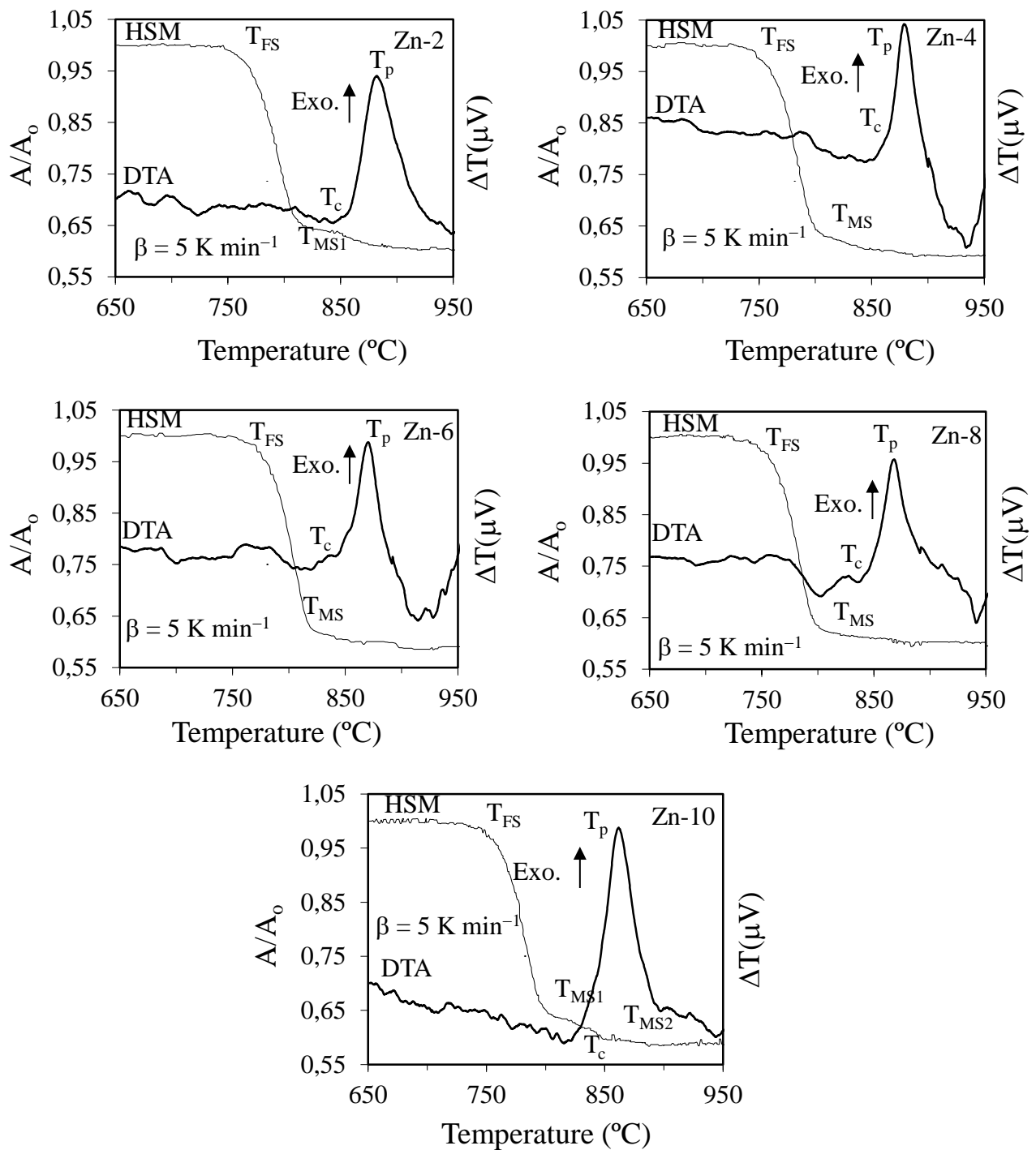


Figure 4.3.2 Comparison of DTA and HSM curves under the same heating rate (5 K min^{-1}) for compositions: (a) Zn-2, (b) Zn-4, (c) Zn-6, (d) Zn-8 and (e) Zn-10.

Table 4.3.1 Thermal parameters measured from DTA and HSM at 5 K min⁻¹ *β = 20 K min⁻¹.

	Zn-0	Zn-2	Zn-4	Zn-6	Zn-8	Zn-10
T _{FS} (±5 °C)	757	753	748	766	747	750
T _{MS1} (±5 °C)	820	809	797	817	797	795
T _{MS2} (±5 °C)	–	883	888	–	–	850
T _g [*] (±2 °C)	752	737	733	725	722	718
T _c (±2 °C)	850	843	852	843	837	822
T _p (±2 °C)	895	881	878	870	868	861
S _c (=T _c -T _{MS1})	30	48	55	26	41	27
A/A ₀ at T _{MS1}	0.66	0.67	0.66	0.63	0.65	0.67

4.3.2.4 Effect of heat treatment of the structure

4.3.2.4.1 Crystalline phase evolution by XRD

The exact nature of the phases produced during the heat treatment is of great interest in bioactive glasses as they are intended to be often exposed to high temperature when it is sintered for different biomedical application. Based on DTA thermographs, T_c was established for all the compositions and used as a criterion for selecting the heat treatment temperature to induce crystallization. In agreement with HSM and DTA, well sintered and dense glass-ceramics were obtained after heat treating the glass–powder compacts at 850 °C for 1 h. Figure 4.3.3 presents the qualitative crystalline phase analysis of the sintered glass-ceramics as depicted by XRD data. Thus heat treating at 850 °C for 1 h resulted in well-defined XRD phase reflections in all the compositions indicating their crystalline nature (Figure 4.3.3). Di (CaMgSi₂O₆; ICSD: 10223) and FA (Ca₅(PO₄)₃F; ICSD: 163790) were the two the primary crystalline phases formed in all the glass-ceramics, followed by rankinite (Ca₃Si₂O₇; ICSD: 2282) as secondary phase. Another phase named petedunnite (CaZnSi₂O₆; ICSD: 158143) crystallized in glass-ceramics with ZnO contents > 4 mol%. Consequently, with the addition of ZnO for MgO, Zn²⁺ replaced Mg²⁺ in the Di, thus forming the major crystalline phase with higher intensity than FA. The presence of FA phase is highly desirable as FA is more stable than HA. Therefore, materials containing FA would be recommended when coatings having low dissolution rate are required [136].

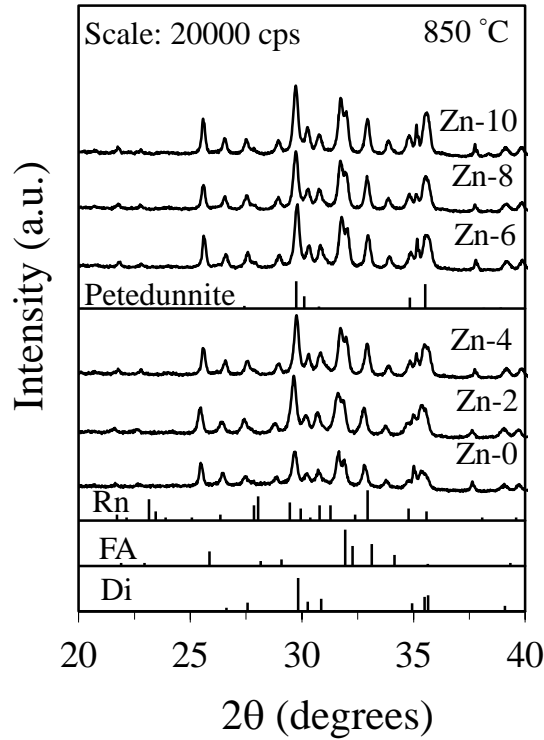


Figure 4.3.3 X-ray diffractograms of glass-ceramics heat treated at 850 °C for 1 h.

Hence, with the addition of ZnO to the parent composition the intensity of XRD peaks corresponding to Di increased whereas the intensity of FA peaks remained almost constant throughout the series.

4.3.2.4.2 MAS-NMR of glass-ceramics

The XRD data was further supported by MAS-NMR studies (Figure 4.3.4). The full width half maximum has reduced considerably in comparison to the original glasses (Figure 4.2.1). Further, as shown in Figure 4.3.4a, all the spectra have a sharp peak centred ~ -84.4 ppm and a small shoulder at -74.5 ppm, which becomes more pronounced with increase of zinc content in glasses, where the former is close to the pure Di [188] while the latter corresponds to the presence of minor phase rankinite [188]. In our study of XRD, a total of two silicate phases pertaining to chain silicates were observed in the glass-ceramics. However, discrimination between these phases is difficult due to the similarity in their silica connectivity. Therefore the resonance around -84 ppm can be due to the contribution from Di and petedunnite (inosilicates).

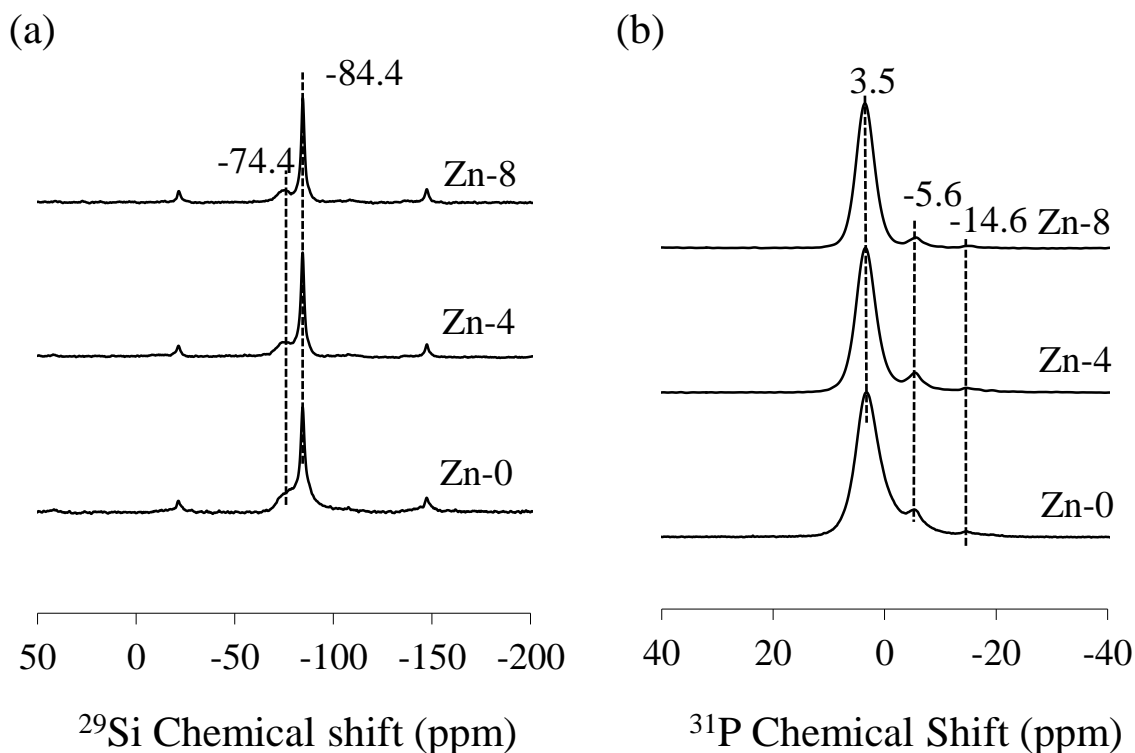


Figure 4.3.4 (a) ^{29}Si MAS-NMR and (b) ^{31}P MAS-NMR spectra of glass-ceramics heat treated at 850 °C for 1 h.

Figure 4.3.4b shows ^{31}P NMR spectra of glass-ceramics heat treated at 850 °C for 1 h. All the spectra have a sharp peak at 3.3 – 3.5 ppm corresponding to an orthophosphate environment and a small shoulder at around –5.3 and –14.6 ppm indicating the presence of pyrophosphate units. The band at 3.5 ppm is close to that reported for FA [136]. Further, the formation of pyrophosphate phase around –5.3 and –14.6 ppm may be due to the reduction in the charge balancing cations, which migrated towards their respective crystalline phases upon heat treatment. Further, Di being a mechanically strong phase renders high mechanical strength to the resultant glass-ceramics. It is worth noting that the presence of petedunnite as a minor phase indicates that zinc predominantly remains in the residual glassy phase.

4.3.2.5 Density and molar volume

The experimental results showed that substitution of MgO by ZnO caused an increase in the density (Table 4.3.2) of the glasses due to the higher density of ZnO (5.6 g cm^{-3}) in respect to MgO (3.6 g cm^{-3}). The molar volume of the glasses increased with increase in Zn content in glasses. The increase in molar volume can attributed to the small bond strength of

Zn–O bond in comparison to Mg–O bond which results in higher bond lengths thus causing an expansion in the network.

Table 4.3.2 Density and molar volume of the investigated glasses.

Glasses	Density (g cm ⁻³)	Molar volume (cm ⁻³ mol ⁻¹)
Zn-0	2.92	20.40
Zn-2	2.95	20.47
Zn-4	2.98	20.51
Zn-6	3.02	20.55
Zn-8	3.05	20.59
Zn-10	3.08	20.66

4.3.2.6 Mechanical Behaviour

Evaluating the mechanical strength of a biomaterial is very important while judging its suitability for a given intended application, such as scaffolds for bone regeneration. It is likely that mechanical strength of a given glass-ceramic will be dependent on the mechanical properties of the constituting crystalline phases, their volume fractions, the size/shape of the crystals formed, and on the interfacial bonding between the amorphous and crystalline phases. The flexural strength was calculated for powder compacts sintered at 850 °C. High flexural strength values were obtained for glass powder compacts, which can be attributed to the predominance of Di in all glass-ceramics (Figure 4.3.5). In general, an increase in mechanical strength with increasing Zn contents in glasses was observed, with the highest mechanical strength being measured for the GC Zn-8. As deduced from HSM and DTA analysis, this enhancement can be attributed to two complementary reasons: (i) an improved sintering ability due to a decrease in the viscosity of glasses translated by decreasing T_g values; (ii) a more extensive subsequent crystallization promoted by the enhanced diffusivity of ionic species in the glassy matrix.

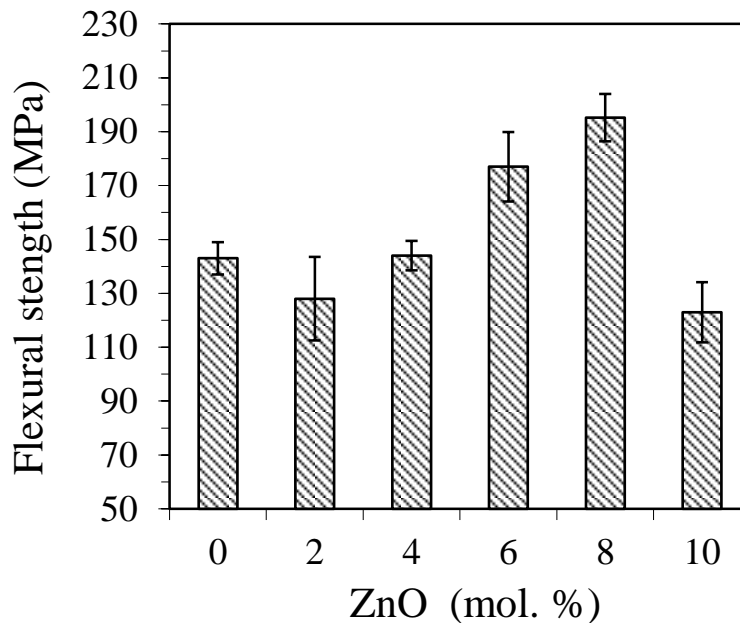


Figure 4.3.5 Flexural strength of the glass-ceramics heat treated at 850 °C for 1 h

4.3.2.7 Apatite forming ability of glass-ceramics

The SEM-EDS results of the glass-ceramic samples before and after immersion in SBF solution for different time periods are shown in Figure 4.3.6. The surface morphology of Zn-0, Zn-4 and Zn-8 samples before immersion in SBF (Figure 4.3.6a) is similar, a situation that was altered for the samples immersed in SBF (Figure 4.3.6b). The EDS data was gathered over the entire areas shown in the SEM micrographs to assure reliable averaging of the signals and the scale of all EDS spectra was always kept constant to enable a direct comparison. Although all the spectra reveal the presence of all glass-constituting elements, their relative intensities changed significantly after immersing the samples in SBF. It can be seen that the EDS spectrum of Zn-0 sample (Figure 4.3.6a) significantly differs from those obtained after immersing in SBF (Figure 4.3.6b). Namely, the intensities of Ca and P became more and more predominant with increasing immersion time. This constitutes an obvious evidence of apatite formation at the surface of the samples.

The formation of HA at the surface of ZnO-containing glass-ceramics is less obvious. Various reasons can be cited for this delayed bio-mineralization process in ZnO-containing glass-ceramics:

1. *Presence of ZnO*: The delayed formation of HA can be due to inter-tetrahedral non-covalent linkages in the residual glassy phase. Similar results have been reported in our previous section. Further, the concomitant presence of Mg^{2+} and

Zn^{2+} inhibits HA crystal growth. Literature reports suggest a Langmuir-type adsorption of these ionic species at active growth sites on the HA crystals [169]

2. *Low residual glassy phase:* The enhanced crystallization of ZnO-containing glass-ceramics (lower T_c values) and the consequent lower amount of residual glassy phase is also expected to decrease the apatite forming ability [189].

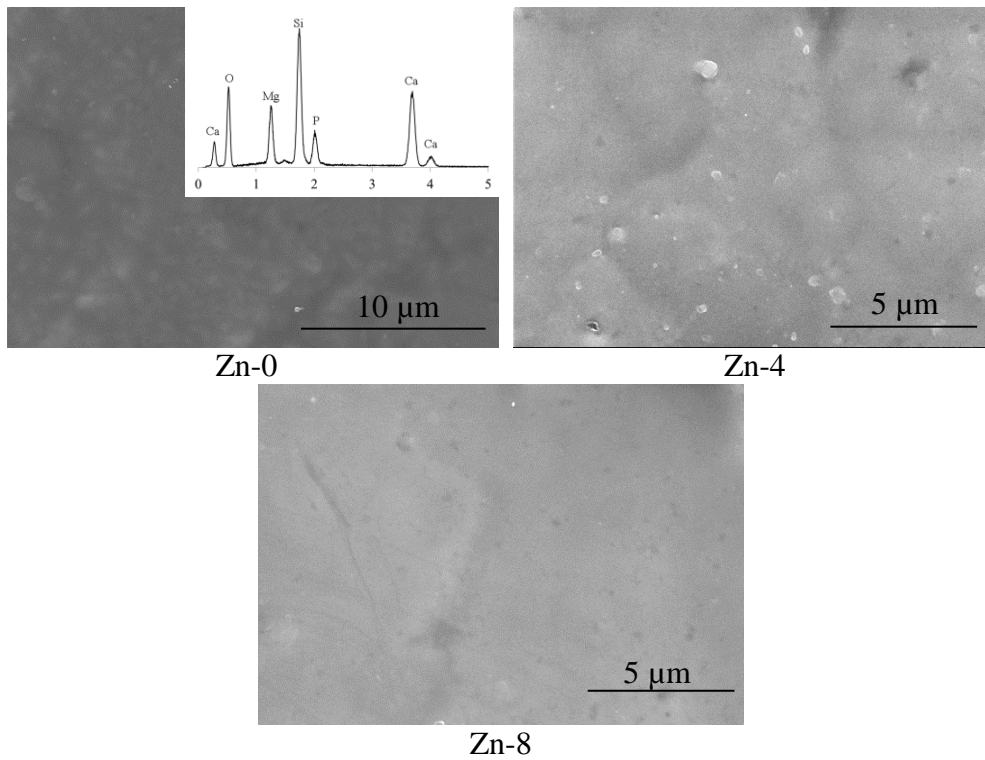


Figure 4.3.6a SEM/EDS micrographs images of unpolished and non-etched glass-ceramics samples before soaking in SBF: Zn-0, Zn-4, and Zn-8.

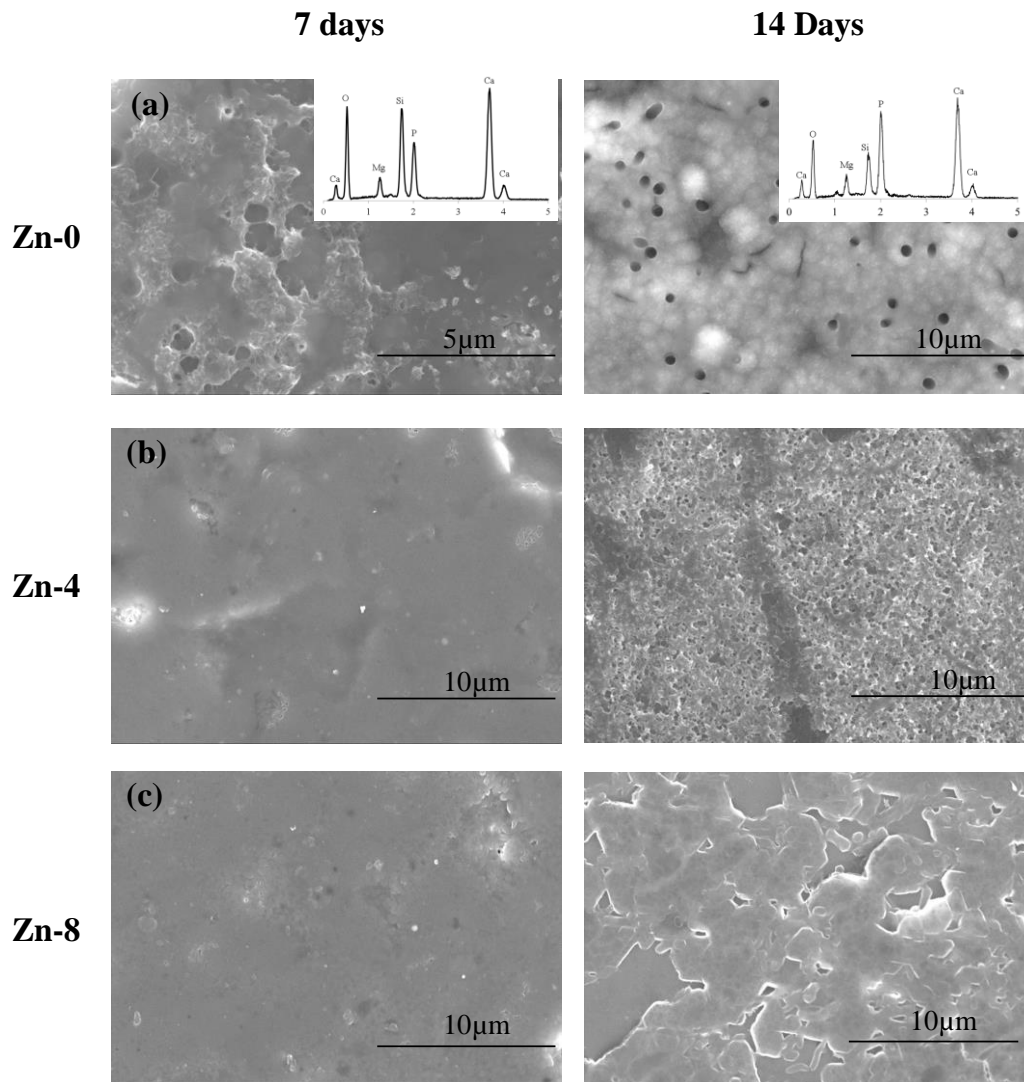


Figure 4.3.6b SEM/EDS micrographs images of unpolished and non-etched glass-ceramics samples after soaking in SBF for 7 and 14 days: (a) Zn-0, (b) Zn-4, and (c) Zn-8.

4.3.2.8 Mesenchymal cell activity and alkaline phosphatase activity

Figure 4.3.7 shows the cell viability on the glass-ceramics and control during culture for up to 7 days, as assessed by a CCK method. Apparently, the growth kinetics of glass-ceramics with 4 mol.% ZnO was significantly higher with respect to that of tissue culture plastic control as well as to that of other investigated glass-ceramics. Interestingly, all other zinc containing glass-ceramics showed lower cell viability in comparison to that for tissue culture plastic.

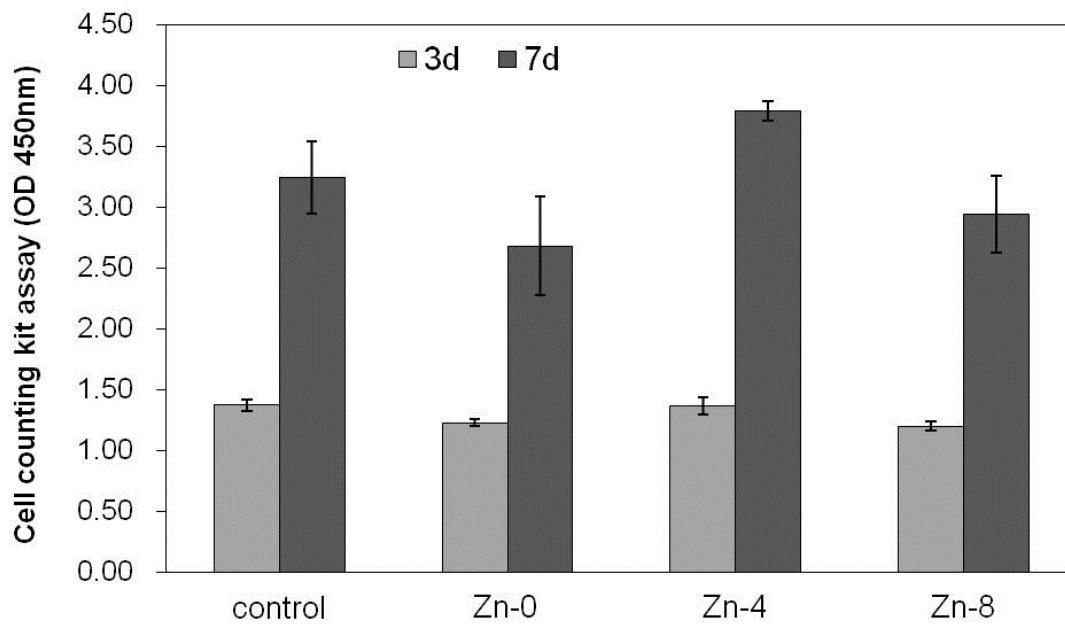


Figure 4.3.7 Influence of ZnO content in glass-ceramics on cell viability during culture for up to 7 days, as assessed by CCK method. Glass-ceramics with 4 mol% ZnO showed highest growth with respect to tissue culture plastic control as well as to that of other investigated glass-ceramics.

The representative cell growth images at day 3 and day 7 on the glass-ceramics samples are presented in Figure 4.3.8. The cells were not readily noticed on the Zn-0 glass-ceramic after 3 days while the cell proliferation was comparatively better on glass-ceramic Zn-8. On the other hand, when grown on Zn-4, the cells were readily observed covering the surface almost completely with active cytoskeletal processes and elongated filopodia indicating that glass-ceramic Zn-4 provides favourable conditions for adherence, spreading and proliferation of MSCs. After 7 days, although the cell proliferation on glass-ceramics other than Zn-4 was better in comparison to that observed after day 3 but still the glass-ceramic Zn-4 exhibited the highest rate of cell proliferation. The lower cell viability in the absence of zinc can be explained by the fact that after iron, zinc is the most abundant trace metal in human organisms and is essential for various metabolic activities as has been discussed above

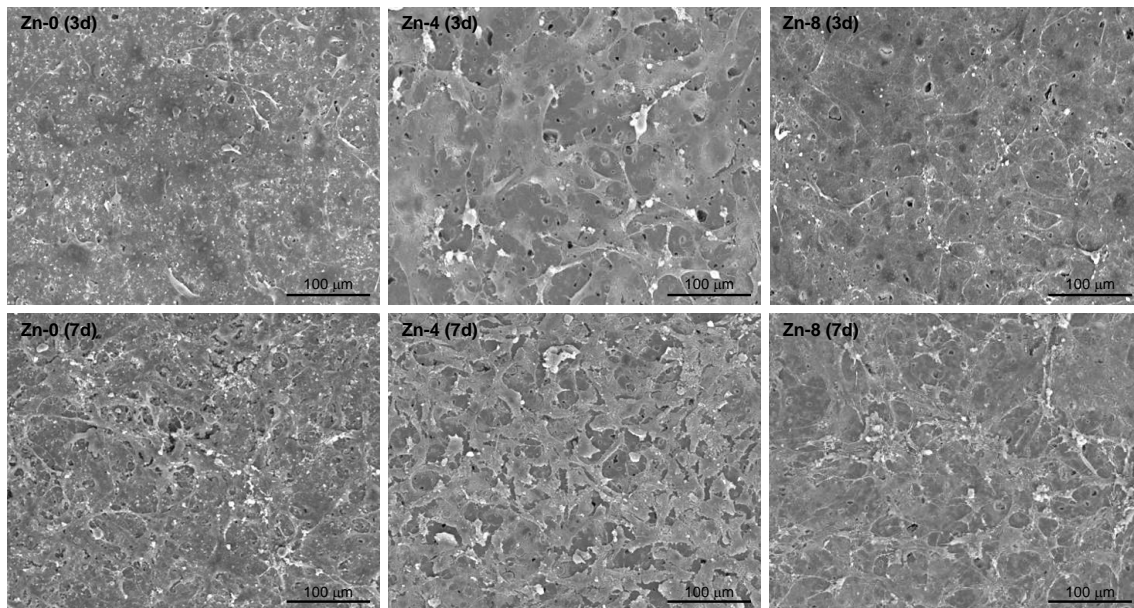


Figure 4.3.8 SEM images of the MSCs grown on the sintered glass powder compacts (Zn-0, Zn-4 and Zn-8) during culture for 3 and 7 days. After 7 days, cell proliferation on glass-ceramics was better in comparison to that observed after 3 days. Glass-ceramic Zn-4 exhibited the highest rate of cell proliferation.

However, the decreasing cell viability with increasing zinc concentration in glasses may be attributed to its dose-dependent effect. Zn^{2+} has been reported to play a dual role in affecting the cell death: although zinc seems to be inhibitor of many forms of apoptosis [190], exposure to excessive concentrations may contribute to neuronal cell death in acute neurological disorders and to apoptosis of human peripheral blood lymphocytes [191]. The mechanism by which Zn^{2+} induces cell death and oxidative stress is still unresolved. According to the available literature, an increase in Zn^{2+} concentration in cellular medium higher than ~2 ppm can lead to cytotoxicity and cell death [44]. Similar results with respect to proliferation of endothelial cells and osteoblasts have also been reported by Aina et al. [120, 157] where it has been shown that 45S5 Bioglass[®] doped with 5 wt% ZnO enhanced cell proliferation on its surface while increasing zinc concentration led to significant release of lactate dehydrogenase (index of cytotoxicity) thus, resulting in cell death. With respect to the bioactivity of glass-ceramic Zn-4, the cell growth kinetics in this sample is significantly higher in comparison to that reported for apatite-wollastonite [192] as well as for diopside-fluoroapatite [105] glass-ceramics, respectively.

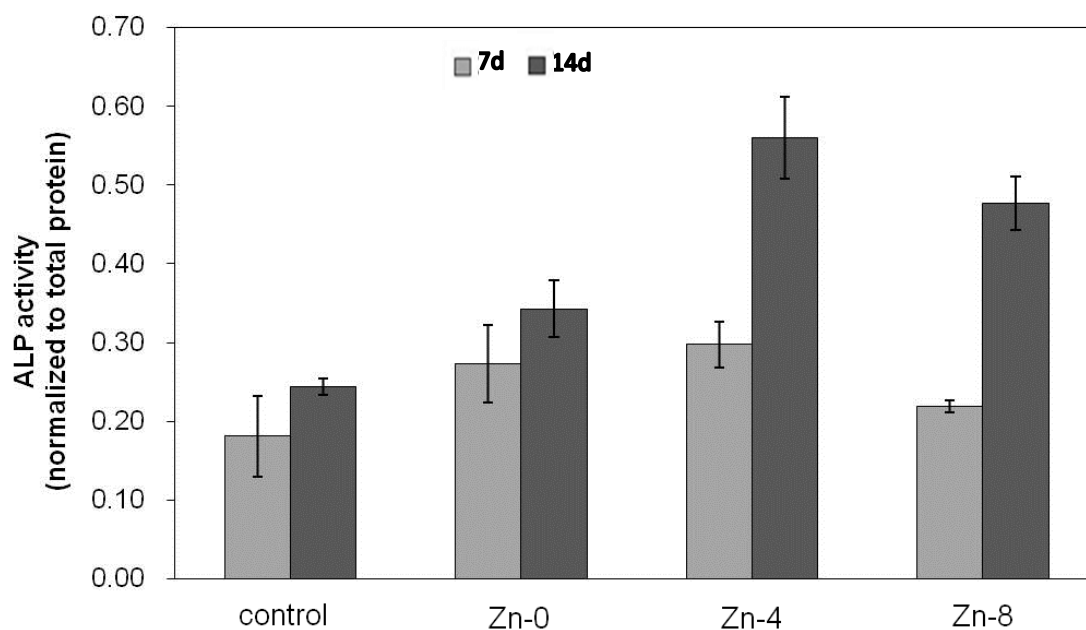


Figure 4.3.9 Alkaline phosphatase activity of the MSCs during culture for 7 and 14 days on the glass compacts (Zn-0 to Zn-8) and on tissue culture plastic control. For all the investigated glass-ceramics, irrespective of their ZnO content, ALP levels were always higher in comparison to that of control ($p < 0.05$, ANOVA, $n=3$)

The osteogenic differentiation of the MSCs cultured on the glass-ceramic samples was investigated in terms of ALP activity (Figure 4.3.9). Under the osteogenic medium used herein, rat bone marrow MSCs have been shown to switch to the lineage of osteoblastic cells [193]. When cultured on the control dish, MSCs showed an increased ALP level from days 7 to 14. The ALP levels for all the investigated glass-ceramics were higher in comparison to control irrespective of their zinc content. However, among all the investigated glass-ceramics, Zn-4 exhibited the highest ALP activity of cells during 7 and 14 days of culture. It should be noted that ALP is a homodimeric metalloenzyme that catalyses the hydrolysis of almost any phosphor monoester with the release of phosphate and alcohol. Its properties have been associated with the mineralization process and phosphate homeostasis in bone tissue [194]. ALP acts as a nucleation centre for hydroxyapatite as it is able to release phosphate and captures calcium ions. In this way, the presence of ALP and a solution rich in Ca^{2+} ions induces the deposition of hydroxyapatite (bone forming mineral) crystals and amorphous calcium phosphate.

4.3.3 Conclusions

A detailed investigation about the influence of adding increasing amounts of ZnO to partially replace MgO in a parent bioactive glass composition (TCP-20) was shown to have consequences in terms of sintering and crystallisation behaviours and on the relevant properties of the resulting glass-ceramics, including mechanical and biological responses. The glass forming ability of the glasses was unaffected by the level of MgO substitution. All the glass compositions investigated exhibited good sintering ability upon heat treating at 850 °C for 1 h thus, resulting in well sintered and mechanically strong glass-ceramics with diopside and fluorapatite as the primary crystalline phases. A minor crystalline phase (petedunnite) was also formed for ZnO > 4 mol%. The ZnO content also revealed to play an essential role on the *in vitro* bioactivity. The glass-ceramic composition with ZnO = 4 mol% exhibited the highest levels of mesenchymal cell proliferation and alkaline phosphatase activity, while further increasing ZnO contents led to a significant decrease in the *in vitro* performance of the investigated glass-ceramics.

4.4 Role of glass structure in defining the chemical dissolution behaviour, bioactivity and antioxidant properties of zinc- and strontium- co-doped alkali-free phosphosilicate glasses

4.4.1 Introduction

Since the chemical degradation of multi-component glasses is strictly related to their atomic and molecular structure [5] the design of bioactive glasses requires a thorough understanding of the relationship between their atomic/molecular structure and dissolution behaviour. In fact, it has been well established that the ionic dissolution products are key to understand the behaviour of their parent inorganic materials *in vitro* and *in vivo*, especially in the context of TE applications [195]. This relationship becomes more important when functional ions (for example: Sr^{2+} , Zn^{2+} , F^- , etc.) are incorporated in the glasses with an aim to enhance their biological efficacy because these ions interact with and modify the phosphosilicate glass matrix, thus, affecting the dissolution behaviour of resultant glass compositions. Therefore, it is of paramount importance to understand the influence of these functional ions on the structure and bioactivity of glasses so as to design glass compositions with controlled chemical dissolution and ion release rates.

Zinc and strontium are two such functional ions whose biological importance has been well documented in literature [42, 56, 59, 121]. Despite being present in trace amounts, both these ions play essential roles in the chemistry of bone [196, 197]. For this reason several studies describing the influence of zinc and/or strontium on various aspects of bioactive glasses and their properties have been reported in literature during the last few years [42, 58, 82, 114, 119-122, 198]. Further, most of the work on strontium and zinc co-doped bioactive glasses available in literature has been published by Boyd and co-authors [125, 154, 199-203] in the $\text{CaO-SrO-ZnO-Na}_2\text{O-SiO}_2$ glass system.

The present section aims at defining the structure-property relationships in a series of alkali-free phosphosilicate glass composition in Di-FA-TCP system co-doped with Zn^{2+} and Sr^{2+} . An attempt has been made to understand the structural role of Sr^{2+} and Zn^{2+} co-doping on the chemical dissolution behaviour of glasses and its impact on their apatite forming ability, osteoblast proliferation and antioxidant behaviour. The very promising glass composition TCP-20 discussed in section 2.1 was adopted as the starting point for synthesis of present series of glasses. The structure of the as-obtained glasses has been investigated by MAS-NMR while the biodegradation of glasses has been investigated by their immersion in Tris-HCl and SBF. Furthermore, the influence of glass structure and the

dissolution behaviour on osteoblast proliferation and oxidative stress levels has been discussed.

4.4.2 Results

4.4.2.1 Glass forming ability

For all the investigated glass compositions with varying Zn^{2+}/Mg^{2+} and Ca^{2+}/Sr^{2+} ratio: (mol%) (36.07-x) CaO – xSrO – (19.24-x) MgO – xZnO – 5.61P₂O₅ – 38.49SiO₂ – 0.59 CaF₂ (x = 0–10), melting at 1570 °C for 1 h was sufficient to obtain bubble-free, transparent and XRD-amorphous glasses (Figure 4.4.1). Table 4.4.1 presents the detailed compositions of the as-designed glasses.

Table 4.4.1 Nominal composition of the as-designed glasses (mol%).

Glass	CaO	MgO	SiO ₂	P ₂ O ₅	ZnO	SrO	CaF ₂
ZS-0	36.07	19.24	38.49	5.61	0.00	0.00	0.59
ZS-2	34.07	17.24	38.49	5.61	2.00	2.00	0.59
ZS-4	32.07	15.24	38.49	5.61	4.00	4.00	0.59
ZS-6	30.07	13.24	38.49	5.61	6.00	6.00	0.59
ZS-8	28.07	11.24	38.49	5.61	8.00	8.00	0.59
ZS-10	26.07	9.24	38.49	5.61	10.00	10.00	0.59

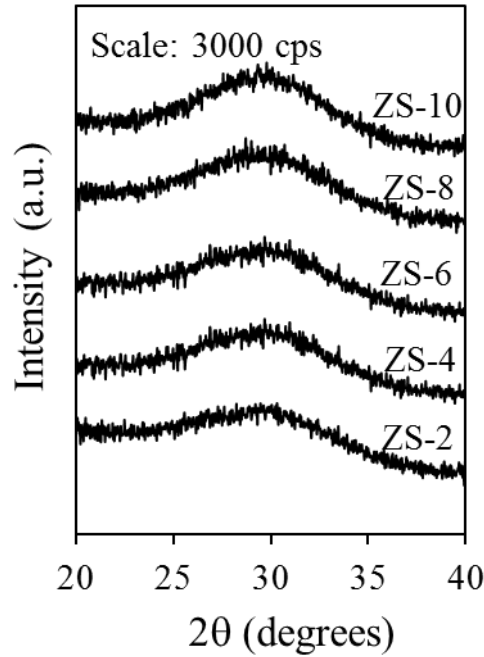


Figure 4.4.1 X-ray diffractograms of glass powders

4.4.2.2 Structure of glasses

The ^{29}Si MAS-NMR results of all the glasses as presented in Figure (4.4.2a, 4.4.3a), depict the dominance of Q^2 (Si) structural units in the glasses. Furthermore, the dominance of Q^2 structural units is confirmed by the quantitative analysis of deconvoluted NMR spectra (Table 4.4.2b). The Q^n distributions for the three compositions are rather close to each other, i.e. the silicate distribution is dominated by Q^2 chain species, with substantial amounts of chain-terminators Q^1 and branched Q^3 species. Further, only slight shift in the peak positions of spectra could be observed and all the spectra are centred between -81 ppm and -82 ppm, thus depicting no significant changes in the silica coordination in glass structure. The ^{31}P MAS-NMR spectra of all the glasses (Figure 4.4.2b) and the corresponding de-convolution (Table 4.4.3) show a predominance of orthophosphate-type species with chemical shifts centred at around 2–2.5 ppm, close to that of the calcium orthophosphate (3.1 ppm) [137]. Besides the dominant Q^0 orthophosphates, Table 4.4.3 also highlights the presence of non-negligible amounts of non-orthophosphate species, in agreement with the MD models, a phosphorus environment thus qualitatively similar to that found for the 45S5 glass [127, 167]. Similar results were obtained for alkali-free bioactive glasses doped with ZnO and SrO on independent basis where insignificant influence on silicate network connectivity was observed by varying SrO/CaO ratio [204] or ZnO/MgO [42] ratio in the glasses while most of the phosphorus component was found in orthophosphate environment.

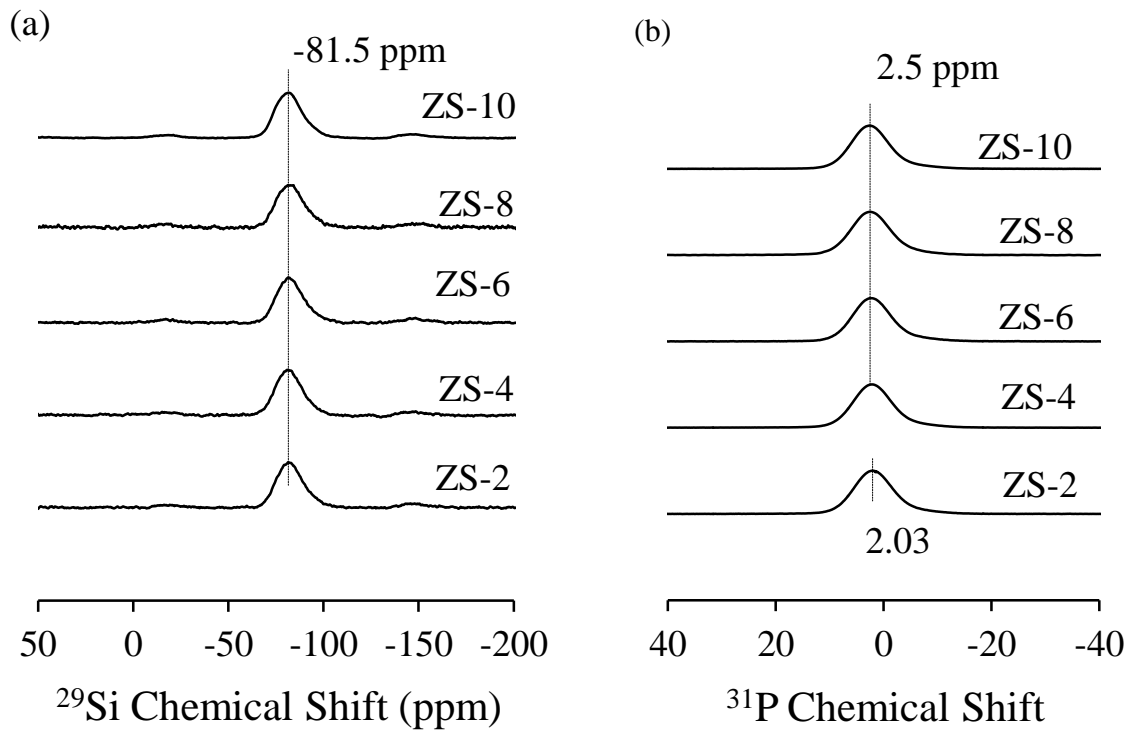


Figure 4.4.2 MAS NMR spectra of investigated glasses showing the peak positions of (a) ^{29}Si and (b) ^{31}P .

Thus NMR results shows that $\text{Zn}^{2+}/\text{Mg}^{2+}$ and $\text{Ca}^{2+}/\text{Sr}^{2+}$ substitutions do not affect the silicate network connectivity of these glasses.

Table 4.4.2 Q^n (Si) distribution for glasses ZS-4 and ZS-10 obtained by NMR deconvolution.

Q^n	ZS-4		ZS-10	
	peak position (ppm)	% integral	peak position (ppm)	% integral
Q^0	-66.5	0.3	-66.0	0.3
Q^1	-75.7	22.7	-75.8	28.8
Q^2	-81.7	50.6	-82.6	48.0
Q^3	-88.3	24.1	-90.5	22.7
Q^4	-96.7	2.2	-107.4	0.1

Table 4.4.3 Q^n (P) distribution for glasses ZS-4 and ZS-10 obtained by NMR deconvolution.

Q^n	ZS-4		ZS-10	
	peak position (ppm)	% integral	peak position (ppm)	% integral
Q^0 (Ca)	3.2	52.3	3.2	67.4
Q^0 (Mg)	0.5	27.5	0.8	17.3
Q^1	-1.0	20.3	-1.9	15.2
Q^2	-	-	-	-

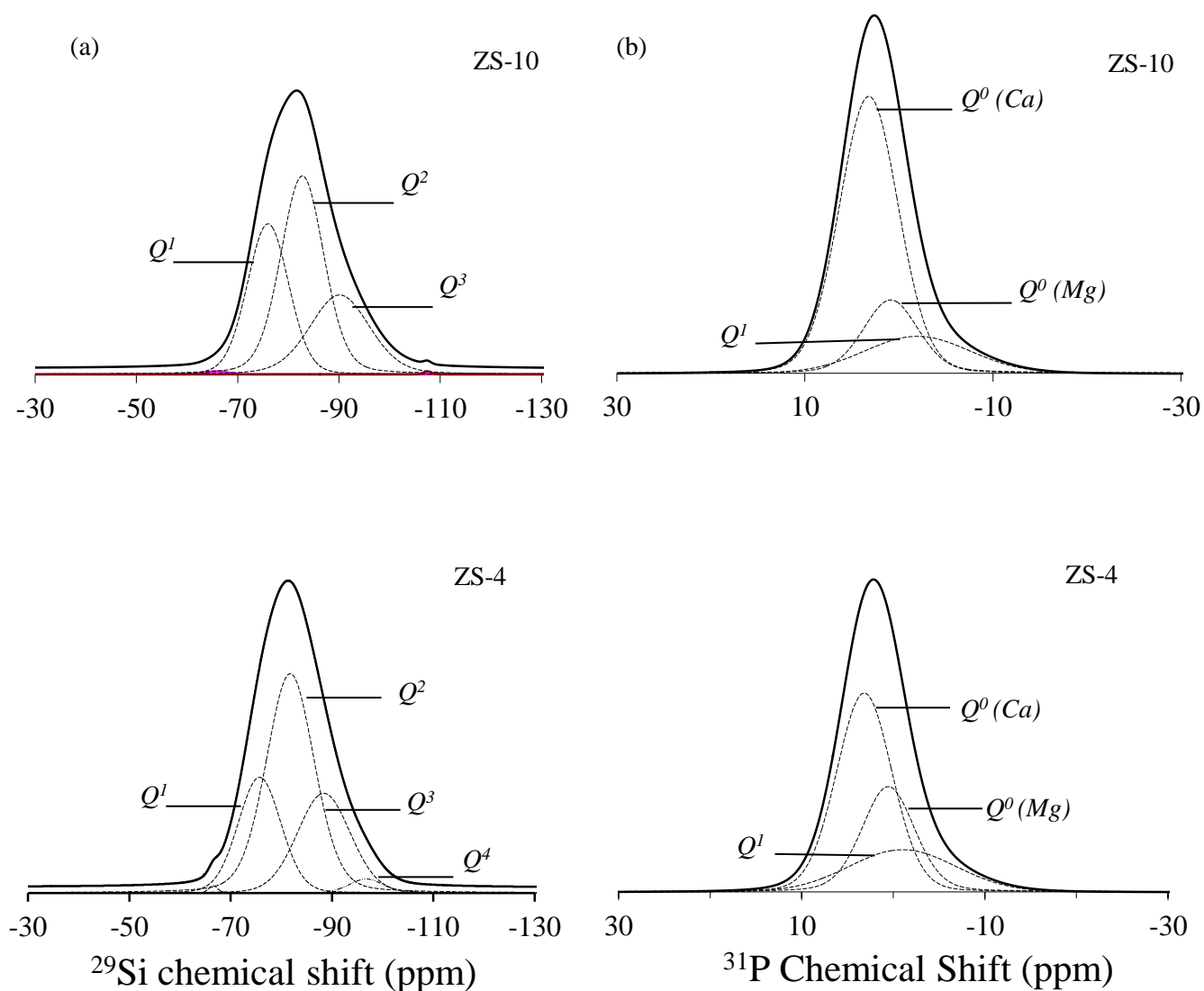


Figure 4.4.3 (a) ^{29}Si MAS NMR spectra and (b) ^{31}P MAS NMR spectra after deconvolution of investigated glasses.

4.4.2.3 SBF immersion studies

In the present case, FTIR spectra of all the glass powders before immersion in SBF solution are presented in Figure 4.4.4a. All the investigated glasses show three broad bands in 350–1300 cm^{-1} region. The broadness clearly shows the disorder in the glass structure with uneven distribution of Q^n units. The band ranging from 800–1300 cm^{-1} corresponds to presence of two optical modes of Si–O–Si groups: Si–O bending mode identified around 800 cm^{-1} and the asymmetric stretching mode Si–O (s) in 1000–1300 cm^{-1} region. The $\sim 500 \text{ cm}^{-1}$ band can be attributed to Si–O–Si bending modes, while the weak shoulder around $\sim 750 \text{ cm}^{-1}$ may be due to Si–O–Si symmetric stretching with simultaneous Si cations motion [205]. Further, the band centred around 559 cm^{-1} corresponds to P–O bending modes [206].

The immersion of glass powders in SBF for varying time durations led to a considerable change in the glass chemistry which is evident from the FTIR data presented in Figure 4.4.4b-4.4.4d. The soaking of glass powders in SBF for 1 h resulted in the appearance of a strong low frequency band around $\sim 503 \text{ cm}^{-1}$ (Figure 4.4.4b) typical for the deformation mode of silica gel-like layer. In addition to that the main IR band now appeared at 1051 cm^{-1} along with a weak shoulder at 1180 cm^{-1} which could be assigned to Si–O–Si stretching vibrations [206]. These bands indicate the development of interfacial high-area silica gel layer, as postulated in Hench's inorganic reactions set [20] and can be observed in all the glasses. The peaks around $\sim 560, 600, 1035 \text{ cm}^{-1}$ present in all the glasses are evidence for the formation of crystalline hydroxyapatite and other crystalline phosphate species as these bands correspond to P–O bending vibrations in a PO_4^{-3} tetrahedron. Further, the bands at 1296 cm^{-1} and 1461 cm^{-1} corresponding to the formation of complex carbonate species imply towards formation of carbonated HA. It is noteworthy that formation of any calcium carbonate (CaCO_3) polymorphs has been negated considering their absence in the XRD data obtained on glasses after immersion in SBF solution as shown in Figure 4.4.5.

The XRD data obtained on glass powders after immersion in SBF solution for varying time durations support the FTIR results as all the glasses exhibit well defined characteristic X-ray peak at $2\theta = 31.77^\circ$ corresponding to the formation of crystalline hydroxyapatite [HA; ($\text{Ca}_5(\text{PO}_4)_3\text{OH}$; ICDD: 00–09–0432] after 1 h of immersion (Figure 4.4.5).

The intensity of the XRD phase reflections for HA increased with increase in SBF immersion time, thus, depicting the high apatite forming ability of these glasses. Interestingly, the apatite forming ability of same parent glass (ZS–0) was observed to

decrease considerably when doped with SrO (at the expense of CaO) or ZnO (at the expense of MgO) on individual basis as has been reported in our previous articles [42, 204].

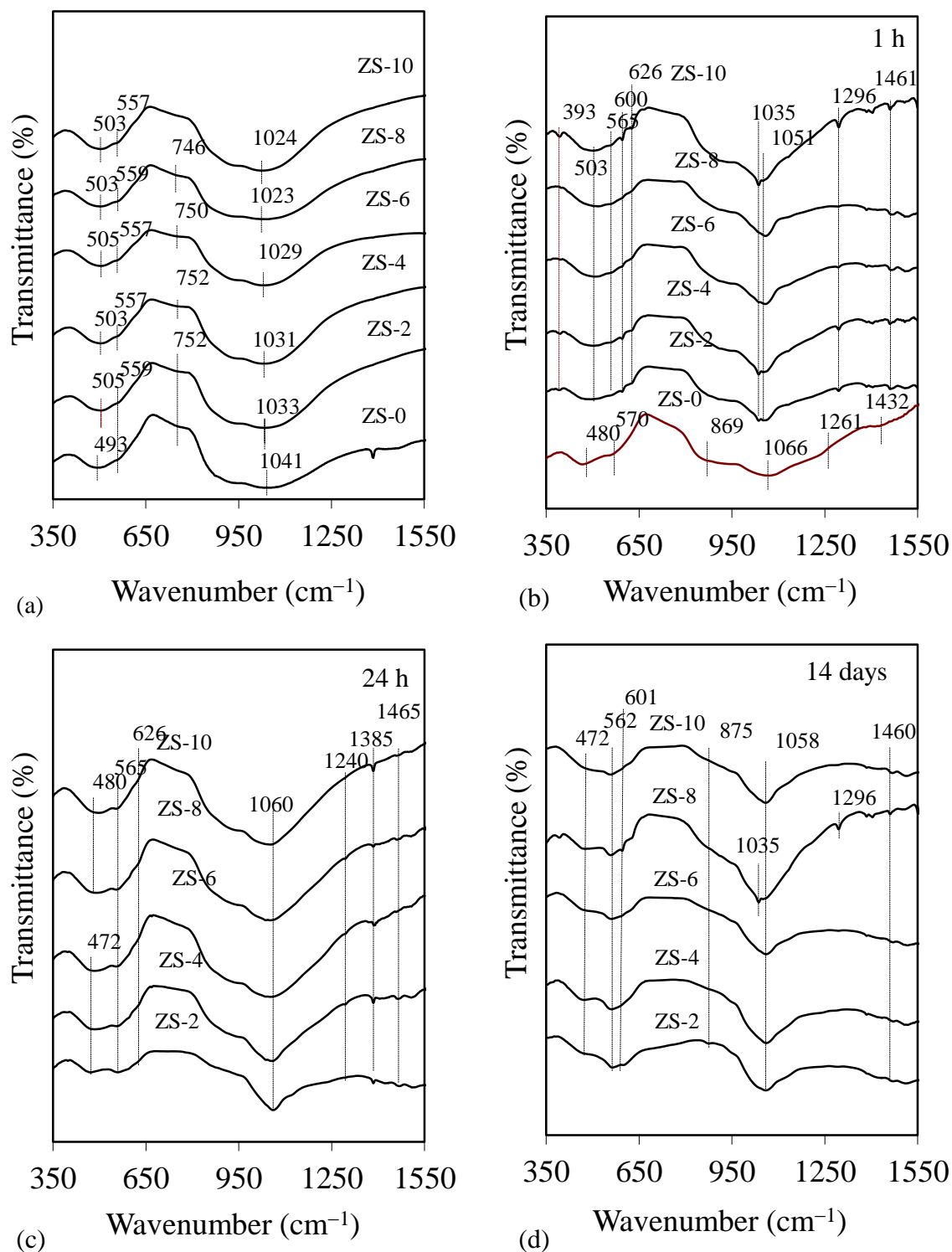


Figure 4.4.4 FTIR spectra of glass powders (a) before, after (b) 1h, (c) 24h, and (d)14 days immersion in SBF.

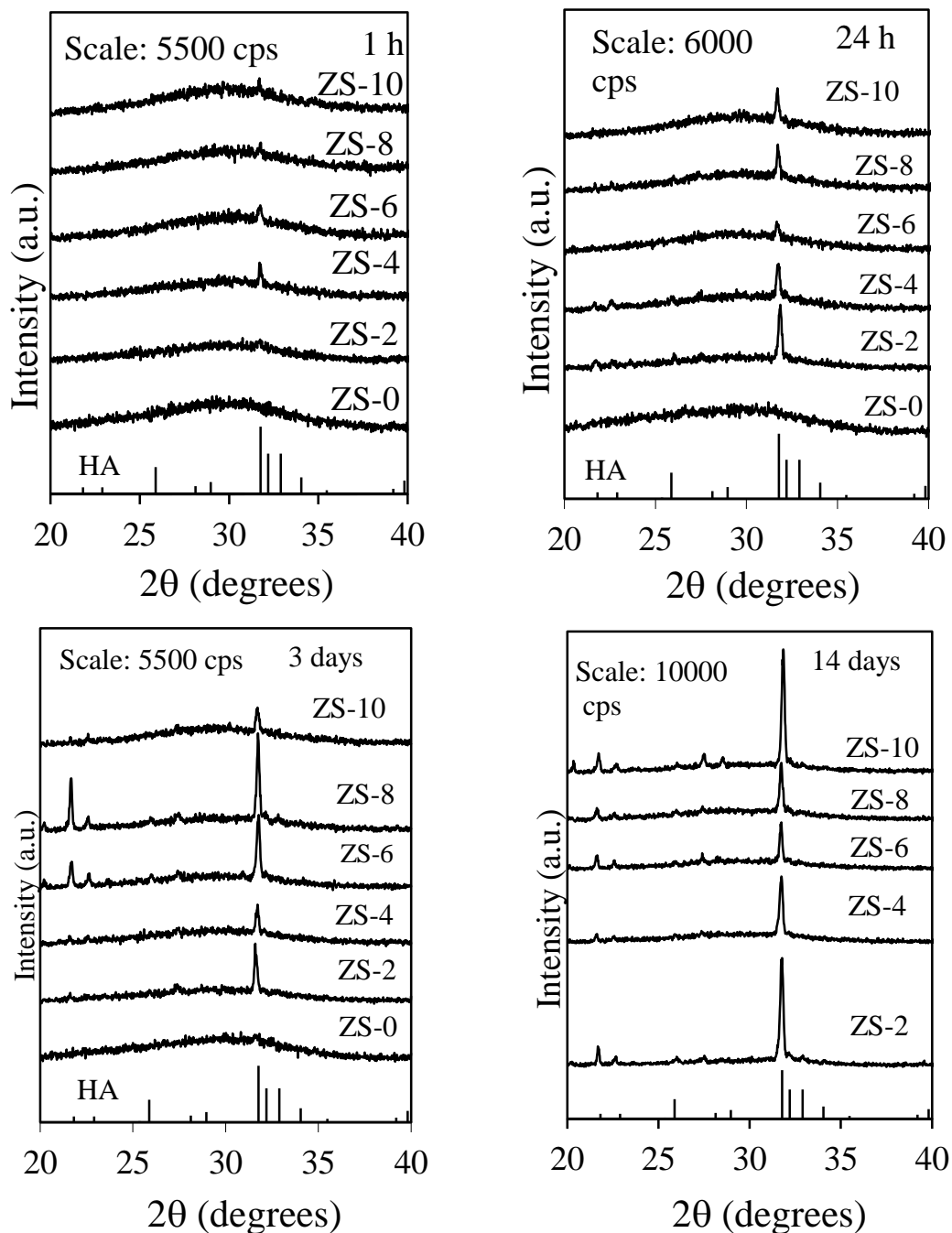


Figure 4.4.5 X-ray diffractograms of glass powders after immersing the glass powders in SBF solution for (a) 1 h (b) 3 h (c) 6 h (d) 24 h (e) 3 days and (e) 14 days.

In order to gain a better insight into the glass dissolution process and apatite forming ability of the investigated glasses, the elemental release profile of these glasses was studied when immersed in SBF solution for initial 24 h. The trends observed for variation in concentration (mg l^{-1}) of different ionic species (Ca^{2+} , Mg^{2+} , PO_4^{3-} , SiO_4^{4-} , Zn^{2+} , Sr^{2+}) in

SBF detected during initial 24 h are presented in Figure 4.4.6. The results obtained have been summarized below:

- i) The trend of Ca^{2+} concentration after 1 h of immersion corresponds to an increase for all glasses which reaches its maximum within 12 h of immersion in SBF solution (Figure 4.4.6a). The increasing Ca^{2+} concentration in SBF during initial immersion for all glasses imply towards the initiation of the bio-mineralization process, where modifier cations in the glass exchange with hydronium ions in the external solution [20]. This increase in the Ca^{2+} concentration may be attributed to the exchange of Ca^{2+} with the hydronium ion present in the SBF solution due to disruption of the glass network. Thereafter, a kind of saturation plateau is reached for all the investigated glasses. The similar dissolution behaviour for all the glass compositions may be ascribed to the similar network connectivity exhibited by all the glasses. The release of Ca^{2+} seems to depend on their actual concentration in parent glasses as increasing SrO/CaO ratio in glasses decreased the Ca^{2+} ion release concentration in the SBF solution.
- ii) The concentration of PO_4^{3-} follows steadily decaying profiles, an indication that the dissolution rate from glasses is lower than the rate of surface deposition of such species.
- iii) The Mg^{2+} ion concentration profile is similar to that of Ca^{2+} in SBF solution and was detected to be highest after 12 h of immersion time for all the glass compositions while no significant variations were observed after prolonged SBF immersions (Figure 4.4.6c), possibly due to attainment of equilibrium between the Mg^{2+} concentration in glass and SBF. In general, the amount of Mg detected after any particular immersion time was highest for ZS-2 and lowest for ZS-8 possibly due to higher magnesium content in ZS-2 as compared to ZS-8.
- iv) Sr^{2+} can accumulate in bone by exchanging with Ca^{2+} in the hydroxyapatite crystal lattice due to the chemical analogy to Ca^{2+} . As shown in Figure 4.4.6d, glass compositions up to ZS-4 exhibit Sr release profiles that are similar to other alkaline earth ions for all compositions with a maximum after 12 h of immersion in SBF solution. With further increasing the ZnO and SrO content to ZS-8, the strontium release profile was observed to steadily increase beyond 12 h. Although we did not make elemental analysis of the SBF solution obtained after immersion of glass ZS-10 for varying time durations, a similar behaviour is expected from this glass too.
- v) In general SiO_4^{4-} ion concentration increases with increase in immersion time, thereafter reaching a saturation plateau after 6–12 h of immersion (Figure 4.4.6e). It is worth noting that Si concentrations reached highest values for ZS-2, an indication that the chemical resistance of glasses somewhat increased with increasing added amounts of doping ions.

vi) The Zn ion release profiles for the investigated glasses over 24 h are shown in Figure 4.4.6f. In all the investigated glasses the Zn ion concentration in SBF increases with 1 h of immersion time, thereafter decreases to a saturation value. Zn^{2+} release from these glasses appears to be independent from the Zn content in the glasses. Also it is worth noting that co-doping of glasses with SrO and ZnO does not prevent the formation of HA on the glasses.

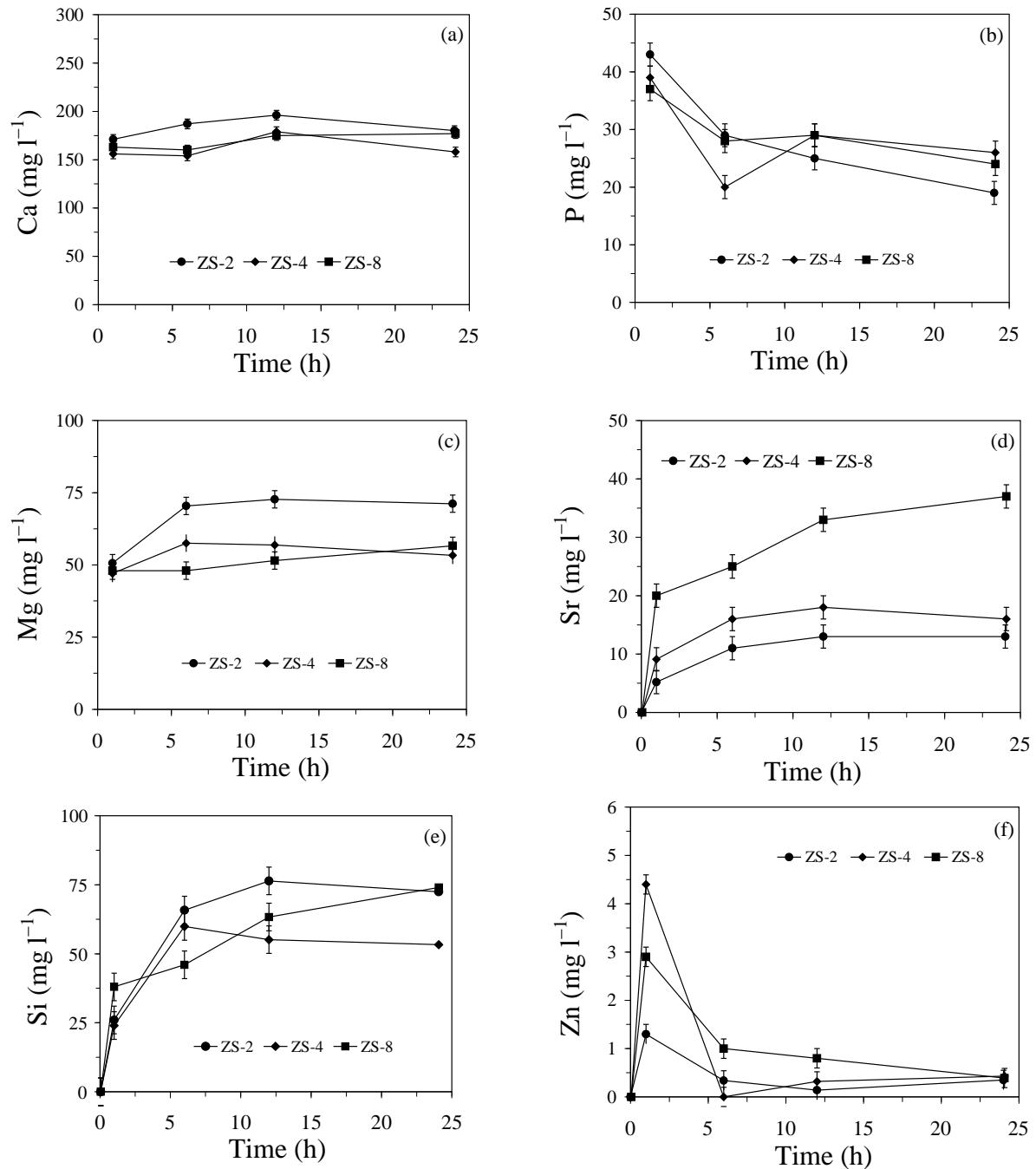


Figure 4.4.6 ICP plots of elemental concentration of (a) Ca, (b) P, (c) Mg, (d) Sr, (e) Si and (f) Zn, in SBF solution versus immersion time for the investigated glass powders.

4.4.2.4 Chemical degradation of glasses in Tris-HCl

All the glasses were XRD amorphous after immersion in Tris-HCl for 120 h, thus negating the possibility of any phase formation due to chemical reaction between the dissolution products (Figure 4.4.7).

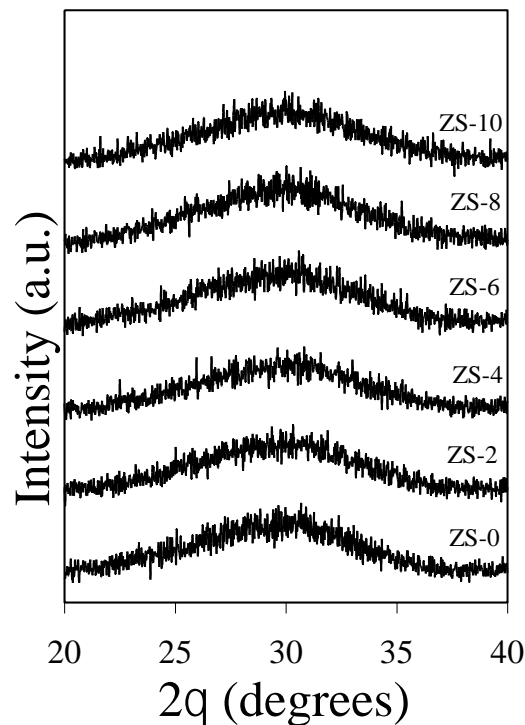


Figure 4.4.7 X-ray diffractograms of glass powder after 120 days of immersion in TRIS-HCL

The variation in pH of Tris-HCl along with weight loss of the glasses with respect to SrO and ZnO content in glasses is presented in Figure 4.4.8a. A slight change in pH of Tris-HCl from 7.54 to 7.24 was observed with increasing SrO and ZnO content in glasses after 120 h of immersion. This depicts good chemical stability of glasses which in turn should support cell viability due to the absence of sudden pH changes in the dissolution medium. A steep decrease in the weight loss of glass was observed with increasing equimolar concentrations of ZnO and SrO content up to 6 mol%. Further increase in ZnO and SrO content in glasses did not lead to any significant change in the weight loss of glasses.

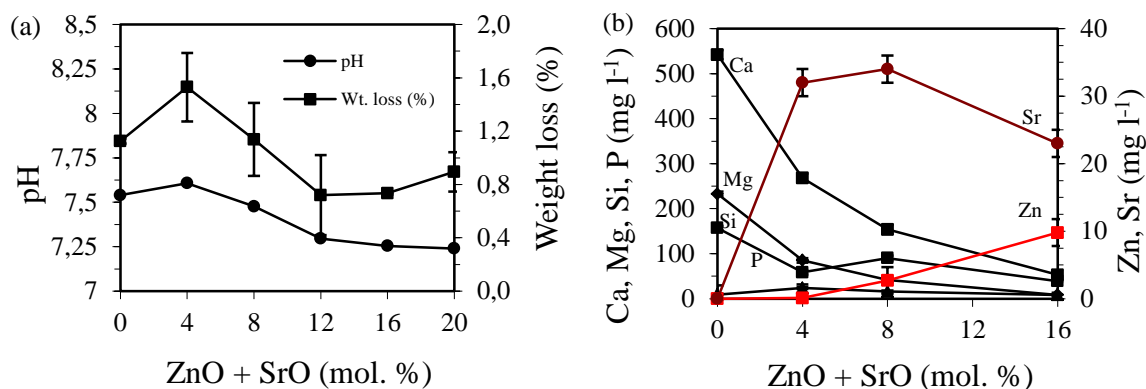


Figure 4.4.8 (a) Graphs depicting the change in solution pH and weight loss of glass powder samples (with respect to variation in ZnO and SrO content in glasses) after immersion in Tris-HCl; (b) ICP-AES plots of elemental concentrations of Ca, Mg, P, Si, Sr and Zn in Tris-HCl after 120 h of immersion of glass powder. It should be noted that Si refers to SiO_4^{4-} and P refers to PO_4^{3-} species.

With respect to the ion release profile the ICP-OES analysis revealed that studied glasses demonstrated SiO_4^{4-} ion release in the range of 39–157 ppm (1 ppm = 1 mg l⁻¹). Also increasing strontium and zinc content in the glasses decreased the release of SiO_4^{4-} species in Tris-HCl as shown in Figure 4.4.8b, thus explaining the lower chemical degradation of glasses. Previous studies have shown that SiO_4^{4-} release levels in the range 0.1–100 ppm from bioactive glass and other biomaterials show stimulatory effects on osteoblasts and the expression of TGF- β mRNA in human osteoblast-like cells [207]. Furthermore, gradual release of soluble silica over time enhances bone bonding due to the increased formation of Si-OH (silanol) groups. Therefore, it is apparent that any bioactive glass releasing SiO_4^{4-} within these ranges will have similar beneficial effects. Hence, all the glasses in the present study may possess beneficial properties towards various biological processes.

Phosphorus being a major component of the inorganic phase of human bone plays an important role in bone formation as mentioned in section 2. In the present study, the ionic concentration of phosphorus released (8.6–24 ppm; Figure 4.4.8b) from the glasses in Tris-HCl lies within the above mentioned limit required to promote favourable biological activity.

Further, Ca^{2+} ion release from experimental glasses in Tris-HCl solution decreased from 268–53 ppm (Figure 4.4.8b) probably owing to the decrease in CaO concentration in glasses. The significance of calcium in bone mineralization is well established and its gradual release over time is bound to enhance therapeutic efficacy of the glasses. Similarly,

Magnesium concentration in the extracellular fluid ranges within 17–25.5 ppm. In the present study the concentration of Mg^{2+} released from the investigated glasses in Tris–HCl solution is higher than the concentration vital for favourable biological properties. However, due to efficient excretion of Magnesium in the urine, incidences related to hyper–magnesium conditions are rare [60]. With respect to release of strontium and zinc from the studied glasses, all the glasses demonstrated a release of 23–32 ppm of strontium and 0.1–9.8 ppm of zinc over 5 days of immersion in Tris–HCl (Figure 4.4.8b). Although, the amount of strontium released from glasses is within the limits of its therapeutic efficacy, the amount of zinc released from glasses with ZnO content >4 mol% is slightly higher than required for biomedical purpose.

4.4.2.5 Cellular response on bioactive glasses

4.4.2.5.1 In vitro proliferation of MG63 cells

Figure 4.4.9 depicts the cell viability on glasses under investigation in comparison with commercially available culture plates, of ZS–2, ZS–4, and ZS–6 and ZS–8 bioactive glasses. MG-63 cells were used for the following reasons firstly, MG-63 cells display suitable integrin molecules required for cell adhesion making them a more appropriate model under the present study, secondly the response of MG-63 cells to 1,25(OH)₂D₃ administration has been shown to be similar to normal human osteoblast cells [208]. Additionally, human and MG63 cells produce cAMP in response to Parathyroid hormone therapy [209, 210]. Moreover, MG-63 cells provide an excellent model for studying the antioxidant properties of bioactive glasses as they have been used in variety of studies especially for their use in capsaicin induced apoptosis via the caspase cascade and the antioxidant enzyme system and Okadaic acid induced apoptosis through the PKR, NF- κ B and caspase pathway. These pathways are similar to the apoptotic death caused by H₂O₂ used and oxidizing agent in the present study which have earlier been used to studying protection of MG63 cells by Melatonin and Simvastatin [211, 212]. Apparently, the proliferation of MG63 cells was 89.0±4.2%, 86.7±3.9%, 80.25±3.6% and 72.8±3.1% on glasses ZS–2, ZS–4, ZS–6 and ZS–8, respectively (Figure 4.4.9a).

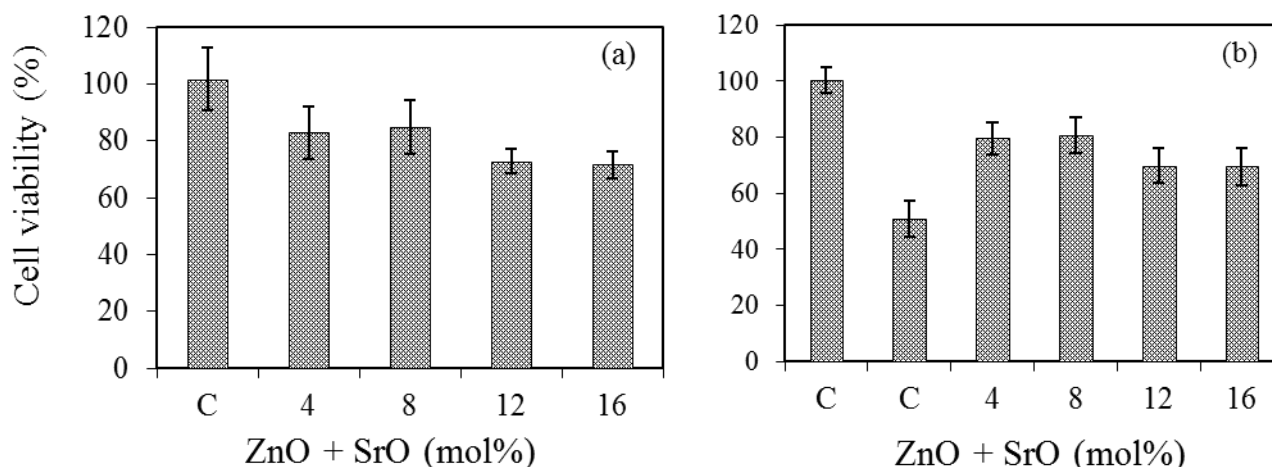


Figure 4.4.9 Plots showing the cell growth kinetics of the glasses (ZS-2, ZS-4, ZS-6, and ZS-8) (a) under normal condition during culture after 4 days under normal conditions (b) under H₂O₂ (250 μM) induced oxidative stress in MG63 cell after 3 days. *(C for control)

The antioxidant potential of investigated glasses was examined on H₂O₂ induced oxidative damage in MG63 cell line after 24 h of cell growth. H₂O₂ is one major contributor to the oxidative damage and leaks from mitochondria in the cells. According to Li et al. [213] H₂O₂ stops cells proliferation in MG63 cells by reducing the levels of cycline B1 and induction of G₂ cell cycle arrest. Although, the cell viability was higher (in comparison to control) in the presence of Sr- and Zn-doped bioactive glasses under investigation; interestingly, the cell viability decreased for SrO- and ZnO-concentration in glasses beyond ZS-4, as is evident from Figure 4.4.9b. Accordingly, the highest cell viability under oxidative stress was observed for glass ZS-2 (163%) followed by ZS-4 (151%), ZS-6 (138%) and ZS-8 (135%) when compared with control cultures at LD50 dose of H₂O₂ (Figure 4.4.9b).

4.4.3 Discussion

From MD simulation results [214], the network connectivity (NC) in the investigated glasses is ~1.95. Based on the qualitative interpretation of the correlation between solubility and NC, an empirical upper limit of NC~3 has been defined separating bioactive (NC <3) from bio-inert (NC >3) glasses [39]. According to O'Donnell and Hill [112], melt-quenched silicate glasses with NC = 2 are good candidates for bioactive materials as biological response and other properties of glasses rapidly change around this value. Invert glasses with NC below 2 usually exhibit very high dissolution rates (due to highly depolymerized glass

structure), being considered less practical in biological systems [112]. However, this empirical interpretation based on NC should be considered only as a qualitative guideline for designing bioactive glasses. As a matter of fact, our investigated glasses having a NC <2 would be expected to exhibit excessive dissolution rates and unsuitable bioactivity, which is at odds with their apatite forming ability in SBF (Figure 4.4.5) and very moderate weight loss in Tris–HCl shown in Figure 4.4.8a.

Further, the ^{29}Si MAS–NMR data reveal the predominance of Q^2 units along with considerable fraction of $Q^1(\text{Si})$ and $Q^3(\text{Si})$ in all the glasses (Table 4.4.2). The phosphate component in the glass is predominantly coordinated in orthophosphate environment thus, not contributing to the glass network backbone. This is again a desired feature because the low connectivity of phosphorus in the glass structure along with its ability to rip off the network modifying cations (mainly Ca^{2+}) from the silicate network not only facilitates the release of additional soluble phosphate species into the contact fluid which will increase the local supersaturation but also accelerate the bone bonding ability of glass by enhancing the HA deposition on the glass surface.

The network modifying role of SrO/CaO along with the intermediate role of ZnO/MgO seems to play the major role in deciding the biological efficacy of the investigated glasses. This is evident from the significant disparity in the leaching behaviour of ZnO and SrO from glasses in SBF solution or Tris–HCl despite the fact that both these oxides have been incorporated in the glasses in the equimolar concentrations. The slow release of zinc (due to its ability to enhance the strength of inter-tetrahedral cross-links) and the comparatively faster release of strontium along with other elements help in enhancing the osteoblast proliferation and anti-oxidative properties of the studied glass compositions. According to literature, strontium when released in concentrations of <10 ppm has the ability to inhibit H_2O_2 induced oxidative stress in osteoblasts (CRL-11372) within a duration of 6–12 h [215]. For concentrations >87.6 ppm, strontium becomes an apoptotic agent and induces the apoptotic effect of H_2O_2 [215]. The blood active Sr^{2+} concentration in postmenopausal osteoporotic patients treated with strontium ranelate (Protelos[®], Servier Laboratories, Ireland) has been measured to be 10.5 ppm [56]. On the other hand, zinc concentrations have been observed to follow a strict dose-dependent behaviour with their therapeutic efficacy being restricted to the dose limits of <2 ppm. According to Aina et al. [157], when the concentration of zinc released from bioactive glasses exceeds 2 ppm, it causes damage to the osteoblasts (MG63) *via* oxidative stress. In a similar study, Bergandi et al. [216] explained

the role of fluoride ions released from F-doped 45S5 Bioglass[®] in inducing the oxidative stress when in contact with MG63 human osteoblast cell line due to inhibition of the pentose phosphate oxidative pathway and, in particular, through the oxidative inhibition of glucose 6-phosphate dehydrogenase. A similar observation has been made in the present study as the glass ZS-2, which releases <1.5 ppm zinc and ~10 ppm strontium in SBF (Figure 4.4.6) exhibits antioxidant behaviour by enhancing the cell viability and negating the effect of oxidative stress induced by H₂O₂ addition in the cell culture medium. Further increasing the ZnO and SrO contents in glasses led to an increase in their released zinc and strontium concentrations. However, the decrease of their antioxidant behaviour could only be clearly noticed for the glass compositions with their respective ZnO and SrO content ≥6 mol%. Interestingly, although our glasses contain equimolar concentrations of ZnO and SrO, the release of Sr²⁺ into the SBF or Tris-HCl solutions is significantly higher than that of Zn²⁺. This depicts the importance of the structural coordination of zinc ions as intermediate in the glass structure (at variance with the stronger network modifying role of strontium, and its higher ionic field strength in comparison to strontium).

Oxidative stress plays a prominent role in bone healing and regeneration. It arises due to the formation of reactive oxygen species (ROS). ROS (•O₂⁻, •OH, H₂O₂, OCl⁻, etc.), which are generally produced in cellular mechanisms during conversion of oxygen to water (in order to produce energy) by mitochondria or during an encounter between white blood cells (WBCs) and pathogens in our body [217]. In case of a bone fracture, oxidative stress injury may be caused by an ischemia-reperfusion mechanism. In such a scenario, tissue damage is caused due to oxidative stress when blood supply returns to the tissue after a period of lack of oxygen. These radicals may cause oxidative injury to the fractured bone as has been seen in other tissues with reperfusion injury [218, 219]. The protection of MG63 cell line from H₂O₂ induced oxidative stress in the present study by alkali-free bioactive glasses (mainly by glasses ZS-2 and ZS-4) may be attributed to the anti-apoptotic effect of zinc and strontium when released in a controlled manner. It has been recently reported that zinc is involved in direct inhibition of H₂O₂ induced apoptosis by activation of the P13K/Akt and MAPK/ERK pathways [220], while in case of strontium, a recent study by Jebahi et al. [221] reports an increase in the Superoxide Dismutase (SOD), Catalase (CAT) and Glutathione Peroxidase (GPx) *in vivo* as the prominent features providing antioxidant behaviour to the materials doped with these trace elements. In the overall context of bone healing and regeneration, the as designed glasses are potential candidates for applications in the treatment of osteoporosis.

4.4.4 Conclusions

The effects of co-doping of zinc and strontium on the structure, chemical dissolution behaviour of alkali-free phosphosilicate glasses and its impact on their apatite forming ability, osteoblast proliferation and antioxidant behaviour have been studied with NMR, FTIR, XRD, chemical degradation and cell culture experiments. An increase in the Zn^{2+}/Mg^{2+} and Sr^{2+}/Ca^{2+} ratio did not induce any significant change in Q^n speciation and network connectivity, as revealed by MAS-NMR. The chemical durability of investigated glass improved (as observed from Tris-HCl studies), however all the glasses exhibit good apatite forming ability. The glass ZS-2 which releases < 1.5 ppm zinc and ≤ 10 ppm strontium in SBF, is exhibiting good antioxidant behaviour by enhancing the cell viability and negating the effect of oxidative stress induced by H_2O_2 addition in the cell culture medium. However, further increase in ZnO and SrO content in glasses led to an increase in their released zinc and strontium concentrations, thus, decreasing their antioxidant behaviour. Thus zinc concentration < 1.5 ppm has an anti-oxidant effect. The anti-oxidant behaviour may be attributed to the anti-apoptotic effect of zinc and strontium when released in a controlled manner. Although promising results suggest possible clinical use of bioactive glass, further investigations of long-term outcomes are going on for the glass to be used in orthopaedic applications.

4.5 Thermo-mechanical behaviour of alkali-free bioactive glass-ceramics co-doped with strontium and zinc

4.5.1 Introduction

TE has emerged as an effective approach in response to the challenges in reconstructive and orthopaedic surgeries which involve restoring the diseased or damaged tissue by applying a combination of functional cells and scaffolds made of synthetic biomaterials. TE offers a feasible solution to the problems associated with the allograft and autograft [23]. This approach requires scaffolds with a well-defined architecture which not only provide temporary mechanical strength but also act as guiding channels for cell proliferation and tissue ingrowths [161]. The ideal scaffold should (i) be biocompatible (non-toxic) and should promote cell adhesion and proliferation; (ii) exhibit mechanical properties that are comparable to those of the tissue to be replaced; (iii) exhibit controlled degradation rate and should degrade into nontoxic products that can be easily resorbed or excreted by the body; and (iv) be capable of being machined easily into required shapes [161]. All these properties are highly dependent on the substrate material properties and it is due to this reason that the choice of the material plays an important role in designing a suitable scaffold.

In today's scenario, bioactive glass-ceramics are considered to be potential materials for bone TE because of a number of salient features not only in relation with their good bioactivity but also owing to their good sintering ability, high mechanical strength and controlled chemical degradability [141, 189, 206]. The aim of the present section is understand the influence of co-doping of Zn^{2+} and Sr^{2+} on the thermal and mechanical behaviour of TCP-20. Although, good amount of literature is available on the influence of these two ions on various properties of bioactive glasses on individual basis as mention in section 4.4, it is rare to find literature describing the influence of both these ions on thermal behaviour of glasses.

4.5.2. Results and Discussion

4.5.2.1 Glass-forming ability

For all the investigated glass compositions shown in Table 4.4.1, melting at 1570 °C for 1 h was sufficient to obtain bubble-free, transparent and XRD-amorphous glasses.

4.5.2.2 Thermal analysis

The DTA thermographs of fine glass powders with $\beta = 20 \text{ K min}^{-1}$ are shown in Figure 4.5.1. All the glass compositions feature a single endothermic dip which corresponds to T_g before T_c followed by an exothermic crystallization curve. The characteristic parameters obtained from DTA thermographs are summarized in the Table 4.5.1. In general, T_g decreases with increase in SrO and ZnO content in glasses. This decrease in T_g can be attributed to decrease in oxygen density (ρ_o) of glasses with addition of SrO and ZnO as shown in Figure 4.5.2. Oxygen density is a measure of compactness of the glass structure and can be calculated by using the following relation [114]:

$$\rho_o = \frac{M(O) \times (2x_{SiO_2} + 5x_{P_2O_5} + x_{SrO} + x_{CaO} + x_{ZnO} + x_{MgO})}{M_v}$$

Where, $M(O)$ is the molecular mass of oxygen atom and x corresponds to the molar concentration of the respective oxides and M_v corresponds to the molar volume of the glasses. In general, the decrease in oxygen density points towards the expansion of glass structure resulting in the weakening of the glass network and an associated decrease in T_g .

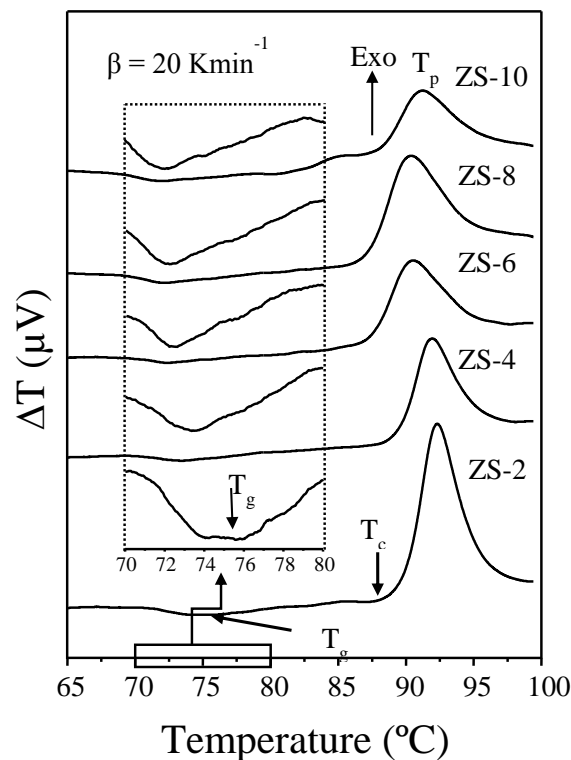


Figure 4.5.1 DTA thermographs of glasses at a heating rate of 20 K min^{-1} .

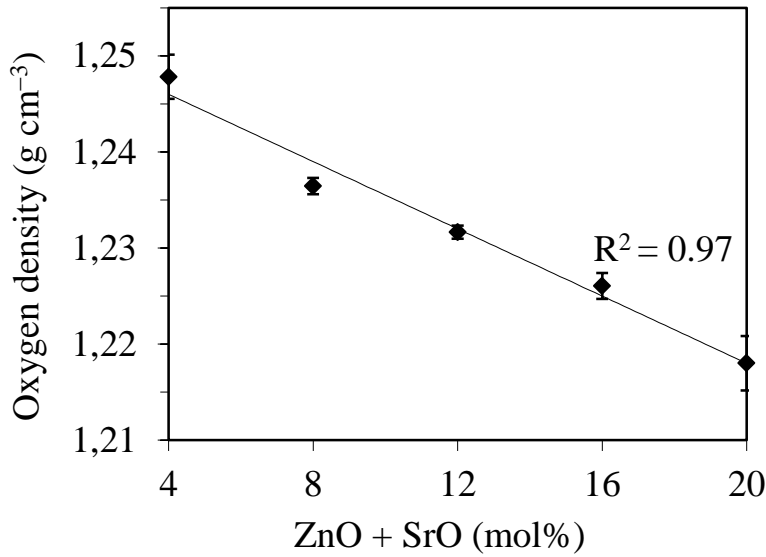


Figure 4.5.2 Oxygen density plotted against percentage zinc and strontium substitution.

Table 4.5.1 Thermal parameters measured from DTA at 20 K min⁻¹.

	ZS-2	ZS-4	ZS-6	ZS-8	ZS-10
T _c (±2 °C)	885	884	871	866	870
T _g (±2 °C)	756	734	725	721	720
ΔT(=T _c -T _g)	129	150	146	145	150

4.5.2.3 Sintering and Crystallization behaviour

Figure 4.5.3 presents variation in the relative area and heat flow with respect to temperature as obtained from HSM and DTA, respectively, for all the investigated glasses at a similar heating rate of 5 K min⁻¹. Table 4.5.2 summarizes the values of the temperature of first shrinkage (T_{FS}; log η = 9.1 ± 0.1, η is viscosity in dPa s), temperature for maximum shrinkage (T_{MS}; log η = 7.8 ± 0.1) and ratio of the final area/initial area of the glass powder compact (A/A₀) at T_{MS1}, as obtained from the HSM data along with temperature for T_c and T_p, as obtained from the DTA of the glasses.

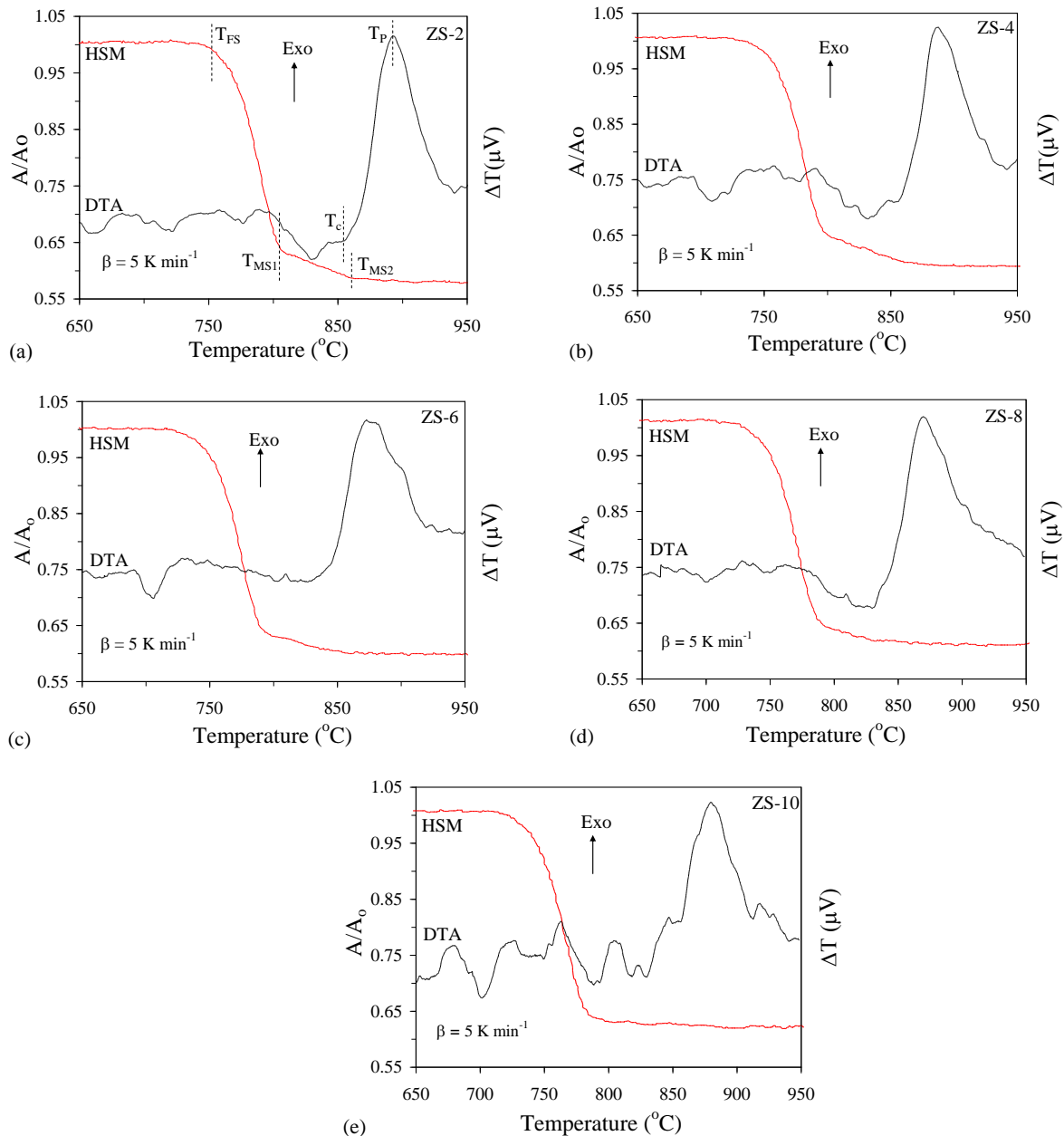


Figure 4.5.3 Comparison of DTA and HSM curves under the same heating rate (5 K min^{-1}) for compositions: (a) ZS-2, (b) ZS-4, (c) ZS-6, (d) ZS-8 and (e) ZS-10.

- (i) T_{FS} decreased monotonically from 765 to 740 °C with increasing SrO/CaO and ZnO/MgO ratios.
- (ii) Two stage sintering behaviours, with the main shrinkage occurring along the first step, were observed for glasses ZS-2, ZS-4 and ZS-6, while a gradual shift to single stage shrinkage was registered for glasses ZS-8 and ZS-10 (Figure 4.5.3). The first sintering stage is accomplished at T_{MS1} while the second one at T_{MS2} . In all the glass compositions T_{MS1} was observed at temperatures lower than T_c (i.e., $T_{MS1} < T_c$). This

feature will ensure the production of well sintered and mechanically strong glass powder compacts. The second stage of densification occurred in competition with crystallization and ended at temperatures higher than T_c . This depicts that shrinkage continued in the glass powders even after onset of crystallization, possibly due to the presence of residual glassy phase in the glass-ceramics.

- (iii) The thermal stability parameter, $\Delta T = T_c - T_g$ varied from 129 °C for ZS-2 to ~150 °C for the remaining compositions (ZS-4 to ZS-10), Table 4.5.1. This suggests that thermal stability was enhanced with the increasing amounts of ZnO and SrO within the composition range, thus favouring densification during sintering. On the other hand, no particular trend could be observed for the variation in S_c values reported in Table 4.5.2. However, all the glasses exhibited a comfortable $T_c - T_{MS}$ difference which enables delaying the nucleation events thus, providing a wide processing window for attaining maximum densification [23].
- (iv) The DTA thermographs of glasses (ZS-2 to ZS-8) exhibited single crystallization exothermic curves. This signifies that the obtained glass-ceramics are formed either as a result of single phase crystallization or of an almost simultaneous precipitation of more than one crystalline phase. The two distinct exothermic events observed for ZS-10 suggests the almost simultaneous precipitation of two crystalline phases
- (v) Values of A/A_0 ranged from 0.65 to 0.67 (Table 4.5.3) for all the glasses implying towards good densification levels of 95–98%.

Table 4.5.2 Thermal parameters measured from DTA and HSM at 5 K min⁻¹

	ZS-2	ZS-4	ZS-6	ZS-8	ZS-10
T_{FS} (± 5 °C)	765	752	748	746	740
T_{MS1} (± 5 °C)	803	794	790	789	782
T_{MS2} (± 5 °C)	862	865	854	–	–
T_c (± 2 °C)	855	856	831	829	855
T_p (± 2 °C)	892	887	872	869	879
$S_c (= T_c - T_{MS1})$	52	62	40	41	73
A/A_0 at T_{MS1} (± 0.02)	0.65	0.67	0.65	0.65	0.65

4.5.2.4 Structural transformation in glasses during heat treatment:

4.5.2.4.1 XRD

In agreement with HSM and DTA data, Figure 4.5.4a shows that amorphous glass powder compacts were obtained for the ZS-2 and ZS-4 samples after sintering for 1 h at 800 °C, while crystalline peaks corresponding to strontium-containing FA (Sr-fluorapatite) ($\text{Sr}_{0.59}\text{Ca}_{4.41}(\text{PO}_4)_3$) (ICDD card: 01-070-3522) with a maximum intensity at $2\theta = 31.75^\circ$ were observed for the other compositions (ZS-6 – ZS-10). Further increase in temperature to 850 and 900 °C led to the crystallization of strontium containing Di phase (Sr-Diopside), ($\text{Sr}_{0.15}\text{Ca}_{0.75}\text{Mg}_{1.1}(\text{Si}_2\text{O}_6)$) (ICDD card: 04-015-0688) in all the glass-ceramics. The XRD data revealed that solid solutions involving partial substitution of Ca^{2+} by Sr^{2+} in FA and Di crystal structures were formed. Considering the higher ionic radius of Sr^{2+} (132 Å) in comparison to that of Ca^{2+} (114 Å), variations in lattice parameters are likely to occur. As a matter of fact, Figure 4.5.4b-c shows slight shifts in the peak positions to lower 2θ angles, especially in case of Sr-FA. Concerning the evolution of the XRD peaks with increasing contents of SrO and ZnO in the glass-ceramics, Figure 4.5.4b-c also show two opposite trends for the two identified crystalline phases. Namely, the intensity of the XRD peaks increases for Sr-FA and decreases for Sr-Di.

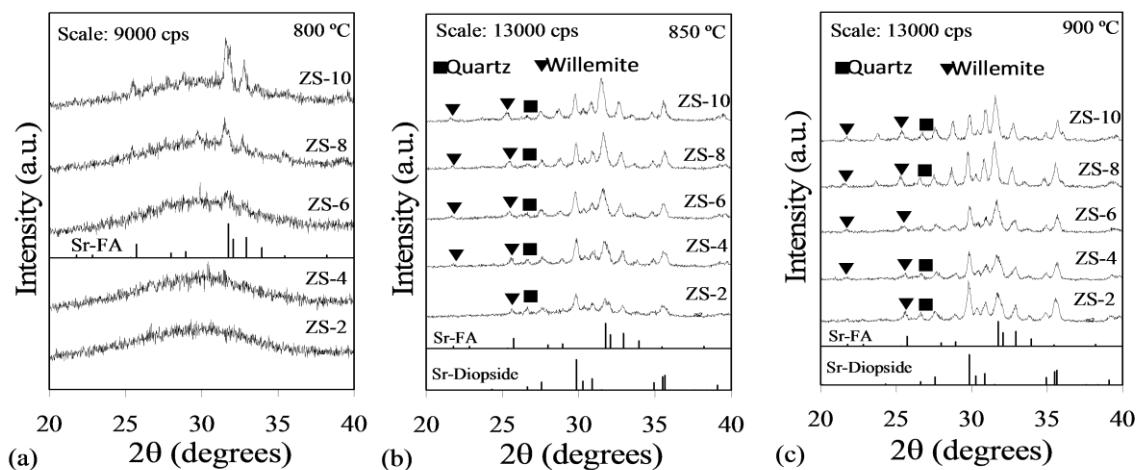


Figure 4

Figure 4.5.4 X-ray diffractograms of glass-ceramics heat treated for 1 h at: (a) 800 °C, (b) 850 °C and (c) 900 °C.

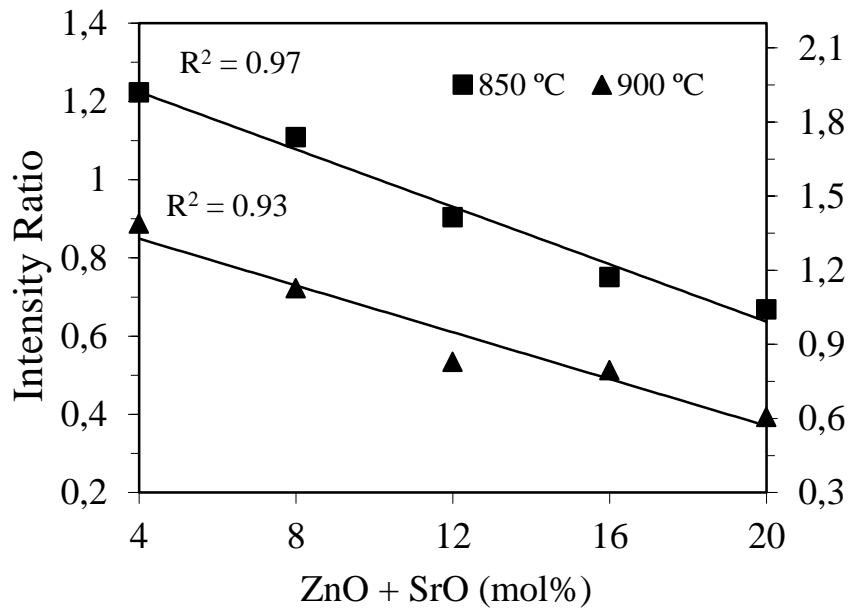


Figure 4.5.5 Intensity ratio of the main XRD intensity peaks of Sr-diopside to Sr-fluorapatite plotted against percentage of zinc and strontium substitution for glass-ceramics heat treated for 1 h at 850 °C and 900 °C.

Figure 4.5.5 shows the variation of the ratio between the highest intensity XRD peaks of Sr-Di / Sr-FA with respect to the ZnO + SrO content in the glass. Linear decreasing intensity trends are observed. The decrease in Sr-Di phase with increasing SrO/CaO and ZnO/MgO ratios can be attributed to the decrease in the Mg content in the glass network due to ZnO substitution. Along with the two major crystalline phases mentioned above, low-quartz (SiO_2) and willemite (Zn_2SiO_4) also precipitate out as minor phases in the glass-ceramics sintered at 850 and 900 °C. It is worth noting that the presence of willemite as minor phase indicates that zinc predominantly remains in the residual glassy phase.

Representative SEM images and EDS data collected in the areas indicated in the SEM micrographs are shown in Figure 4.5.6 for glass-ceramics ZS-8 samples sintered for 1 h at different temperatures. At 800 °C, the microstructure is essentially amorphous and the few FA crystals are still isometric. With increasing the sintering temperature, the typical elongated morphology of FA became evident. Although the results are informative, there are significant deviations in the measured atomic percentages of the different elements relatively to those planned for the starting glass compositions or relatively to their proportions in the crystalline phases. This is not surprising considering that the area being analysed is larger than a single crystal and the measured result is influenced by the surrounding area. In

contrast, there is a good agreement between the XRD results (Figure 4.5.4) and the SEM observations (Figure 4.5.6).

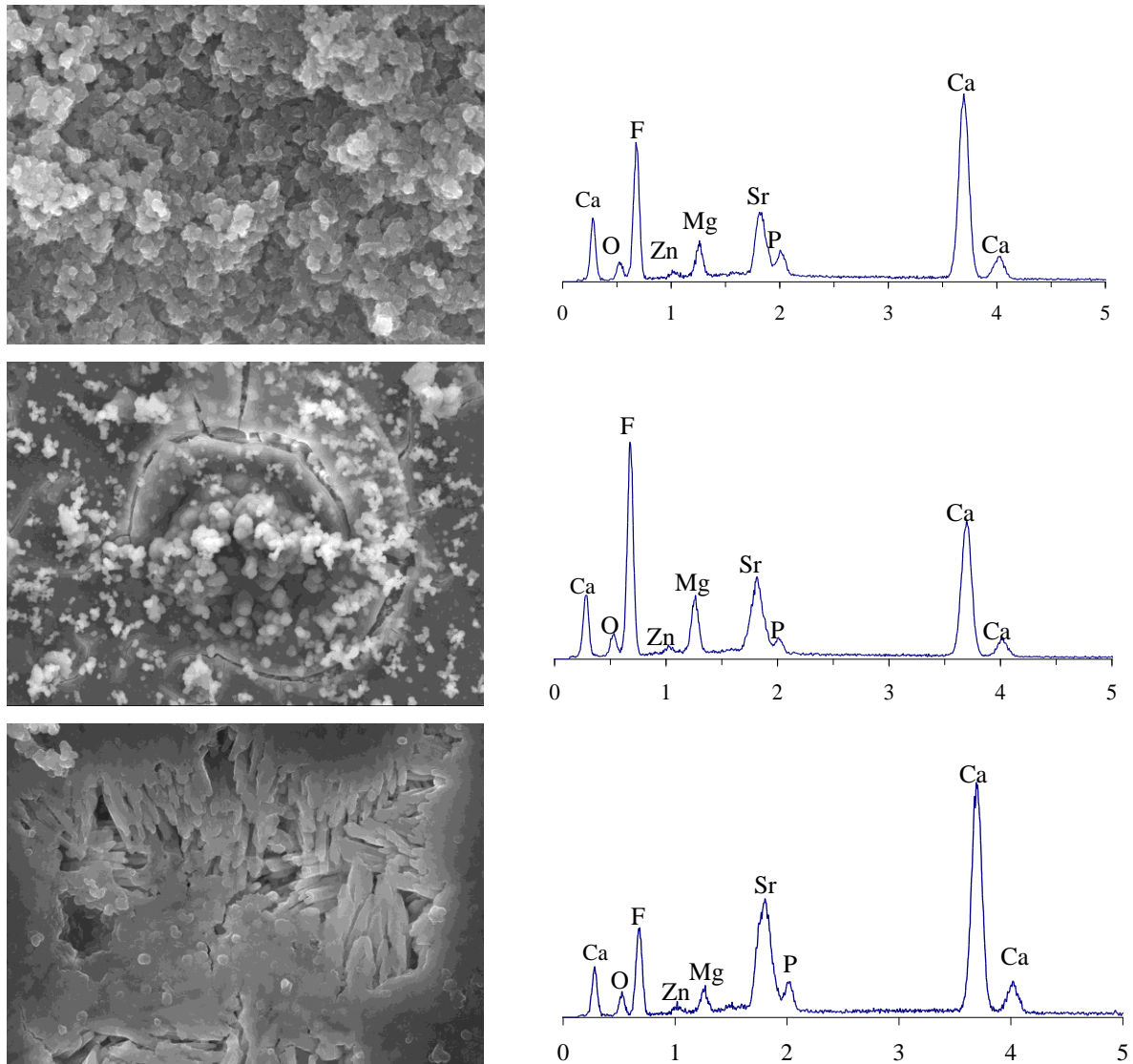


Figure 4.5.6 SEM images and EDS results of glass-ceramic ZS-8 sintered for 1 h at: (a) 800 °C, (b) 850 °C, (c) 900 °C, after a heating rate ramp of 5 K min⁻¹.

4.5.2.5 Mechanical Behaviour:

The flexural strength was calculated for powder compacts sintered at 800, 850 and 900 °C (Figure 4.5.7). Despite their highly amorphous nature, the glass powder compacts sintered at 800 °C exhibited flexural strength of ~ 60 – 70 MPa depicting their good sintering ability.

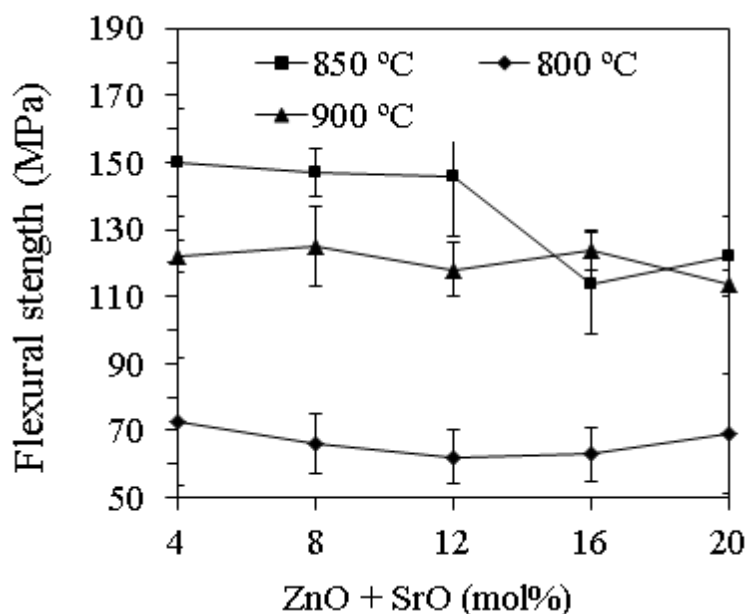


Figure 4.5.7 Flexural strength of glass-ceramics heat treated for 1 h at: (a) 800 °C, (b) 850 °C and (c) 900 °C, using a heating rate of 5 K min⁻¹.

Further, higher values of flexural strength were obtained for glass-ceramics sintered at 850 °C as sintering at 900 °C led to a decrease in their mechanical strength. The variation in mechanical strength with the sintering temperature can be explained on the basis of crystalline phase evolution, including the type of predominating phase and, eventually, the size of crystals formed in these glass-ceramics. The mechanical strength was firstly enhanced with the predominate formation of Di, a mechanically strong crystalline material. Therefore, the relatively higher intensity XRD peaks of Di in glass-ceramics sintered at 850 °C in comparison to their counterparts sintered at 800 and 900 °C suggests an enhanced fraction of this phase that confers to these samples higher mechanical strength. At 900 °C, FA became the dominant crystalline phase in glass-ceramics with higher SrO and ZnO content. This resulted in lower mechanical strength owing to the poor mechanical properties of FA in comparison to Di [131].

4.5.3 Discussions

We have investigated the influence of strontium and zinc oxides on the sintering and mechanical behaviour of alkali-free bioactive phosphosilicate glass-ceramics. The increase in SrO and ZnO concentration leads to the expansion of the glass structure and to concomitant decreases in T_g . all the investigated glasses exhibit good sintering behaviour and good

flexural strength with Sr-diopside and Sr-fluorapatite evolved as the major crystalline phases in the glass-ceramics along with willemite and quartz as minor phases. Due chemical similarity between strontium and calcium increase in concentration of SrO at the expense of CaO led to the partial replacement of Ca^{2+} by Sr^{2+} in the FA crystal structure whereas ZnO predominantly remained in the glassy phase.

4.6 Understanding the influence of composition on structure bioactive and thermal behaviour of Diopside – Tricalcium phosphate based glasses

4.6.1 Introduction

The present work aims at gaining an insight about the influence of composition on the structure, bioactivity and thermal behaviour in alkali-free bioactive glasses in the CaO–MgO–SiO₂–P₂O₅ system designed along Di–TCP binary join by varying Di/TCP ratio and These glass compositions are derived from the ternary Di–FA–TCP system which has been extensively studied in this thesis. Furthermore, the glass compositions derived from these binary and ternary systems have been regarded with much of interest to biomaterials community for their potential applications in bone regeneration and tissue engineering [131-134, 139, 140, 222].

Table 4.6.1 Nominal composition of the as-designed glasses (mol%).

Glasses	CaO	MgO	SiO ₂	P ₂ O ₅
Di-0	75	–	–	25
Di-10	68.13	3.43	6.87	21.57
Di-20	61.82	6.59	13.18	18.41
Di-30	55.99	9.5	19.02	15.49
Di-40	50.57	12.22	24.42	12.79
Di-50	45.55	14.73	29.44	10.28
Di-60	40.88	17.06	34.12	7.94
Di-70	36.52	19.24	38.48	5.76
Di-80	32.44	21.28	42.57	3.71
Di- 90	28.60	23.20	46.40	1.80
Di-100	25.00	25.00	50.00	–

4.6.2 Results

4.6.2.1 Glass forming ability

For all the investigated compositions (Table 4.6.1), we could obtain amorphous glasses only from compositions with Di \geq 50 wt%. The melting of compositions with Di content varying between 30–50 wt% at 1570 °C for 1 h resulted in a highly viscous liquid which was prone to spontaneous crystallization even after quenching in cold water, thus resulting in a white, opaque material. Decreasing further the Di content to 20 wt% led to the

formation of highly viscous, non-homogeneous melt under the same experimental conditions. Therefore, the present study will be dedicated towards the investigation of structure, bioactivity and chemical degradation of glasses with Di content varying between 50 – 100 wt%.

4.6.2.2 Structure of glasses by MAS-NMR

The ^{29}Si MAS-NMR spectra of the glasses are shown in Figure 4.6.1a. All glasses exhibit a broad peak with full width half maximum in the range of 16–17 ppm centred around –81 to –82 ppm indicative of dominance of Q^2 units silicate species [188]. There is a slight change in the peak position towards higher ppm up to Di-90; afterwards the peak shifts towards less negative ppm.

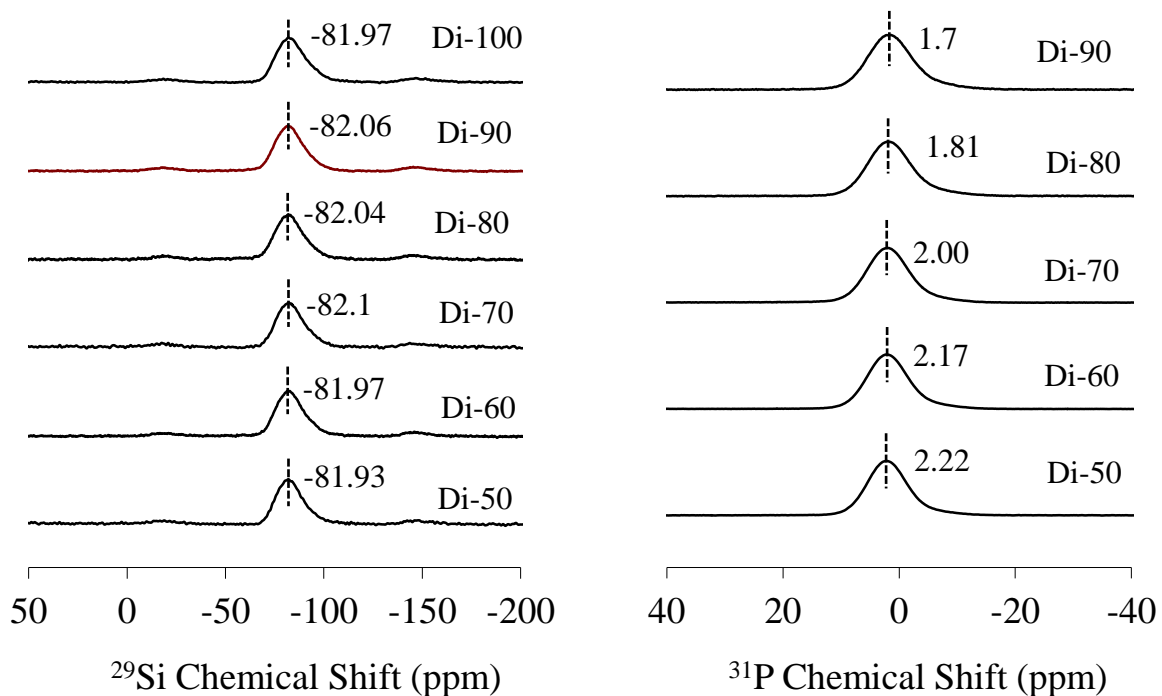


Figure 4.6.1 MAS NMR spectra of investigated glasses showing the peak positions of (a) ^{29}Si and (b) ^{31}P .

Figure 4.6.1b represents the ^{31}P spectra of the investigated glass samples. Irrespective of the content of the modifiers in the glasses, all the spectra are characterised by a relatively symmetric peak with chemical shift within the range of 1–3 ppm with an approximate line width of 8–9 ppm. The line width and the chemical shift values correspond to phosphorus in

orthophosphate environment (Ca–Mg orthophosphate). A downfield shift from 2.2–1.7 ppm was observed with the increments in Di content.

In general, infrared spectra of all investigated glasses exhibit three broad transmittance bands in the region of 300–1300 cm^{-1} (Figure 4.6.2). This lack of sharp features is indicative of the general disorder in the silicate and phosphate network mainly due to a wide distribution of Q^n units occurring in these glasses. The most intense bands in the 800–1300 cm^{-1} region correspond to the stretching vibrations of the SiO_4 tetrahedron with a different number of BO atoms [205]. In all the glasses this band further split in two transmittance bands, a low frequency band at 940 cm^{-1} and a second band in the range 1030–1038 cm^{-1} . The high frequency bands can be assigned to the Si–O asymmetric stretching mode of BOs, whereas the $\sim 940 \text{ cm}^{-1}$ may be attributed to the Si–O asymmetric stretching mode of the NBOs [205, 223]. While the weak 750 cm^{-1} shoulder may be due to Si–O–Si symmetric stretching with simultaneous Si cation motions. Further, a weak shoulder $\sim 600 \text{ cm}^{-1}$ corresponds to P–O bending modes [206].

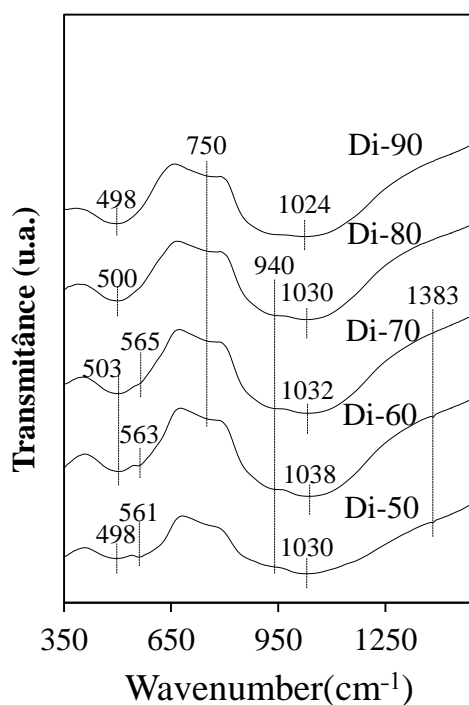


Figure 4.6.2 FTIR spectra of the investigated glasses

4.6.2.3 SBF immersion studies

The immersion of glass powders in SBF for varying time durations led to a considerable change in the glass chemistry that occurred due to the reaction between glass

and SBF (Figure 4.6.3). The soaking of glass powders in SBF for 1 h resulted in the splitting of a strong low frequency band in the region 350–650 cm^{-1} into two small bands at $\sim 470 \text{ cm}^{-1}$ and $\sim 563 \text{ cm}^{-1}$ (Figure 4.6.3a). The band centred around 470 cm^{-1} can be ascribed to a deformation mode of the silica gel layer that develops on the dissolution of glass particles [83], while small band at $\sim 563 \text{ cm}^{-1}$ characteristic phosphates as it corresponds to P–O bending vibrations in a $(\text{PO}_4)^{3-}$ tetrahedron. The band now occurring at $\sim 1060 \text{ cm}^{-1}$ and a nearby shoulder, centred at $\sim 1240 \text{ cm}^{-1}$ are attributed to Si–O–Si vibration [147]. These bands indicate the development of interfacial high–area silica gel layer, as postulated in Hench’s inorganic reactions set [20] and can be observed in all the glasses. After 6 h of immersion the bands pertaining to the formation of complex carbonates 875, 1430, 1485 cm^{-1} and silica gel layer ($\sim 1235 \text{ cm}^{-1}$) became more evident (not shown). Further, an increase in immersion time up to 24 h (Figure 4.6.3b), resulted in the sporadic appearance of new bands around 798 and 960 cm^{-1} , indicating towards silica gel layer, and also, band at $\sim 560 \text{ cm}^{-1}$ suggests the presence of non-apatitic or amorphous calcium phosphate, which is usually taken as an indication of the presence of precursors to HA. Immersion of glass powder for 3 days (Figure 4.6.3c) led to the formation of well-defined bands in all the glasses at ~ 563 and 604 cm^{-1} , attributed to crystalline apatite. After 14 days of immersion (Figure 4.6.3d), no new bands formation could be seen apart from the increase in intensity of the bands corresponding to crystalline apatite i.e., at ~ 563 and 604 cm^{-1} , indicating an increase in crystallinity. In addition, a small band at $\sim 1420 \text{ cm}^{-1}$ along with a broad but intense band at $\sim 850 \text{ cm}^{-1}$ present in all glasses.

In agreement with the FTIR results, the XRD patterns of the samples immersed in SBF for different time periods are displayed in Figure 4.6.4. Although there are a few sporadic peaks apparently related to hydroxyapatite (HA) even after 1 h of immersion (see Di–80), the indubitable formation of crystalline HA at the surface of the samples Di–50 – Di–90 only becomes clearly evident after 3 days of immersion. With the increase in immersion time to 14 days, the intensity of XRD peaks increased irrespective of the glass composition (Di–50 – Di–90). Further, the formation of any calcium carbonate (CaCO_3) polymorphs along the entire immersion period was not observed whereas, formation of calcite under similar testing conditions has been reported for pure Di glass [105].

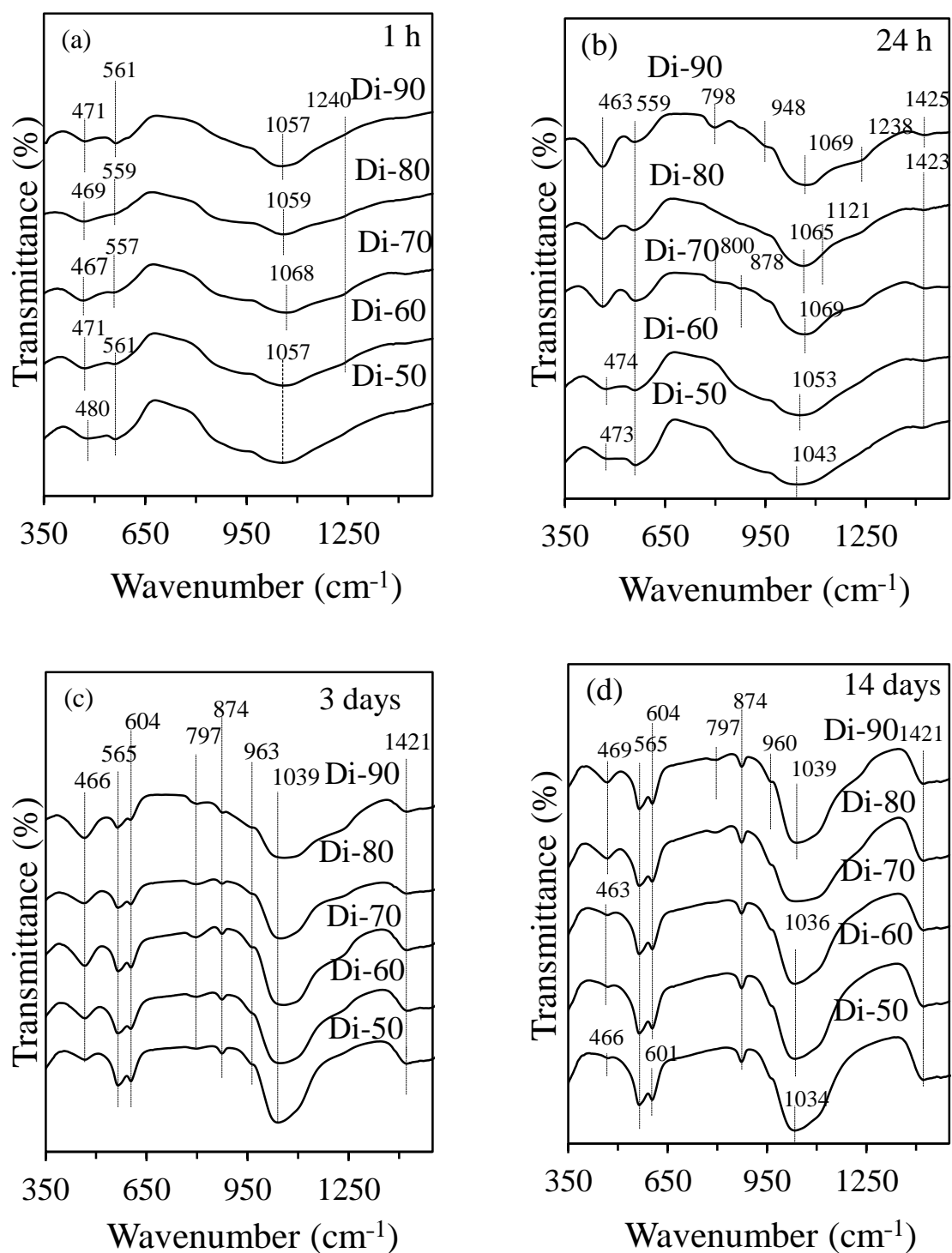


Figure 4.6.3 FTIR spectra of glasses powders after immersion in SBF solution for (a) 1 h, (b) 24 h, (c) 3 days, and (d) 14 h.

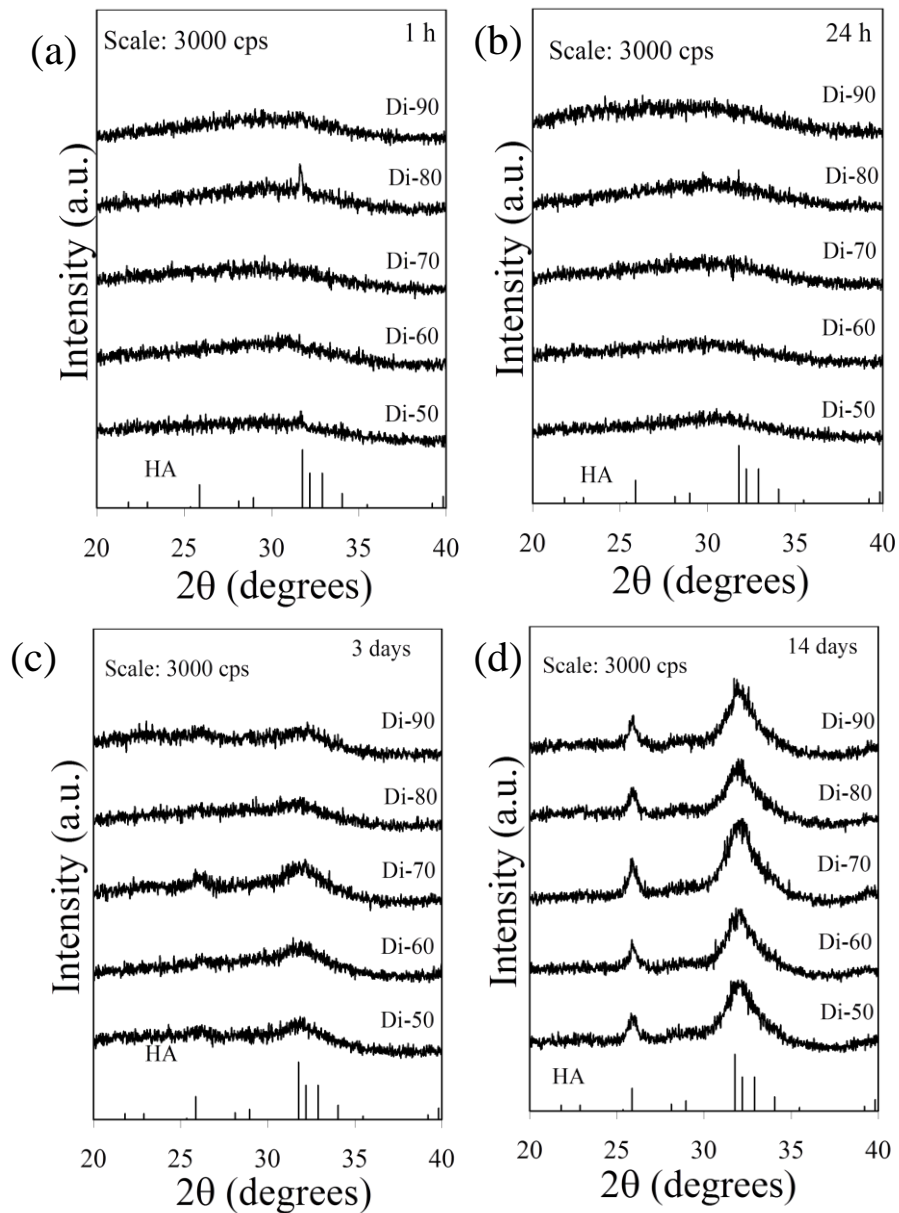


Figure 4.6.4 X-ray diffractograms of glass powders before and after immersion in SBF solution for (a) 1 h (b) 24 h (c) 3 days and (d) 14 days. HA refers to hydroxyapatite.

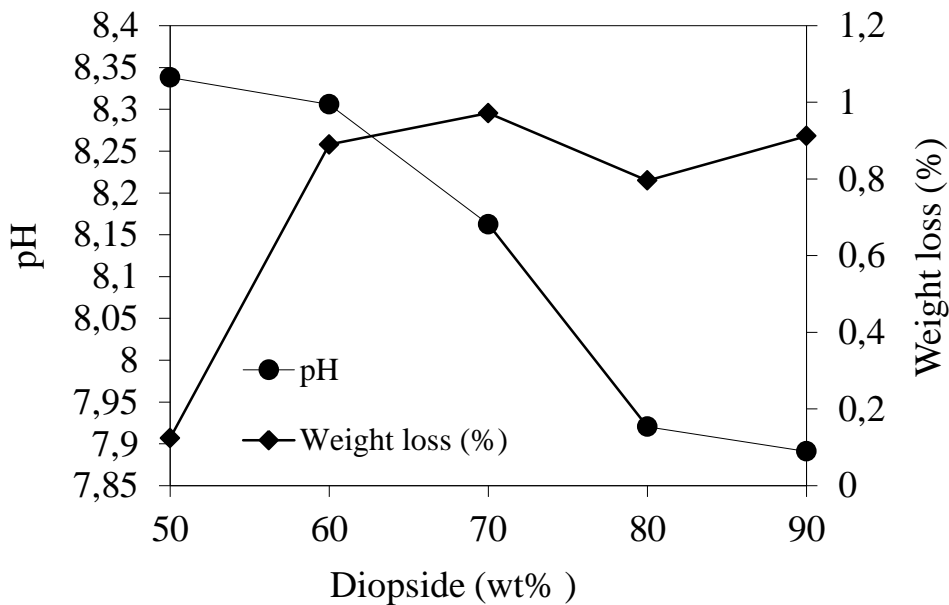


Figure 4.6.5 Variations in pH and weight loss of glass powders upon immersion in Tris-HCl solution for 7 days

4.6.2.4 Chemical degradation of glasses in Tris-HCl

Chemical durability of the glasses is a critically dependent on the pH and the nature of the solution. The leaching behaviour depends on the diffusability of the ions which determined by the ionic field strength of the ions and structure of the glasses. In the present case, a slight in pH of Tris-HCl solution from 7.8 to 8.33 was observed with increasing TCP content (Figure 4.6.5). The increase in the final pH value with increasing TCP content can be attributed to the increase in the CaO content in the glass. However, the weight loss of the analysed samples (Figure 4.6.5), does not reflect well the expected mass balance through the ion exchange, in particular less weight loss of the sample Di-50 (~0.12%).

Glasses with TCP content varying between 10 – 40 wt.% did show some stability in observed weight loss, thus approaching more the expected trend when one considers that the weight losses derived only from the passage of species from the solid to the solution. Further, all the glasses were XRD amorphous (Figure 4.6.6) after immersion in Tris-HCl solution for 7 days.

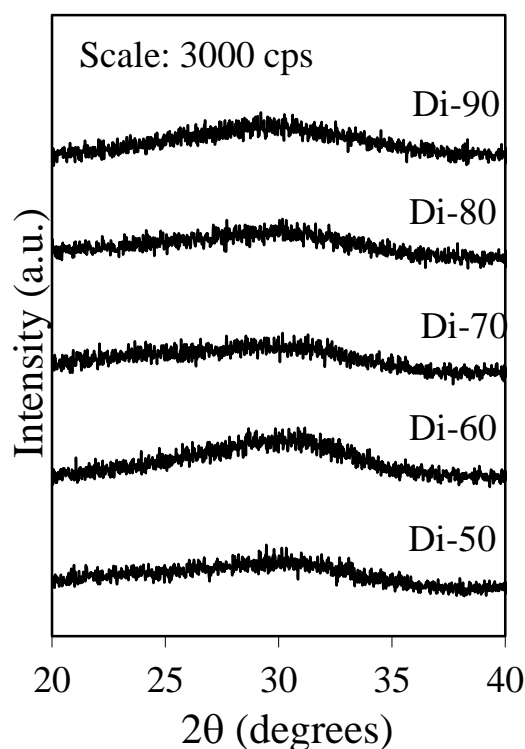


Figure 4.6.6 X-ray diffractograms of glass powder after 120 days of immersion in TRIS-HCL

Table 4.6.2 Thermal parameters measured from DTA at 20 K min⁻¹.

Glasses	T _g (±2)	T _c (±2)	ΔT
Di-50	747	825	78
Di-60	748	861	113
Di-70	748	881	133
Di-80	749	901	152
Di-90	736	880	144
Di-100	744	839	95

4.6.2.5 Thermal analysis

The DTA thermographs of fine glass powders with $\beta = 20 \text{ K min}^{-1}$ are shown in Figure 4.6.7. All the glass compositions feature a single endothermic dip between 748–736 °C before the T_c, corresponding to T_g, estimated from the inflection temperature in DTA curve where the first derivative is null [224]. This thermal event was then followed by a single exothermic crystallization peak/band for glasses Di-60 to Di-100, whereas two crystallization peaks points (T_{p1} and T_{p2}) were observed in glass Di-50. We could not

observe any significant differences in the variation of T_g values with varying Di/TCP ratio in the glasses. The characteristic thermal parameters, T_g , T_c and thermal stability, defined as $\Delta T (=T_c - T_g)$ obtained from DTA thermographs are summarized in the Table 4.6.2. The thermal stability parameter, $\Delta T = T_c - T_g$ varied from 78 °C for Di-50 to ~152 °C for Di-80.

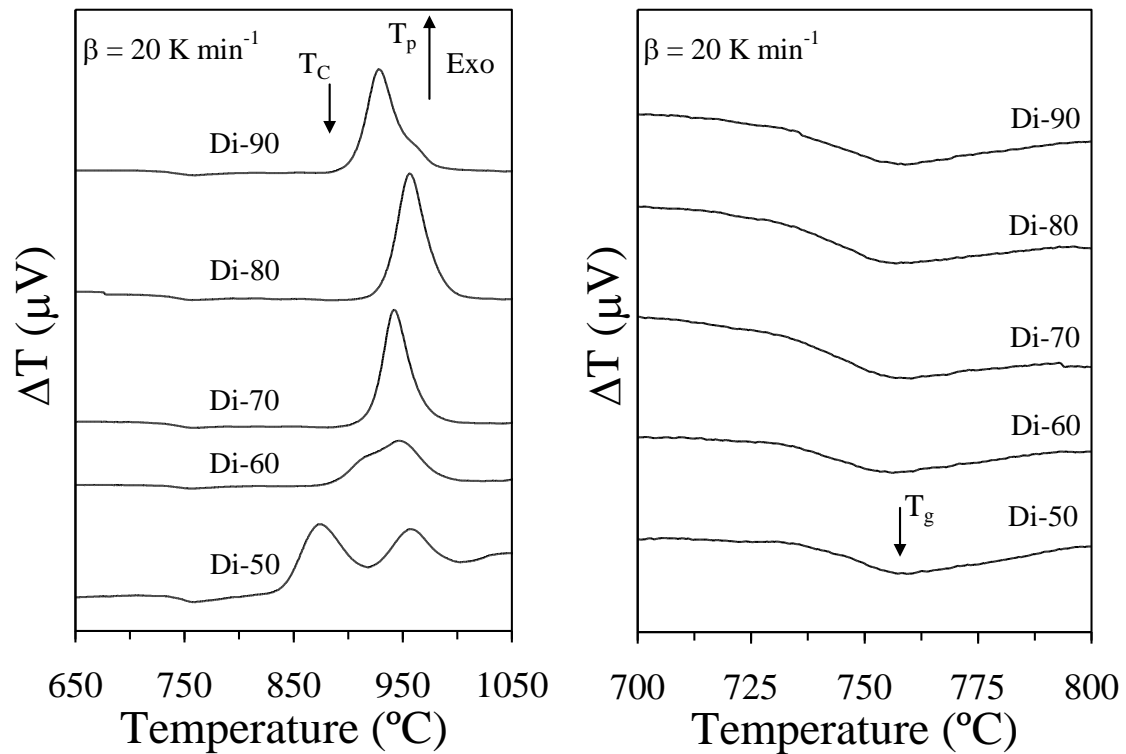


Figure 4.6.7 DTA thermographs of glasses at a heating rate of 20 K min⁻¹

4.6.2.6 Sintering and crystallization behaviours

The variations in the relative area and heat flow as functions of the heat treatment temperature as obtained from HSM and DTA, respectively, under a similar heating rate of 5 K min⁻¹ are presented in Figure 4.6.8a–f for all the investigated glasses. The DTA thermographs of glasses with Di contents varying between 60 and 100 wt.% exhibit single crystallization exothermic peaks Figure (4.6.8b–f), confirming the crystallization behaviour discussed above observed under a higher heating rate of 20 K min⁻¹. Table 3 summarizes the values of some relevant thermal parameters including the temperature of first shrinkage (T_{FS} ; $\log \eta = 9.1 \pm 0.1$, η is viscosity in dPa s), temperature for maximum shrinkage (T_{MS} ; $\log \eta = 7.8 \pm 0.1$) and ratio of the final area/initial area of the glass powder compact (A/A_0) at T_{MS1} , as obtained from the HSM data. The temperatures corresponding T_c , and T_p obtained from

the DTA of the glasses are also reported. From these DTA and HSM results the following observations can be made:

1. The temperature of first shrinkage (T_{FS}) showed a slight increase with increasing TCP contents in the glasses before decreasing abruptly to at Di-50;
2. The first sintering stage is accomplished at T_{MS1} while the second one at T_{MS2} . In all the glass compositions (except the extreme ones Di-50 and Di-100), T_{MS1} was lower than T_c meaning that maximum shrinkage was reached before onset of crystallization. The second stage of densification T_{MS2} occurred in much smaller extent and in competition with crystallization, ending at temperatures around T_c . This general trend is more obvious in the intermediate glass compositions from Di-60 to Di-90.
3. The sintering parameter, defined as $S_c = T_c - T_{MS}$, reflects the extent of separation between the sintering and crystallization events in the temperature scale. The S_c values for all investigated glasses are reported in Table 4.6.3. Initially the sintering ability increased with increase in TCP content until glass Di-80, while further TCP increments led to its degradation. In case of Di-100, T_{MS} coinciding with T_c , $S_c (T_c - T_{MS}) = 0$ as shown in Figure 4.6.8f.
4. The values of the A/A_0 ratio between the area (A) of the sample at T_{MS} to its initial area (A_0) decreased from 0.94 in Di-50 (the less prone composition for sintering) to 0.66 in Di-90. Except for Di-50, all other glass-powder compacts exhibited good densification with A/A_0 ratios varying within the range of 0.72 – 0.66.

Table 4.6.3 Thermal parameters (°C) and A/A_0 ratio derived from DTA and HSM at 5 K min^{-1} .

	$T_{FS} (\pm 5)$	$T_{MS1} (\pm 5)$	$T_{MS2} (\pm 5)$	$T_c (\pm 2)$	$T_p (\pm 2)$	$T_{p2} (\pm 2)$	S_c	A/A_0
Di-50	737	786	932	795	845	910	9	0.94
Di-60	786	826	–	831	881	903	5	0.72
Di-70	763	850	–	874	905	–	24	0.75
Di-80	774	812	–	899	955	–	87	0.68
Di-90	777	824	–	857	895	–	33	0.66
Di-100	756	823	–	823	853	–	0	0.69

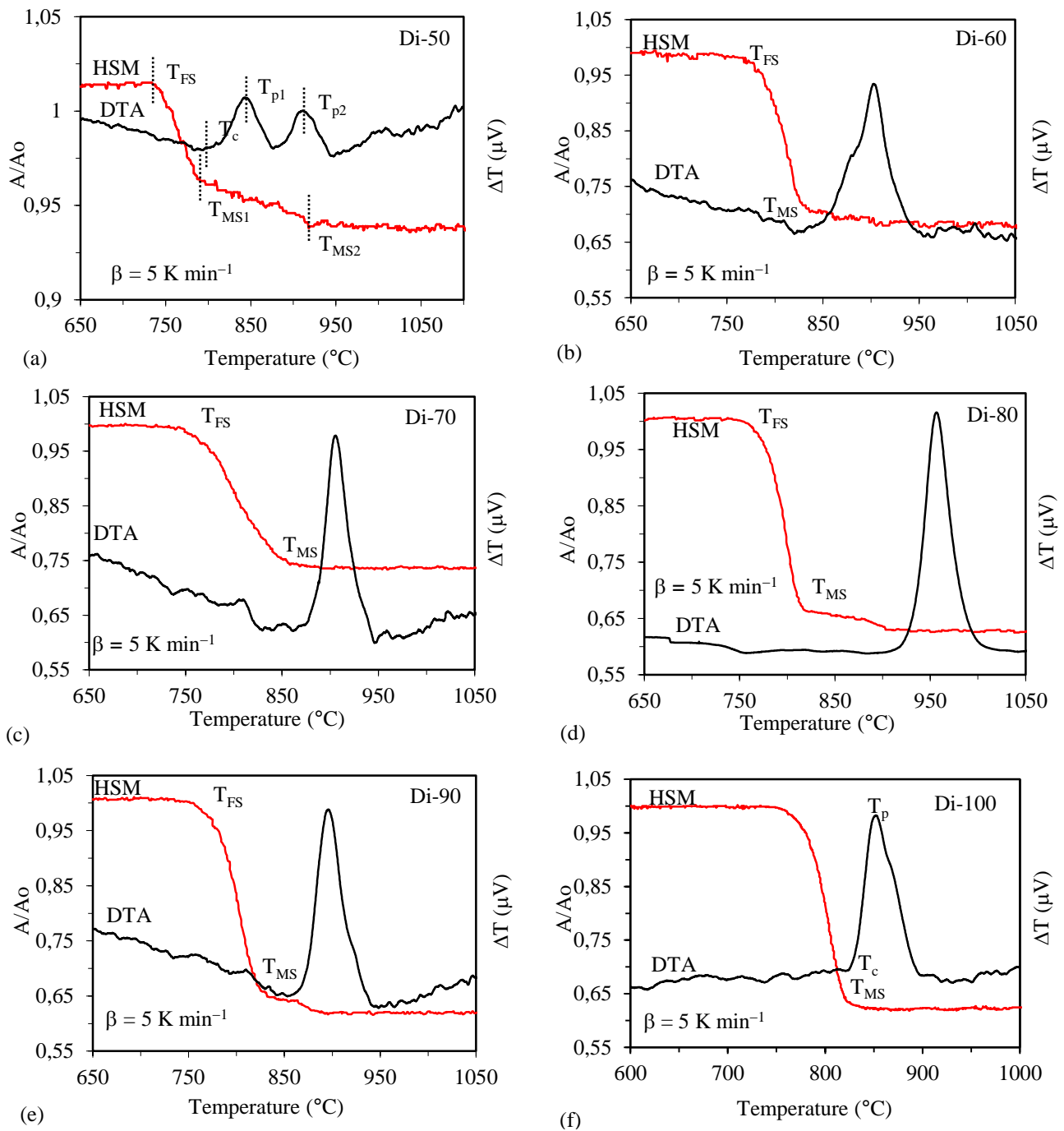


Figure 4.6.8 Comparison of DTA and HSM curves under the same heating rate (5 K min^{-1}) for compositions: (a) Di-50, (b) Di-60 (c) Di-70, (d) Di-80 (e) Di-90 and (f) Di-100

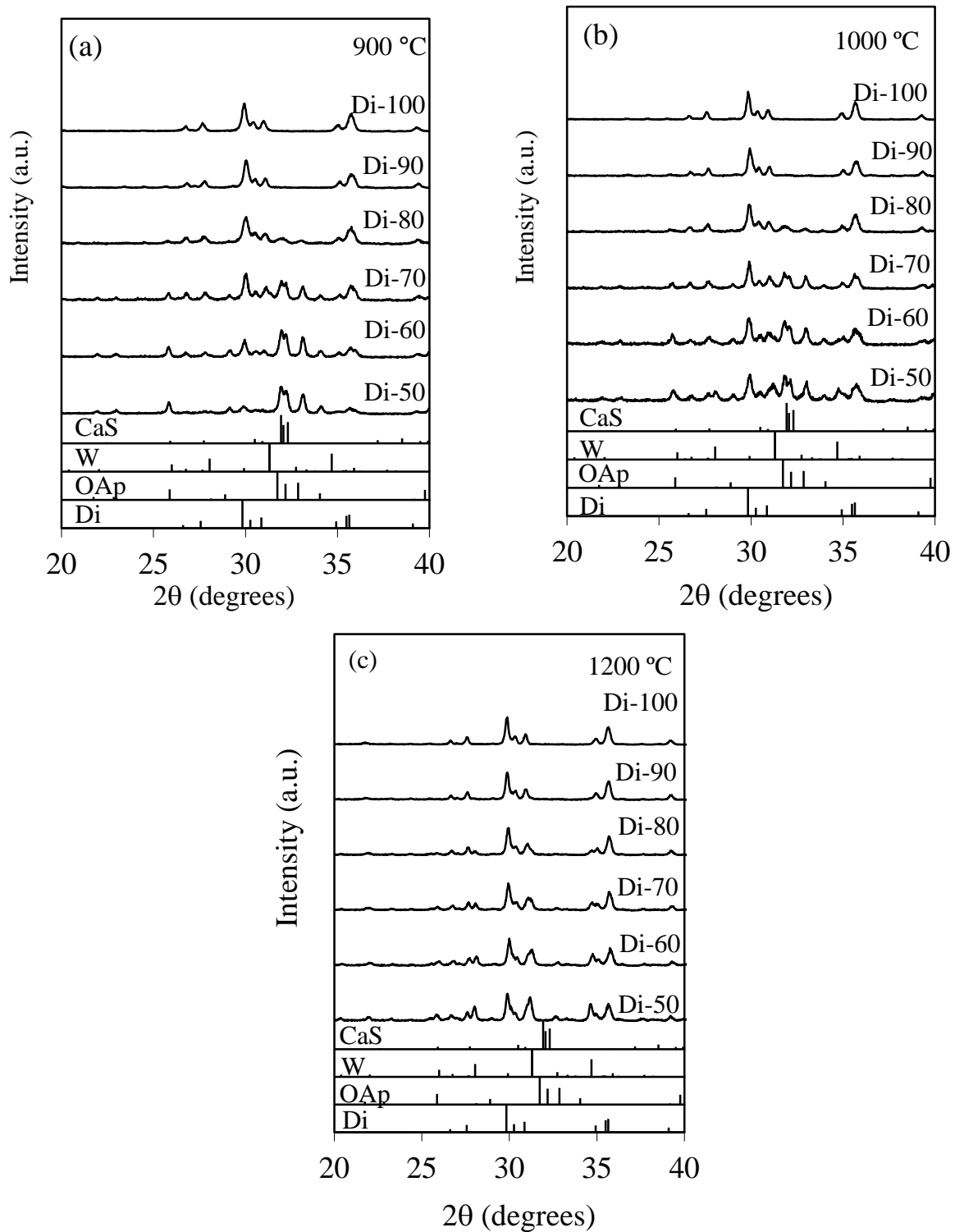


Figure 4.6.9 X-ray diffractograms of glass-ceramics heat treated at (a) 900 (b) 1000, and (c) 1200 °C for 1 h. (Di: Diopside, OAp: oxyapatite, W: Whitlockite, CaS: Calcium Silicate)

4.6.2.7 Structural transformations during heat treatment

Figure 4.6.9 shows the XRD patterns of the glass powder compacts heat treated for 1 h at 900, 1000 and 1200 °C. The peak at $2\theta = 29.83^\circ$ position appeared in all glasses and became more intense as the Di content is increased. The peak around of $2\theta = 31.74^\circ$ was restricted to the composition with higher TCP contents (Di-50 to Di-70). In addition, a number of low intensity peaks were also present as minor crystalline phase, being more prominent in these compositions (Di-50 to Di-70). The crystalline phase assemblage did not change much upon further increasing the heat treatment temperature to 1000 °C (Figure 4.6.9b), traces of new peaks at $2\theta = 31.30^\circ$ start appearing at this temperature especially for Di-50 to Di-70 compositions. Further, with the increase in the heat treatment temperature to 1200 °C peaks $\sim 2\theta = 31.74^\circ$ disappeared along with some minor phases and new peaks with maxima at $2\theta = 31.30^\circ$ appeared as the prominent phases (Figure 4.6.9c).

4.6.2.8 Density

The experimental density data measured for bulk glasses and glass-ceramics heat treated at different temperatures are reported in Table 2.6.4. The density of glass Di-50 was not measured due to its partial crystallization upon casting/slow cooling. It can be seen that density of the glass tends to decrease with increasing proportions of Di. All the glass-ceramics, except Di-50, exhibited good densification ability, achieving densities that are superior in comparison to those of bulk glasses. The density values show a general increasing trend with temperature increasing followed by its reversion with further augmenting the sintering temperature, with small composition dependent variations.

Table 4.6.4 Density (kg m^{-3}) of glasses and glass-ceramics.

Compositions	Bulk glass	Glass ceramics heat treated at		
		900 °C	1000 °C	1200 °C
Di-50*	-	2,819±47	2,863±60	2,893±16
Di-60	2.945	2,951±12	2,972±4	2,964±15
Di-70	2.921	2,972±60	2,953±6	2,962±1
Di-80	2.897	2,933±1	2,973±6	2,924±3
Di-90	2.871	2,930±7	2,936±6	2,925±11
Di-100	2.852	2,897±3	2,936±17	2,892±4

* Partial crystallisation upon casting

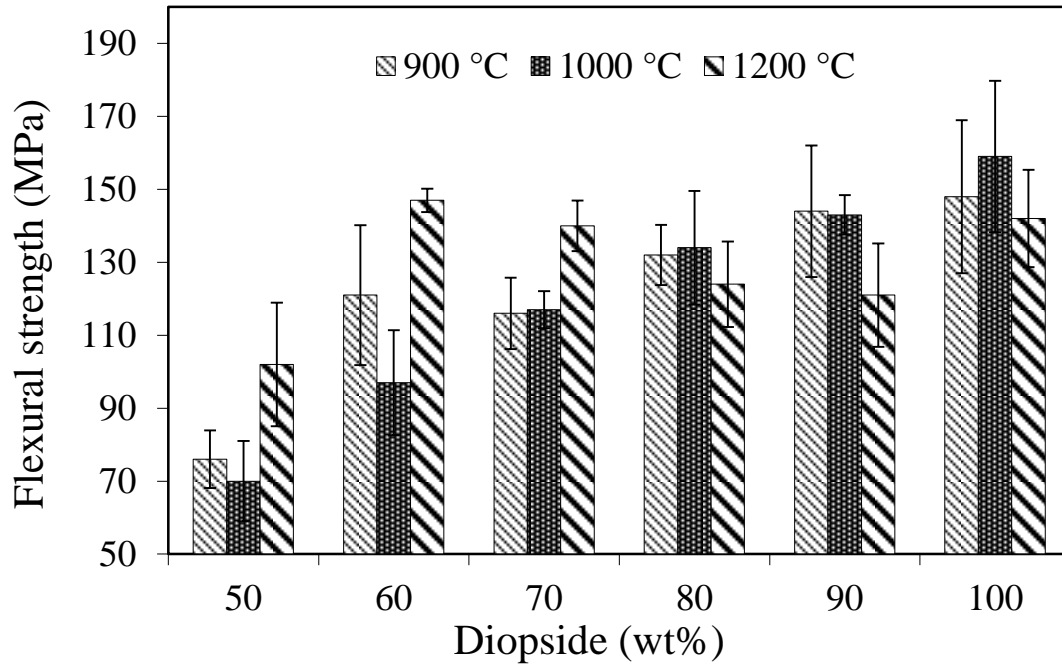


Figure 4.6.10 Flexural strength of glass-ceramics heat treated for 1 h at (a) 900 °C (b) 1000 °C, and (c) 1200 °C.

4.6.2.9 Mechanical properties

The 3-point bending strength was calculated for glass powder compacts sintered for 1 h at 900, 1000 and 1200 °C (Figure 4.6.10). In general, the flexural strength increased from Di-50 – Di-100 in all the glass powder compacts heat treated at 900 and 1000 °C. Interestingly, for the glass-ceramics sintered at 1200 °C a point of inflection was observed after Di-70, i.e., at 1200 °C there was a gradual decrease in the flexural strength of the glass-ceramics with increasing Di content.

4.6.2.10 Cell culture studies

hMSCs' metabolic activity on Di-60, Di-70 and Di-90 and Tissue culture polystyrene (TCPS) after 1, 3, 7, 14 and 21 days under both conditions are shown in Figure 4.6.11.

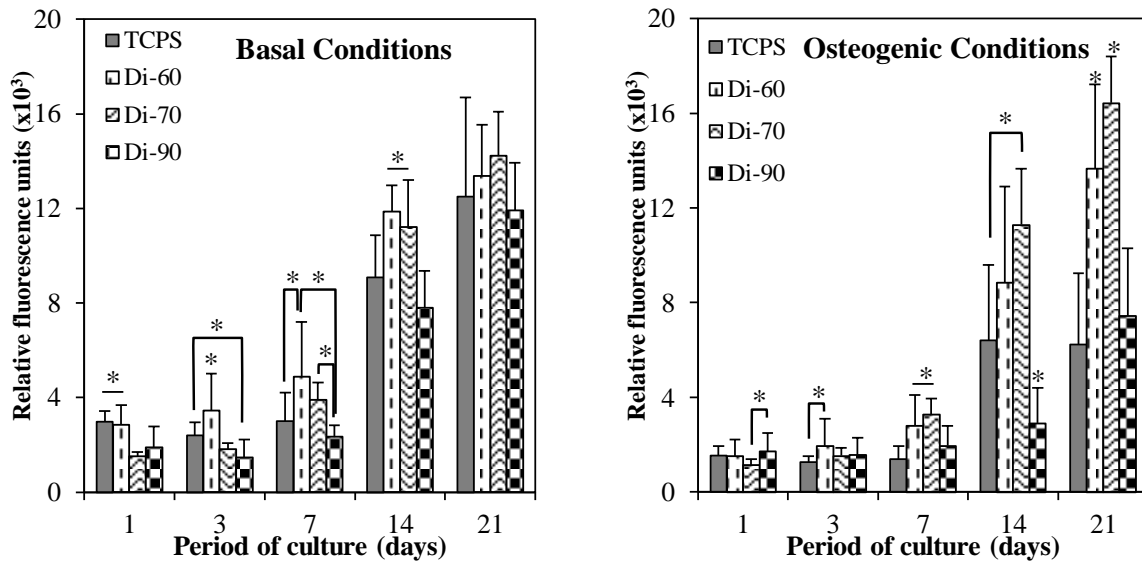


Figure 4.6.11 Metabolic activities of hMSCs on Di-60, Di-70 and Di-90 and TCPS after 1, 3, 7, 14 and 21 days.

An increase in cells' metabolic activity was observed under both basal and osteogenic conditions for the culture period tested. On day 14 of culture in a basal medium, the metabolic activity of cells on Di-60 and Di-70 showed superior and significant statistical difference when compared with the control. However, no statistically significant difference was found after 21 days. Under osteogenic conditions, by day 14, cells' metabolic activity was inferior and exhibited significant statistical difference with Di-90 in comparison with the control. On day 21, cell's on Di-70 presented a higher metabolic activity than cells on Di-60, D-90 and the control. At this time point, it was also possible to notice a potential recovery of cells' metabolic activity on Di-90.

4.6.3 Discussions

The gradual replacement of Di ($\text{CaO} \cdot \text{MgO} \cdot 2\text{SiO}_2$) by TCP ($3\text{CaO} \cdot \text{P}_2\text{O}_5$) changes the balance between glass formers and glass modifiers, implying structural variations that will influence the properties of glasses. The decreasing contents of Si lead to the formation of an increasing number of non-bridging oxygens in the glass structure. Further, no abrupt change in the glass structure was observed with increasing amounts of Di. However, the change in peak position towards more negative ppm values with increase in content of Di may be attributed to addition of silica and removal of phosphate from the glass network. On the

contrary, the up field peak shift in case of Di-100 can be attributed to complete removal of phosphate ion and simultaneous movement of modifier ions towards SiO₂ which were earlier attached to P₂O₅.

Figure 4.6.1b shows that ³¹P MAS-NMR continuously shifts for all the glasses lying predominantly in the range for calcium orthophosphate (1–3 ppm), and a small amount of magnesium orthophosphate (0.5 ppm) can be expected. This therefore suggests that phosphorus is present in mixed calcium and magnesium orthophosphate. The phosphate component in the glass is predominantly coordinated in orthophosphate environment thus, not contributing to the glass network backbone. This facilitates the release of additional soluble phosphate species into the surrounding fluid, increasing their local super-saturation levels and accelerating the bone bonding ability of glass by enhancing the HA deposition on the glass surface. Further Lockeyer et al. [225] attributed the presence of orthophosphate-like environment as a result of phase separation in glasses. All the glasses prepared by Lockeyer et al [225] were annealed for 6 h at 450 °C before slow cooling. However, the compositions under investigation were rapidly quenched in water, thus reducing the possibility of phase separation. Further, as the cation field strength and electronegativity of the modifiers significantly affect the ³¹P chemical shift in glasses. The peak shift observed in the spectra with increasing Di contents can be attributed to the increase in the Mg²⁺ (high field strength) and the concomitant decrease in the amount of Ca²⁺ content (low field strength).

In terms of bioactive behaviour, all the investigated glasses have shown good *in vitro* bio-mineralization activity in terms of the formation ability of an HCA surface layer over 14 days of soaking in SBF (Figure 4.6.3), except for pure Di (Di–100) [104]. The inability of Di–100 to form a HCA surface layer after 14 days of immersion can be attributed the relatively high amount of MgO which retards the formation of apatite-like calcium phosphate [148]. However, the presence of ACP could be detected for these glasses after 24 h of immersion (Figure 4.6.3). Further, despite the differences in P₂O₅ content, all the investigated alkali-free glasses show similar rate of biomineralisation in contrast to the results reported by O'Donnell et al. [226] and Mneimne et al. [227]. The possible reason behind these different behaviours could be attributed to high alkali content (22–29 mol%) of the bioglass compositions used by O'Donnell et al [228] and Mneimne et al. [227]. The eventual association of P with Na in the form Na-orthophosphate is likely to contribute to faster rates of dissolution and release of phosphates species from these glasses into the surrounding fluid in comparison to alkali-free counter parts. Interestingly, the presence of varying amounts of

magnesium did not apparently affect the rate of apatite formation in our alkali-free bioactive glasses, even though a suppressing role in apatite formation has been reported in literature for Mg [229]. However, the results obtained in this study are in line with findings reported elsewhere [99] about the negligible effects of Mg on the apatite forming ability of other bioactive glass compositions. Thus, it seems reasonable to conclude that the effects of MgO on the properties of bioactive glasses do not exclusively depend on the added amount of MgO but also on the presence and relative contents of other oxides in each glass composition [229].

The foremost requirement for optimizing the fabrication of glass–ceramics scaffolds is to understand the sintering and crystallization behaviours of the glass powder compacts and avoid the overlapping of these two thermal events. A thorough understanding of the transformations that occur during the thermal treatment of glasses and how they depend on the starting compositions is therefore essential for designing biomedical applications/devices based on bioactive glasses that have to undergo high temperature treatments. We could not observe any significant differences in the variation of T_g values with varying Di/TCP ratio in the glasses. Further, the presence of single crystallization exotherm anticipates that the glass–ceramics are formed as a result of either single phase crystallization (Di–100) or an almost simultaneous precipitation of different crystalline phases (Di–60 – Di–90), while the appearance of two crystallization peaks points (T_{p1} and T_{p2}) in Di–50 glass points towards the separate precipitation of two different crystalline phases. Further, good sintering behaviour was observed in the glasses as T_{MS1} was lower than T_c , meaning that maximum shrinkage was reached before onset of crystallization. Further, the higher values of the sintering parameter, $S_c = (T_c - T_{MS})$ for intermediate compositions (Table 4.6.3) clearly explain why these compositions perform better upon sintering. The observed decrease in the sintering ability for the higher added amounts of TCP is attributed to the formation of phosphate rich phases that degrade the sintering ability by enhancing the crystallization tendency of the glasses. In case of Di–100, T_{MS} coinciding with T_c ($T_c - T_{MS} = 0$), (Figure 4.6.8f). However, well sintered glass powder compacts were obtained as maximum shrinkage was achieved just before the onset of crystallization. This is confirmed by the density data reported in Table 4.6.4. The lowest density of Di–50 glass-ceramics is in good agreement with its poorer densification ability as deduced from the DTA-HSM results, with T_{MS2} coinciding with the onset of crystallization. Some bubbling was observed upon immersing the Di-50 glass-ceramics in diethyl phthalate due to the presence of some open pores, a tendency that decreased with increasing temperature, but was not completely eliminated. The absence of

bubbling for the remaining glass-ceramics samples and their higher sintered density values in comparison to the parent bulk glasses attest their good sintering ability, in good agreement with the predictions derived from DTA-HSM studies. Density data confirm that the compositions within the range of Di-60 to Di-80 exhibit the higher sintering ability, being the most interesting ones for scaffolds fabrication. The general tendency of density to decrease with heat treatment increasing can be attributed to the elimination of a few pores left at lower temperatures and or to the formation of increasing amounts of denser crystalline phases. The reversion of this trend with temperature further increasing might be due to partial re-melting of crystalline phases, crystalline phase transformations. Therefore, exact information about the nature of crystalline phases formed upon heat treating the bioactive glasses is of great interest as they determine the relevant final properties of the glass-ceramic materials. Besides being composition dependent, the phase assemblage might be also affected in a certain extent by the heat treatment schedule.

In the present study, Di ($\text{CaMgSi}_2\text{O}_6$) (ICDD: 01-072-1497) and oxyapatite (ICDD: 65-1659) were the principal crystalline phases formed at 900 °C (Figure 4.6.9a). The presence of oxyapatite was restricted to the composition with higher TCP contents (Di-50 to Di-70). Calcium silicate (Ca_2SiO_4) (ICDD: 01-086-0401) was also present as minor crystalline phase, being more prominent in these compositions (Di-50 to Di-70) as evident from the X-ray diffractograms. The crystalline phase assemblage did not change much upon further increasing the heat treatment temperature to 1000 °C, but traces of whitlockite ($\text{Ca}_{2.71}\text{Mg}_{0.29}(\text{PO}_4)_2$) (ICDD: 01-070-0682) start appearing at this temperature especially for Di-50 to Di-70 compositions. The absence of calcium silicate and whitlockite phases in the glass-ceramics with higher Di contents can be attributed to the gradual depletion in Ca required to form those phases and the concomitant increasing amounts of MgO that tend to enhance the viscosity of the melts. Further increasing the heat treatment temperature to 1200 °C led to the dissolution of oxyapatite and calcium silicate phases, favouring the formation of whitlockite along with Di as the prominent phases. The dissolution of oxyapatite and calcium silicate at 1200 °C can be attributed to increase in the amount of Di phase and the associated decrement of calcium content in the residual glassy phase available for apatite/ Ca_2SiO_4 formation.

Mechanical strength of the scaffolds is a very important aspect to take into consideration when designing glass-ceramics for bone tissue engineering applications. The mechanical strength of glass-ceramics is dependent on the mechanical properties of the

constituting crystalline phases and the densification ability of glass-powder compacts. In the present investigation the mechanical strength of the glass-ceramics (Di-60 – Di-100) exhibit good mechanical strength which can be attributed the mechanical properties of the constituting crystalline phases and high density obtained by the glass-ceramics (2,890–2,970 kg m⁻³). In case of Di-50, the poor sintering/densification ability and lower mechanical strength of the dominant phase can attributed to the lower mechanical strength upon sintering. Further glass-ceramics with higher amounts of Di (a mechanically stronger phase) [230] exhibit high mechanical strength values when heat treated up to 1000 °C. Further, the overall decrease in the mechanical strength of the resultant glass-ceramics heat treated at 1200 °C can be due to the decline in the densification ability of the glass-ceramics and formation of considerable volume fraction of whitlockite (a mechanically weaker phase), explaining the overall decrease in the mechanical strength of the resultant glass-ceramics.

The cell culture studies showed an excellent cellular response to the investigated glass compositions, with the exception of the cells tested with osteogenic supplements and Di-90. Under these conditions, cells had lower metabolic activity than control, Di-60 and Di-70. Since Di-90 has higher amount of silica and MgO than the other compositions, the release of the compounds to the culture medium may induce some levels of cytotoxicity towards the hMSCs. Previous studies have shown that high Si concentrations can be cytotoxic [231, 232]. However this behaviour was more prominent under osteogenic conditions, which might be attributed to the inhibition of the stimulatory effect of osteogenic supplements in the presence of high Si concentrations [233]. At the end of the culture period, these cells seem to recover from the imposed toxic levels as suggested by an increase in their metabolic activity. This behaviour has been reported by several authors [231, 234]. On the contrary, Di-60 and Di-70 promoted a good cell adhesion, metabolic activity into an osteoblastic phenotype, suggesting a potential stimulatory effect of these materials on hMSCs by the release of soluble factors or by the fastest formation of a CaP layer [235]. It has been reported the Si-, Ca- and Mg-containing bioactive ceramics can release soluble ionic products to stimulate the proliferation and osteogenic differentiation of osteoblasts and human mesenchymal stem cells [236-238].

4.6.4 Conclusions

An attempt has been made gain an insight into composition - structure - bioactivity relationships of alkali-free bioactive glasses in the CaO-MgO-SiO₂-P₂O₅ system. The glasses have been designed in the Di (CaO•MgO•2SiO₂) – TCP (3CaO•P₂O₅) binary join by

varying the Di/TCP ratio. We could obtain amorphous glasses only from compositions with Di \geq 50 wt%. The melting of compositions with Di contents varying between 30-50 wt% at 1570 °C for 1 h resulted in a highly viscous liquids which were prone to spontaneous crystallization even after quenching in cold water, thus resulting in a white, opaque material. Further decrease in Di content to 20 wt% led to the formation of highly viscous, non-homogeneous melts under the experimental conditions. Further, there was no significant change in the structure of the glass with decrease in Di content as investigated glasses have predominantly Q^2 (Si) units while phosphorus is mostly in orthophosphate type environment. As expected from the structure of the glasses, all other investigated glasses have shown good *in vitro* bio-mineralisation activity in terms of the formation ability of an HCA surface layer over 14 days of soaking in SBF. All the glasses exhibited considerably lower weight loss in comparison to 45S5 Bioglass[®] in Tris-HCl with Di-50 exhibiting lowest weight loss. The cell culture studies showed an excellent cellular response to the investigated glass compositions, with the exception of the Di-90. Further, all the glasses exhibit good thermal stability and processing window wide enough for the fabrication of scaffolds. TCP addition resulted in slight T_g variations. Good densification was achieved for the glass powder compacts at all investigated temperatures, resulting in well sintered and mechanically strong glass-ceramics. Diopside, oxyapatite were the major phases present at 900 °C and 1000 °C with calcium silicate and whitlockite as the minor phases. At 1200 °C, diopside and whitlockite were the major phases present with no other minor phase detected.

Chapter 5

General conclusions

5. General conclusions

The present work aimed at developing alkali-free bioactive glasses in the ternary system of Di-FA-TCP having high bioactivity, lower dissolution rate and good sintering behaviour for bone regeneration and tissue engineering applications. In this pursuit, an attempt was made to understand the structure-property relationships in alkali-free bioactive glasses. Further, the influence of various functional ions on the structure and their implications on the biodegradation, sintering and crystallization behaviour of bioactive glasses was studied. In terms of structure, the glasses are almost similar to 45S5 Bioglass®, while significantly differing in the properties that are relevant for the intended applications. The designed alkali-free bioactive glasses exhibit: (i) higher bioactivity and slower chemical degradation in comparison to 45S5 Bioglass®; (ii) enhanced sintering ability resulting in well sintered and mechanically strong glass-ceramics with high residual amorphous content; (iii) good ability to be dispersed in aqueous media and to fabricate scaffolds for bone regeneration and tissue engineering applications with good mechanical properties and high bioactivity; (iv) the pH of the media is kept at moderate values owing to the absence of alkali metals in the composition, making them non-cytotoxic.

Further, the addition of zinc to the parent glasses enhanced their chemical durability and the sintering ability without causing a substantial change in the structure. The flexural strength of 200 MPa achieved for Zn-8 We is comparable to that of the A-W glass-ceramics. Glasses doped with equimolar concentrations of ZnO and SrO showed excellent bioactivity despite of their very low degradation in comparison to 45S5 Bioglass®. In addition, the glass ZS-2 released doses of zinc and strontium into the SBF that are within the considered therapeutic ranges (< 1.5 ppm Zn and ≤ 10 ppm Sr), and exhibited good antioxidant behaviour by enhancing the cell viability and negating the effect of oxidative stress induced by H₂O₂ addition in the cell culture medium. Thus zinc concentration < 1.5 ppm has an anti-oxidant effect.

Moreover, we have elucidated that a straightforward correlation between the glass structure as evaluated by the network connectivity (Q_n units) and dissolution behaviour of alkali-free bioactive glasses is difficult to establish as the bulk molecular structure of glasses does not completely control the hydroxyapatite formation on the surface of bioactive glasses. The structural coordination of functional ions in the glass plays a crucial role in deciding their elemental release profile thus, affecting the bioactivity of glasses. In the investigated alkali-free bioactive glasses, all the glasses had almost similar molecular structure (Q_n and NC).

However, the structural coordination of zinc (five-coordinated) and strontium (six coordinated) played an important role in deciding their biodegradation and sintering and crystallization behaviour. Also, in order to obtain a comprehensive picture about the dissolution mechanism and surface reactivity of glasses, it is of utmost importance to explore the surface chemistry of bioactive glasses and correlate it with their molecular structure.

Chapter 6

Future works

6. Future works

During this research work, an attempt has been made to develop diopside based Alkali-free bioactive glasses for bone regeneration applications. We have succeeded in shedding some light on the composition-structure-property relationships in the glasses and the effect of various functional ions on the biodegradation, sintering, thermal and in vitro behaviour of bioactive glasses, which render them suitable for further experimentation as potential candidates in various bone regeneration applications. However, a lot work still needs to be accomplished in order to understand the biodegradation behaviour of the glasses. Therefore, in our opinion, the future work in this area may be addressed to the following issues:

1. Surface chemistry of the glasses is highly important aspect to study the bioactive phenomenon. It could be interesting to study the relation of surface chemistry of glasses with their biodegradation behaviour and compare them with alkali-containing counterparts.
2. In addition, biologically relevant additives (Co, Mn, Cu etc.) can be added to study their effect on bio-degradation behaviour in order to enhance the therapeutic efficacy of the glasses
3. Further in depth in vitro tests are required to see the interaction of bioglass with variety to cellular environments.
4. Also, in vivo tests of glasses/glass-ceramics are required to further establish its application in human biomedicine.

References

References

- [1] Shelby JE. Introduction to Glass Science and Technology : Edition 2. 2005.
- [2] Hench L. The story of Bioglass®. J Mater Sci: Mater Med 2006;17:967-78.
- [3] Hench LL. Bioceramics - from Concept to Clinic. J Am Ceram Soc 1991;74:1487-510.
- [4] Hench LL, DeDeaHW, RVM. Glass and Medicine. Int J Appl Glass Sci;1:104--17.
- [5] Tilocca A. Structural models of bioactive glasses from molecular dynamics simulations. Proc R Soc A;2009;465:1003-27.
- [6] Tilocca A, Cormack AN, de Leeuw NH. The formation of nanoscale structures in soluble phosphosilicate glasses for biomedical applications: MD simulations. Faraday Discuss 2007;136:45-55.
- [7] Tilocca A, Cormack AN, de Leeuw NH. The structure of bioactive silicate glasses: New insight from molecular dynamics simulations. Chem Mater 2007;19:95-103.
- [8] Lefebvre L, Chevalier J, Gremillard L, Zenati R, Thollet G, Bernache-Assolant D, et al. Structural transformations of bioactive glass 45S5 with thermal treatments. Acta Materialia 2007;55:3305-13.
- [9] Bretcanu O, Chatzistavrou X, Paraskevopoulos K, Conradt R, Thompson I, Boccaccini AR. Sintering and crystallisation of 45S5 Bioglass® powder. J Eur Cer Soc 2009;29:3299-306.
- [10] Lefebvre L, Gremillard L, Chevalier J, Zenati R, Bernache-Assolant D. Sintering behaviour of 45S5 bioactive glass. Acta Biomater 2008;4:1894-903.
- [11] Wallace KE, Hill RG, Pembroke JT, Brown CJ, Hatton PV. Influence of sodium oxide content on bioactive glass properties. J Mater Sci: Mater Med 1999;10:697-701.
- [12] Jones JR, Hench LL. Regeneration of trabecular bone using porous ceramics. Curr Opin Solid St M 2003;7:301-7.
- [13] Johnell O, Kanis JA. An estimate of the worldwide prevalence and disability associated with osteoporotic fractures. Osteoporosis Int 2006;17:1726-33.
- [14] Gullberg B, Johnell O, Kanis JA. World-wide projections for hip fracture. Osteoporosis Int 1997;7:407-13.
- [15] Cooper C, Campion G, Melton LJ. Hip-Fractures in the Elderly - a Worldwide Projection. Osteoporosis Int 1992;2:285-9.
- [16] Nandi SK, Roy S, Mukherjee P, Kundu B, De DK, Basu D. Orthopaedic applications of bone graft & graft substitutes: a review. Indian J Med Res 2010;132:15-30.
- [17] Hench LL, Polak JM. Third-generation biomedical materials. Science 2002;295:1014.

- [18] Charnley J. Anchorage of the Femoral Head Prosthesis to the Shaft of the Femur. *J Bone Joint Surg Br* 1960;42:28-30.
- [19] Buddy D. Ratner ASH, Frederick J. Schoen and Jack E. Lemons 2012. 3 ed: Elsevier
- [20] Hench LL. Bioceramics. *J Am Ceram Soc* 1998;81:1705-28.
- [21] Hench LL, Paschall HA. Direct Chemical Bond of Bioactive Glass-Ceramic Materials to Bone and Muscle. *J Biomed Mater Res* 1973;7:25-42.
- [22] Kulkarni RK, Moore EG, Hegyeli AF, Leonard F. Biodegradable poly(lactic acid) polymers. *J Biomed Mater Res* 1971;5:169-81.
- [23] Goel A, Kapoor S, Rajagopal RR, Pascual MJ, Kim HW, Ferreira JMF. Alkali-free bioactive glasses for bone tissue engineering: A preliminary investigation. *Acta Biomater* 2012;8:361-72.
- [24] Shapoff CA, Alexander DC, Clark AE. Clinical use of a bioactive glass particulate in the treatment of human osseous defects. *Compendium of continuing education in dentistry (Jamesburg, NJ : 1995)* 1997;18:352-4, 6, 8 passim.
- [25] Jones JR. Review of bioactive glass: From Hench to hybrids. *Acta Biomater* 2013;9:4457-86.
- [26] Hench LL, Splinter RJ, Allen WC, Greenlee TK. Bonding mechanisms at the interface of ceramic prosthetic materials. *J Biomed Mater Res* 1971;5:117-41.
- [27] Xynos ID, Edgar AJ, Buttery LDK, Hench LL, Polak JM. Ionic products of bioactive glass dissolution increase proliferation of human osteoblasts and induce insulin-like growth factor II mRNA expression and protein synthesis. *Biochem Biophys Res Commun* 2000;276:461-5.
- [28] Xynos ID, Edgar AJ, Buttery LDK, Hench LL, Polak JM. Gene-expression profiling of human osteoblasts following treatment with the ionic products of Bioglass[®] 45S5 dissolution. *J Biomed Mater Res* 2001;55:151-7.
- [29] Leach JK, Kaigler D, Wang Z, Krebsbach PH, Mooney DJ. Coating of VEGF-releasing scaffolds with bioactive glass for angiogenesis and bone regeneration. *Biomaterials* 2006;27:3249-55.
- [30] Gorustovich AA, Roether JA, Boccaccini AR. Effect of Bioactive Glasses on Angiogenesis: A Review of In Vitro and In Vivo Evidences. *Tissue Eng Part B-Re* 2010;16:199-207.
- [31] Kaur G, Pandey OP, Singh K, Homa D, Scott B, Pickrell G. A review of bioactive glasses: Their structure, properties, fabrication, and apatite formation. *J Biomed Mater Res A* 2014;102:254-74.

- [32] Liu X, Rahaman MN, Fu QA. Oriented bioactive glass (13-93) scaffolds with controllable pore size by unidirectional freezing of camphene-based suspensions: Microstructure and mechanical response. *Acta Biomater* 2011;7:406-16.
- [33] Jung SB, Day DE, Day T, Stoecker W, Taylor P. Treatment of Non-Healing Diabetic Venous Stasis Ulcers with Bioactive Glass Nanofibers. *Wound Repair Regen* 2011;19:A30-A.
- [34] Abou Neel EA, Pickup DM, Valappil SP, Newport RJ, Knowles JC. Bioactive functional materials: a perspective on phosphate-based glasses. *J Mater Chem* 2009;19:690-701.
- [35] Li R, Clark AE, Hench LL. An investigation of bioactive glass powders by sol-gel processing. *J Appl Biomater* 1991;2:231-9.
- [36] Pereira MM, Clark AE, Hench LL. Calcium phosphate formation on sol-gel-derived bioactive glasses in vitro. *J Biomed Mater Res* 1994;28:693-8.
- [37] Martinez A, Izquierdo-Barba I, Vallet-Regi M. Bioactivity of a CaO - SiO₂ binary glasses system. *Chem Mater* 2000;12:3080-8.
- [38] Balamurugan A, Balossier G, Kannan S, Michel J, Rebelo AHS, Ferreira JMF. Development and in vitro characterization of sol-gel derived CaO-P₂O₅-SiO₂-ZnO bioglass. *Acta Biomater* 2007;3:255-62.
- [39] Hill R. An alternative view of the degradation of bioglass. *J Mater Sci Lett* 1996;15:1122-5.
- [40] Strnad Z. Role of the Glass Phase in Bioactive Glass-Ceramics. *Biomaterials* 1992;13:317-21.
- [41] Edén M. The split network analysis for exploring composition–structure correlations in multi-component glasses: I. Rationalizing bioactivity-composition trends of bioglasses. *J Non-Cryst Solids* 2011;357:1595-602.
- [42] Goel A, Kapoor S, Tilocca A, Rajagopal RR, Ferreira JMF. Structural role of zinc in biodegradation of alkali-free bioactive glasses. *J Mater Chem B* 2013;1:3073-82.
- [43] Sanders DM, Hench LL. Mechanisms of Glass Corrosion. *J Am Ceram Soc* 1973;56:373-7.
- [44] Hoppe A, Güldal NS, Boccaccini AR. A review of the biological response to ionic dissolution products from bioactive glasses and glass-ceramics. *Biomaterials* 2011;32:2757-74.
- [45] Hench LL, Boccaccini AR, Day RM, Gabe SM. Third-generation gene-activating biomaterials. *Mater Sci Forum* 2003;426-4:179-84.

- [46] Hench LL. Genetic design of bioactive glass. *Journal of the European Ceramic Society* 2009;29:1257-65.
- [47] Jugdaohsingh R. Silicon and bone health. *J Nutr Health Aging* 2007;11:99-110.
- [48] Carlisle EM. Silicon - a Requirement in Bone-Formation Independent of Vitamin-D1. *Calcified Tissue Int* 1981;33:27-34.
- [49] Carlisle EM. In vivo requirement for silicon in articular cartilage and connective tissue formation in the chick. *J Nutr* 1976;106:478-84.
- [50] Schwarz K. A bound form of silicon in glycosaminoglycans and polyuronides. *Proc Natl Acad Sci U S A* 1973;70:1608-12.
- [51] Reffitt DM, Ogston N, Jugdaohsingh R, Cheung HFJ, Evans BAJ, Thompson RPH, et al. Orthosilicic acid stimulates collagen type 1 synthesis and osteoblastic differentiation in human osteoblast-like cells in vitro. *Bone* 2003;32:127-35.
- [52] Hott M, De Pollak C, Modrowski D, Marie PJ. Short-term effects of organic silicon on trabecular bone in mature ovariectomized rats. *Calcified Tissue Int* 1993;53:174-9.
- [53] Seaborn CD, Nielsen FH. Dietary silicon and arginine affect mineral element composition of rat femur and vertebra. *Bio Trace Elem Res* 2002;89:239-50.
- [54] Seaborn CD, Nielsen FH. Dietary silicon affects acid and alkaline phosphatase and Calcium uptake in bone of rats. *J Trace Ele Exp Med* 1994;7:11-8.
- [55] Kim MH, Bae YJ, Choi MK, Chung YS. Silicon Supplementation Improves the Bone Mineral Density of Calcium-Deficient Ovariectomized Rats by Reducing Bone Resorption. *Bio Trace Elem Res* 2009;128:239-47.
- [56] Bonnelye E, Chabadel A, Saltel F, Jurdic P. Dual effect of strontium ranelate: Stimulation of osteoblast differentiation and inhibition of osteoclast formation and resorption in vitro. *Bone* 2008;42:129-38.
- [57] Marie PJ, Hott M, Modrowski D, Depollak C, Guillemain J, Deloffre P, et al. An Uncoupling Agent Containing Strontium Prevents Bone Loss by Depressing Bone-Resorption and Maintaining Bone-Formation in Estrogen-Deficient Rats. *J Bone Miner Res* 1993;8:607-15.
- [58] Gentleman E, Fredholm YC, Jell G, Lotfibakhshaiesh N, O'Donnell MD, Hill RG, et al. The effects of strontium-substituted bioactive glasses on osteoblasts and osteoclasts in vitro. *Biomaterials* 2010;31:3949-56.
- [59] Agren MS. Studies on zinc in wound healing. *Acta dermato-venereologica Supplementum* 1990;154:1-36.

- [60] Staiger MP, Pietak AM, Huadmai J, Dias G. Magnesium and its alloys as orthopedic biomaterials: A review. *Biomaterials* 2006;27:1728-34.
- [61] Zreiqat H, Howlett CR, Zannettino A, Evans P, Schulze-Tanzil G, Knabe C, et al. Mechanisms of magnesium-stimulated adhesion of osteoblastic cells to commonly used orthopaedic implants. *J Biomed Mater Res* 2002;62:175-84.
- [62] Rude RK, Gruber HE, Wei LY, Frausto A, Mills BG. Magnesium deficiency: Effect on bone and mineral metabolism in the mouse. *Calcified Tissue Int* 2003;72:32-41.
- [63] Rude RK, Gruber HE, Norton HJ, Wei LY, Frausto A, Kilburn J. Dietary magnesium reduction to 25% of nutrient requirement disrupts bone and mineral metabolism in the rat. *Bone* 2005;37:211-9.
- [64] Saris NEL, Mervaala E, Karppanen H, Khawaja JA, Lewenstam A. Magnesium - An update on physiological, clinical and analytical aspects. *Clinica Chimica Acta* 2000;294:1-26.
- [65] Vormann J. Magnesium: Nutrition and metabolism. *Mol Aspects Med* 2003;24:27-37.
- [66] Cashman KD. Calcium intake, calcium bioavailability and bone health. *Br J Nutr* 2002;87:S169-77.
- [67] Maeno S, Niki Y, Matsumoto H, Morioka H, Yatabe T, Funayama A, et al. The effect of calcium ion concentration on osteoblast viability, proliferation and differentiation in monolayer and 3D culture. *Biomaterials* 2005;26:4847-55.
- [68] Marie PJ. The calcium-sensing receptor in bone cells: A potential therapeutic target in osteoporosis. *Bone* 2010;46:571-6.
- [69] Valerio P, Pereira MM, Goes AM, Leite MF. Effects of extracellular calcium concentration on the glutamate release by bioactive glass (BG60S) preincubated osteoblasts. *Biomed Mater* 2009;4.
- [70] Hinoi E, Takarada T, Yoneda Y. Glutamate signaling system in bone. *J Pharmacol Sci* 2004;94:215-20.
- [71] Julien M, Khoshniat S, Lacreusette A, Gatius M, Bozec A, Wagner EF, et al. Phosphate-Dependent Regulation of MGP in Osteoblasts: Role of ERK1/2 and Fra-1. *J Bone Miner Res* 2009;24:1856-68.
- [72] Meleti Z, Shapiro IM, Adams CS. Inorganic phosphate induces apoptosis of osteoblast-like cells in culture. *Bone* 2000;27:359-66.
- [73] Sepulveda P, Jones JR, Hench LL. In vitro dissolution of melt-derived 45S5 and sol-gel derived 58S bioactive glasses. *J Biomed Mater Res* 2002;61:301-11.

- [74] Kansal I, Reddy A, Muñoz F, Choi S-J, Kim H-W, Tulyaganov DU, et al. Structure, biodegradation behavior and cytotoxicity of alkali-containing alkaline-earth phosphosilicate glasses. *Mater Sci Eng C* 2014;44:159-65.
- [75] Hench LL, Spilman DB, Hench JW. Fluoride-containing Bioglass™ compositions. Google Patents; 1988.
- [76] Andersson OH, Liu GZ, Karlsson KH, Niemi L, Miettinen J, Juhanoja J. In vivo Behavior of Glasses in the SiO₂-Na₂O-CaO-P₂O₅-Al₂O₃-B₂O₃ System. *J Mater Sci: Mater M* 1990;1:219-27.
- [77] Brink M, Turunen T, Happonen RP, YliUrpo A. Compositional dependence of bioactivity of glasses in the system Na₂O-K₂O-MgO-CaO-B₂O₃-P₂O₅-SiO₂. *J Biomed Mater Res* 1997;37:114-21.
- [78] Gomez-Vega JM, Saiz E, Tomsia AP, Oku T, Suganuma K, Marshall GW, et al. Novel Bioactive Functionally Graded Coatings on Ti6Al4V. *Adv Mater* 2000;12:894-8.
- [79] Kokubo TS, Masazumi; Nagashima, Yukihito; Tashiro, Megumi; Nakamura, Takashi; Yamamuro, Takao; Higashi, Shoichiro. Apatite- and Wollastonite-Containing Glass-Ceramics for Prosthetic Application. *Bull Inst Chem Res Kyoto Univ* 1982;60:260-8.
- [80] Elgayar I, Aliev AE, Boccaccini AR, Hill RG. Structural analysis of bioactive glasses. *J Non-Cryst Solids* 2005;351:173-83.
- [81] Vogel M, Voigt C, Gross UM, Muller-Mai CM. In vivo comparison of bioactive glass particles in rabbits. *Biomaterials* 2001;22:357-62.
- [82] Lusvardi G, Zaffe D, Menabue L, Bertoldi C, Malavasi G, Consolo U. In vitro and in vivo behaviour of zinc-doped phosphosilicate glasses. *Acta Biomater* 2009;5:419-28.
- [83] Lusvardi G, Malavasi G, Menabue L, Aina V, Morterra C. Fluoride-containing bioactive glasses: Surface reactivity in simulated body fluids solutions. *Acta Biomater* 2009;5:3548-62.
- [84] Zhang D, Hupa M, Hupa L. In situ pH within particle beds of bioactive glasses. *Acta Biomater* 2008;4:1498-505.
- [85] Chen QZ, Li YA, Jin LY, Quinn JMW, Komesaroff PA. A new sol-gel process for producing Na₂O-containing bioactive glass ceramics. *Acta Biomater* 2010;6:4143-53.
- [86] Waltimo T, Brunner TJ, Vollenweider M, Stark WJ, Zehnder M. Antimicrobial effect of nanometric bioactive glass 45S5. *J Dent Res* 2007;86:754-7.
- [87] Brauer DS, Karpukhina N, O'Donnell MD, Law RV, Hill RG. Fluoride-containing bioactive glasses: Effect of glass design and structure on degradation, pH and apatite formation in simulated body fluid. *Acta Biomater* 2010;6:3275-82.

- [88] Shibuya T, Morita Y, Matsui A. No alkali containing biocompatible glass ceramic with apatite, wollastonite and diopside crystals mixed. Google Patents; 1988.
- [89] Andersson OH, Peltola JK. Bioactive glass as a bone substitute. Google Patents; 1993.
- [90] Brink M, Karlsson K, Yli-Uro A. Novel bioactive glasses and their use. Google Patents; 1997.
- [91] Hill RG, Stevens MM. Bioactive glass. Google Patents; 2007.
- [92] O'donnell M, Hill RG. Multicomponent Glasses for use in Personal Care Products. Google Patents; 2011.
- [93] Brink M. The influence of alkali and alkaline earths on the working range for bioactive glasses. *J Biomed Mater Res* 1997;36:109-17.
- [94] Kokubo T, Hayashi T, Sakka S, Kitsugi T, Yamamuro T. Bonding between bioactive glasses, glass-ceramics or ceramics in a simulated body fluid. *Yogyo Kyokai Shi/J Cer Soc Japan* 1987;95:785-91.
- [95] Kitsugi T, Yamamuro T, Nakamura T, Kokubo T, Takagi M, Shibuya T, et al. Bonding behavior between two bioactive ceramics in vivo. *J Biomed Mater Res* 1987;2 1:1109-1123.
- [96] Kasuga T, Nakagawa K, Yoshida M, Miyade E. Compositional dependence of formation of an apatite layer on glass-ceramics in simulated physiological solution. *J Mater Sci* 1987;22:3721-4.
- [97] Ohura K, Nakamura T, Yamamuro T, Ebisawa Y, Kokubo T, Kotoura Y, et al. Bioactivity of $\text{CaO}\cdot\text{SiO}_2$ Glasses Added with Various Ions. *J Mater Sci: Mater M* 1992;3:95-100.
- [98] Galliano PG, Lopez JMP. Thermal-Behavior of Bioactive Alkaline-Earth Silicophosphate Glasses. *J Mater Sci: Mater M* 1995;6:353-9.
- [99] Salinas AJ, Román J, Vallet-Regi M, Oliveira JM, Correia RN, Fernandes MH. In vitro bioactivity of glass and glass-ceramics of the $3\text{CaO}\cdot\text{P}_2\text{O}_5\text{-CaO}\cdot\text{SiO}_2\text{-CaO}\cdot\text{MgO}\cdot 2\text{SiO}_2$ system. *Biomaterials* 2000;21:251-7.
- [100] Oliveira JM, Correia RN, Fernandes MH. Surface modifications of a glass and a glass-ceramic of the $\text{MgO}\cdot 3\text{CaO}\cdot\text{P}_2\text{O}_5\text{-SiO}_2$ system in a simulated body fluid. *Biomaterials* 1995;16:849-54.
- [101] Oliveira JM, Correia RN, Fernandes MH, Rocha J. Influence of the CaO/MgO ratio on the structure of phase-separated glasses: A solid state ^{29}Si and ^{31}P MAS NMR study. *J Non-Cryst Solids* 2000;265:221-9.

- [102] Oliveira JM, Correia RN, Fernandes MH. Effects of Si speciation on the in vitro bioactivity of glasses. *Biomaterials* 2002;23:371-9.
- [103] Kamitakahara M, Ohtsuki C, Kozaka Y, Ogata S, Tanihara M, Miyazaki T. Preparation of porous glass-ceramics containing whitlockite and diopside for bone repair. *J Ceram Soc Jpn* 2006;114:82-6.
- [104] Kansal I, Goel A, Tulyaganov DU, Santos LF, Ferreira JMF. Structure, surface reactivity and physico-chemical degradation of fluoride containing phospho-silicate glasses. *J Mater Chem* 2011;21:8074-84.
- [105] Kansal I, Goel A, Tulyaganov DU, Pascual MJ, Lee HY, Kim HW, et al. Diopside (CaO•MgO•2SiO₂)-fluorapatite (9CaO•3P₂O₅•CaF₂) glass-ceramics: potential materials for bone tissue engineering. *J Mater Chem* 2011;21:16247-56.
- [106] Kansal I, Goel A, Tulyaganov DU, Rajagopal RR, Ferreira JMF. Structural and thermal characterization of CaO-MgO-SiO₂-P₂O₅-CaF₂ glasses. *J Eur Cer Soc* 2012;32:2739-46.
- [107] Rawlings RD. Composition Dependence of the Bioactivity of Glasses. *J Mater Sci Lett* 1992;11:1340-3.
- [108] Hupa L, Hupa M. Recent Research on Composition Dependence of the Properties of Bioactive Glasses. *Advances in Bioceramics and Biotechnologies: John Wiley & Sons, Inc.;* 2010. p. 145-56.
- [109] Peitl O, Zanotto ED, Serbena FC, Hench LL. Compositional and microstructural design of highly bioactive P₂O₅-Na₂O-CaO-SiO₂ glass-ceramics. *Acta Biomater* 2012;8:321-32.
- [110] Linati L, Lusvardi G, Malavasi G, Menabue L, Menziani MC, Mustarelli P, et al. Qualitative and Quantitative Structure-Property Relationships Analysis of Multicomponent Potential Bioglasses. *J Phys Chem B* 2005;109:4989-98.
- [111] Lusvardi G, Malavasi G, Tarsitano F, Menabue L, Menziani MC, Pedone A. Quantitative Structure-Property Relationships of Potentially Bioactive Fluoro Phospho-silicate Glasses. *J Phys Chem B* 2009;113:10331-8.
- [112] O'Donnell MD, Hill RG. Influence of strontium and the importance of glass chemistry and structure when designing bioactive glasses for bone regeneration. *Acta Biomater* 2010;6:2382-5.
- [113] Lusvardi G, Malavasi G, Cortada M, Menabue L, Menziani MC, Pedone A, et al. Elucidation of the structural role of fluorine in potentially bioactive glasses by experimental and computational investigation. *J Phys Chem B* 2008;112:12730-9.

- [114] Fredholm YC, Karpukhina N, Law RV, Hill RG. Strontium containing bioactive glasses: Glass structure and physical properties. *J Non-Cryst Solids* 2010;356:2546-51.
- [115] Bonhomme C, Gervais C, Folliet N, Pourpoint F, Coelho Diogo C, Lao J, et al. ⁸⁷Sr Solid-State NMR as a Structurally Sensitive Tool for the Investigation of Materials: Antiosteoporotic Pharmaceuticals and Bioactive Glasses. *J Am Chem Soc* 2012;134:12611-28.
- [116] Martin RA, Twyman HL, Rees GJ, Smith JM, Barney ER, Smith ME, et al. A structural investigation of the alkali metal site distribution within bioactive glass using neutron diffraction and multinuclear solid state NMR. *Phys Chem Chem Phys* 2012;14:12105-13.
- [117] Pedone A, Charpentier T, Menziani MC. The structure of fluoride-containing bioactive glasses: new insights from first-principles calculations and solid state NMR spectroscopy. *J Mater Chem* 2012;22:12599-608.
- [118] Watts SJ, Hill RG, O'Donnell MD, Law RV. Influence of magnesia on the structure and properties of bioactive glasses. *J Non-Cryst Solids* 2010;356:517-24.
- [119] Fredholm YC, Karpukhina N, Brauer DS, Jones JR, Law RV, Hill RG. Influence of strontium for calcium substitution in bioactive glasses on degradation, ion release and apatite formation. *J Roy Soc Interface* 2012;9:880-9.
- [120] Aina V, Malavasi G, Fiorio Pla A, Munaron L, Morterra C. Zinc-containing bioactive glasses: Surface reactivity and behaviour towards endothelial cells. *Acta Biomater* 2009;5:1211-22.
- [121] Lao J, Jallot E, Nedelec J-M. Strontium-Delivering Glasses with Enhanced Bioactivity: A New Biomaterial for Antiosteoporotic Applications? *Chem Mater* 2008;20:4969-73.
- [122] Lao J, Nedelec JM, Jallot E. New strontium-based bioactive glasses: physicochemical reactivity and delivering capability of biologically active dissolution products. *J Mater Chem* 2009;19:2940-9.
- [123] Navarro M, Ginebra M-P, Clément J, Salvador M, Gloria A, Planell JA. Physicochemical Degradation of Titania-Stabilized Soluble Phosphate Glasses for Medical Applications. *J Am Ceram Soc* 2003;86:1345-52.
- [124] Dias AG, Gibson IR, Santos JD, Lopes MA. Physicochemical degradation studies of calcium phosphate glass ceramic in the CaO–P₂O₅–MgO–TiO₂ system. *Acta Biomater* 2007;3:263-9.

- [125] Murphy S, Wren A, Towler M, Boyd D. The effect of ionic dissolution products of Ca–Sr–Na–Zn–Si bioactive glass on in vitro cytocompatibility. *J Mater Sci: Mater Med* 2010;21:2827-34.
- [126] Serra J, González P, Liste S, Chiussi S, León B, Pérez-Amor M, et al. Influence of the non-bridging oxygen groups on the bioactivity of silicate glasses. *J Mater Sci: Mater Med* 2002;13:1221-5.
- [127] Tilocca A. Short- and medium-range structure of multicomponent bioactive glasses and melts: An assessment of the performances of shell-model and rigid-ion potentials. *J Chem Phys* 2008;129.
- [128] Tilocca A. Sodium migration pathways in multicomponent silicate glasses: Car-Parrinello molecular dynamics simulations. *J Chem Phys* 2010;133.
- [129] Hill RG, Brauer DS. Predicting the bioactivity of glasses using the network connectivity or split network models. *J Non-Cryst Solids* 2011;357:3884-7.
- [130] Tas AC. Synthesis of biomimetic Ca-hydroxyapatite powders at 37 degrees C in synthetic body fluids. *Biomaterials* 2000;21:1429-38.
- [131] Nonami T, Tsutsumi S. Study of diopside ceramics for biomaterials. *J Mater Sci: Mater Med* 1999;10:475-9.
- [132] De Aza PN, Luklinska ZB, Anseau M. Bioactivity of diopside ceramic in human parotid saliva. *Journal of biomedical materials research Part B, Appl Biomater* 2005;73:54-60.
- [133] Nakajima S, Harada Y, Kurihara Y, Wakatsuki T, Noma H. [Physicochemical characteristics of new reinforcement ceramic implant]. *Shika gakuho Dental science reports* 1989;89:1709-17.
- [134] Nakajima S. [Experimental studies of healing process on reinforcement ceramic implantation in rabbit mandible]. *Shika gakuho Dental science reports* 1990;90:525-53.
- [135] Yoganand C, Selvarajan V, Lusvarghi L, Goudouri OM, Paraskevopoulos KM, Rouabhia M. Bioactivity of CaO-MgO-SiO₂ glass ceramics synthesized using transferred arc plasma (TAP) process. *Mater Sci Eng C* 2009;29:1759-64.
- [136] Jana C, Braun M. ¹⁹F NMR spectroscopy of glass ceramics containing fluorapatites. *Biomaterials* 1996;17:2065-9.
- [137] Abo-Mosallam HA, Hill RG, Karpukhina N, Law RV. MAS-NMR studies of glasses and glass-ceramics based on a clinopyroxene-fluorapatite system. *J Mater Chem* 2010;20:790-7.

- [138] Tulyaganov DU, Agathopoulos S, Fernandes HR, Ventura JM, Ferreira JMF. Preparation and crystallization of glasses in the system tetrasilicic mica-fluorapatite-diopside. *J Eur Cer Soc* 2004;24:3521-8.
- [139] Wang Z, Guo Z, Bai H, Li J, Li X, Chen G, et al. Clinical evaluation of β -TCP in the treatment of lacunar bone defects: A prospective, randomized controlled study. *Mater Sci Eng C* 2013;33:1894-9.
- [140] Kotobuki N, Kawagoe D, Nomura D, Katou Y, Muraki K, Fujimori H, et al. Observation and quantitative analysis of rat bone marrow stromal cells cultured in vitro on newly formed transparent beta-tricalcium phosphate. *J Mater Sci: Mater Med* 2006;17:33-41.
- [141] Ashizuka M, Ishida E. Mechanical properties of silicate glass-ceramics containing tricalcium phosphate. *J Mater Sci* 1997;32:185-8.
- [142] Tilocca A. Structure and dynamics of bioactive phosphosilicate glasses and melts from ab initio molecular dynamics simulations. *Phys Rev B* 2007;76.
- [143] Tilocca A, Cormack AN. Structural effects of phosphorus inclusion in bioactive silicate glasses. *J Phys Chem B* 2007;111:14256-64.
- [144] Bohner M, Lemaître J. Can bioactivity be tested in vitro with SBF solution? *Biomaterials* 2009;30:2175-9.
- [145] Fujibayashi S, Neo M, Kim HM, Kokubo T, Nakamura T. A comparative study between in vivo bone ingrowth and in vitro apatite formation on $\text{Na}_2\text{O-CaO-SiO}_2$ glasses. *Biomaterials* 2003;24:1349-56.
- [146] Kokubo T, Takadama H. How useful is SBF in predicting in vivo bone bioactivity? *Biomaterials* 2006;27:2907-15.
- [147] Cerruti M, Morterra C. Carbonate formation on bioactive glasses. *Langmuir* 2004;20:6382-8.
- [148] Pérez-Pariante J, Balas F, Vallet-Regí M. Surface and Chemical Study of $\text{SiO}_2\cdot\text{P}_2\text{O}_5\cdot\text{CaO}\cdot(\text{MgO})$ Bioactive Glasses. *Chem Mater* 2000;12:750-5.
- [149] Karlsson KH, Fröberg K, Ringbom T. A structural approach to bone adhering of bioactive glasses. *J Non-Cryst Solids* 1989;112:69-72.
- [150] Jones JR, Sepulveda P, Hench LL. Dose-dependent behavior of bioactive glass dissolution. *J Biomed Mater Res* 2001;58:720-6.
- [151] Lara C, Pascual MJ, Duran A. Glass-forming ability, sinterability and thermal properties in the systems RO-BaO-SiO_2 ($\text{R} = \text{Mg, Zn}$). *J Non-Cryst Solids* 2004;348:149-55.

- [152] Magallanes-Perdomo M, Pena P, De Aza PN, Carrodeguas RG, Rodriguez MA, Turrillas X, et al. Devitrification studies of wollastonite-tricalcium phosphate eutectic glass. *Acta Biomater* 2009;5:3057-66.
- [153] Lusvardi G, Malavasi G, Menabue L, Menziani MC, Pedone A, Segre U, et al. Properties of zinc releasing surfaces for clinical applications. *J Biomater Appl* 2008;22:505-26.
- [154] Murphy S, Boyd D, Moane S, Bennett M. The effect of composition on ion release from Ca-Sr-Na-Zn-Si glass bone grafts. *J Mater Sci: Mater Med* 2009;20:2207-14.
- [155] Du RL, Chang J. Preparation and characterization of Zn and Mg doped bioactive glasses. *J Inorg Mater* 2004;19:1353-8.
- [156] Du RL, Chang J, Ni SY, Zhai WY, Wang JY. Characterization and in vitro bioactivity of zinc-containing bioactive glass and glass-ceramics. *J Biomater Appl* 2006;20:341-60.
- [157] Aina V, Perardi A, Bergandi L, Malavasi G, Menabue L, Morterra C, et al. Cytotoxicity of zinc-containing bioactive glasses in contact with human osteoblasts. *Chem Biol Interact* 2007;167:207-18.
- [158] Kamitakahara M, Ohtsuki C, Inada H, Tanihara M, Miyazaki T. Effect of ZnO addition on bioactive CaO-SiO₂-P₂O₅-CaF₂ glass-ceramics containing apatite and wollastonite. *Acta Biomater* 2006;2:467-71.
- [159] Du RL, Chang J. The influence of Zn on the deposition of HA on sol-gel derived bioactive glass. *Bio Med Mater Eng* 2006;16:229-36.
- [160] Salinas AJ, Shruti S, Malavasi G, Menabue L, Vallet-Regi M. Substitutions of cerium, gallium and zinc in ordered mesoporous bioactive glasses. *Acta Biomater* 2011;7:3452-8.
- [161] Rahaman MN, Day DE, Bal BS, Fu Q, Jung SB, Bonewald LF, et al. Bioactive glass in tissue engineering. *Acta Biomater* 2011;7:2355-73.
- [162] Oudadesse H, Dietrich E, Gal YL, Pellen P, Bureau B, Mostafa AA, et al. Apatite forming ability and cytocompatibility of pure and Zn-doped bioactive glasses. *Biomed Mater* 2011;6.
- [163] Oudadesse H, Dietrich E, Lucas-Girot A, Le Gal Y, Jeanne S, Cathelineau G. Effects of Mg and Zn on the surface of doped melt-derived glass for biomaterials applications. *Appl Surf Sci* 2008;255:391-5.
- [164] Bini M, Grandi S, Capsoni D, Mustarelli P, Saino E, Visai L. SiO₂-P₂O₅-CaO Glasses and Glass-Ceramics with and without ZnO: Relationships among Composition, Microstructure, and Bioactivity. *J Phys Chem C* 2009;113:8821-8.

- [165] Saino E, Grandi S, Quartarone E, Maliardi V, Galli D, Bloise N, et al. In vitro calcified matrix deposition by human osteoblasts onto a zinc-containing bioactive glass. *Eur Cell Mater* 2011;21:59-72; discussion
- [166] Roy B, Jain H, Saha SK, Chakravorty D. Comparison of structure of alkali silicate glasses prepared by sol-gel and melt-quench methods. *J Non-Cryst Solids* 1995;183:268-76.
- [167] Linati L, Lusvardi G, Malavasi G, Menabue L, Menziani MC, Mustarelli P, et al. Medium-range order in phospho-silicate bioactive glasses: Insights from MAS-NMR spectra, chemical durability experiments and molecular dynamics simulations. *J Non-Cryst Solids* 2008;354:84-9.
- [168] Termine JD, Peckauskas RA, Posner AS. Calcium phosphate formation in vitro: II. Effects of environment on amorphous-crystalline transformation. *Arch Biochem Biophys* 1970;140:318-25.
- [169] Wang L, Nancollas GH. Calcium Orthophosphates: Crystallization and Dissolution. *Chem Rev* 2008;108:4628-69.
- [170] Dorozhkin SV, Epple M. Biological and Medical Significance of Calcium Phosphates. *Angew Chem Int Ed* 2002;41:3130-46.
- [171] Ebisawa Y, Kokubo T, Ohura K, Yamamuro T. Bioactivity of CaO•SiO₂-based glasses: in vitro evaluation. *J Mater Sci: Mater Med* 1990;1:239-44
- [172] Hoppe A, Guldal NS, Boccaccini AR. A review of the biological response to ionic dissolution products from bioactive glasses and glass-ceramics. *Biomaterials* 2011;32:2757-74.
- [173] Aina V, Bonino F, Morterra C, Miola M, Bianchi CL, Malavasi G, et al. Influence of the Chemical Composition on Nature and Activity of the Surface Layer of Zn-Substituted Sol-Gel (Bioactive) Glasses. *J Phys Chem C* 2011;115:2196-210.
- [174] Courtheoux L, Lao J, Nedelec JM, Jallot E. Controlled bioactivity in zinc-doped sol-gel-derived binary bioactive glasses. *J Phys Chem C* 2008;112:13663-7.
- [175] Haimi S, Gorianc G, Moimas L, Lindroos B, Huhtala H, Raty S, et al. Characterization of zinc-releasing three-dimensional bioactive glass scaffolds and their effect on human adipose stem cell proliferation and osteogenic differentiation. *Acta Biomater* 2009;5:3122-31.
- [176] Popp JR, Love BJ, Goldstein AS. Effect of soluble zinc on differentiation of osteoprogenitor cells. *J Biomed Mater Res A* 2007;81A:766-9.
- [177] Dellamea G, Gasparotto A, Bettinelli M, Montenero A, Scaglioni R. Chemical Durability of Zinc-Containing Glasses. *J Non-Cryst Solids* 1986;84:443-51.

- [178] Bock CW, Katz AK, Markham GD, Glusker JP. Manganese as a replacement for magnesium and zinc: Functional comparison of the divalent ions. *J Am Chem Soc* 1999;121:7360-72.
- [179] Cassingham NJ, Stennett MC, Bingham PA, Hyatt NC, Aquilanti G. The Structural Role of Zn in Nuclear Waste Glasses. *Int J Appl Glass Sci* 2011;2:343-53.
- [180] Le Grand M, Ramos AY, Calas G, Galois L, Ghaleb D, Pacaud F. Zinc environment in aluminoborosilicate glasses by ZnK-edge extended x-ray absorption fine structure spectroscopy. *J Mater Res* 2000;15:2015-9.
- [181] Calas G, Cormier L, Galois L, Jollivet P. Structure–property relationships in multicomponent oxide glasses. *Comptes Rendus Chimie* 2002;5:831-43.
- [182] Li P, Ohtsuki C, Kokubo T, Nakanishi K, Soga N, Nakamura T, et al. Apatite Formation Induced by Silica Gel in a Simulated Body Fluid. *J Am Ceram Soc* 1992;75:2094-7.
- [183] Fu Q, Saiz E, Rahaman MN, Tomsia AP. Bioactive glass scaffolds for bone tissue engineering: state of the art and future perspectives. *Mater Sci Eng C* 2011;31:1245-56.
- [184] Pawlowski L. *The Science and Engineering of Thermal Spray Coatings*. England: John Wiley & Sons Ltd; 2008.
- [185] Luo Y-R. *Comprehensive Handbook of Chemical Bond Energies*: CRC Press; 2010
- [186] Toyoda S, Fujino S, Morinaga K. Density, viscosity and surface tension of 50RO-50P(2)O(5) (R : Mg, Ca, Sr, Ba, and Zn) glass melts. *J Non-Cryst Solids* 2003;321:169-74.
- [187] Doremus RH. *Glass Science*. 2nd ed: John Wiley & Sons, Inc., New York; 1994. p. pp105.
- [188] Chapter 4 ²⁹Si NMR. In: Kenneth JDM, Mark ES, editors. *Pergamon Materials Series*: Pergamon; 2002. p. 201-68.
- [189] Li P, Yang Q, Zhang F, Kokubo T. The Effect of Residual Glassy Phase in a Bioactive Glass-Ceramic on the Formation of Its Surface Apatite Layer *In vitro*. *J Mater Sci: Mater Med* 1992;3:452-6.
- [190] Chai FG, Truong-Tran AQ, Ho LH, Zalewski PD. Regulation of caspase activation and apoptosis by cellular zinc fluxes and zinc deprivation: A review. *Immunol Cell Biol* 1999;77:272-8.
- [191] Choi DW, Koh JY. Zinc and brain injury. *Annu Rev Neurosci* 1998;21:347-75.
- [192] Zhang H, Ye XJ, Li JS. Preparation and biocompatibility evaluation of apatite/wollastonite-derived porous bioactive glass ceramic scaffolds. *Biomed Mater* 2009;4.

- [193] SA O, SH K, JE W, JJ K, US S, HW K. Effects on growth and osteogenic differentiation of mesenchymal stem cells by the zinc-added sol-gel bioactive glass granules. *Journal of Tissue Engineering* 2010;2010:475206.
- [194] Verne E, Ferraris S, Vitale-Brovarone C, Spriano S, Bianchi CL, Naldoni A, et al. Alkaline phosphatase grafting on bioactive glasses and glass ceramics. *Acta Biomater* 2010;6:229-40.
- [195] Hench LL, Xynos ID, Polak JM. Bioactive glasses for in situ tissue regeneration. *J Biomat Sci Polym E* 2004;15:543-62.
- [196] Nielsen SP. The biological role of strontium. *Bone* 2004;35:583-8.
- [197] Siccardi AJ, Padgett-Vasquez S, Garris HW, Nagy TR, D'Abramo LR, Watts SA. Dietary Strontium Increases Bone Mineral Density in Intact Zebrafish (*Danio rerio*): A Potential Model System for Bone Research. *Zebrafish* 2010;7:267-73.
- [198] Fujikura K, Karpukhina N, Kasuga T, Brauer DS, Hill RG, Law RV. Influence of strontium substitution on structure and crystallisation of Bioglass[®] 45S5. *J Mater Chem* 2012;22:7395-402.
- [199] Boyd D, Carroll G, Towler MR, Freeman C, Farthing P, Brook IM. Preliminary investigation of novel bone graft substitutes based on strontium-calcium-zinc-silicate glasses. *J Mater Sci-Mater M* 2009;20:413-20.
- [200] Boyd D, Towler MR, Watts S, Hill RG, Wren AW, Clarkin OM. The role of Sr²⁺ on the structure and reactivity of SrO-CaO-ZnO-SiO₂ ionomer glasses. *J Mater Sci: Mater Med* 2008;19:953-7.
- [201] Looney M, O'Shea H, Boyd D. Preliminary evaluation of therapeutic ion release from Sr-doped zinc-silicate glass ceramics. *J Biomater Appl* 2013;27:511-24.
- [202] Towler MR, Boyd D, Freeman C, Brook IM, Farthing P. Comparison of in vitro and in vivo Bioactivity of SrO-CaO-ZnO-SiO₂ Glass Grafts. *J Biomater Appl* 2009;23:561-72.
- [203] Xiang Y, Du JC, Skinner LB, Benmore CJ, Wren AW, Boydd DJ, et al. Structure and diffusion of ZnO-SrO-CaO-Na₂O-SiO₂ bioactive glasses: a combined high energy X-ray diffraction and molecular dynamics simulations study. *RSCAdvances* 2013;3:5966-78.
- [204] Goel A, Rajagopal RR, Ferreira JMF. Influence of strontium on structure, sintering and biodegradation behaviour of CaO-MgO-SrO-SiO₂-P₂O₅-CaF₂ glasses. *Acta Biomater* 2011;7:4071-80.
- [205] Omori K. Analysis of Infrared Absorption Spectrum of Diopside. *Am Mineral* 1971;56:1607.

- [206] Peitl O, Zanotto ED, Hench LL. Highly bioactive $P_2O_5-Na_2O-CaO-SiO_2$ glass-ceramics. *J Non-Cryst Solids* 2001;292:115-26.
- [207] Christodoulou I, Buttery LDK, Saravanapavan P, Tai GP, Hench LL, Polak JM. Dose- and time-dependent effect of bioactive gel-glass ionic-dissolution products on human fetal osteoblast-specific gene expression. *J Biomed Mater Res B* 2005;74B:529-37.
- [208] Clover J, Gowen M. Are Mg-63 and Hos Te85 Human Osteosarcoma Cell-Lines Representative Models of the Osteoblastic Phenotype. *Bone* 1994;15:585-91.
- [209] Lajeunesse D, Frondoza C, Schoffield B, Sacktor B. Osteocalcin Secretion by the Human Osteosarcoma Cell-Line Mg-63. *J Bone Miner Res* 1990;5:915-22.
- [210] Lajeunesse D, Kiebzak GM, Frondoza C, Sacktor B. Regulation of Osteocalcin Secretion by Human Primary Bone-Cells and by the Human Osteosarcoma Cell-Line Mg-63. *Bone Miner* 1991;14:237-50.
- [211] Chen L. Okadaic acid induces apoptosis through the PKR, NF-kappa B and caspase pathway in human osteoblastic osteosarcoma MG63 cells. *Toxicol in Vitro* 2011;25:1796-802.
- [212] Wang Y, Wei YD, Zhang HY, Shi YF, Li YL, Li RG. Arsenic trioxide induces apoptosis of p53 null osteosarcoma MG63 cells through the inhibition of catalase. *Med Oncol* 2012;29:1328-34.
- [213] Li M, Zhao L, Liu J, Liu A-L, Zeng W-S, Luo S-Q, et al. Hydrogen Peroxide Induces G2 Cell Cycle Arrest and Inhibits Cell Proliferation in Osteoblasts. *The Anat Rec: Adv Integ Anat Evol Biol* 2009;292:1107-13.
- [214] Kapoor S, Goel A, Tilocca A, Dhuna V, Bhatia G, Dhuna K, et al. Role of glass structure in defining the chemical dissolution behavior, bioactivity and antioxidant properties of zinc and strontium co-doped alkali-free phosphosilicate glasses. *Acta Biomater* 2014;10:3264-78.
- [215] Senkoylu A, Yilmaz A, Ergun M, İlhan M, Simsek A, Altun N, et al. Effect of Strontium Ranelate on Hydrogen Peroxide-Induced Apoptosis of CRL-11372 Cells. *Biochem Genet* 2008;46:197-205.
- [216] Bergandi L, Aina V, Garetto S, Malavasi G, Aldieri E, Laurenti E, et al. Fluoride-containing bioactive glasses inhibit pentose phosphate oxidative pathway and glucose 6-phosphate dehydrogenase activity in human osteoblasts. *Chem Biol Interact* 2010;183:405-15.

- [217] Rosenfeldt F, Wilson M, Lee G, Kure C, Ou R, Braun L, et al. Oxidative stress in surgery in an ageing population: Pathophysiology and therapy. *Exp Gerontol* 2013;48:45-54.
- [218] Cornell CN, Lane JM. Newest Factors in Fracture Healing. *Clinical Orthopaedics and Related Research* 1992;277:297-311.
- [219] Prasad G, Dhillon MS, Khullar M, Nagi ON. Evaluation of oxidative stress after fractures. A preliminary study. *Acta orthopaedica Belgica* 2003;69:546-51.
- [220] Liang D, Yang M, Guo B, Cao J, Yang L, Guo X, et al. Zinc Inhibits H₂O₂-Induced MC3T3-E1 Cells Apoptosis via MAPK and PI3K/AKT Pathways. *Bio Trace Elem Res* 2012;148:420-9.
- [221] Jebahi S, Oudadesse H, El Feki H, Rebai T, Keskes H, El Feki A. Antioxidative/oxidative status of muscular tissue surrounding strontium-substituted bioactive glass implanted in bone of ovariectomised rats. *Fund Clin Pharmacol* 2012;26:94-.
- [222] Wu C, Chang J. Degradation, bioactivity, and cytocompatibility of diopside, akermanite, and bredigite ceramics. *Journal of biomedical materials research Part B, Appl Biomater* 2007;83:153-60.
- [223] Aronne A, Sigaev VN, Champagnon B, Fanelli E, Califano V, Usmanova LZ, et al. The origin of nanostructuring in potassium niobosilicate glasses by Raman and FTIR spectroscopy. *J Non-Cryst Solids* 2005;351:3610-8.
- [224] Fiore G, Ichim I, Battezzati L. Thermal analysis, fragility and viscosity of Au-based metallic glasses. *J Non-Cryst Solids* 2010;356:2218-22.
- [225] Lockyer MWG, Holland D, Dupree R. Nmr Investigation of the Structure of Some Bioactive and Related Glasses. *J Non-Cryst Solids* 1995;188:207-19.
- [226] O'Donnell MD, Watts SJ, Hill RG, Law RV. The effect of phosphate content on the bioactivity of soda-lime- phosphosilicate glasses. *J Mater Sci: Mater Med* 2009;20:1611-8.
- [227] Mneimne M, Hill RG, Bushby AJ, Brauer DS. High phosphate content significantly increases apatite formation of fluoride-containing bioactive glasses. *Acta Biomater* 2011;7:1827-34.
- [228] O'Donnell MD, Watts SJ, Law RV, Hill RG. Effect of P₂O₅ content in two series of soda lime phosphosilicate glasses on structure and properties – Part I: NMR. *J Non-Cryst Solids* 2008;354:3554-60.
- [229] Diba M, Tapia F, Boccaccini AR, Strobel LA. Magnesium-Containing Bioactive Glasses for Biomedical Applications. *Int J Appl Glass Sci* 2012;3:221-53.

- [230] Kapoor S, Goel A, Pascual MJ, Ferreira JMF. Thermo-mechanical behaviour of alkali free bioactive glass-ceramics co-doped with strontium and zinc. *J Non-Cryst Solids* 2013;375:74-82.
- [231] Zhang N, Molenda JA, Mankoci S, Zhou X, Murphy WL, Sahai N. Crystal structures of CaSiO₃ polymorphs control growth and osteogenic differentiation of human mesenchymal stem cells on bioceramic surfaces. *Biomater Sci* 2013;1:1101-10.
- [232] Han P, Wu C, Xiao Y. The effect of silicate ions on proliferation, osteogenic differentiation and cell signalling pathways (WNT and SHH) of bone marrow stromal cells. *Biomater Sci* 2013;1:379-92.
- [233] Zhang NL, Molenda JA, Fournelle JH, Murphy WL, Sahai N. Effects of pseudowollastonite (CaSiO₃) bioceramic on in vitro activity of human mesenchymal stem cells. *Biomaterials* 2010;31:7653-65.
- [234] Bidarra SJ, Barrias CC, Barbosa MA, Soares R, Granja PL. Immobilization of Human Mesenchymal Stem Cells within RGD-Grafted Alginate Microspheres and Assessment of Their Angiogenic Potential. *Biomacromolecules* 2010;11:1956-64.
- [235] Magallanes-Perdomo M, De Aza AH, Mateus AY, Teixeira S, Monteiro FJ, De Aza S, et al. In vitro study of the proliferation and growth of human bone marrow cells on apatite-wollastonite-2M glass ceramics. *Acta Biomater* 2010;6:2254-63.
- [236] Sun HL, Wu CT, Dai KR, Chang J, Tang TT. Proliferation and osteoblastic differentiation of human bone marrow-derived stromal cells on akermanite-bioactive ceramics. *Biomaterials* 2006;27:5651-7.
- [237] Huang Y, Jin XG, Zhang XL, Sun HL, Tu JW, Tang TT, et al. In vitro and in vivo evaluation of akermanite bioceramics for bone regeneration. *Biomaterials* 2009;30:5041-8.
- [238] Zhai WY, Lu HX, Wu CT, Chen L, Lin XT, Naoki K, et al. Stimulatory effects of the ionic products from Ca-Mg-Si bioceramics on both osteogenesis and angiogenesis in vitro. *Acta Biomater* 2013;9:8004-14.